UMR-CNRS 6538 "Domaines Océaniques"
Institut Universitaire de la Mer (UBO)

Laboratoire Environnements Sédimentaires
Géosciences Marines

THÈSE

Présentée

à l'UNIVERSITÉ DE BRETAGNE OCCIDENTALE

Ecole Doctorale des Sciences de la Mer

Pour l'obtention du grade de

DOCTEUR

Spécialité: **GÉOSCIENCES MARINES**

par

GWÉNAËL JOUËT

Enregistrements stratigraphiques des cycles climatiques et glacio-eustatiques du Quaternaire terminal
---
Modélisations de la marge continentale du Golfe du Lion

Volume II

Soutenue le 12 novembre 2007, devant le jury composé de :

François GUILLOCHEAU	Professeur, Université de Rennes 1, Rennes	Rapporteur
Bilal HAQ	Professeur, NSF, Arlington, Virginie, USA	Rapporteur
Jacques DEVERCHERE	Professeur, IUEM-UBO, Brest	Examinateur
Serge BERNÉ	Chercheur CR3, IFREMER, Brest	Directeur de thèse
Didier GRANJEON	Chercheur, IFP, Paris	Examinateur
Pascal LE ROY	Maître de Conférences, IUEM-UBO, Brest	Examinateur
Michel TESSON	Professeur, Université de Perpignan, Perpignan	Examinateur

UMR-CNRS 6538 "Domaines Océaniques"
Institut Universitaire de la Mer (UBO)

Laboratoire Environnements Sédimentaires
Géosciences Marines

THÈSE

Présentée

à l'UNIVERSITÉ DE BRETAGNE OCCIDENTALE

Ecole Doctorale des Sciences de la Mer

Pour l'obtention du grade de

DOCTEUR

Spécialité: GÉOSCIENCES MARINES

par

GWÉNAËL JOUËT

Enregistrements stratigraphiques des cycles climatiques et glacio-eustatiques du Quaternaire terminal
---
Modélisations de la marge continentale du Golfe du Lion

Volume II

Soutenue le 12 novembre 2007, devant le jury composé de :

François GUILLOCHEAU	Professeur, Université de Rennes 1, Rennes	Rapporteur
Bilal HAQ	Professeur, NSF, Arlington, Virginie, USA	Rapporteur
Jacques DEVERCHERE	Professeur, IUEM-UBO, Brest	Examinateur
Serge BERNÉ	Chercheur CR3, IFREMER, Brest	Directeur de thèse
Didier GRANJEON	Chercheur, IFP, Paris	Examinateur
Pascal LE ROY	Maître de Conférences, IUEM-UBO, Brest	Examinateur
Michel TESSON	Professeur, Université de Perpignan, Perpignan	Examinateur

TABLE DES MATIÈRES

ANNEXE - I

PUBLICATIONS ET COMMUNICATIONS

ANNEXE-I. LISTE DES PUBLICATIONS ET COMMUNICATIONS

A-I.1. Articles en préparation ou soumis

Jouet, G., Berné, S., Sierro, F.J., Bassetti, M.A., Canals, M., Dennielou, B., Flores, J.A. and the Team PROMESS-1. **Submitted**. Sedimentary response to millenial-scale sea-level changes in the NW Mediterranean. Letters to Nature.

Bassetti, M.A., Berné, S., **Jouet, G.**, Dennielou, B., Sultan, N., Taviani, M., Gaillot, A., Flores, J.A., Gelfort, R. and Lafuerza, S., **Submitted**. Facies and high-resolution stratigraphy of late Quaternary forced-regressive shorefaces from the Gulf of Lions (Western Mediterranean Sea). Geochemistry, Geophysics, and Geosystems.

Dennielou, B., Jallet, L., Sultan, N., **Jouet, G.**, Berné, S., Voisset, M. and Giresse, P., **Submitted**. Post-glacial persistence of gravity deposits and of erosive processes in the deep basin of the Gulf of Lions (Western Mediterranean): linking the shelfal and the deep basin sedimentary record. Marine Geology.

Lafuerza, S., Sultan, N., Canals, M., Frigola, J., Berné, S., **Jouet, G.**, Galavazi, M. and Sierro, F.J., **Submitted-a**. Overpressure within upper continental slope sediments from CPTU data, Gulf of Lion, NW Mediterranean Sea. International Journal of Earth Sciences.

Lafuerza, S., Frigola, J., Canals, M., Jouet, G., Bassetti, M.A., Sultan, N. and Berné, S., **Submitted-b**. Subsea-floor stratigraphic profiling and soil classification from piezocone tests: A case study in the Gulf of Lion (NW Mediterranean Sea). Geochemistry, Geophysics, and Geosystems.

Sierro, F.J., Andersen, N., Bassetti, M.A., S., B., Canals, M., Curtis, J.H., Dennielou, B., Flores, J.A., Frigola, J., Gonzales-Mora, B., Grimalt, J.O., Hodell, D.A., **Jouet, G.**, Pérez-Folgado, M. and Schneider, R., **Submitted**. Flooding events in the Western Mediterranean continental shelf, millennial climate oscillations and global sea level changes. Science.

van Welden, A., Bout-Roumazeilles, V., Berné, S., **Jouet, G.**, Gorini, C. and Sierro, F.J**., *in prep*.** Sedimentation in the Gulf of Lions during the last 25 ky BP in the light of clay mineralogy and grain size parameters. Marine Geology.

A-I.2. Articles publiés dans des revues internationales à comité de lecture

Jouet, G., Hutton, E.W.H., Syvitski, J.P.M. and Berné, S., *in press*. Response of the Rhône deltaic margin to loading and subsidence during the last climatic cycle. Computer and Geosciences.

Berné, S., **Jouet, G.**, Bassetti, M.A., Dennielou, B. and Taviani, M., *in press*. Late glacial to Preboreal sea-level rise recorded by the Rhône deltaic system (NW Mediterranean). Marine Geology.

Beaudouin, C., **Jouet, G.**, Suc, J.-P., Berné, S. and Escarguel, G., **2007**. Vegetation dynamics in southern France during the last 30 ky BP in the light of marine palynology. Quaternary Science Reviews, 26(7-8): 1037-1054.

Jouet, G., Berné, S., Rabineau, M., Bassetti, M.A., Bernier, P., Dennielou, B., Flores, J.A., Sierro, F.J. and Taviani, M., **2006**. Shoreface migrations at the shelf edge and sea-level changes around the Last Glacial Maximum (Gulf of Lions, NW Mediterranean). Marine Geology, 234: 21-42.

Bassetti, M.A., **Jouet, G.**, Dufois, F., Berné, S., Rabineau, M. and Taviani, M., **2006**. Sand bodies at the shelf edge in the Gulf of Lions (Western Mediterranean): deglacial history and modern processes. Marine Geology, 234: 93-109.

Labaune, C., **Jouet, G.**, Berné, S., Gensous, B., Tesson, M. and Delpeint, A., **2005**. Seismic stratigraphy of the Deglacial deposits of the Rhône prodelta and the adjacent shelf. Marine Geology, 222-223: 299-311.

A-I.3. Autres publications

Satra, C., Boyer, J., Berné, S., Tesson, M., Guennoc, P., Alix, A.S., Bassetti, M.A., **Jouet, G.**, Leroux, E., Mazé, J.P., Normand, A., Pierre, D., Labaune, C., Gensous, B. and Guérin, K., **2004**. Projet Beachmed - Rapport final de phase C : Présentation des données. In: D.G. 2004-21 (Editor). Ifremer, Brest.

Satra, C., Boyer, J., Labaune, C., Berné, S., Tesson, M., Gensous, B., **Jouet, G.**, Pierre, D. and Mazé, J.P., **2004**. Projet Beachmed - Rapport final de phase B : présentation des données. In: D.G. 2004-15 (Editor). Ifremer, Brest.

A-I.4. Communications internationales *(1er auteur)*

Jouet, G., Berné, S., Sierro, F.J., Bassetti, M.A., Flores, J.A., Gaudin, M., Dennielou, B. and Rabineau, M., **2006**. Sedimentary imprints of millennial-scale sea-level fluctuations during the last 130 ka on the Rhône deltaic margin (Gulf of Lions, NW Mediterranean), Sea-level changes: Records, processes and modelling - SEALAIX'06, Giens (France), pp. 100. (Poster)

Jouet, G., Gaudin, M., Bassetti, M.A., Berné, S., Rabineau, M., Dennielou, B., Sierro, F.J., Flores, J.A. and Taviani, M., **2006**. Climatic and environmental variations during the last 130 ka: Investigations from sedimentary record on the Rhône deltaic margin (Gulf of Lions, NW Mediterranean), 17th International Sedimentological Congress (ISC2006), Fukuoka (Japan), pp. 117.

Jouet, G., Berné, S., Bassetti, M.A., Gaudin, M., Rabineau, M., Dennielou, B., Sierro, F.J., Flores, J.A. and Taviani, M., **2006**. Last climatic cycle investigated from sedimentary record on the Rhône deltaic margin (Gulf of Lions, NW Mediterranean), European Geosciences Union Conference (EGU), Vienna (Austria), pp. 273. (Poster)

Jouet, G., Berné, S., Rabineau, M., Granjeon, D. and Vella, C., **2006**. Variabilité climatique pendant la dernière déglaciation: conséquences sur la sédimentation de la marge deltaïque du Golfe du Lion, Colloque du GDR-Marges, Paris (France), pp. 98. (Poster)

Jouet, G., Hutton, E.W., Syvitski, J.P., Rabineau, M. and Berné, S., **2006**. Continental margin's response to loading and subsidence variations: stratigraphic modelling of the Rhône deltaic margin during the Last Climatic Cycle (Gulf of Lions, NW Mediterranean), Work Session, Boulder (Colorado).

Jouet, G., Rabineau, M., Berné, S. and Granjeon, D., **2005**. An overview of the stratigraphic simulations on the Rhône deltaic margin (Gulf of Lions, South-East of France), Consortium Dionisos - IFP, Paris (France).

Jouet, G., Berné, S., Rabineau, M., Granjeon, D. and Vella, C., **2005**. Stratigraphic simulations of the last deglaciation on the Rhône deltaic margin (over the last 20 000 years), Joint Eurostrataform - Promess-1 Annual Meeting, Salamanca (Spain)

Jouet, G., Berné, S., Rabineau, M., Granjeon, D. and Vella, C., **2005**. Simulations stratigraphiques de la dernière déglaciation sur la marge deltaïque du Golfe du Lion (derniers 20 000 ans), 10ème Congrès Français de Sédimentologie (ASF). Livre des résumés. Publ. ASF, Presqu'île de Giens (France), pp. 173.

Jouet, G., Rabineau, M., Berné, S., Bassetti, M.A. and Dennielou, B., **2004**. Marine isotope stage 3 to present signature in shelf margin deltaic sedimentary sequences in the Gulf of Lions, Joint EuroDelta - EuroStrataform Annual Meeting, Venice (Italy), pp. 55.

Jouet, G. and Rabineau, M., **2004**. Workpackage 7: Stratigraphic modelling, Promess-1 2nd Annual Meeting, Brest (France).

Jouet, G., Rabineau, M. and Berné, S., **2004**. Marine isotope stage 3 to present signature in shelf margin deltaic sedimentary sequences in the Gulf of Lions: imbrication of cyclicities, Conference EuroStrataform US, Keystone (Colorado).

Jouet, G., Rabineau, M. and Berné, S., **2004**. Stratigraphic modelling on a shelf margin deltaic sedimentary sequence associated to the glacio-eustatic cycles in the Gulf of Lions, PROxies in Paleoclimatology: Education and Research (Proper cours), Amsterdam (Netherlands).

Jouet, G., Rabineau, M., Berné, S., Baztan, J., Beaudouin, C., Duval, F. and Jégou, I., **2003**. Marine isotope stage 3 to present signature in shelf margin deltaic sedimentary sequences in the Gulf of Lions: imbrication of cyclicities, Conference ComDelta (Comparing Mediterranean and Black Sea Prodeltas) - EuroDelta, Aix-en-Provence (France), pp. 50-51. (Poster)

Jouet, G., Rabineau, M. and Berné, S., **2003**. Origines des séquences sédimentaires emboîtées sur la marge externe du Golfe du Lion du stade isotopique 3 à l'Actuel (derniers 50 000 ans), 9$^{\text{ème}}$ Congrès Français de Sédimentologie (ASF). Livre des résumés. Publ. ASF, Bordeaux (France), pp. 278. (Poster)

A-I.5. Autres communications *(1er auteur)*

Jouet, G., Rabineau, M. and Berné, S., **2005**. Comment s'enregistrent les climats du passé dans les sédiments marins ?, Forum des doctorants de l'Ecole Doctorale des Sciences de la Mer, IUEM-Brest (France). (Poster)

Jouet, G., Berné, S., Rabineau, M., Granjeon, D., Labaune, C. and Bassetti, M.A., **2005**. Simulations stratigraphiques de la dernière déglaciation sur la marge deltaïque du Golfe du Lion, Séminaire UMR6538, Brest (France).

Jouet, G. and Rabineau, M., **2005**. Traitements et interprétations en sédimentologie marine, Séminaire UMR6538, Crozon (France).

Jouet, G., Rabineau, M. and Berné, S., **2005**. Comment s'enregistrent les climats du passé dans les sédiments marins ?, Stage résidentiel CIES, Rennes (France).

Jouet, G., Rabineau, M. and Berné, S., **2004**. Simulations stratigraphiques 3D des séquences sédimentaires associées aux cycles glacio-eustatiques sur la marge du Golfe du Lion, Réunion annuelle de l'URM17, Brest (France), pp. 10.

Jouet, G., Rabineau, M. and Berné, S., **2004**. Enregistrement du climat dans les sédiments marins: observations sur la plateforme externe du Golfe du Lion pour les derniers 50 000 ans, Forum des doctorants de l'Ecole Doctorale des Sciences de la Mer, IUEM-Brest (France).

ANNEXE - II

PUBLICATION SUR LE PLEISTOCENE

ANNEXE-**II.** Publication sur le Pléistocène

A-II.1. Facies and high-resolution stratigraphy of late Quaternary forced-regressive shorefaces from the Gulf of Lions (Western Mediterranean Sea).

(Bassetti, Berné, Jouet *et al*., submitted)

10

Facies and high-resolution stratigraphy of late Quaternary forced-regressive shorefaces from the Gulf of Lions (Western Mediterranean Sea)

M.A. Bassetti

Université de Perpignan IMAGES, 52 avenue Paul Alduy, Perpignan , France

S. Berné, G. Jouet, B. Dennielou and N. Sultan

IFREMER, Géosciences Marines, BP 70, 29280 Plouzané, France,

M. Taviani

ISMAR/CNR via Gobetti 101, Bologna, Italy

A. Gaillot

IFREMER, NSE, BP 70, 29280 Plouzané, France

J.-A. Flores

Universidad de Salamanca, Facultad de Ciencias, Plaza Merced s/n, Salamanca, Spain,

R. Gelfort

Institut für Geowissenschaftliche Gemeinschaftsaufgaben (GGA), Stilleweg 2, 30655, Hannover, Germany

S. Lafuerza

GRC Geociències Marines, Departament d'Estratigrafia i Paleontologia i Geociències Marines, Universitat de Barcelona, Martí i Franquès s/n, 08028 Barcelona, Spain

Abstract

Thick forced regressive units deposited on the wide continental shelf of the Gulf of Lions (Western Mediterranean) have recorded the composite effect of sea-level changes during the Quaternary. They are mostly composed of coastal siliciclastic and bioclastic wedges showing clinoform geometry.

These deposits have been intensively explored through high-resolution seismic investigations, but only recently it was possible to ground-truth seismic interpretations, thanks to a long (100 m) borehole that crossed the succession and recovered a large part of the mainly sandy deposits (~84% recovery).

A multiproxy analysis of the sedimentary succession shows that: (1) the stratal architecture of the shelf margin is controlled by major bounding surfaces that are polygenic erosion surfaces made of coarse-grained material incorporating abundant and diverse shells, including cold-water fauna (presently absent from the Mediterranean Sea). Between each surface, coarsening upwards units with steep (up to 5°) foresets are made of massive (more than 20 m thick) sands with possible swaley and hummocky cross-stratifications, passing seawards to sands with muddy intervals, then to alternating sands and silts highly bioturbated. Each prograding wedge corresponds to a forced-regressive shoreface, deposited during the overall sea-level falls during (relatively slow) interglacial/ glacial transitions and therefore represent the record of 100 ky cyclicity (2) detailed examination of the architecture and chrono-stratigraphy of the recent-most sequence shows that second-order bounding surfaces, corresponding to abrupt shallowing of sedimentary facies, separate stepped downward-stepping parasequences within the main sequence. These events are in phase with millennial-scale glacial sea-level variability inferred from the Red Sea. They provide a comprehensive and well-constrained Pleistocene analogue to the numerous shoreface deposits attributed to *falling-stage systems tracts* recognized in the stratigraphic record.

1. Introduction

Prograding beach-shoreface deposits are a common component of the stratigraphic record (i.e. *Walker and Plint* [1992]). They correspond to one of the key "facies models" utilised by sedimentologists studying the stratigraphic record, and the analysis of their evolution through time is at the origin of most of sequence-stratigraphic paradigms (i.e. *Posamentier et al.* [1992]). They are very sensitive to base-level changes, thus they can also be utilized, under certain conditions, as "dipsticks" for sea-level changes (i.e. *Rabineau et al.* [2005]). In addition, because of their high well-sorted sand content, they also represent interesting potential reservoirs for hydrocarbons. However, the shallow marine processes that are recorded in detail within shoreface-foreshore-shelf parasequences are barely known. This is mostly due to the lack of lithological data on Quaternary shoreface deposits, which are mainly known through high-resolution seismic investigations or from interpretation of geological outcrops interpreted as ancient shoreface deposits. The term "shoreface" is used here in the sense of *Van Wagoner et al.* [1990], i.e. sediments deposited between the foreshore and the storm wave base.

The Gulf of Lions, in the NW Mediterranean Sea has been the field of intense high-resolution seismic investigations during the last 10 years [*Berné et al.*, 2004]. Because of high sediment supply and rapid subsidence offers an exceptional record of shelf/slope sequences linked to glacio-eustatic sea-level changes during the last 500 ky. However, attempts to core the sandy forced-regressive shoreface deposits that constitute one of the key component of the shelf/slope succession was largely unsuccessful, due to the presence of coarse shell lags making piston and vibra-coring operations very difficult. The maximum recovery using these conventional techniques were cores about 2.5 m long [*Aloïsi*, 1986; *Berné et al.*, 1998; *Bassetti et al.*, 2006]. For similar reasons, leg ODP 174A on the New Jersey continental shelf encountered great difficulties for recovering, with "Advanced Piston Coring", the sandy successions that constitute most of Quaternary deposits on this margin [Initial Reports, leg 174A, *Austin et al.*, 1998]. Similarly, attempts to core a sand ridge in the North Sea experienced major difficulties, with an overall recovery less than 16% [*Davis and Balson*, 1992]. The most comprehensive investigation of sandy clinoforms was conducted by a consortium of oil companies, which successfully drilled shelf-edge deltas of the Mississippi margin [*Winn et al.*, 1995]. However, the borehole described by these authors is located beyond the shelf edge, and the authors do not provide description of sedimentary facies associated to clinoforms.

In June-July 2004, a drilling operation was funded by the European Community in order to investigate the Adriatic and the Gulf of Lions deltaic margins (PROMESS 1).

Within the PROMESS 1 project, two sites were drilled in the Gulf of Lions: PRGL1 (300 m long), located at the interfluves of Bourcart and Herault canyons at a water depth of 298 m, and PRGL2 (100 m long), located at the seaward termination of the Last Glacial Maximum shoreline (103 m water depth) (Figure 1). In particular, PRGL2 drilled through sedimentary discontinuities related to submarine and/or subaerial erosion that can be tied to correlative conformities towards the slope. It is mainly studied for its seismic and sedimentary facies, physical and geotechnical properties. On the other hand, the site PRGL1, located at the interfluves Bourcart and Herault canyons, shows a long and continuous depositional sequence that have great potentiality for multy-proxy investigations (micropaleontology, paleomagnetism, palynology, geochemistry). It provides a continuous paleoclimatic record and chrono-stratigraphic framework that can be linked, through the correlation of seismic surfaces, to site PRGL2 [*Flores et al, 2005; Berné et al., this volume, Sierro et al, submitted*].

Interpretations of the prograding sediment wedges that were drilled during the cruise at site PRGL2 are here provided, since the drilling operations were successfully terminated with the satisfactory core recovery of 84%, despite the marked lithological variability and the presence of thick sandy intervals. The correspondence between sedimentary and seismic facies is here demonstrated, thanks to the newly acquired sedimentological data that permit to characterize in detail the seismic response to lithological changes. For intervals with no recovery, litologies may be predicted from Continuous Penetrating Tests [*Lafuerza et al. this volume*].

The major objectives of our study are to:
- the sedimentary facies and environments responsible for the clinoform seismic facies;
- shed lights on the sedimentary environments in which the clinostrafied bodies formed;
- understand how the different facies record the changing sea-level and how important surfaces can be recognized from subsurface and sedimentological data.

2. Regional setting

The Gulf of Lions is a passive, prograding and subsiding margin, located in the north-western sector of the Mediterranean Sea bounded, to the west and east, by Pyrenean and Alpine orogenic belts, respectively (see the synthesis by *Berné and Gorini* [2005]). It comprises a wide (about 70 km) shelf and a continental slope that is incised by numerous canyons descending down to the abyssal area of the Algero-Balearic Basin. Because of high sediment supply (mainly from the Alps through the Rhône River) and very limited tectonic activity, it is a favourable environment for studying the deposition and preservation of sequences controlled by glacio-eustatism.

During the last 500 ka, sea level has been oscillating between its present position and about 100 m below the present sea level. Because the shelf edge is located between 105 and 165 m water depth, a large portion of the continental shelf was exposed during glacial periods. As a result, the stratigraphic record displays major erosional surfaces deriving from subaerial and shallow marine erosion during sea-level falls, lowstands and sea-level rises.

The cyclically stacked Plio-Quaternary sequences have been object of seismic investigations over the last 30 years by several authors that proposed a number of conceptual and/or numerical stratigraphic models [*Monaco*, 1971; *Aloïsi* 1986; *Tesson et al.*, 1990, 2000; *Berné et al.* 1998, 2004; *Lofi et al.*, 2003; *Rabineau et al.*, 2006]. A review of these investigations is given by *Rabineau et al.* [2005]. Most of the middle and outer continental shelf consists of prograding wedges that display internal reflections showing alternating low angle (<1°) and high angle (>4°) clinoforms. Based on shallow cores and stratigraphic modelling, this elementary "motif" was

interpreted as the result of alternating deposition of high energy (sandy upper shorefaces) and low energy (muddy lower shorefaces or "offshore" deposits) during late Quaternary sea-level changes. The large (>100 km) lateral extent of these sand bodies attest for a global (sea-level) control on their deposition. However, there was controversy as to the nature of the prograding shorefaces; some authors interpreted them as the product of deposition during the falling stages of sea-level [*Aloïsi*, 1986; *Berné et al.*, 1998; *Rabineau et al.*, 2005] whereas other proposed that they could correspond to transgressive parasequences (in the sense of *Van Wagoner* [1990] formed during the early stages of sea-level rises [*Tesson et al.*, 2000]. Similarly, the timing of deposition was a matter of controversy, some authors considering that the main bounding surfaces separating each prograding unit corresponded to sequence boundaries linked to the 100 ky glacial/interglacial cycles [*Aloïsi*, 1986; *Rabineau*, 2001; *Lobo et al.*, 2005] whereas others considered that they were formed in response to higher-order (20ky) cyclicities [*Tesson et al.*, 1993; 2000].

3. Methods

The data were collected onboard SRV "Bavenit" of the Russian company "Amige", operated by Fugro. In order to evaluate sediment types to be cored, and for geotechnical characterisation, we first performed a continuous CPTU (Cone Penetrator Test Unified) at site PRGL2-1, distant a few m from the PRGL2-2 site where continuous coring was carried out. The test was made with a static penetrometer measuring:

1.   cone resistance (KPa);

2.   sleeve friction (KPa);

3.   pore pressure acting on the cone (KPa).

The CPTU equipment and the procedures adopted during the cruise operations are in accordance with the International Reference Test Procedure published by the Society of Soil Mechanisms and Geotechnical Engineering (ISSMGE, 1999). Estimation of sediment types based on geotechnical properties was done using the method of Soil Classification established after Ramsey (2002).

An important application of CPTU measurements is the determination of the stratigraphy and lithology of buried sediments. Thanks to the combination of three CPTU measurements (cone resistance, lateral friction, pore pressure, *Ramsey*, [2002], it is possible to define the soil type based on a soil classification chart (see details in *Lafuerza et al.*, this volume). It relies on a large CPTU database adapted and improved by different authors to diagrams of soil classification [*Robertson*, 1990; *Ramsey*, 2002].

All geotechnical data were combined for soil characterization, considering that the pore pressure (u_2) is mainly related to the permeability of sediments, whereas the resistance to cone penetration (qt) and the lateral friction (fs) can be directly correlated to a particular lithology.

Core sections, from 0.80 to 1.5 m in length, were recovered using a suite of FUGRO corers, including a piston corer, a "WIP" corer and a FUGRO corer. Overall, about 50% of the drilled section consisted of sand, making core recovery difficult. However, within very sandy intervals, the strategy consisted to core down to the maximum of penetration, then, when core recovery was less than 50 cm, to drill only 50 cm in order to minimize the gaps. This time-consuming operation allowed overall recovery of 84%.

Physical properties of collected cores were measured onboard using a GEOTEK Multi-Sensor Core Logger (MSCL), by means of:

1.   gamma-ray density;

2.   P-wave velocity;

3.   magnetic susceptibility

Magnetic susceptibility was measured a second time in the laboratory on split cores. To link lithological, seismic and geotechnical data, a time-depth conversion was constructed using P-wave velocities from MSCL. From this calculation, all logs were converted into a time scale (ms, Two Way Travel Time). In addition, velocities of fine-grained intervals were measured using a pair of transducers oriented along the core axis. The very good match between major lithological changes and boundaries of seismic units demonstrates the validity of the method.

All cores were visually described, and X-ray images were realized for the most significant sections with the SCOPIX system [*Migeon et al.,* 1999]. The X-ray radiography was particularly useful for enhancing subtle sedimentary structures not easily identified on freshly-cut core surfaces.

Measurements of carbonate content (Bernard calcimeter, precision ±2%) and grain size analyses with a laser microgranulometer (Coulter counter LS130; size range 0.4 μm to 1 mm) were made on the total sediment fraction on samples collected every 20 cm (to the exception of gravel beds).

In order to establish a biostratigraphic control, the cores were analysed onboard for calcareous nannoplancton [*Colmenero and Gravalosa,* personal communication], additional samples being analysed after core splitting in the laboratory.

The chronostratigraphy of the youngest sequence is based on AMS ^{14}C dating of biogenic carbonates (mainly foraminifera). In addition, attempts were made on few samples to date total

organic carbon or wood fragments. Approximately 10 mg of biogenic carbonates were handpicked under the binocular microscope and AMS ^{14}C dates were obtained by the Poznan Radiocarbon Laboratory of the Adam Mickiewicz University (Poland). All ages reported here are given in calibrated ages, using the Cal v5.1 version [*Hugens et al.* 2004] or the polynomial in *Bard et al.*, 1998. The ages reported herein are δ^{13}C-normalised conventional ^{14}C years. For ages between 0 and 21,880, ^{14}C BP calendar (i.e. calibrated) ages were calculated using the Calib 5.0.2 sofware [*Stuiver and Reimer*, 1993] with the Marine04 calibration curve [*Hughen et al.*, 2004], no deviation from the mean global reservoir correction (-408 yr). For ages beyond 21,880 a ^{14}C BP, the Glacial Polynomial [*Bard et al.*, 1998] was used. Calendar ages are given with 1 sigma standard error.

Beyond the radiocarbon dating resolution, chronostratigraphy was obtained by estimations on the abundance of the biostratigraphically significant coccolith taxa, following the criteria of *Raffi and Flores (1995)*. These estimates have to be utilized with cautioun considering the general scarcity of coccoliths in the observed samples.

Finally, the macrofauna fauna (molluscs) was sorted and analysed for generating additional information on the environments and, possibly, on the paleo-bathymetry.

In addition to core data, spectral gamma ray measurements were performed in situ by means of wireline logging. Total gamma counts and Potassium (^{40}K), Thorium (^{232}Th) and Uranium (^{238}U) fractions were recorded. Because open hole logging deemed to be too risky in such unconsolidated marine sediments, logging took place from within the drill string and bottom hole assembly (BHA). While this ensured a safe operation, gamma counts were severely diminished by the surrounding steel. From the BHA design, steel thicknesses were established and data corrected for using the ENCOR algorithm as developed by *Hendriks (2003)*. From total gamma counts, sand content was estimated using $V_{sand} = 1 - (GR-GR_{min})/(GR_{max}-GR_{min})$ with $GR_{min} = 40$ gAPI and $GR_{max} = 90$ gAPI.

4. Results

4.1. Seismic sequences, seismic facies and their lithostratigraphic correlation

The overall seismic stratigraphic organization of the shelf/upper slope is presented by Berné et al., (this volume) and summarized in Figure 2. Prograding wedges, attributed to forced-regressive systems tracts [*Hunt and Tucker*, 1992] formed in response to 100 ky glacio-eustatic cycles, thicken seaward. These wedges are bounded by erosion surfaces that become correlative

conformities on the upper continental slope, where they have been precisely dated (*ibid*). These seismic surfaces are called ***major seismic surfaces***, meaning that they are traceable throughout the Gulf of Lions and that they correspond to fourth order glacio-eustatic cycles [*Rabineau et al.*, 2005]. They bound major seismic units. ***Second-order seismic surfaces*** have not been correlated at the regional scale, but they present, within major seismic units, erosional geometries, or distinct changes in clinoform geometries. They have been correlated to distinct and well-dated climatic/sea-level events thanks to long piston cores [*Jouet et al.*, 2006] or to the Promess 1 drill sites (Jouet et al., submitted, Berné et al., this volume).

In the vicinity of PRGL2, seismic facies seen on multi-channel and sparker profiles (Figure 3) are characterized by various clinoform geometries, bounded by a hierarchy of bounding surfaces (in the sense of *Brookfield*, 1997). From the top to the bottom of the borehole, 6 major seismic units are identified. :

-   **Unit U150** is characterized by steep (up to 5°) clinoforms pinching out seaward and forming a ~48 ms (42 m) thick wedge interpreted as forced regressive and lowstand shoreface (Jouet et al., 2006). The top of this seismic unit is, at the resolution of sparker data (Figure 3B), an erosion surface that truncates the clinoforms (the topsets of these clinoforms are not preserved). Cemented sands (C.S. in Figure 3), interpreted as beach rocks by *Berné et al.* [1998]; *Jouet et al.* [2006] are visible 1 km south of the drill site (Figure 3). Within U150, several 2nd order bounding surfaces are identified. D63 is an erosion surface that bounds relatively low-angle clinoforms (landward) from higher-angle clinoforms (seaward). It was dated between 41 and 38 cal ka BP and was attributed to a drop of sea-level during the overall sea-level fall between Marine Isotope Stage (MIS) 3 and MIS 2 [*Jouet et al.*, 2006]. D64 and D65 display more subtle changes, but they are traceable in a strike direction over 15 km. They are clinoforms similar to the high-angle clinoforms previously described, but their bottomsets have a distinct high-amplitude signature and they can be traced down to the position of PRGL1, more than 25 km seaward. These bottomsets form a downlap surface for high-angle clinoforms deposited subsequently (Figure 3), suggesting that accommodation space was created by regressive marine erosion. These second-order bounding surfaces allow to identify, within U150, 4 seismic sub-units, labelled U147, U151a, U151b, U152 (Figure 3). In addition, a sub-horizontal second-order bounding surface truncates the upper part of the clinoforms of U150. It is sometimes difficult to distinguish it from the sea-floor on seismic profiles, but shallow cores and ultra-high resolution seismic profiles have shown that it is a *ravinement* surface linked to the last deglacial sea-level rise [*Bassetti et al.*, 2006]. Locally, this surface underlies transgressive sand bodies of unit U155 (Figure 3).

- **Unit U129** is a seaward-thickening wedge made of very low-angle clinoforms (high-amplitude, parallel reflections). Its upper termination (D55) is an erosion surface (D55) that becomes seaward a correlative conformity.

- **Unit U100** consists of wavy structures, that could be interpreted either as submarine retrogressive slides or sediment waves (see the review by *Lee et al.*[2002]. These structures are asymmetrical with a steep side facing upslope, suggesting landward migration if they are sediment waves. Their internal structure is characterized by alternating high- and low-amplitude reflectors suggesting changes in the lithology of sediments.

- **Unit U80** displays seismic facies similar to that of U150, with clinoforms dipping at angles up to 5°. The topsets are better preserved and their sigmoid shape is clearly visible (Figure 3).

Below these prisms, 2 major erosional, bounding surfaces are observed at the position of PRGL2-2 (D45, D40, D35 and D30). D45-40-35 corresponds to 3 amalgamated erosion surfaces that separate seaward (Figure 2). Hereafter, it will be named D45. Between these erosion surfaces, **Unit U57** is a <5 m-thick seismic unit, difficult to correlate laterally. It displays very-high amplitude, sub-horizontal reflections.. The bottom of the borehole reached seismic **Unit U40**, that corresponds to the infill of an axial incision (in the sense of *Baztan et al.* [2005]) that cuts across a major buried canyon connected to the present Bourcart Canyon.

At the core scale, 14 sedimentary units were identified on the basis of their sedimentological facies (Table 1). They are bounded by 5 coarse-grained intervals whose positions perfectly correspond to the 5 major bounding surfaces previously described on seismic profiles (Figure 4).

1) U151-U152 (sedimentary units 1-2-3)

The sedimentary facies that are equivalent to seismic units U151 and U152 show clear, and quite sharp lithological changes that correspond to foreset-bottomset transition. From top to the bottom, they consist of:

(a) **Sedimentary unit 1** (0 to 28.75 mbsf) is topped by a coarse to medium sand interval, 1.90 m thick, with shell debris. Below this coarse lag, it displays fine to medium-grained sand, well sorted and homogeneous with scattered rounded pebbles. They are characterized by planar lamination, tabular cross-bedding and minor wavy laminations. Occasionally, thin (1-2 cm) mud interbeds are observed, especially within the lower part of this interval (Plate 1, sections 8A, 10A, 14A, Plate 3, *[1]*). It is worthy to remark that sands, which appear structureless to the naked-eye inspection, reveal detailed sedimentary structures or bioturbation (Plate 1, sections 8A and 10A) in the X-ray radiographs (Plates 1 and 2). Swaley cross-stratification [*Leckie and Walker, 1982*]

or HCS (*Harms et al.* [1975]) can be inferred at levels (very gently dipping laminations truncated by more inclined erosion surfaces, Plate 1, section 14A) but these large-scale sedimentary structures are not easy to recognize at core scale. The bottom of the sedimentary unit corresponds to 80 cm-thick, highly bioturbated interval of silty clay. This sedimentary unit, which displays an overall coarsening-upward pattern, corresponds to seismic unit U152.

(b) Sedimentary unit 2 (28.75 to 41.51 mbsf) consists of mud-sand alternations with mm-thick sandy beds, laminated and intensively burrowed, separated by 1 to 10 cm-thick muddy beds (Plate 3, [*2-3-4*]). Some fining-upward/graded beds probably resulting from waning flows can be found, but bioturbation partly homogenized the sediments (Plate 1, sections 35, 39). The bottom of unit 2 is marked by a very distinct transition toward massive silty clay with sparse bioturbation and organic matter below ~39 mbsf. In detail, this unit can be divided into 4 coarsening-upward sub-units. Each sub-unit displays clay or silty clay at the bottom and fine to very fine sand beds alternating with mud at the top (with progressive increase of the abundance and thickness of sandy beds toward the top) (Figure 5A, Plate 1, section 35, 39, 40, Plate 3, [*3-4-5*]) These coarsening upward sub-units are respectively situated between:

- 28.74 and 29.49 mbsf,
- 29.49 and 33.90 mbsf,
- 33.90 and 40.32 mbsf,
- 40.32 and 41.40mbsf.

(c) Sedimentary unit 3, (41.51 to 42.32 mbsf) is made of very coarse-grained material, mainly composed of shell fragments. In detail, 2 coarse-grained intervals with an erosional base can be distinguished, separated by about 15 cm of marine clay (Figure 5B).

2) U129 (sedimentary units 4)

Sedimentary unit 4 (from 42.30 to 45.41 mbsf) consists of alternating beds made of fine sand and bioturbated clay or silty clay, with rare primary laminations (Plate 1, section 47).

3) U100 (sedimentary units 5-6)

Recovery was excellent for this interval, and the hole crossed mainly the upstream flank of the sediment waves.

The upper limit is an erosional surface with pebbles up to 2 cm in diameter. Below this surface, fine-grained sediments are observed in (a) **sedimentary unit 5**, (45.41-63.60 mbsf), with highly bioturbated silty clay (Plate 3, *[6]*) and rare 1 mm to several cm thick silt/fine sand beds (up to

about 10 cm, Plate 1 section 61). The boundary between sedimentary unit 4 and 5, which marks a shallowing (in an upward direction) of sedimentary environments, corresponds to seismic surface D55.

(b) **Sedimentary unit 6** (63.60-66.80 mbsf) is characterized by 2 coarse-grained intervals about 50 cm-thick each, separated by bioturbated fine-grained interval, parallel laminations preserved in the sandy beds. These beds have sharp (erosional?) basal contacts and are, locally, gradational. Organic matter and shell debris are scattered within the sediments. The coarse-grained intervals have extremely abundant biogenic material in a muddy sand matrix (Plate 3, [7]). The bioclastic gravel contains the rest of different mollusc species and sometimes the shells are pretty well preserved. It has an erosional contact with the underlying deposits. This unit is very similar to sedimentary unit 3 and it corresponds to seismic surface D50.

4) U80 (sedimentary units 7-8-9)

Between 66.8 and 84.40 mbsf, 3 sedimentary units equivalent to sedimentary units 1 to 3 are present.

(a) **Sedimentary unit 7** (66.70 to 77.80 mbsf) consists of well-sorted fine to very fine sand with planar and cross-bedding. Recovery was difficult within this massive sand interval.

(b) **Sedimentary unit 8** (from 77.80 to 81.40 mbsf) consists of mud-sand alternations with intense bioturbation and occasional horizontal laminations in (mm to 5 cm-thick) sand beds (Plate 2, sections 88, 90). Normal grading and erosional bases in sandy beds are also observed (Plate 2, sections 90, 91, Plate 3, [8]). The lowest part (about 1 m) of (c) **Sedimentary unit 9** (81.90 to 84.4 mbsf) was not recovered due to very coarse-grained material found in core shoes (medium sand with aboundant shell debris, Plate 3, [9]). The recovered interval is composed at the base of a 50 cm-thick interval of medium to coarse sand rich in shell fragments and well-preserved shells, topped by a coarsening-upward 1.40 m-thick interval of fine-grained muddy sand with sparse shell fragments becoming rich in shell fragments at the top. This unit corresponds to seismic surface D45-40-35.

5) Units 57 and 40 (sedimentary units 10-11-12-13-14)

The lowest part of the borehole corresponds, on seismic profiles, to an interval where bounding surfaces linked to various glacio-eustatic cycles are almost amalgamated. Very coarse intervals were encountered and made recovery difficult. However, from the recovered material and indirect information from geotechnical measurements, 4 sedimentary units can be described.

(a) **Sedimentary unit 10** (84.40 to 88.28 mbsf) is made of dark grey clayey silt with very stiff intervals of homogeneous very fined-grained sand badly recovered.

(b) **Sedimentary 11** (from 88.28 to 92.37 mbsf) corresponds to sandy/gravel deposits where sedimentary structures are difficult to characterize because of limited recovery. The bottom of this unit is a distinct erosional surface. Above the erosion surface, a heterogeneous, fining-upward interval of rounded gravels and shell fragments in a muddy sand matrix is observed. The upper part of this level is showed in Plate 2, section 103, where coarse-grained beds alternate with sand. Only core shoes are available for interval 89.6 to 92.00 mbsf; they consist of coarse sand with large shell debris.

(c) **Sedimentary unit 12** (92.37 to 94.15 mbsf) is made of medium to coarse-grained muddy sand with pebbles and shell fragments. Pebbles up to 2 cm in diameter are found incrusted by serpulids.

(d) **Sedimentary unit 13** (94.15 to 99.24 mbsf) is an interval consisting of silty clay interbedded with graded sand beds (Figure 5C, Plate 2, section 111), few mm to 10 cm thick. In details, it consists of fining upward sub-units with a very coarse base containing abundant bioclasts (including *Turritella*), mud clasts and a top with intensively bioturbated fine sands. Horizontal and cross-bedding are observed in sand beds (see Plate 2, section 113 at about 97 mbsf). Just below it a crudely graded interval starting with 5 cm of coarse material (worm tubes, shell debris ans silty sand) passing to poorly sorted sand with shell debris is showed at 97.41 mbsf (Plate 2, section 113).

(e) **Sedimentary unit 14** (99.24 to 100.13 mbsf) is very coarse, with large rounded clasts and shell fragments in a muddy sand matrix (Plate 2, section 114, Plate 1, [10]). The bottom of the unit is made of rounded pebbles up to 3 cm in diameter (Figure 5C, Plate 3, [10]).

4.2. Comparison of geotechnical and lithological data

The sand or sand-dominant intervals (0-30 mbsf; 67-78 mbsf; 82-97 mbsf) are characterized by relatively high values of qt (up to 60^3 kPa) and fs (up to 800 kPa) (Figure 6). In contrast, fine-grained intervals (29-63 mbsf, 78-82 mbsf) display low values of qt and fs. Overall, the soil-type diagram (Figure 6) evidences with high precision the correspondence between geotechnical and lithological characteristics of soils (as discussed in *Lafuerza et al.*, this volume), as relatively homogeneous intervals and alternances can be distinguished (see sedimentary units 1, 7, 11 in Figure 6), if we exclude the very coarse-grained sands or gravels, that exceed the maximum resistance detected by the penetrometer ($> 10^5$ kPa). With this exception, we may use

geotechnical data to interpolate with good confidence the lithological information for non-recovered intervals.

4.3. Grain size, carbonate content and radiography

Downhole grain-size profile (Figure 7) shows that the main feature in the PRGL2-2 is the change from sediments composed largely of silt-clay alternations (bottomsets of seismic clinoforms of U152, U151, sediment waves) to sediments consisting primarily of sand (foresets of seismic clinoforms of U152 and U80). In fact, the foresets of U152 and U80 (0-20 mbsf and 68-78 mbsf, respectively) are made of >90% of well sorted sands. By extrapolation to the thickest (non-cored) part of seismic unit U80, situated immediately landward of PRGL2, one could expect as much as 30 m of massive sand within this unit.

The carbonate content displays anti-correlation with sand composition, with a percentage of 20% or less in sandy intervals and a slightly higher $CaCO_3$ component (between 25 and 35%) in the fine-grained interval (20-66 mbsf). The carbonate of the foresets mainly derives from biogenic production of phythal biota of the middle shelf (ostracods and benthic foraminifera). The contribution from *in situ* skeletal biota is less important in the sand-silt alternation (bottomsets). One exception to this anti-correlation comes from the coarsest parts of units 3, 6, 9 and 13, as well as the top of unit 1, where abundant shells and shell fragments are accumulated.

4.4. Chronostratigraphy and faunal content

1) ^{14}C dates

Radiocarbon dating has been carried out for the first 42 m of the borehole that fall within the radiocarbon dating resolution (Table 2).

We obtained good results for the top of the borehole (U155) and for the fine-grained interval of seismic U151 (Figure 8), whereas significant age inversions affect the sandy interval of U152 (Figure 8). Within the ^{14}C ages that are clearly distorted because of reworked material, we can nonetheless discern certain logic: from the top to the bottom, the measured ages show a gradual transition from older (about 36,000 cal yr BP) to younger (26,000 cal yr BP) sediments. Thus, rather than discarding them, we can use these data for discussing the nature of erosion during falling sea-levels and eventually, the origin of sediments deposits during forced regression (see Discussion).

The age of U155 (about 15,000 cal yr BP) is consistent with the transgressive origin of the sand ridges that cannibalized the top of shoreface deposits [*Berné et al.*, 1998; *Bassetti et al.*, 2006]. Below the ravinement surface linked to the last deglacial sea-level rise (D70 in Figure 3), U152

corresponds to regressive deposits whose deposition ended around 20 ky cal BP [*Jouet et al.*, 2006]. If we consider that the bottom of U151 has an age of ca. 31 cal ky bP, it implies that the shoreface sediments drilled by PRGL2-2 (about 42 m thick) were deposited within ca. 11 ky. This time span encompasses, in particular, two climatic cold events, Heinrich Event (HE) 2 and HE 3 [*Heinrich*, 1988]. These events, occured around 25,000 and 29.000 cal y BP, respectively [*Hemming*, 2004], i.e. at about 35 and 40 mbsf along the borehole. During the same interval, there is growing evidence that global sea-level experienced rapid changes with magnitude up to 30 m (see below).

2) Coccoliths

Coccolithophore assemblages observed in the studied samples of PRGL2-2 are dominated by Noelaerhabdaceae. The abundance of the different species of this group varies along the hole. Taxa such as *Helicosphaera carteri* and *Syracosphaera* spp. have been observed in some samples although they do not show a continuous record. This fact is probably due to the general scarcity of coccoliths in some horizons.

Reworked nannofossils is a common feature of all studied samples and they are even present in the samples almost barren of coccoliths. The age of basal sediments remains undetermined because of poor preservation of nannoplancton in sedimentary units 7 to 14, however, significant events are identified in the upper layers that allow a correlation with the SPECMAP curve (Figure 8):

First Occurrence of *Emiliania huxleyi*: *E. huxleyi* is identified at 60.56 mbsf. The age of this event was established by *Thierstein et al.* [1977] at 268 ky (top of MIS- 8). It has to be taken into account that this First Occurrence horizon (lower limit of the present-day Nannofossil Zone NN21 of *Martini* [1971] could have been influenced by the low coccolithophore abundances in the samples.

Age of the top of the hole: The coccolithophore assemblage compositions and the high abundances present in the uppermost interval indicate that this horizon is younger than the Last Glacial period (scarcity of *E. huxleyi* >4 μm).

Other events: The preliminary sampling resolution and the low abundance of coccoliths in most samples do not allow giving an accurate depth for the other events as in other holes (PRGL1-4, *Sierro et al, submitted*). However, the following horizons can be approximated (Figure 3):

-Reversal in *Gephyrocapsa caribbeanica/Gephyrocapsa oceanica* - small *Gephyrocapsa*: *G. caribbeanica* and *G. oceanica* decrease their abundances and small *Gephyrocapsa* becomes the dominant group in the coccolithophore assemblage at about 62.93 mbsf (bottom of section 69).

This event has been dated by *Villanueva et al.* [2002] and *Flores et al.* [2003] between 260 and 245 ky (top of MIS 8).

-Reversal in small *Gephyrocapsa–Gephyrocapsa muellerae*: This last species increases around 43.73 mbsf (bottom of section 45). This probably approximates the event occurring during the middle of MIS 6 (between 160-170 ky, as idenfied by *Villanueva et al.* [2002].

-Acme of *Emiliania huxleyi*/Reversal in *Gephyrocapsa muellerae - Emiliania huxleyi*: This last species increases its abundances at about 41.34 mbsf, indicating the approximate position of MIS 4.

3) Macrofauna

Macrofossils, mostly benthic molluscs are found at different levels of the sedimentary record in PRGL2 (Figure 9). The richest mollusc deposits are associated to the major discontinuities.

The fine-grained intervals are poorer in macrofossils and mainly contain benthic forams (rarely planktic), ostracods and debris of different origins (echinoid spines, ossicles, wood fibres, shell fragments) together with juvenile and little-size bivalves (*Abra alba, Parvicardium, Timoclea ovata...,* unidentified Cardidae , Gastropods).

Seismic units, but especially erosional unconformities, can be characterized by the faunal content as follow:

(a) seismic units U151 and U152 are characterized by a very poor faunal content. Rare worn fragments of bivalves are found together with partly reworked benthic foraminifera (mainly *Ammonia* and *Elphidium* foraminifera);

(b) D60 corresponds to an interval rich in molluscs but with low-diversity faunal assemblage: *Abra* sp., *Corbula* sp. and *Turritella communis* indicate shore to sublittoral deposits, characterized by significant clay supply;

(c) relatively high-diversity high-abundance assemblages are identified in correspondence of D50: species pertain to bivalves (*Myrtea spinifera, Nucula sp., Nuculana commutate*), scaphopods (*Dentalium*), gastropods (*Turritella communis*), serpulids plychaetes (*Ditrupa arietina*). The association *Ditrupa arietina- Turritella communis* is considered characteristic of prodeltaic conditions, i.e. very dynamic coastal environments subject to rapid sedimentary fluxes, flood deposits, etc.;

(d) very diverse macrofossil assemblages indicating relatively starved subtidal (open) shelf conditions are observed in correspondence of D45 and D30 where *D. arietina* and *T. communis* is associated with the solitary coral *Caryophyllia* and a number of bivalves e.g.Veneridae species, *Dosinia lupinus, Nuculana commutata, Parvicardium* sp, *Mytilus* sp., etc.

(e) the bottom part of the core is clearly characterized by an high degree of reworking: worn and chalky fragments, many encrusted by coralline algae testify that the deposits are sourced from sublittoral shelf environments, as suggested by the co-presence of *Crenella decussata* and *Obtusella macilenta.*

Another interesting finding is the presence of cold-water boreo-celtic guests, molluscs of eco-biostratigraphic and climatic significance such as *Modiolus modiolus, Arctica islandica,* cf. *Mya truncata/Panopea norvegica* which are known entering the Mediterranean during glacial periods (*Malatesta and Zarlenga* [1988]). They occur consistently in correspondence of major bounding surfaces. Lag deposits are at the origin of impedance reflections creating very-high amplitude contrasts on seismic profiles (major bounding surfaces).

5. Discussion

Integration of geophysical multi-proxy borehole data allows us to propose a synthetic interpretation of Quaternary depositional units and surfaces in the Gulf of Lions (Table 2). The remarkable correspondence between geotechnical properties and lithological data is here used for lithological prediction of non-recovered intervals. It gives reliable lithological prediction at the major facies transitions but the content of sand strongly influences the cone penetration only when the sand layers are > 3 cm thick. Therefore, integration with sedimentological data and fossil content is necessary to define sequence boundaries. These boundaries observed on seismic data correspond to erosion surfaces overlain by muddy gravel or coarse sand, mixed with abundant biogenic material (shell fragments).

5.1. Nature and origin of major erosion surfaces

A striking feature along PRGL2-2 is the perfect match between major seismic reflections (including the sea-floor) and very coarse intervals with shells and shell debris. The mollusc assemblages refer to diverse environments, from open shelf to sub-littoral, traducing an intense reworking. Cold-water Pleistocene species are found within D60, D50, D45 and D30. They have also been described within D70 on shallow cores [*Bassetti et al.,* 2006]. However, these cold species are generally mixed with temperate species. All the borehole data confirm previous seismic and sequence stratigraphic interpretations (see summaries *in Berné et al.* [2004]; *Rabineau et al.* [2005]. Major seismic discontinuities (D30 to D70) are polygenic erosion surfaces that first formed as sequence boundaries at the top of prograding wedges during sea-level falls driven by 100ky glacio-eustatic cycles, subsequently reworked by marine ravinement during sea-level rises. Transgressive deposits being very thin or absent on the outer shelf, except

at the position of sand ridges (U155 in Figure 11) they eventually become surfaces of condensation during highstands. This explains the important mixture of glacial and "warm" fauna living at different water depths. If we look in details at sediments corresponding to seismic surfaces D60, D50 and D45, we can note that they correspond in fact to 2 coarse-grained intervals, separated by 10 to 1 m cm of very fine sand or silty clay material. These fine-grained intervals might correspond to transgressive deposits separating a *ravinement* surface (at the base) and a condensed interval (at the top), as described for D70 by *Bassetti et al.* [2006]. The limited thickness (<1m) of these transgressive deposits does not allow distinction surfaces on seismic profiles.

As to the basal coarse-grained interval (sedimentary unit 13) which corresponds to seismic surface D30, it displays material such as rounded pebbles encrusted by coralline algae. This suggests the vicinity of a river and of possible sediment starvation within the photic zone. On seismic profiles, these deposits correspond to the infill of an axial incision within the Bourcart canyon. This is the first sedimentological evidence of connection between a river and an axial incision in the Gulf of Lions, supporting the scenario proposed by *Baztan et al.* [2005].

5.2. Nature and significance of prograding bodies

1) Synthesis of sedimentological and biostratigraphic information on U151/U152

The sedimentary facies association that we observe within U151/U152 represents a typical coarsening upwards trend that can be observed on wave-dominated shelves [*Walker and Plint*, 1992], with the vertical superposition of 3 main different facies (from top to bottom):

(a) planar to very low-angle stratified sand and possibly swaley cross-stratification (Figure 7, sedimentary unit 1, section 8A), indicative of efficient wave reworking. This interval lies above an intensely bioturbated sand (Plate 1, sedimentary unit 1, section 10A);

(b) cross stratified, well-sorted fine sands and possible hummocky cross-stratifications, with parallel internal laminations (Plate 1, sedimentary unit 1, section 14A). The HCS unit represents deposition above storm wave base, but probably not far from this wave base [*Dumas and Arnott*, 2006];

(c) bioturbated mud with interbedded thin sand beds (Plate 1, sedimentary unit 2, sections 35 and 39). Storm-generated event beds, intensively bioturbated with sharp erosional base, corresponding to moderate-energy storm-dominated shelf zone with fair weather mud drapes [*Aigner and Reineck*, 1982]

The relative position of these facies strongly supports the interpretation of U151/U152 as a complex formed at the foreshore-shoreface transition (sedimentary unit 1) characterized by a high-energy (coastal) dominated setting marked essentially by (a) massive, well-sorted fine to medium sand with low carbonate content; (b) horizontal lamination and possible swaley cross stratification, indicative of efficient winnowing by wave action; (c) possible hummocky cross-stratification indicative of a storm-dominated lower shoreface environment.

Short-lived, episodic storm beds are preferably recorded in the "offshore" facies (bottomsets, sedimentary unit 2) as testified by the highly heterolithic character of deposits, mainly consisting of fine-grained beds alternating with repeated, distally deposited, storm beds. Bioturbation of the finer section (silty clay) indicates prolonged intervals of calm conditions between the deposition of tempestites.

2) Integration of sedimentological and seismic data

The upper 20 m massive sands of sedimentary unit 1 correspond to the steep (up to 5°) foresets of seismic unit U152. They pass progressively to sands with thin muddy interbeds between 20 and 30 mbsf where clinoforms are dipping more gently. The abrupt deepening of sedimentary facies below 30 mbsf corresponds to seimic surface D65. The alternating bioturbated sands and muds observed below this surface (sedimentary unit 2) correspond to the bottomsets of clinoforms of unit U151. Despite the dominant sandy lithology of clinoforms, the impedance contrast at the origin of reflectors on seismic profiles (foresets of U152) is certainly due to the presence of cm-thick clayey levels, or packets of such levels.

Sedimentary structures and paleo-environmental indications given by fauna and micro-fauna confirm earlier interpretations, based on seismic stratal architectures (*Aloïsi* [1986] and subsequent workers): U151 and U152 represent wave-dominated shorefaces deposited during an overall sea-level fall at the end of the last glacial cycle. The age of the bottomsets confirm, in particular, that U151/U152 did not form during a short-lived stillstand during an overall transgression [*Tesson et al.*, 2000] but before Last Glacial Maximum.

The shoreface deposits observed here are, however, significantly different from typical shoreface deposits observed in modern (highstand) settings, which commonly show much lower dip angle of clinoforms (0.3° on average, *Walker and Plint, 1992*). On the other hand, examples of clinoforms with steep dip angles are reported in the stratigraphic record in forced regressive shelf-margins [*Hart and Long, 1996; Surlyk and Noe-Nygaard, 2005; Massari et al. 1999, Hanken et al., 1996*]. On Quaternary margins, there are also worldwide examples of sandy (or

supposedly sandy) shelf or shelf-edge shoreface or deltaic clinoforms with angles of dip similar to that of the Gulf of Lions' shorefaces (*Suter and Berryhill*, [1985]; *Trincardi and Field*, [1991]; *Sydow et al.* [1992]; *Hernandez-Molina* [1994], *Chiocci and Orlando* [1996] *Winn et al.* [1998], *Trincardi and Correggiari* [2000], *Hiscott* [2001], *Anderson et al.* [2004] and others). Possibly, the difference in slope angles between present-day shorefaces and Pleistocene/Ancient examples would be due to the fact that the latest record phases of active progradation with abundant sand supply, whereas modern examples correspond to equilibrium profiles of sand-starved shorelines.

The thickness of the Gulf of Lions' shoreface deposits is also quite different from values reported from modern examples. It reaches up to 30 m for U152 (including 20 m of massive sands), and even 40 m for U80 (where the sand thickeness is estimated to more than 30 m with comparison to U152. These values have to be compared to the thickness of Holocene shorefaces, that are in the range of 10-20 m [*Hampson and Storms*, 2003]. An explanation for this difference is that modern shorefaces prograde over inner shelves where accommodation is limited because of their low gradient, whereas the shorefaces studied here developed at the shelf edge. In addition, it can be observed that the steep clinoforms of U151/152 and U80, as well as over prograding units of the Gulf of Lions, developed immediately seaward of a step of the underlying surface (Figure 2). Probably this step provided more accommodation for shoreface deposition, as proposed by *Trincardi and Field*, [1991] for Thyrrhenian Sea shorefaces, or as observed at the outcrop scale by *Massari et al.* [1999].

Besides this morphological control, *Hampson and Storms* [2003] proposed that the main driving processes at the origin of the architecture of modern and ancient shorefaces are different. According to these authors, modern shorefaces represent a much shorter time-span, and therefore are manly controlled by wave climate and/or sediment supply. In contrast, the shape of shorefaces from the geological record would be the product of shoreline trajectory (*Helland-Hansen and Martinsen*, [1996]) during changing relative sea-level rise. This could account both for the larger thickness of ancient shorefaces and for differences in clinoform dipping angles. Thanks to the available chrono-stratigraphic framework, we will explore this hypothesis.

5.3. Regressive parasequences linked to rapid climate changes

Units 151 and 152 were deposited during the overall sea-level fall that took place between the highest sea-level of Marine Isotope Stage (MIS) 3 (around 50 ky BP) and the lowest sea-level of MIS 2 (Last Glacial Maximum), around 22 ky BP. Even if the position of global sea-level during MIS 3 is still debated (ranging from -35 m to -95 m, see compilation of sea-level curves in *Jouet*

et al., [2006]), the MIS3-MIS2 interval is a period of overall cooling and lowering of sea-level, punctuated by rapid climate changes generally referred to as Dansgaard Oeschger (D/O) cycles [*Dansgaard et al.*, 1993; *Bond et al.*, 2003], with Heinrich Events (HE, *Heinrich* [1988]) occurring at the end of some of the coldest stadials.

In the lithological succession corresponding to U152/U151, we observed coarsening upward units and sub-units (indicative of a general regressive pattern) separated by fine-grained flooding surface. In particular, such flooding surfaces are observed at about 29 mbsf and 40 mbsf. They correspond to seismic reflections D64 and D65, and they are marked by relatively abrupt deepening of sedimentary facies marked in Figure 10.

If we consider the chrono-stratigraphic constraints obtained from shallow cores retrieved landward and seaward of PRGL2 [*Jouet et al.*, 2006], as well as the numerous ^{14}C dates obtained within U151/152 at PRGL2, we find that:

- D65 formed between 24.131 and 22.700 cal y BP (from *Jouet et al.*[2006]) a time frame consistent with an age <25.007 cal y BP found at 33.75mbsf on PRGL2-2, about 4 m below the position of D65 (considering an average sedimentation rate of 1m/ky),

- D64 formed between 30.409 and 27.751 cal y BP (if we assign a depth of about 40 mbsf for D64 at the position of the borehole).

Finally, the ages of both surfaces fall within the time-intervals assigned to HE 2 and HE 3 (respectively ~ 25 and 30 ky cal BP, *Hemming* [2004]). They also correspond to the end of marked periods of sea-level falls (in the order of 10 m) observed in the Red Sea [*Siddall et al.*, 2003; *Arz et al.*, 2007].

On seismic profiles, a very pronounced downward shift surface corresponds to seismic surface D63, that marks a very distinct erosional boundary between bottomsets of U147 and steep (probably sandy) clinoforms of U151 (Figure 10). At the resolution of seismic data, this surface is merged with the main sequence boundary (D60), however, we noticed within sedimentary unit 3 the presence of a distinct fine-grained interval separating 2 very coarse intervals interpreted as *ravinement* surfaces. This interval has not been dated on PRGL2-2. However, it was dated previously on a piston core at ~ 41 cal ky BP [*Jouet et al.*, 2006], whereas an age of ~ 38 cal ky BP is found at the deep borehole PRGL1. (*Jouet et al.*, submitted, *Berné et al.*, this volume). The importance of the erosion linked to D63, as it is seen on seismic profiles, can be explained by a much higher magnitude of sea-level drop between 43 and 40 ky cal BP (about 30 m according to *Arz et al.* [2007]). According to these authors, the magnitude of the ensuing sea-level rise was in

the same order (Figure 10), within only ~2,000 y (about 1.5 cm/yr), i.e. a rate in the same range as that of melt water pulses during the deglacial.

Finally, we can recognize, within the prograding shoreface deposits linked to the overall sea-level fall between MIS 3 and MIS 2, a sedimentary *motif* linked to higher-order incremental sea-level falls and subsequent rises (Figure 10) that erode the upper and seaward terminations of previous deposits and initiate a new phase of forced regression deposition, separated by minor transgressions that are all preserved in the sedimentary record. These 2nd order bounding surfaces, created by these pulsations are genetically similar to the major bounding surfaces, in the sense that they represent surfaces linked to a fall and rise of sea-level, but their lithologic expression is different from that of major bounding surfaces (D60, D50, D45, D30) because the magnitude sea-level changes and duration of processes at their origin are shorter. The scenario also allows us to explain the age inversion observed within the ^{14}C data from U152 In a context of general sea-level fall, the uppermost clinoform samples are sourced from deposits reworked from the entire emerged shelf (and therefore older on an average). On the other hand the deeper borehole (PRGL1-4) that has a more distal (i.e. younger) source, since the shelf was still partly submerged at that time.

Our scenario of shoreface preservation in response to pulsed sea-level falls is quite similar to that proposed from the interpretation of ancient shoreface deposits. The concept was initially proposed by *Plint* [1988] and subsequently developed and applied to several ancient examples [*Walker and Plint*, 1992; *Hunt and Tucker*, 1992; *Posamentier and Allen*, 1993; *Mellere and Steel*, 2000]. A synthesis of the stratigraphic expression of such *"falling stage systems tracts"* is given by *Plint and Nummedal* [2000]. In the rock record, good examples of stepwise downstepping clinoform units separated by *ravinement* surfaces, very similar to our Gulf of Lions shoreface deposits, are given for instance by *Surlyk and Noe-Nygaard* [2005] from the lowermost Cretaceous of East Greenland. In modern (late Holocene) shoreface deposits, the effect of rapid, even if limited, sea-level falls (<1 m, in relation with tectonic uplift) is well documented by *Tamura et al.* [2007] who shows intra-shoreface erosion following such sea-level falls. Such surfaces are also reproduced by numerical experiments explaining that sea-level fall and/or increase of the wave-height can be at the origin of these surfaces [*Storms and Hampson*, 2005]. As well as the thickness of our shelf-edge shorefaces (compared to modern examples), it could be explained by more space available at the shelf edge, especially because the (generally fine-grained) underlying deposits did not undergo compaction during long-lasting emersion and are therefore more sensitive to marine erosion during sea-level falls.

6. Summary and conclusions

1. The prograding bodies in the Gulf of Lions are formed by massive sand with clinoforms dipping at 5° maximum that show a progressive transition to silt-silty clay alternation basinwards and form coarsening-upward sedimentary sequences with a sedimentological *motif* summarized in Figure 10;

2. Main clinostratified bodies are bounded by easily recognizable erosional surfaces that display a common pattern (coarse grained material, shell and shell hash with species indicative of various marine environments). Macrofauna (molluscs, corals) together with the lithological characteristics prove their polygenic origin (marine regressive ravinement, subaerial, marine transgressive ravinement and eventually condensation during highstands). Theses surfaces form the ***major bounding surfaces*** corresponding to 100-ky glacial-interglacial cycles;

3. Within the last glacial/interglacial sequence, cyclic changes of sedimentary environments and radiocarbon dates suggest that the clinostratified bodies are composed of several higher-order (para)sequences, bounded by flooding surfaces. These ***second order bounding surfaces*** are probably linked to rapid sea-level changes during the overall MIS3-MIS2 sea-level fall, as they are recorded on high-resolution sea-level records of the Red Sea [*Siddall et al., 2003*; *Arz et al.,* 2007];

4. Each parasequence (about 40 m thick, including about 20 m of massive sand) formed within about 5-10 ky, and progradation during this interval was in the range of 1-2 km. The sea-level drops at their origin are comprised between 10 and 30 m. These deposits represent good Pleistocene analogues to the numerous stepwise downstepping shorefaces described in the rock record.

5. The detection of river-derived material at the bottom of the borehole (units 14), delineates the direct influence of fluvial discharging events into the continental shelf. It constitutes the first evidence in this area of connection between a river and axial incision within a canyon.

Appendix A

Mollusc fauna components (PRGL2)

POLYPLACOPHORA
Leptochiton sp.

GASTROPODA
Acmaea unicolor
Acmaea sp.
Lepetella laterocompressa
Anatoma sp.
Calliostoma sp.
Gibbula magus
Gibbula sp.
Jujubinus sp.
Clelandella miliaris
Skeneidae sp.
Bittium sp.
Cerithidium submammillatum
Cerithidium sp.
Turritella communis
Turritella sp,
Rissoa sp.
Turboella sp.
Putilla sp.
Alvania cancellata
Alvania punctura
Alvania testae
Alvania sp.
Obtusella sp.
Rissoide sp.
Caecum trachea
Caecum sp.
Calyptraea chinensis
Capulus ungaricus
Euspira catena
Euspira sp.
Naticidae sp,
Epitonium sp.
Melanella sp.
Trophon muricatus
Trophon sp.
Buccinum undatum
Nassarius mutabils
Nassarius reticulates
Nassarius (Telasco) sp.
Nassarius sp.
Mitrella minor
Mitrella sp.
Bela brachystoma
Bela sp.

Raphitoma sp.
Teretia teres
Chrysallida, sp.
Eulimella sp.
Odostomia sp.
Pyramidellidae sp.
Actaeon tornatilis
Retusa truncatula
Retusa sp.
Ringicula auriculata
Cylichna cylindracea
Cylichna sp.
Diacria sp.
Creseis sp.
Limacina trochiformis
Limacina sp.
Substitute *Spiratella sp*

BIVALVIA
Nucula sulcata
Nucula, sp.
Nuculana commutata
Nuculana sp.,
Arca sp.
Anadara corbuloides
Bathyarca grenophia,
Bathyarca sp.
Striarca lactea
Mytilus edulis/galloprovincialis
Crenella cf. *prideauxi*
Modiolus modiolus
Musculus sp.
Mytilidae sp.
Pecten jacobaeus
Aequipecten opercularis
Aequipecten sp.
Hyalopecten similis
Chlamys glabra (=syn:
Proteopecten glaber)
Chlamys sp.
Pectinidae spp,
Anomia, ephippium
Anomia sp.
Limatula sp.
Neopycnodonte cochlear
Ostreidae sp.
Lucinella divaricata
Myrtea spinifera

Diplodonta apicalis
Lasaeidae sp.
Leptonidae sp.
Mysella dentata
Mysella sp.
Montacutidae sp.
Neoleptonidae sp.
Glans aculeata
Astarte sulcata
Acanthocardia deshayesii
Acanthocardia echinata
Acanthocardia sp.
Parvicardium minimum
Parvicardium sp,
Plagiocardium papillosum
Laevicardium oblungum
Spisula subtruncata,
Spisula sp.
Tellina sp.
Gari fervensis
Abra alba

Abra prismatica,
Abra sp.
Arctica islandica
Venus casina
Chamelea gallina
Timoclea ovata
Dosinia lupinus
Dosinia sp.
Pitar rudis
Veneridae sp.
Mya truncata
Corbula gibba
Hiatella artica
Hiatella sp.
Thracia sp.
Pandora sp.

SCAPHOPODA
Dentalium inaequicostatum,
Dentalium sp.
Pulsellum lofotense

Acknowledgements

References

Anderson, J.B., Rodriguez, A., Abdulah, K.C., Fillon, R.H., Banfield, L.A., McKeown, H.A.Wellner, J.S (2004). Late Quaternary Stratigraphic evolution of the northern Gulf of Mexico margin: a synthesis *in: Stratigraphic evolution of the northern Gulf of Mexico margin Late Quaternary* edited by J.B. Anderson and R.H. Fillon, *SEPM*, pp. 1-23, Tulsa.

Aigner, T., Reineck, H.-E. (1982). Proximality trends in modern storm sands from the Helegoland Bight (North Sea) and their implication for basin analysis. *Seckembergiana Marit., 14,* 183-215

Aloïsi, J.-C., (1986) Sur un modèle de sédimentation deltaïque: Contribution à la connaissance des marges passives. PhD thesis, University of Perpignan, 162 p.

Arz, H.W., Lamy, F., Ganopolski, A., Nowaczyk, N., Pätzold, J. (2007). Dominant Northern Hemisphere climate control over millennial-scale glacial sea-level variability *Quaternary Science Reviews, 26 (3-4),* 312-321. doi:10.1016/j.quascirev.2006.07.016

Austin, J.A., Jr., Christie-Blick, N., Malone, M.J., et al., 1998. *Proc. ODP, Init. Repts.,* 174A [CD-ROM]. Available from: Ocean Drilling Program, Texas A&M University, College Station, TX 77845–9547, U.S.A.

Bard, E., Arnold, M., Hamelin, B., Tisnerat-Laborde, N. and Cabioch, G. (1998). Radiocarbon calibration by means of mass spectrometric 230Th/234U and 14C ages of corals. An updated data base including samples from Barbados, Mururoa and Tahiti. *Radiocarbon,* 40(3): 1085-1092.

Bassetti, M.A., Jouet, G., Dufois, F., Berné, S., Rabineau, M., and Taviani, M. (2006), Deglacial sedimentary processes and deposits in the outer continental shelf of the Gulf of Lions (western Mediterranean). *Marine Geology, 234(1-4), 93-109*

Baztan, J., Berné, S., Olivet, J.-L., Rabineau, M., Aslanian, D., ,Gaudin, M., Réhault, J.-P., Canals, M., (2005). Axial incision: The key to understand submarine canyon evolution (in the western Gulf of Lion). *Marine and Petroleum Geology 22, 805–826*

Berné, S., Rabineau, M., Flores, J.A., Sierro F.J. (2004) The impact of Quaternary global changes on strata formation. *Oceanography 17 (4),* 92-103.

Berné, S., Lericolais, G., Marsset, T., Bourillet, J.F. and de Batist, M. (1998), Erosional shelf sand ridges and lowstand shorefaces. Examples from tide and wave dominated environments of France. *Journal of Sedimentary Research, 68(4),* 540-555.

Berné, S., Gorini, C. (2005), The Gulf of Lions: An overview of recent studies within the French 'Margins' programme. *Marine and Petroleum Geology, 22,* 691-693.

Berné, S., Jouet, G., Dennielou, B., Bassetti, M.A., Flores, J.A., Gaillot, A., Riboulot, V., Sierro, F.J., Suc, J.P.Thouveny, N., in preparation. Stratigraphic signature of sea-level changes during the last 500 kyrs. The Gulf of Lions revisited by the Promess 1 drilling operation. *Geochemistry, Geophysics, Geosystems, submitted*

Brookfield, M.E. (1977). The origin of bounding surfaces in ancient eolian sandstones. *Sedimentology*, 24, 303-332.

Chiocci, F.L., Orlando, L. (1996). Lowstand terraces on Tyrrhenian Sea steep continental slopes. *Marine Geology, 134 (1-2)*, 127-143

Dansgaard, W., Johnsen, S.J., Clausen, H.B., Dahl-Jensen, D., Gundestrup, N.S., Hammer, C.U., Hvidberg, C.S., Steffensen, J.P., Sveinbjörnsdottir, A.E., Jouzel, J., and Bond, G., 1993, Evidence for general instability of past climate from a 250 ky ice-core record, Nature, 364, 218-220.

Davis, R.A., Balson, P.S. (1992), Stratigrpahy of a North Sea sand ridge. *Journal of Sedimentary Research; 62(1),* 116-121

Dumas, S., Arnott, R.W.C. (2006). Origin of hummocky and swaley cross-stratification. The controlling influence of unidirectional current strength and aggradation rate. Geology; 34 (12); 1073-1076; doi: 10.1130/G22930A.1

Flores, J.-A., Marino, M., Sierro, F.J., Hodell, D.A. and Charles, C.H. (2003) Calcareous plankton dissolution pattern and coccolithophore assemblages during the last 600 ky at ODP Site 1089 (Cape Basin, South Atlantic): paleoceanographic implications. *Palaeogeography, Palaeoclimatology, Palaeoecology, 196(3-4)*, 409-426.

Hampson, G.J., Storm, J.E. (2003), Geomorphological and sequence stratigraphic variability in wave-dominated, shoreface-shelf parasequences. *Sedimentology, 50, 667-701*

Hanken, N.-M., Bromley, R.G., Miller, J. (1996), Plio-pleistocene sedimentation in coastal grabens, north-east Rhodes, Greece. *Geol. J., 31,* 271-296

Helland-Hansen, W., Martinsen, O.J. (1996), Shoreline trajectories and sequences: description of variable depositional-dip scenarios. *Journal of Sedimentary Research*, 66, 670-688

Hart, B.S., Long, B.F. (1996), Forced regressions and lowstand deltas: Holocene Canadian examples. *Journal of Sedimentary Research, 66(4),* 820-829.

Heinrich, H. (1988) Origin and consequences of cyclic ice rafting in the Northeast Atlantic Ocean during the past 130,000 years. *Quaternary Research, 29,* 142-152.

Hemming, S.R. (2004). Heinrich events: massive late Pleistocene detritus layers of the North Atlantic and their global climate imprint. *Rev. Geophys 42 (1).* doi:10.1029/2003RG000128

Hendriks, P. H. G. M. (2003). In-depth gamma-ray studies: borehole measurements. Ph.D. thesis, Rijksuniversiteit Groningen, Holland.

Hernandez-Molina, F.J., Somoza, L., Rey, J., Pomar, L. (1994). Late Pleistocene-Holocene sediments on the Spanish continental shelves: Model for very high resolution sequence stratigraphy. *Marine Geology, 120 (3-4),* 129-174

Hiscott, R.N. (2001). Depositional sequences controlled by high rates of sediment supply, sea-level variations, and growth faulting: the Quaternary Baram Delta of northwestern Borneo. *Marine Geology,* 175, (1-4), 67-102

Hughen, K.A., Baillie, M.G.L., Bard, E., Beck, J W., Bertrand, C. J.H., Blackwell, P. G., Buck, C. E., Burr, G. S., Cutler, K. B., Damon, P. E.,Edwards, R. L., Fairbanks, R. G., Friedrich, M., Guilderson, T. P., Kromer, B., McCormac, G., Manning, S., Ramsey, C. B., Reimer, P. J., Reimer, R. W., Remmele, S., Southon, J. R., Stuiver, M., Talamo, S., Taylor, F.W., van der Plicht, J.,Weyhenmeyer, C. E. (2004). Marine04 Marine radiocarbon age calibration, 26 - 0 ka BP. *Radiocarbon, 46:* 1059-1086

Hunt, D., Tucker, M.E. (1992) Stranded parasequences and the forced regressive wedge systems tract: deposition during base-level fall, *Sedimentology, 81* (1-2), 1-9

Jouet, G., Berné S., Sierro, F., Bassetti, M.A., Canals, M., Dennielou, B., Flores, J.A. & the PROMESS-1 Team. Sedimentary response to millennial-scale sea_level changes in the NW Mediterranean.

Jouet, G., Berné, S., Rabineau, M., Bassetti, M.A., Bernier, P. and Dennielou, B. (2006), Shoreface migrations at the shelf edge and sea-level changes around the Last Glacial Maximum (Gulf of Lions, NW Mediterranean). *Marine Geology 234(1-4) 21-42*

Lafuerza, S., Frigola, J., Canals, M.,Jouet, G., Bassetti, M.A., Sultan, N., Berné, S. Subsea-floor stratigraphic profiling and soil classification from piezocone tests: A case study in the Gulf of Lion (NW Mediterranean Sea). *This volume*

Leckie, D.A., Walker, R.G. (1982) Storm and tide-dominated shorelines in Cretaceous Moosebar-Lower Gates interval-outcrop equivalents of deep basin gas trap in western Canada. *J. sedim. Petrol., 59,* 862-870.

Lee, H.J., Syvitski, J.P.M., Parker, G., Orange, D., Locat, J., Hutton, E.W.H.Imran, J., (2002). Distinguishing sediment waves from slope failure deposits: field examples, including the 'Humboldt slide', and modelling results. *Marine Geology,* 192, 79-104.

Lofi, J., Rabineau, M., Gorini, C., Berne, S., Clauzon, G., De Clarens, P., Tadeu Dos Reis, A., Mountain, G.S., Ryan, W.B.F., Steckler, M.S., Fouchet, C. (2003). Plio-Quaternary prograding clinoform wedges of the western Gulf of Lion continental margin (NW Mediterranean) after the Messinian Salinity Crisis. *Marine Geology, 198,* 289-317.

Lobo, F.J., Dias, J.M., Hernández-Molina, F.J., González, R., Fernández-Salas, L.M., Díaz Del Río, V. (2005). Late Quaternary shelf-margin wedges and upper slope progradation in the Gulf of Cadiz margin (SW Iberian Peninsula). *Geological Society of London, Special Publications,* 244; 7-25

Malatesta, A., Zarlenga, F. (1986). Northern guests in the Pleistocene Mediterranean Sea. *Geologica Romana,* 25, 91-154

Martini, E. (1971) Standard Tertiary and Quaternary calcareous nannoplankton zonation, *in:* Farinacci, A., ed., Proc. 2nd Planktonic Conference Roma 1970, vol. 2. Edizioni Tecnosciencia, Rome, p. 739-785.

Mellere D.; Steel R.J. (2000). Style contrast between forced regressive and lowstand/ transgressive wedges in the Campanian of south-central Wyoming (Hatfield Member of the Haystack Mountains Formation), in *Sedimentary responses to forced regressions. Geological Society Special Publications. 172* edited by D. Hunt and R. Gawthorpe, pp. 141-162

Massari, F., Sgavetti, M., Rio, D., D'Alessandro, A., Prosser, G. (1999), Composite sedimentary record of falling stages of Pleistocene glacio-eustatic cycles in a shelf setting (Crotone basin, south Italy). *Sed. Geol., 127, 85-110*

Migeon, S., Weber O., Faugères J.C. and Saint-Paul, J. (1999) SCOPIX: A new imaging system for core analysis. *Geo-Mar. Lett.,18,* 251–255

Monaco, A. (1971), Contribution à l'étude géeologique et sédimentologique du plateau continental du Roussillon. *PhD thesis, Univeisity of Perpignan,* pp. 295

Plint, A.G. (1988), Sharp-based offshore sequences and «offshore bars» in the Cardium Formation of Alberta: their relationship to relative changes in sea level, in *Sea Level Changes- An Integrated approach. Society of Economic paleontologists and Mineralogists vol. 42* edited by C.K. Wilgus , B.S. Hastings, C.G. St. C. Kendall, H.W. Posamantier, C.A. Ross and J.C. Van Wagoner, pp. 357-370, Special Publications

Plint, A.G. (1991), High frequency sea level oscillations in Upper Cretaceous shelf clastics of th Alberta foreland basin: possible evidence of a glacio-eustatic control? In *Sedimentation, tectonics and eustacy, Ass. of Sedimentologists Special Publication, 12* edited by D.I.M. Macdonald, pp. 409-428

Plint, A.G., Nummendal, D. (2000), The falling stage system tract: recognition and importance in sequence stratigraphy analysis *in Sedimentary responses to forced regressions. Geological Society, vol. 172*, edited by D. Hunt and Gawthorpe, pp. 1-18, London, Special Publication

Posamantier, H.W., Allen, G.P. (1993) Variability of the sequence stratigraphic model: effect of local basin factors. *Sedimentary Geology, 86*, 91-109

Posamantier, H.W., Allen, G.P., James, D.P. and Tesson, M. (1992) Forced regression in a sequence stratigraphic framework: concepts, examples, and exploration significance. *American Association of Petroleum Geologists Bullettin, 76*, 1687-1709

Posamantier, H.W., Morris W.R. (2000), Aspects of the stratal architecture of forced regressive deposits *in Sedimentary responses to forced regressions. Geological Society, vol. 172*, edited by D. Hunt and Gawthorpe. pp. 19-46, London, Special Publication

Rabineau, M. (2001) Un modéle geometrique et stratigraphique des sequences de depots quaternaries sur la marge du Gulf du Lion: enregistrement des cycles climatique de 100.000 ans. University of Lille. 394 pp.

Rabineau, M., Berné, S., Aslanian, D., Olivet, J.-L., Joseph., P., Guillocheau, F., Bourillet, J-F, Ledrezen, E. and Granjeon, D. (2005), Sedimentary sequences in the Gulf of Lion: a record of 100,000 years climatic cycles. *Marine and Petroleum Geology, 22*, 775-804

Rabineau, M., Berné S. , Olivet, J.-L., Aslanian, D., Guillocheau, F., Joseph, P. (2006). Paleo sea levels reconsidered from direct observation of paleoshoreline position during Glacial Maxima (for the last 500,000 yr). *EPSL*, 252(1-2), 119-137

Raffi, I., Flores, J.A. (1995), Pleistocene through Miocene calcareous nannofossils from Eastern Equatorial Pacific Ocean (Leg 138) *in Proceedings of the ODP Program, Scientific Results vol. 138, Ocean Drilling* edited by N.G. Pisias, L.A. Mayer, T.R. Janecek, A. Palmer-Julson and T.H. van Handel, pp. 233–286, College Station

Ramsey, N. (2002), A calibrated model for the interpretation of cone penetration tests (CPTs) in North Sea quaternary soils. Proc. Offshore Site Investigation and Geotechnics: diversity and sustainability, London, UK, p. 341-356

Robertson, P. K. (1990), Soil classification using the cone penetration test. *Can. Geotech J*, 27, 151-158.

Siddall, M., Rohling, E.J., Almogi-Labin, A., Hemleben, Ch., Meischner, D., Schmelzer, I., Smeed, D.A. (2003). Sea-level fluctuations during the last glacial cycle. *Nature* 423, 853-858, doi:10.1038/nature01690

Storm, J.E.A., Hampson, G.J. (2005), Mechanisms for forming discontinuity surfaces within shoreface-shelf parasequences: sea level, sediment supply, or wave regime? *Journal of Sedimentary Research, 75(1), 67-81.*

Stuiver, M., and Reimer, P. J., 1993, Extended 14C database and revised CALIB radiocarbon calibration program, Radiocarbon 35:215-230.

Surlyk, F., Noe-Nygaard, N. (2005), A forced regressive shelf-margin wedge formed by transition-slope progradation: lowermost Cretaceous Rauk Plateau Member, Jameson Land, East Greenland. *Bullettin of Geological Society of Denmark, 52, 227-243*

Suter, J.R., Berryhill, H.L.J. (1985). Late Quaternary shelf-margin deltas, Northwest Gulf of Mexico. Am. Petrol. Geol. Bull., 69, 77-91.

Sydow, J., H. H. Roberts, A.H. Bouma, and R. D. Winn (1992) Constructional subcomponents of a shelf-edge delta, northeast Gulf of Mexico: Gulf Coast *Association of Geological Societies Transactions, 42,* 717-726.

Tamura, T., Nanayama, F., Saito, Y., Murakami, F., Nakashima, R., Watanabe, K. (2007), Intra-shoreface erosion in response to rapid sea-level fall: depositional record of a tectonically uplifted strand plain, Pacific coast of Japan. *Sedimentology,* doi: 10.1111/j.1365-3091.2007.00876.x

Tesson, M., Gensous, B., Allen, G. and Ravenne, C. (1990), Late Quaternary lowstand wedges on the Rhône continental shelf, France. *Marine Geology, 91,* 325-332.

Tesson, M., Allen, G.P., Ravenne, C. (1993). Late Pleistocene shelf-perched lowstand wedges on the Rhone continental shelf *in:Sequence Stratigraphy and facies associations, IAS Special Publication 18,* edited by H.W Posamantier, C.P. Summerhayes, B.U. Haq, G.P. Allen, pp.183-196, Oxford

Tesson, M., Posamantier, H.W. and Gensous, B. (2000) Stratigraphic organization of Late Pleistocene deposits of the western part of the Gulf du Lion shefl (Languedoc shelf), western Mediterranean Sea, using high-resolution seismic and core data. *AAPG Bullettin, 84(1),* 119-150.

Trincardi, F.Field, M. (1991). Geometry, lateral variability and preservation of downlapped regressive shelf deposits: Eastern Tyrrhenian margin, Italy. *Journal of Sedimentary Petrology, 61,* 775-790.

Trincardi, F.Correggiari, A. (2000). Quaternary forced regression deposits in the Adriatic Basin and the record of composite sea-level cycles. In: D. Hunt and R.L. Gawthorpe (Editors), Sedimentary responses to forced regressions. Geological Society, London, pp. 245-269.

Thierstein, H.R., Geitznauer, K.R., Molfino, B. and Shackleton, N.J. (1977), Global synchroneity of late Quaternary coccolith datum levels: validation by oxygen isotopes. *Geology, 5,* 400-404.

Van Wagooner, J.C., Mitchum, R.M., Campion, K.M., Rahamanian, V.D. (1990), Siliciclastic sequence stratigraphy in well logs, cores and outcrops. *AAPG Methods in Exploration, 7, 55 pp.*

Villanueva, J., Flores, J.-A. and Grimalt, J.O. (2002), A detailed comparison of the Uk'$_{37}$ and coccolith records over the past 290 kyears: implications to the alkenone paleotemperature method. *Organic Geochemistry, 33,* 897-905.

Walker, R.G., Plint, A.G. (1992), Wave- and storm-dominated shallow marine systems *in Facies Models: Response to Sea Level Changes, Geological Association of Canada* edited by R.G. Walker and N.P. James, pp. 219-238, Toronto.

Winn, R.D., Roberts, H.H., Kohl, B., Fillon, R.H., Bouma,A., and Constans, R.E.(1995), Latest Quaternary deposition on the outer shelf, northern Gulf of Mexico: facies and sequence stratigraphy from the Mainpass Block 303 shallow core: *Geological Society of America Bullettin, 107,* 851-86.

Figure captions

Figure 1: General bathymetry of the Gulf of Lions. The grey pattern corresponds to the sand distribution on continental shelf. The red dotted line marks the shoreface position at the Last Glacial Maximum.

Figure 2: Multi-channel, high-resolution sesmic profiles at the drill site: (A) Shelf-slope seismic line (Marion....) showing depositional sequences bounded by discontinuities on the shelf that can be followed into correlative conformities on the slope (PRGL1 site); (B) close_up view at the position of PRG2-2 (line Calimero8). See position in Fugure 1.

Figure 3: High resolution multi-channel (A) and very high-resolution (sparker) (B) seismic profiles showing the detail on the last sequence (bounded by D60 and D70 discontinuities). Post-glacial transgressive deposits (U155) ly above the clinostratified sequence.

Figure 4: Correlation between seismic and lithological data after the conversion of mbsf depths into mstwtt on the basis of P-wave velocities from MSCL. Sedimentary units 1-14 are detailed in Table 1.

Figure 5: Detailed logs of selected cores. (A) Part of a sub-unit of sedimentary unit 2 showing an overall coarsening upward pattern with storm-generated beds based by an interval of clay, intensively bioturbated and with an high content of organic matter; (B) Coarse grained interval of the sedimentary unit 3 (corresponding to seismic surface D60), consisting of 2 coarse-grained beds (with shells and heterogeneous biogenic material) separated by about 1 m of marine clays; (C) the fining upward basal coarse-grained interval (sedimentary unit 14) made of sand and gravel (channel infill deposits).

Figure 6: Geotechnical and physical properties measured at PRGL2 site. Lithological characteristics and soil types show an outstanding correspondence that can be used for lithological prediction of not-recovered intervals. The main lithologies are estimated by the combination of resistance to cone penetration (qt) and friction resistance (fs) for sediments comprised between clay and medium sand. Thick coarse grained horizons are not evidenced by this methodology. Between 2 and 5,5 mbsf the lack of pore pressure measurements (due to the high permeability of sand) does not allow establishing the lithological correspondence. In addition, slight discrepancies between lithological prediction and real lithology are observed

(see transition between sedimentary units 1-2 and 6-7). In fact, the CPTU has been measured 3 m away from PRGL2-2 and lateral facies changes might be possible.

Figure 7: Total sand fraction, carbonate content and GR curve at PRGL2 and correlation with corresponding sedimentary units. Note that the grain size analysis only takes into account the <2 mm fraction, therefore gravel and shell beds are not shown in the vertical profile.

Figure 8: Chronostratigraphy of PRGL2 and correlation with the SPECMAP curve. ^{14}C dates provide an accurate chronology of the last sequence (U151-152). Deeper in the borehole, the detection of significant nannoplacton events are utilized down to MIS 8. The bottom of the hole has been dated on the basis of seismic correlations with the PRGL1 borehole (see Figure 2, Berné et al. this volume). The Specmap curve is from *Martinson et al.* [1987].

Figure 9: Synthetic scheme of mollusc assemblages examined in correspondence of erosional surfaces. Examples of the described assemblages are shown in the photos.

Figure 10 : Synthetic interpretation of the last forved-regressived unit (last 100 kyr glcial-intergacial cycle comprised between D60 and the sea-floor) showing the stratigraphic signature of higher-order, stepped sea-level falls creating 2nd order bounding surfaces (D63, D64, D65). Note the good match between the ages of these surfaces and the Heinrich events 4, 3, 2, respectively. D-", in particular, shows a drastic shallowing of sedimentary facies that could be explained by the 30m sea-level fall measure by *Arz et al.* [2007] in Red Sea. For clarity, post LGM deposits (U155) have not been represented.

Plates

Plate 1: X-ray images (see position in depth in Figures 4 and 7) evidencing sedimentary facies and structures: horizontal lamination and swaley cross bedding (8A), bioturbated sand (10A), hummocks and associated parallel lamination (14A), bioturbated storms beds in mud (35, 39), bioturbated clays with rare laminated silty beds (40, 47 and 61).

Plate 2: X-ray images (see position in depth in Figure 4 and 7) evidencing sedimentary facies and structures: intensively bioturbated clays with laminated sand beds (81), heterolithic facies (90 and 91 comparable to 35 and 39 in Plate 1), muddy shelly lag deposits with associated silty-sand bioturbated layers (103), alternating sand and mud couplets, slightly bioturbated

(111), bioclastic material lag (worm tubes can be distinguished) with bioturbated clay passing upwards to horizontally laminated silty clay (113), sand/clay alternations with sparse biogenic material (114).

Plate 3: Photos from selected cores:

1- section 8B/37-57 cm (8.50-8.70 mbsf): mud intervals in massive sands;

2- section 32/2-22 cm (32.61-32.80 mbsf): silty clay with fine sand beds, large burrow;

3- section 34/23-43 cm (34.43-34.63 mbsf): Lenticular/wavy fine sand/silt beds and clay. Erosional basal contacts;

4- section 36/25-45 cm (36.05-36.25 mbsf): lenticular (rippled?) fine sand beds and clay/silty clay. Some scours at the bottom of sand beds;

5- section 40/30-50 cm (39.30-39.50 mbsf): Intensively bioturbated silty clay with organic matter spots;

6- section 69/1-21 cm(62.21-62.40 mbsf): very bioturbated clay/silty clay;

7- section 74/20-40 cm (66.40-66.60 mbsf): muddy bioclastic gravel;

8- section 91/30-50 cm(80.94-81.10 mbsf): graded silty sand beds in silty clay;

9- section 95/0-20 cm (83.60-83.80 mbsf): very coarse-coarse muddy sand with very abundant shells and shell fragments, including complete bivalves;

10- section 116/64-84 cm (99.57-100.13 mbsf): Sandy gravel with large rounded clasts (up to 3cm)
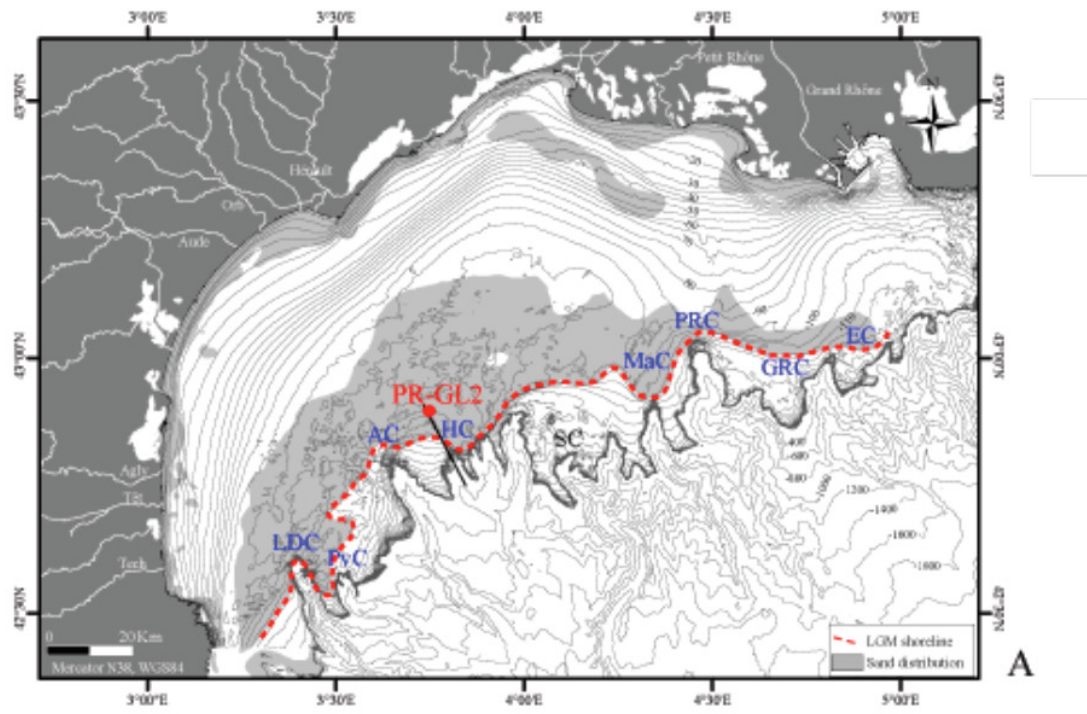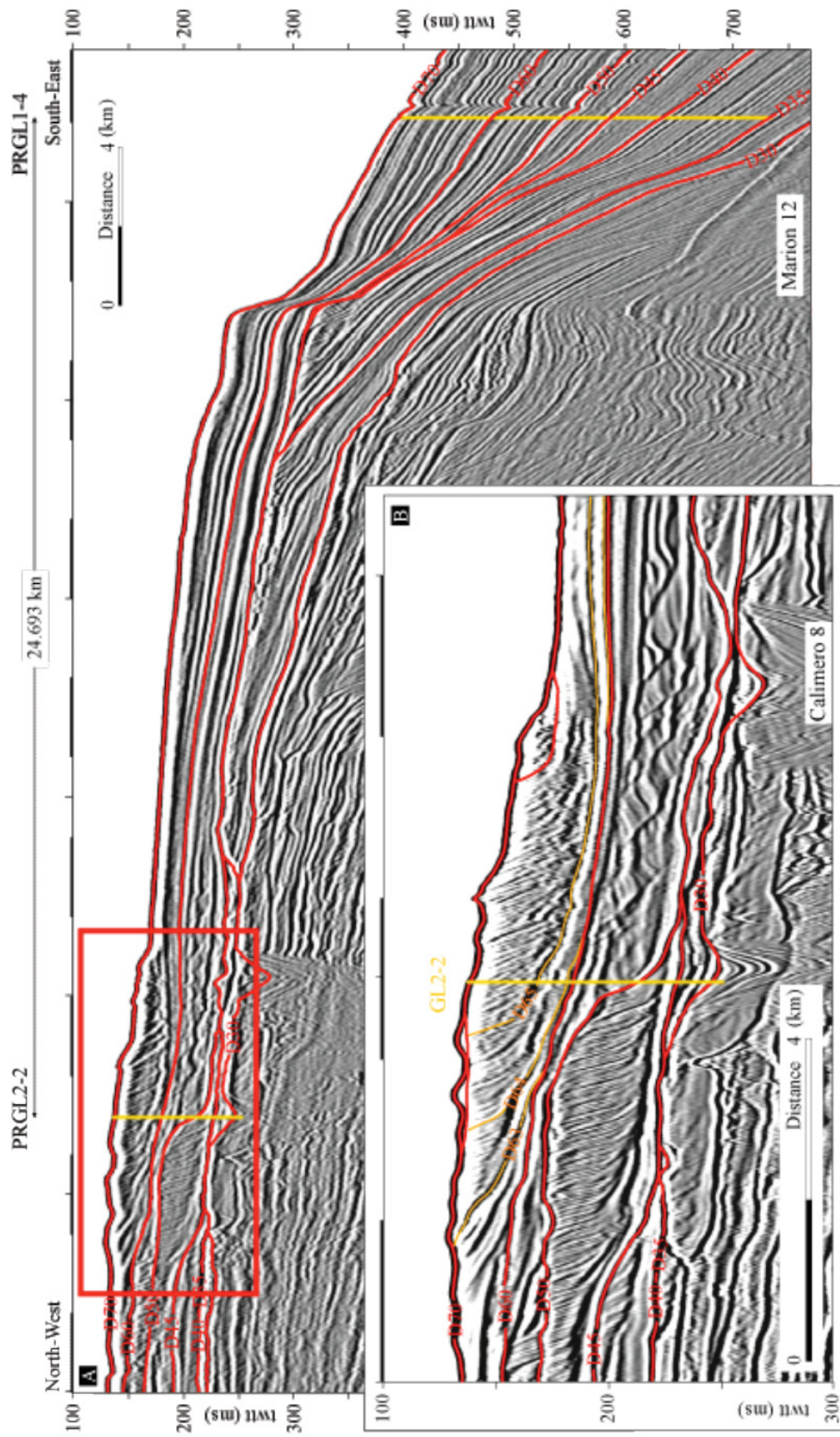
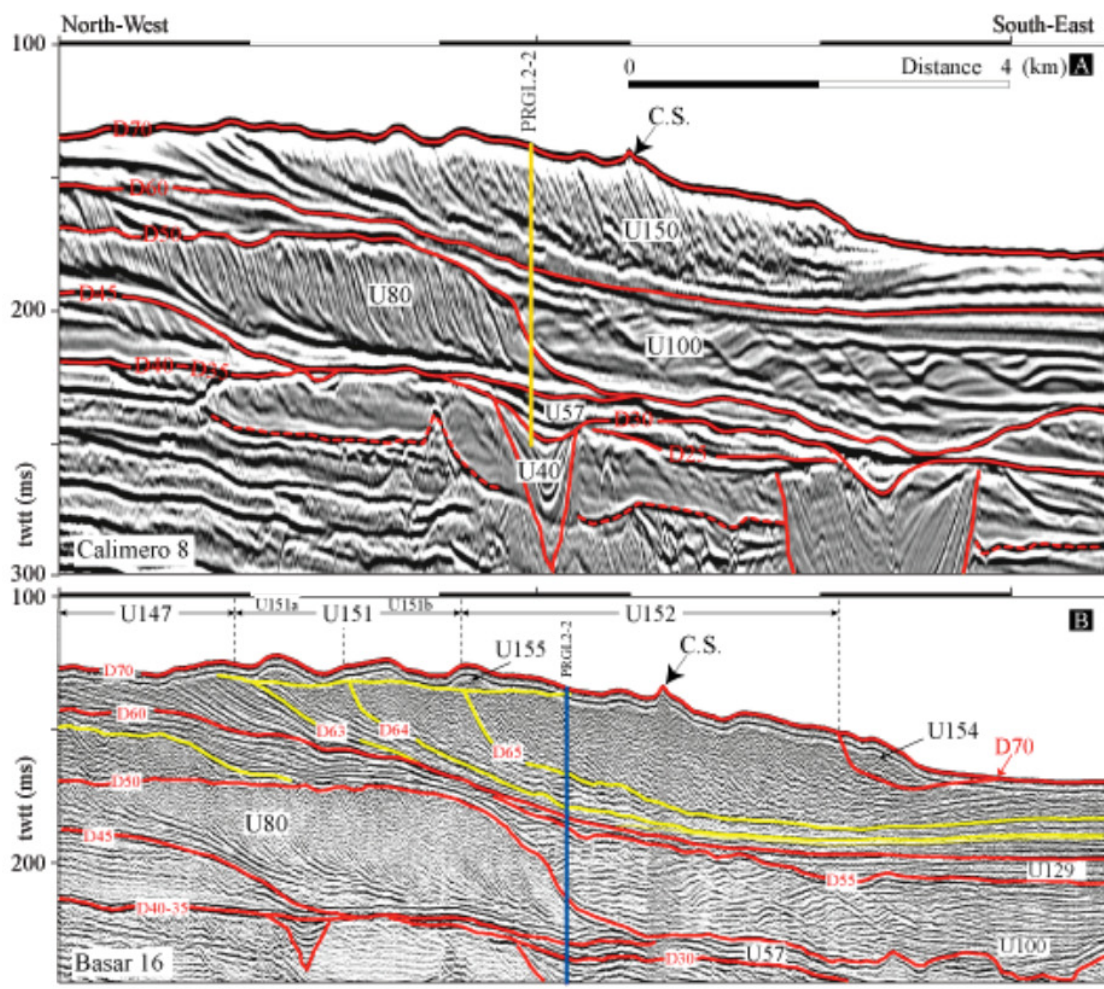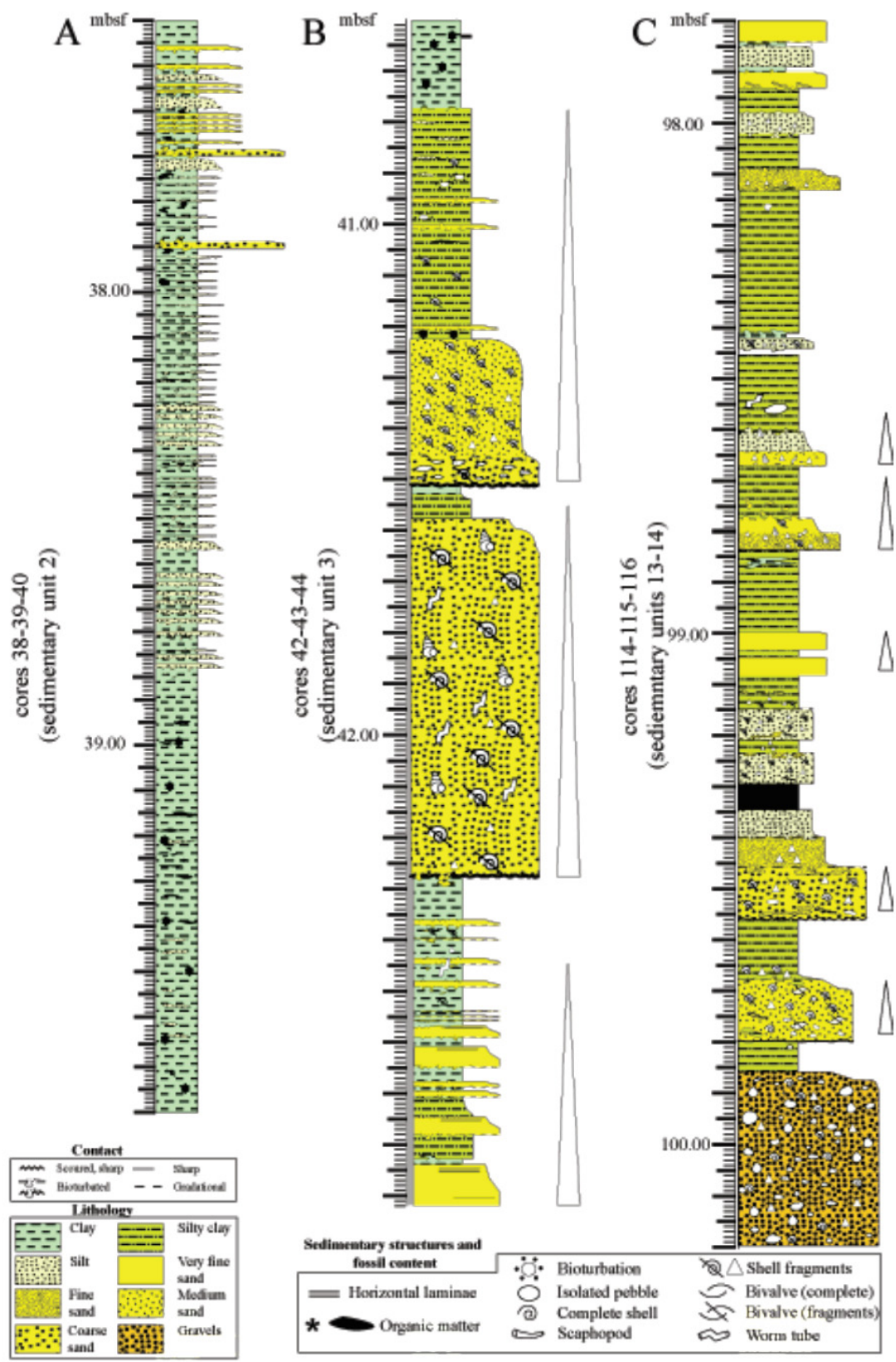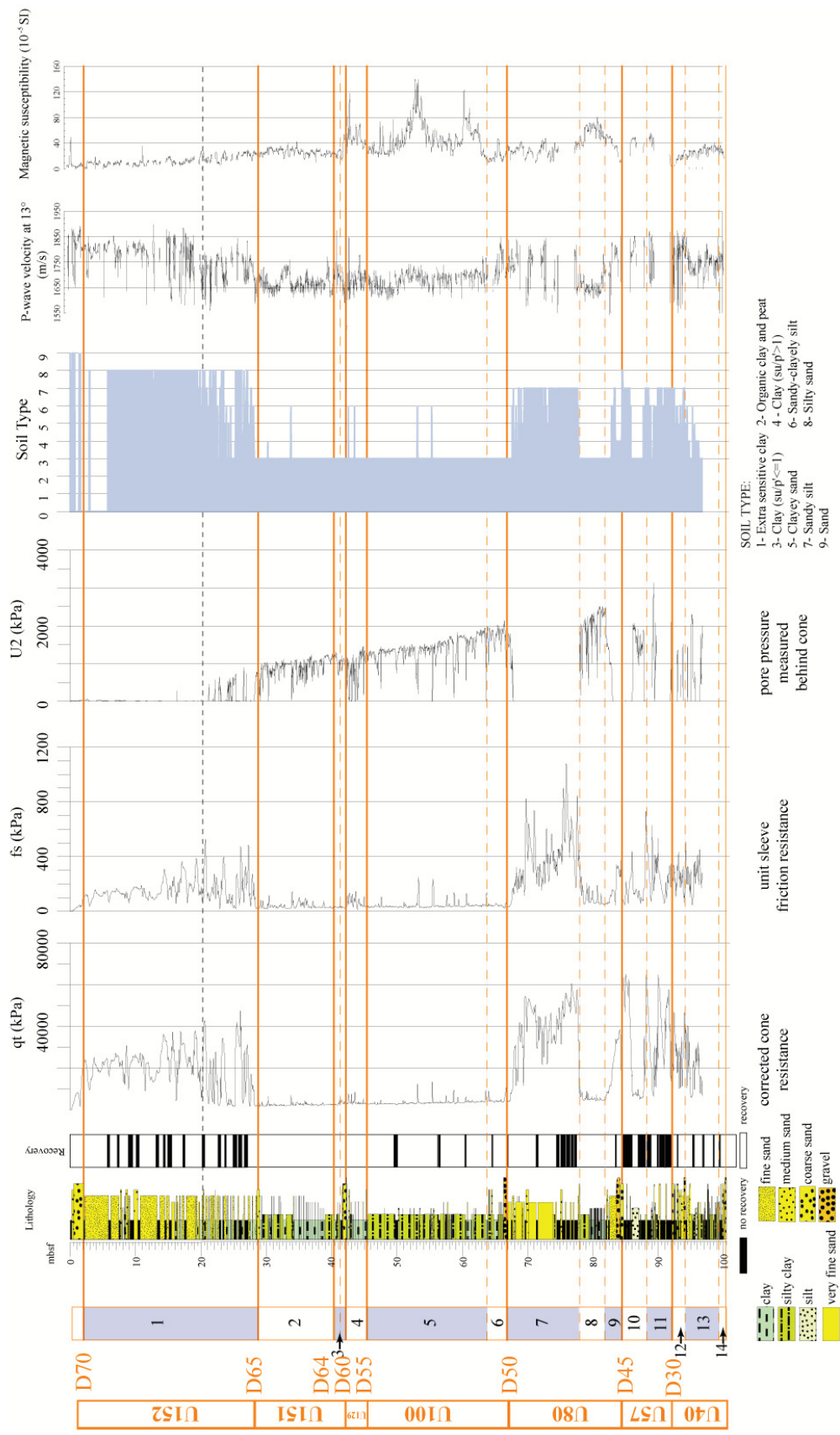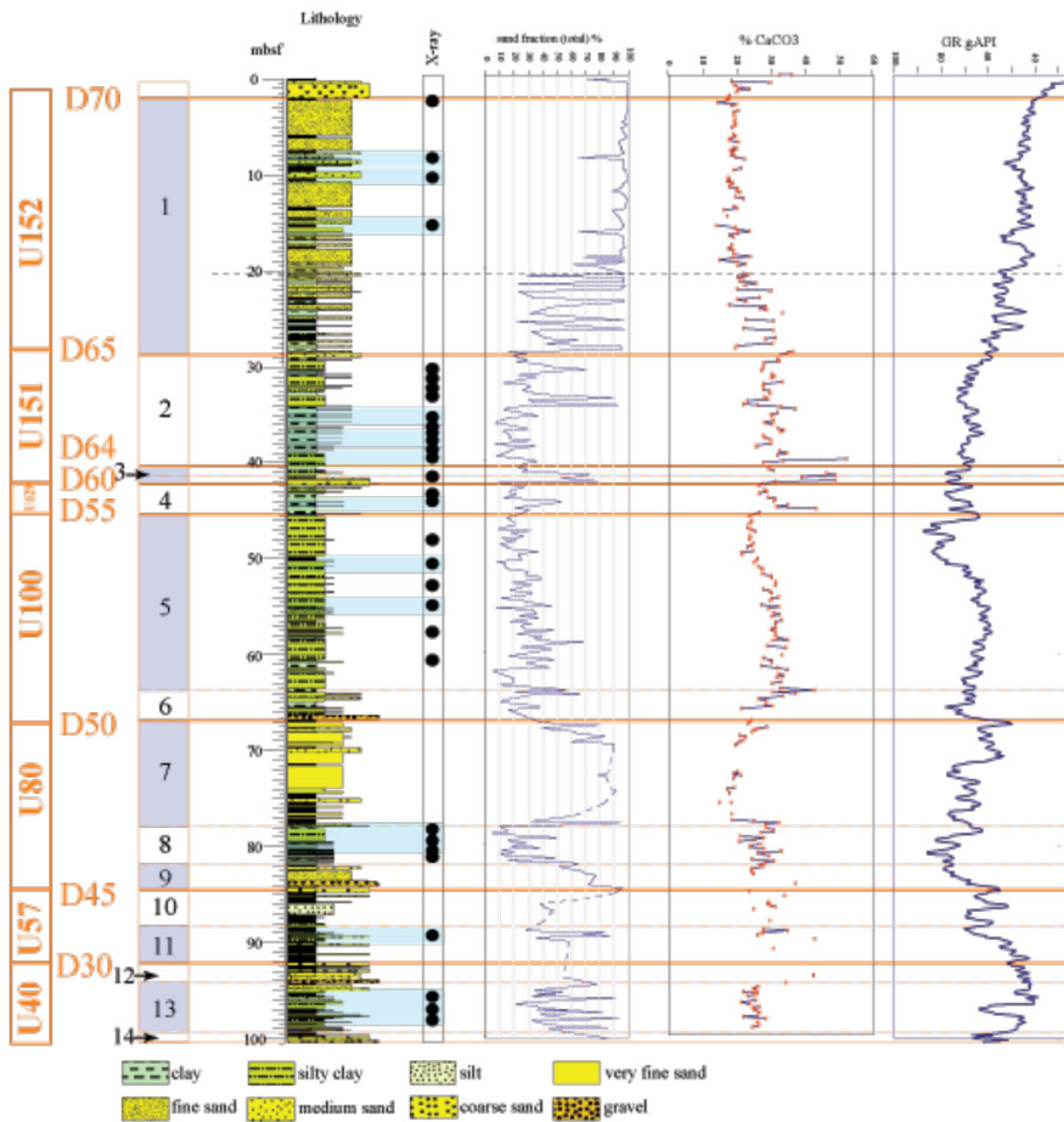Figure 1_Bassetti et al_G3

Figure 2_Bassetti et al._G3

Figure 3_Bassetti et al._G3

Figure 4_Bassetti et al._G3

A mbsf

38.00

39.00

cores 38-39-40
(sedimentary unit 2)

B mbsf

41.00

42.00

cores 42-43-44
(sedimentary unit 3)

C mbsf

98.00

99.00

100.00

cores 114-115-116
(sediemntary units 13-14)

Contact

Scoured, sharp — Sharp
Bioturbated — — Gradtional

Lithology

Clay / Silty clay
Silt / Very fine sand
Fine sand / Medium sand
Coarse sand / Gravels

Sedimentary structures and fossil content

Horizontal laminae
Organic matter

Bioturbation / Shell fragments
Isolated pebble / Bivalve (complete)
Complete shell / Bivalve (fragments)
Scaphopod / Worm tube

Figure 5_Bassetti et al_G3

50
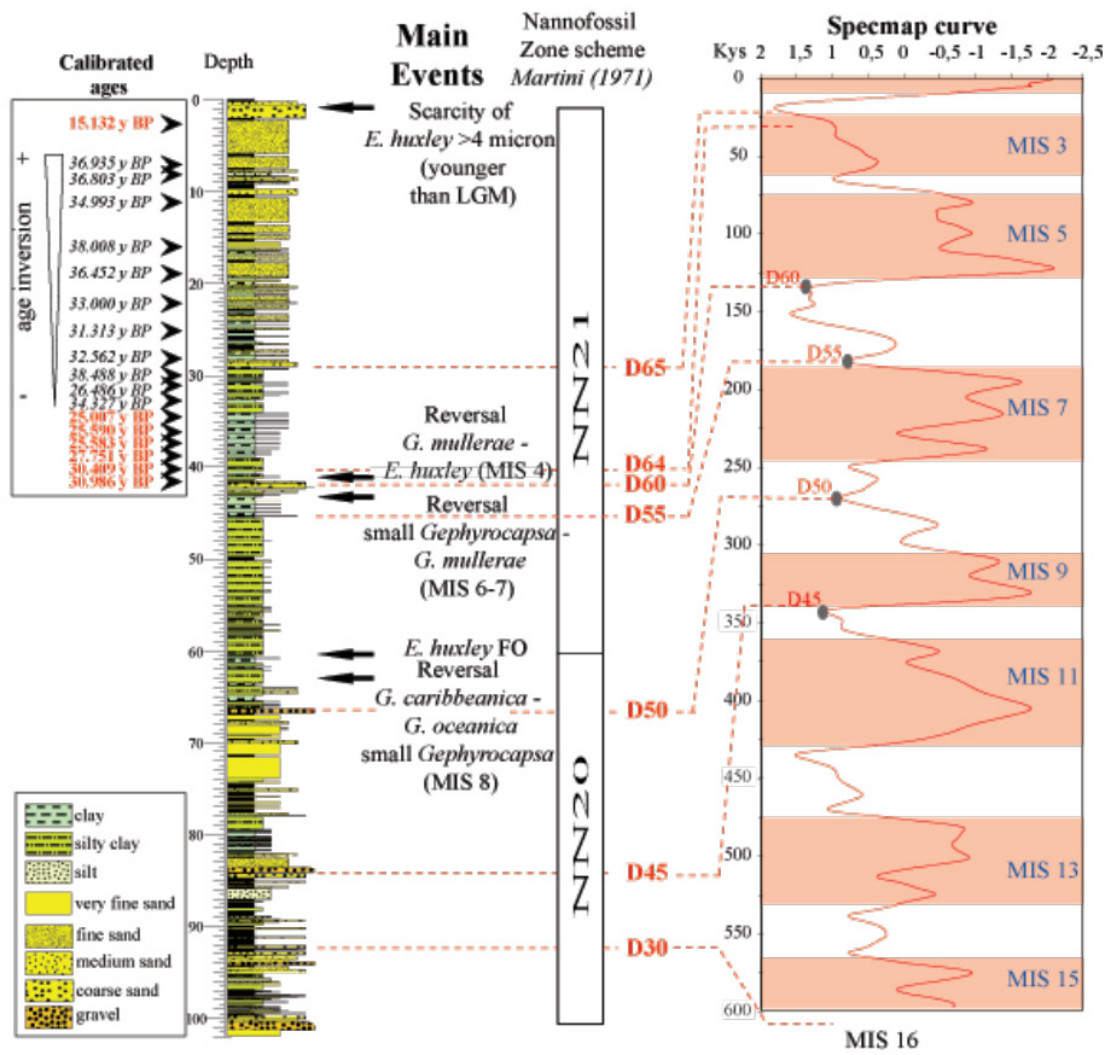
Figure 6 _ Bassetti et al._G3

Figure 7_Bassetti et al._G3
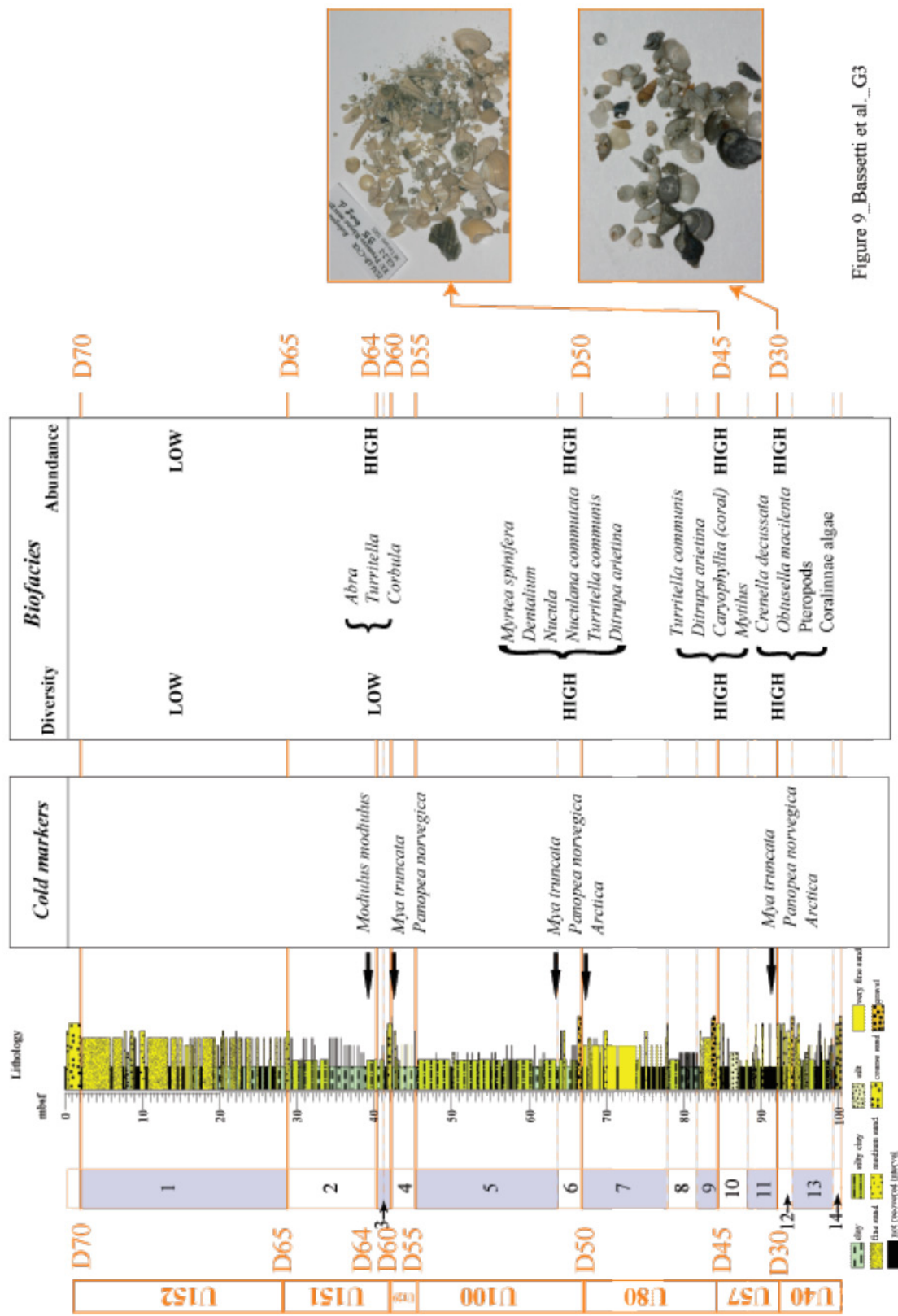
Figure 8_Bassetti et al._G3
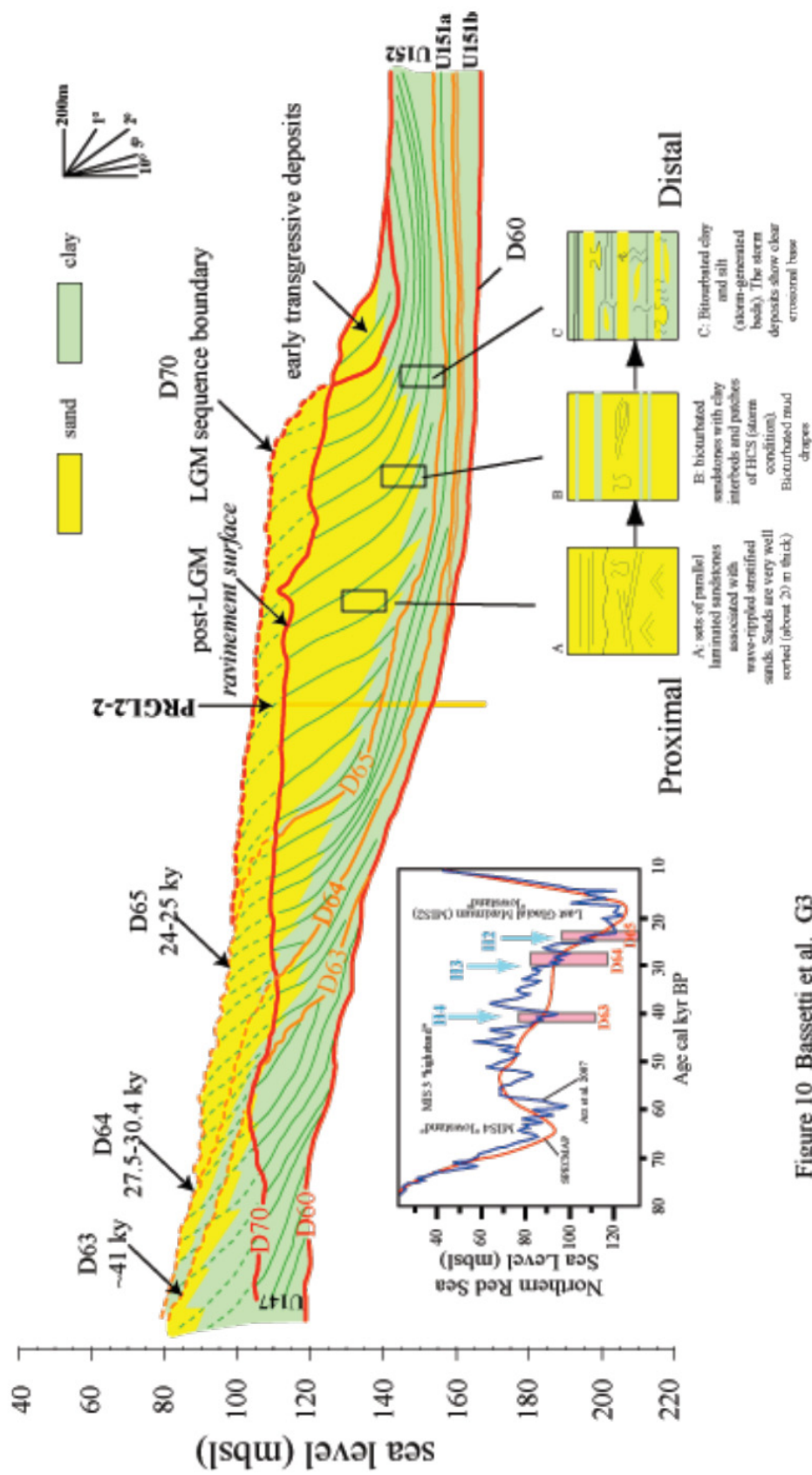
Figure 9_Bassetti et al._G3
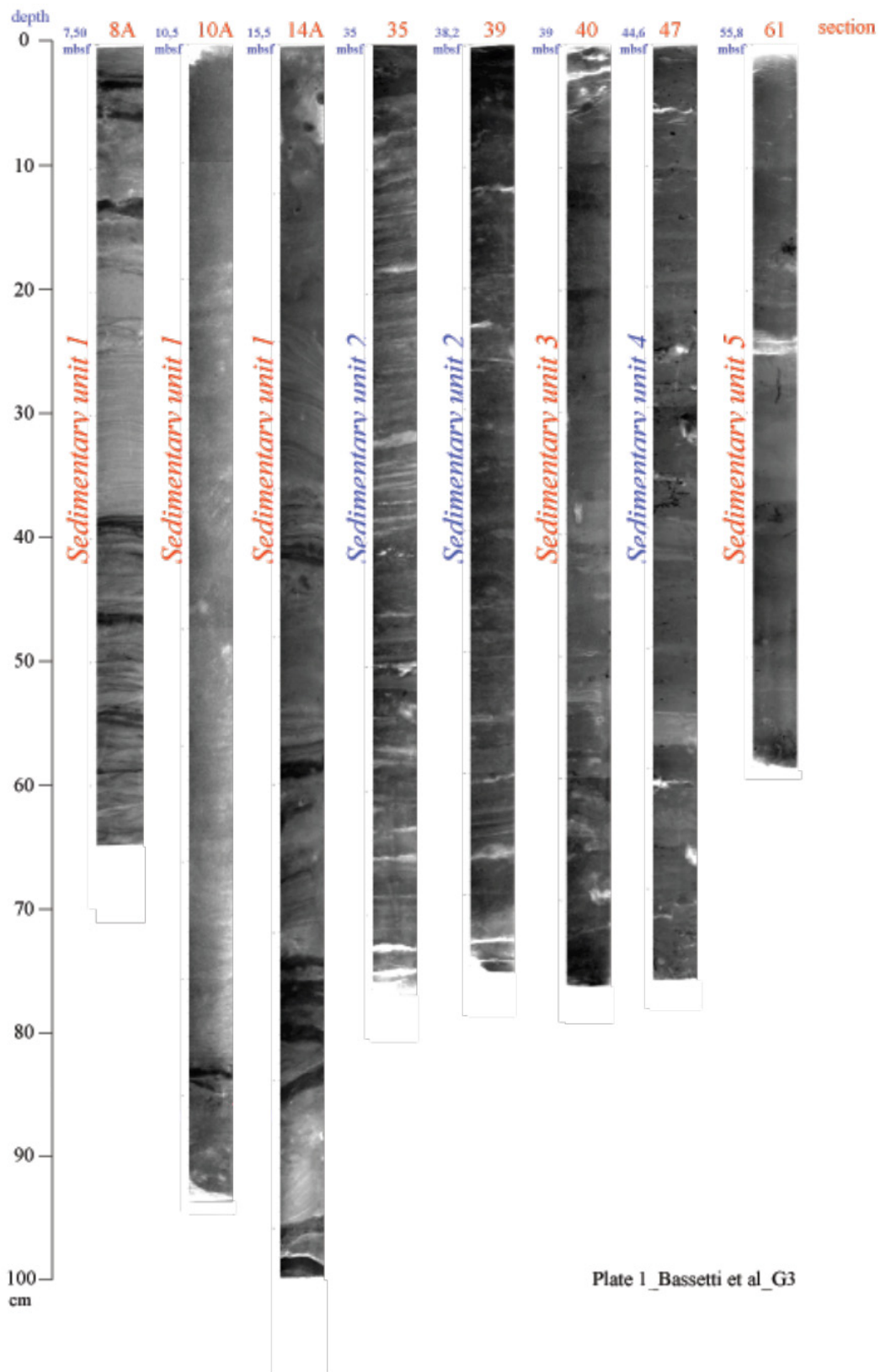
Figure 10_Bassetti et al._G3

55

Plate 1

Plate 1_Bassetti et al_G3

Plate 2
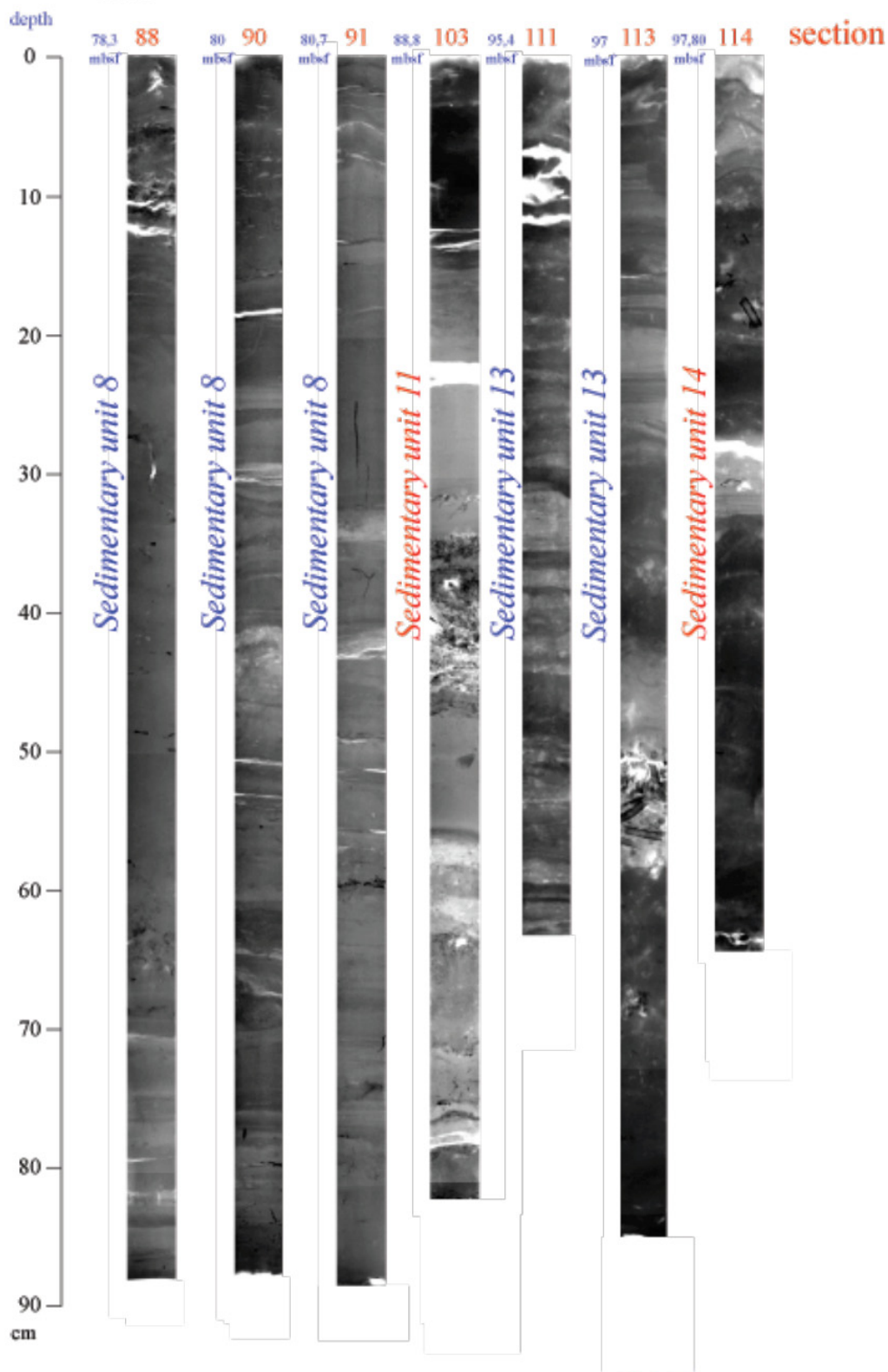
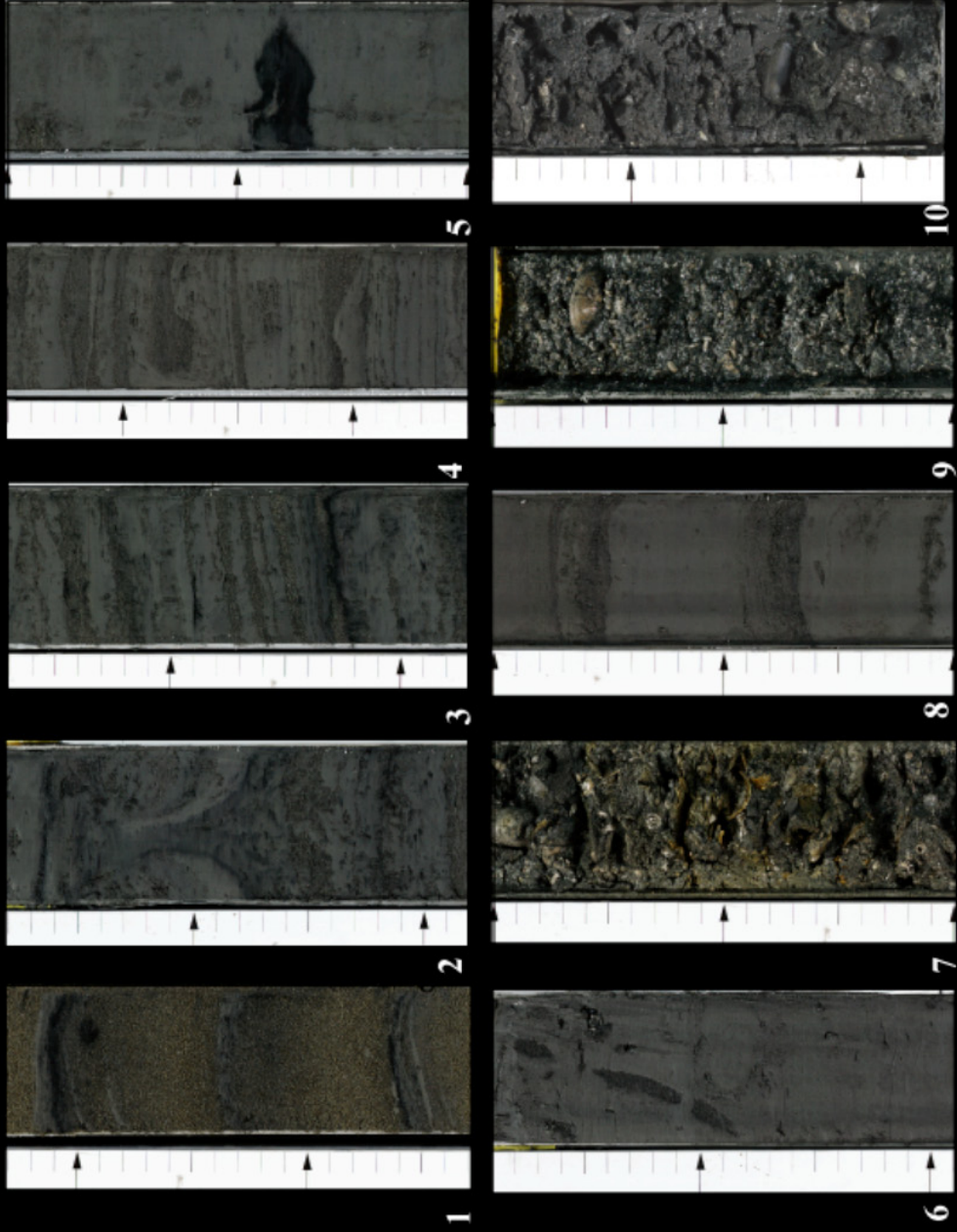

Plate 2_Bassetti et al._G3

Plate 3

Core number	mbsf	Unit	Facies description	Seismic expression	Environment/deposits
2-27	0-28.75	1	Fine to very fine grained sand, well sorted and homogeneous with scattered pebbles and rare shells. Mud interbeds. Planar lamination, tabular cross-bedding. Minor wavy lamination. Spare to moderate bioturbation .	Oblique reflectors with truncated topsets	Foreshore-upper shoreface
27-42/43	28.75-41.51	2	Silt-mud couplets (mm thick), intensively bioturbated. The silt laminae do not show gradation and have sharp (erosional) bases and tops. Minor wavy lamination.	Tangential reflectors downlapping seawards	Lower shoreface-offshore transition
43-44	41.51-42.32	3	Coarse grained, muddy sand with abundant shells (fragments)	Planar scour surface	Basal *ravinement* Submarine erosion
44-47	42.32-45.41	4	Clay-silt couplets with spare bioturbation and organic matter. Scattered shell debris. The interval is based by coarse grained, muddy sand with abundant shells (fragments)	Planar reflectors, onlapping landwards	Minor lobe of distibutary channel
48-70	45.41-63.60	5	Dark grey silty clay, with rare sand interbeds. Sparse organic matter and shell debris.	Undulated reflectors	Sediment waves
70-74	63.60-66.80	6	Very coarse-grained muddy sand, mixed with pebbles. Abundant and well preserved shells.	Planar scour surface	Basal *ravinement* Submarine erosion

Core number	mbsf	Unit	Facies description	Seismic expression	Environment/deposits
74-87	66,80-77.80	7	Fine to very fine grained sand, well sorted and homogeneous with scattered pebbles and rare shell debris. Planar lamination, tabular cross-bedding. Spare to moderate bioturbation	Oblique reflectors with toplap terminations below a planar scour	Foreshore-upper shoreface
87-91	77.80-81.40	8	Mud-sand alternations. The sand horizons show horizontal lamination and they are intensively bioturbated	Tangential reflectors downlapping seawards	Lower shoreface-offshore
92-96	81.90-84.4	9	Poorly sorted, muddy sand (medium to coarse-grained) with abundant biogenic material (shells) *Poor recovery between 84.50 and 86.00 mbsf*- medium to coarse grained sand with shell debris	Planar scour surface	Basal *ravinement* Submarine erosion
96-102	84.4-88.28	10	Silty clay-sand alternations with rare shell fragments and scattered pebbles	Convex, parallel reflectors	Mouth bar
103-107B	88.28-92.37	11	Strongly heterogeneous and containing abundant shell fragments. Roughly graded coarse grained intervals at the top	Parallel reflectors	Mouth bar, debris flow deposits
107B-109	92.37-94.15	12	Very coarse-grained deposits	Parallel reflectors	Basal *ravinement* Submarine erosion
109-115	94.15-99.24	13	Alternating coarse to fine-grained graded sand beds and burrowed silty clay	Concave, parallele reflectors	Mouth bar, debris flow deposits
115-116	99.24-100.13	14	Very coarse clastic material made of large rounded clasts and abundant shell fragments passing upwards to roughly grades coarse sand bes	Concave, parallele reflectors	Channel infill

Table1: definition of sedimentary units in PRGL2-2

core	sample depth (cm)	sample weight (mg)	Material	dating technique	Conventional C14 age (BP)	reservoir age	calibrated age (y BP)	calibration reference	Calibration curve
PRGL2-2-4A 60-61	252.0-252.9	49	bivalve	AMS	13220 ± 60	400	14998-15240 **(15132)**	Hughen et al. (2004)	calib5_1 marine04.14c
PRGL2-2-7 100-101	700.0-701.0	12	benthic Foraminifera (*Elphidium+Ammonia*)	AMS	31780 ± 320	400	36584-37287 **(36935)**	Bard et al. (1998) Glacial polynomial	
PRGL2-2-8A 40-41	790.0-791.0	18	benthic Foraminifera (*Elphidium+Ammonia*)	AMS	31660 ± 310	400	36463-37144 **(36803)**	Bard et al. (1998) Glacial polynomial	
PRGL2-2-10A 80-81	1128.0-1129.0	16	benthic Foraminifera (*Elphidium+Ammonia*)	AMS	30020 ± 260	400	34705-35282 **(34993)**	Bard et al. (1998) Glacial polynomial	
PRGL2-2-14A 60-61	1610.0-1611.0	33	benthic Foraminifera (*Elphidium*)	AMS	32760 ± 340	400	37637-38380 **(38008)**	Bard et al. (1998) Glacial polynomial	
PRGL2-2-16A 80-81	1930.0-1931.0	42	benthic Foraminifera (*Elphidium*)	AMS	31340 ± 300	400	36122-36782 **(36452)**	Bard et al. (1998) Glacial polynomial	
PRGL2-2-18 60-61	2190.0-2191.0	23	benthic Foraminifera (*Elphidium*)	AMS	28230 ± 220	400	32753-33246 **(33000)**	Bard et al. (1998) Glacial polynomial	
PRGL2-2-23 08-09	2548.0-2549.0	32	benthic Foraminifera (*Elphidium*)	AMS	26730 ± 190	400	31099-31528 **(31313)**	Bard et al. (1998) Glacial polynomial	
PRGL2-2-26 70-71	2840.9-2841.7	30	benthic Foraminifera (*Elphidium*)	AMS	27840 ± 210	400	32327-32798 **(32562)**	Bard et al. (1998) Glacial polynomial	
PRGL2-2-29 08-09	3028.0-3029.0	4600	Total Organic Carbon (TOC)	AMS	33200 ± 500	400	37944-39033 **(38488)**	Bard et al. (1998) Glacial polynomial	
PRGL2-2-29 58-59	3078.0-3079.0	14	benthic Foraminifera (*Elphidium*)+ 1 juvenil valve	AMS	22500 ± 150	400	26313-26659 **(26486)**	Bard et al. (1998) Glacial polynomial	
PRGL2-2-32 21-22	3279.5-3280.5	4520	Total Organic Carbon (TOC)	AMS	29420 ± 330	400	33960-34694 **(34327)**	Bard et al. (1998) Glacial polynomial	
PRGL2-2-33 31.5-37	3371.5-3378.0	24	2 valves of one bivalve	AMS	21190 ± 140	400	24786-25332 **(25007)**	Hughen et al. (2004)	calib5_1 marine04.14c
PRGL2-2-34 09-12	3429.0-3432.0	14	benthic Foraminifera (*Elphidium+Ammonia*)	AMS	29560 ± 250	400	34205-34761 **(34383)**	Bard et al. (1998) Glacial polynomial	
PRGL2-2-35 67.5-68.5	3567.5-3568.5	5700	Total Organic Carbon (TOC)	AMS	28720 ± 310	400	33201-33893 **(33893)**	Bard et al. (1998) Glacial polynomial	
PRGL2-2-35 68.5-70	3568.5-3570.0	9,5	Foraminifera	AMS	21590 ± 150	400	25407-25742; 25876-26000 **(25590)**	Hughen et al. (2004)	calib5_1 marine04.14c
PRGL2-2-36 58	3638	10	Wood	AMS	17480 ± 250	400	19933-20448 **(20216)**	Hughen et al. (2004)	calib5_1 marine04.14c
PRGL2-2-37 50-59	3710.0-3719.0	16,6	Foramifera	AMS	22120 ± 120	400	25445-25722 **(25583)**	Bard et al. (1998) Glacial polynomial	
PRGL2-2-38 65-66	3805.0-3806.0	5700	Total Organic Carbon (TOC)	AMS	27330 ± 260	400	31245-31832 **(31538)**	Bard et al. (1998) Glacial polynomial	
PRGL2-2-40 30-35	3930.0-3935.0	11,02	Foraminifera	AMS	24000 ± 500	400	27177-28325 **(27751)**	Bard et al. (1998) Glacial polynomial	
PRGL2-2-41 CS	>4055.1 and ≤4060.0	17,36	Foramifera	AMS	26330 ± 200	400	30182-30636 **(30409)**	Bard et al. (1998) Glacial polynomial	
PRGL2-2-42 25-30	4085.0-4090.0	1110	Shell: *Astarte sulcata*	AMS	26840 ± 170	400	30794-31178 **(30986)**	Bard et al. (1998) Glacial polynomial	

Table 2 : 14C dates in PRGL2-2

ANNEXE - III

PUBLICATIONS SUR LE DERNIER CYCLE GLACIAIRE

ANNEXE-III. PUBLICATIONS SUR LE DERNIER CYCLE GLACIAIRE

A-III.1. Shoreface migrations at the shelf edge and sea-level changes around the Last Glacial Maximum (Gulf of Lions, NW Mediterranean).
(Jouet *et al*., 2006)

A-III.2. Vegetation dynamics in Southern France during the last 30 ka BP in the light of marine palynology.
(Beaudouin, Jouet *et al*., 2007)

A-III.3. Response of the Rhône deltaic margin to loading and subsidence during the last climatic cycle.
(Jouet *et al*., *in press*)

A-III.4. Sedimentary response to millennial-scale sea-level changes in the NW Mediterranean.
(Jouet *et al*., submitted)

Shoreface migrations at the shelf edge and sea-level changes around the Last Glacial Maximum (Gulf of Lions, NW Mediterranean)

G. Jouet [a,b,*], S. Berné [a], M. Rabineau [b], M.A. Bassetti [a], P. Bernier [c], B. Dennielou [a], F.J. Sierro [d], J.A. Flores [d], M. Taviani [e]

[a] *Géosciences Marines, IFREMER, BP 70, Plouzané, France*
[b] *UMR-CNRS 6538 Domaines Océaniques, I.U.E.M., Plouzané, France*
[c] *UMR-CNRS 5125 Paléoenvironnements et Paléobiosphère, Université C. Bernard Lyon1, Villeurbanne, France*
[d] *Universidad de Salamanca, Departamento de Geología, Salamanca, Spain*
[e] *ISMAR-CNR, Via P. Gobetti, 101 Bologna, Italy*

Abstract

The Bourcart–Hérault canyon interfluve in the Gulf of Lions (NW Mediterranean) was the site of very high sedimentation (up to 2.5 m/kyr) around the Last Glacial Maximum, due to the vicinity of major fluvial systems that fed the shelf edge. Shoreface deposits and offshore muds deposited during each glacial/interglacial 100 kyr-cycle, created a repeated motif with high-angle and low-angle clinoforms on seismic profiles. New detailed morphological, sedimentological and paleo-environmental data, constrained by ^{14}C dating, allow us to propose a scenario for the evolution of this critical area between 46 and 15 cal. kyr BP. The major seismic sequence (S5), formed as a forced regression during the overall sea-level fall between MIS-3 and MIS-2, can be sub-divided into several prograding units, which indicate that relative sea-level changes were punctuated by intervals of increased fall or slow-down, or even stillstand. Similarly, the onset of sea-level rise was marked by steps, during which wave-cut terraces formed, and can be tracked all around the Gulf of Lions. Three stillstands or slow-downs of sea-level change are identified and dated by deposits found at 90 m relative sea-level (21 cal. kyr BP), 110–115 m rsl (18–17 cal. kyr BP), and 98–105 m rsl (before 15.9 cal. kyr BP). Cementation of beach rocks, that now form eroded pinnacles culminating at 90 m, occurred during the 21 kyr stillstand. The position of relative sea-level during the maximum lowstand is not known, but should be deeper than 115 m. Periods of increased northwesterly winds favoured transport of coarser sediment at the shelf edge, in relation with deep water cascading: this created a distinct sandy interval during the period of Heinrich event 2 (around 24 cal. kyr BP), at the origin of amplitude anomaly on very high-resolution seismic data. The increased sea-level rise, around 15 cal. kyr BP, resulted in an abrupt decrease of sedimentation.
© 2006 Elsevier B.V. All rights reserved.

Keywords: Last Glacial Maximum; relative sea-level; high-resolution sedimentary record; Western Mediterranean; Heinrich events

1. Introduction

* Corresponding author. Géosciences Marines, IFREMER, BP 70, Plouzané, France. Tel.: +33 2 98 22 48 19 or +33 2 98 49 87 17; fax: +33 2 98 22 45 70.
   E-mail address: gjouet@ifremer.fr (G. Jouet).

During the last two decades, a sub-continuous record of Quaternary paleoclimatic evolution has been obtained from marine and continental studies or ice cores. The important climatic changes, which were amplified since

900 kyr (MIS-22/23, Ruddiman et al., 1986; Thunell et al., 1991), led to dramatic variations in sea-level and oceanic circulation, sediment erosion and transport; these changes have had a major impact on the architecture and sedimentary environments of continental margins. The relative sea-level changes can be deduced from the oxygen isotope ratio ($\delta^{18}O$) of foraminifera (Imbrie et al., 1984; Martinson et al., 1987; Labeyrie, 1987, 1989; Shackleton, 2000; Waelbroeck et al., 2002), and the "isotopic" sea-level curves are constrained by coral reefs studies (Fairbanks, 1989; Bard et al., 1990; Chappell and Polach, 1991; Bard et al., 1996). Sea-level is, thus, inferred from species living only at a given water depth and their relative position with respect to a reference level (e.g. present day sea level). Nevertheless, all of these methods have intrinsic uncertainties and there is a need of independent documentation of sea-level position. In this paper, a sea-level estimation method using a geological approach is presented, based on data collected in Western Mediterranean area.

The Gulf of Lions (Fig. 1) is a passive continental margin that is located far from main ice-sheets, with a relatively constant subsidence rate and a high sediment supply; it therefore represents an ideal area for studying the impact of sea-level changes on sedimentary strata and sequences. The main sediment source is from the alpine glaciers and the Rhône watershed (100,000 km²), with additional supply from the Pyrénées and Massif Central rivers (Aude, Agly, Tech, Têt, Orb and Hérault, in Fig. 1). The combination of high sedimentation supply and significant subsidence rate (250 m/Myr at the shelf edge, Rabineau, 2001) generates the progressive filling of available space, and the preservation of the depositional sequences at the shelf edge. It is also well-documented that part of the remaining sediment supply is bypassed and feeds the prograding continental
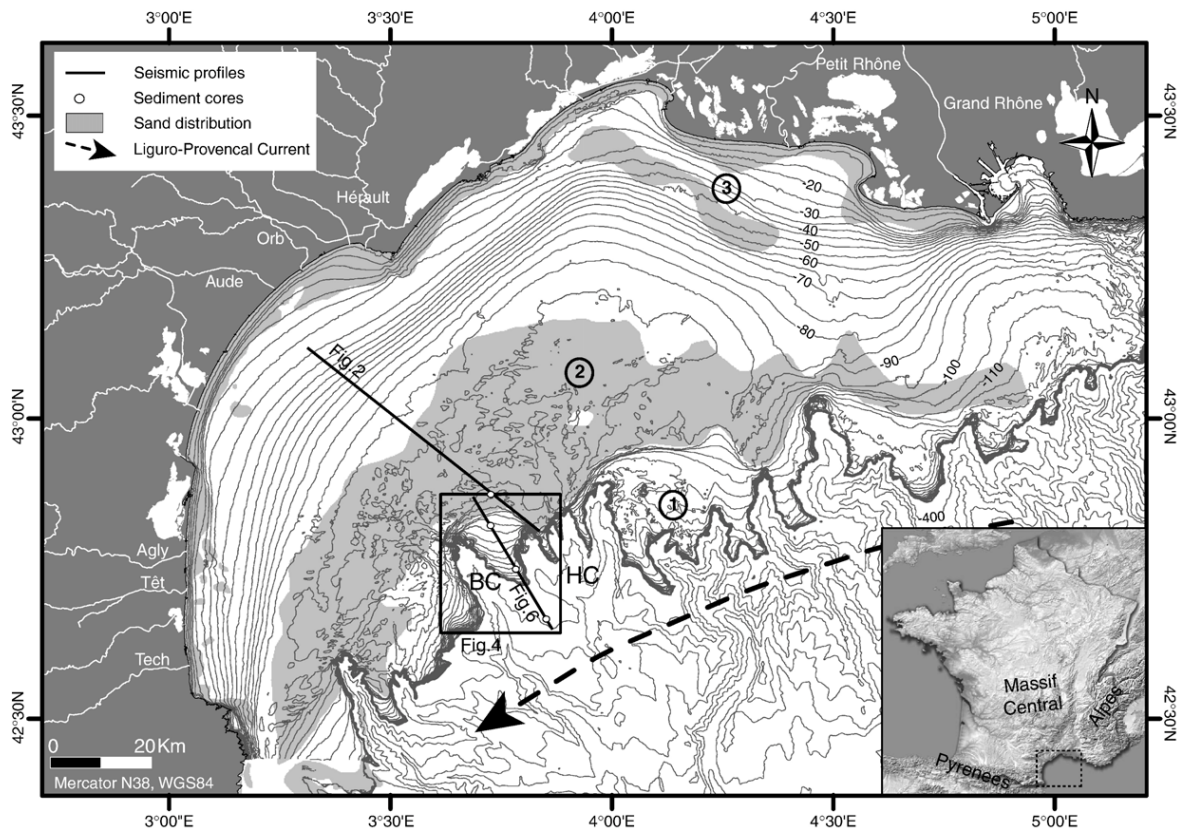

Fig. 1. Geographic and hydrographic settings of the Gulf of Lions. The present day morphology and the sand distribution on the continental shelf (Aloïsi, 1986) illustrate the effect of the last deglacial sea-level rise with (1) Pleistocene prodeltaic/lower shoreface muds beyond about 120 m water depth, (2) Pleistocene shoreface sands between about 80 m and 120 m water depth, (3) a deglacial littoral prism with prodeltaic muds (between about 20 and 80 m water depth) and shoreface sands (between the coastline and about 20 m water depth). The general circulation is mainly driven by the anti-clockwise flow of the Liguro-Provençal or Northern Current (Millot, 1990). Seismic profiles and sediment cores are localised on the Bourcart–Hérault interfluve. BC: Bourcart Canyon; HC: Hérault Canyon.

slope (Lofi et al., 2003), the Rhône deep sea fan (Droz and Bellaiche, 1985) and the Pyreneo–Languedocian sedimentary ridge (Berné et al., 1999).

The objective of this paper is to investigate the architecture of prodeltaic/shoreface sediments deposited around the Last Glacial Maximum (between 46 and 15 cal. kyr BP) at the shelf edge, and to propose a scenario for sea-level oscillations during this period.

2. Geological and environmental settings

2.1. Stratigraphic organisation of the Gulf of Lions continental margin

The Palaeozoic and Mesozoic metamorphic basement of the Rhône margin (Biju-Duval, 1984) is covered by a Neogene to Quaternary sedimentary mega-sequence (Bentounsi, 1990; Gorini et al., 1993; Gueguen, 1995; Sioni, 1997). The margin was formed after a period of rifting during the Oligocene–Aquitanian, followed by deposition of thick Neogene sequences (see the review by Berné and Gorini, 2005). At the end of the Miocene, the Messinian salinity crisis (Hsü et al., 1973; Clauzon, 1974) represented a major event all over the Mediterranean: a sea-level drawdown led to a pronounced erosion surface on the margins and deposition of deep-basin evaporitic

sequence. On the other hand, the Plio-Quaternary sedimentation was characterized by important margin progradation (about 70 km in about 5 Myr; Lofi et al., 2003). On the basis of recent seismic investigations, the Upper Quaternary sequences are observed to show the stacking of several prograding wedges bounded by discontinuities (D30, D40, D50, D60 and D70 in Fig. 2) they converge in a landward direction, with a pinch out at about 80 m water depth. In detail, the prograding wedges display two major types of seismic facies: (1) PI prisms with gently dipping clinoforms (< 1°), and (2) PII prisms with relatively high-angle clinoforms (from 3° to 7°). This elementary motif (PI/PII) is repeated vertically and allowed to define 5 major sequences (S1 to S5; Rabineau et al., 2005) bounded by major discontinuities (Fig. 2). The regressive deposits represent the most significant element constituting outer shelf sequences, when in fact the transgressive deposits are limited to a thin veneer of reworked sands that top the regressive shoreface deposits (Berné et al., 1998; Bassetti et al., 2006-this volume). Some authors considered that each of these wedges corresponded to 100 kyr-glacio-eustatic cyles (Aloïsi, 1986; Rabineau, 2001), whereas others proposed that they were linked to higher-frequency (20–40 kyr) cyclicities (Tesson et al., 1993; Gensous et al., 1993; Tesson et al., 1994; Gensous and Tesson, 1996). Stratigraphic
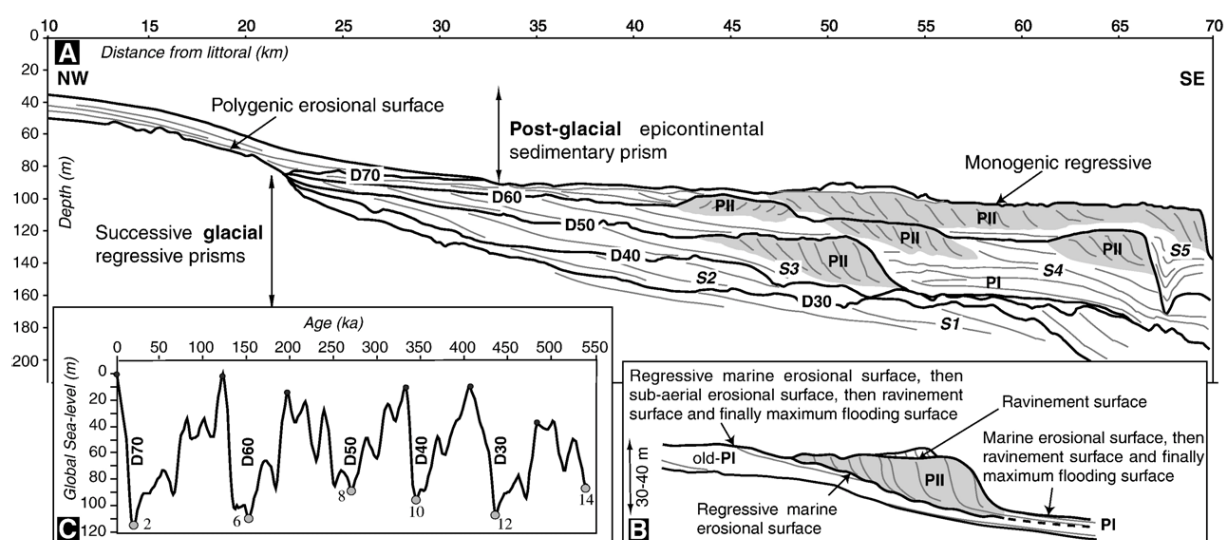

Fig. 2. Stratigraphic interpretation from high-resolution Sparker seismic lines P-1110 (position in Fig. 1). A) The NW–SE transect across the platform illustrates the stacking of the last 5 sedimentary sequences (S1 to S5) bounded by major discontinuities (D30 to D70). Vwater = 1500 m.s [-1] and Vsed = 1600 m.s [-1] are used for depth conversions. B) Recognition of the sedimentary motif (modified from Rabineau et al., 2005). Deposits are organized with a horizontal motif consisting of: (1) PI prisms with gently dipping clinoforms (< 1°) and (2) PII prisms with relatively high-angle clinoforms (from 3 to 7°). Thin black lines are time-lines. PI corresponds to the seaward termination of PII, beyond the action of waves, and could be partly preserved during a general sea-level fall, whereas PII is seaward transferred due to the regressive erosion. C) Correlation between the sedimentary sequences on the shelf and the last 5 glacial/interglacial 100 kyr-glacio-eustatic cycles (Rabineau et al., 2005). Each major erosional surface (D30 to D70) corresponds to a relative low sea-level of the Specmap eustatic curve (Imbrie et al., 1984).

modelling supports the 100-kyr hypothesis because other explanations would imply unrealistic subsidence rates (Rabineau et al., 2005).

The present day morphology of the continental shelf clearly illustrates the effect of the lowest sea-level during glacial and the deglacial sea-level rise (Fig. 1) with (1) Pleistocene lowstand shoreface sands between about 80 m and 120 m water depth, (2) Pleistocene lowstand prodeltaic/lower shoreface muds beyond about 120 m water depth and (3) the deglacial (transgressive and high-stand) littoral prism (Aloïsi et al., 1977) with prodeltaic muds (between about 20 and 80 m water depth) and shoreface sands (between the coastline and about 20 m).

2.2. Hydrodynamics

The Gulf of Lions is a wave-dominated shelf with moderate energy. However, wave heights associated to SE winds can be in excess of 8 m with periods of about 10 s. During winter, dominant N and NNW winds (Mistral and Tramontane) generate cascading of cold dense water with strong associated currents, especially in canyon heads situated to the SW of the Gulf of Lions (Palanques et al., 2006-this volume). The general circulation (Fig. 1) is mainly governed by the anti-clockwise flow of the Liguro–Provençal or Northern Current (Millot, 1990). This current roughly follows the shelf edge, but it locally deviates in relation with sea-floor morphology, creating secondary anti-cyclonic gyres extending to the upper part of the canyons and sweeping the interfluves (Durrieu de Madron, 1992). The hydrodynamism on the platform is slightly modified and locally associated to the coastal wind and swell-induced currents (Millot, 1990, 1999).

2.3. Climate and sea-level changes during the Last Glacial Cycle

The Quaternary is characterized by cyclic climate and sea-level changes (Shackleton, 1987) that strongly impact the sedimentary architecture of continental margins. Within these Milankovitch cycles, more rapid fluctuations in $\delta^{18}O$ have been identified at the millennial scale (Dansgaard et al., 1993); the Dansgaard–Oeschger oscillations (D/O) determine asymmetrical cycles with a progressive cooling at a regional scale followed-up by an abrupt increase of temperatures (Bond et al., 1993). The coldest intervals occur during Heinrich events (Ruddiman, 1977; Heinrich, 1988), approximately every 11 kyr (Bond et al., 1992). Even if the Mediterranean Sea lies far from the former ice sheets, these events are identified within Mediterranean sediments. For instance, in the Alboran Sea, Cacho et al. (1999) suggested that, during Heinrich events 1–5, polar waters reached the Mediterranean Sea through the Strait of Gibraltar and induced a weakening of the thermohaline circulation. The modelling of paleocirculation at the LGM (Myers et al., 1999) indicates a similar direction in the Liguro–Provençal current but certainly amplified by the low sea-level. Similarly, on the continent, the reduced evaporation and the strengthening of storms would lead to a decrease in precipitation and change in the hydrological cycle (Bartov et al., 2002). The low temperatures and a significant increase in wind intensity (Myers et al., 1999) resulted in enhanced wind erosion of the watershed during LGM (Ehlers, 1996). It has been proposed that the sedimentary flux, during the maximum of glaciation, was 3 to 3.5 times greater than the present one (Bossuet et al., 1996).

During the last glacial cycle, the Mediterranean Sea was connected to the global ocean and therefore followed the same trends for absolute sea-level changes (Fig. 3). The various isotopically-derived sea-level curves for the last 120 kyr (Labeyrie, 1987, 1989; Shackleton, 2000; Waelbroeck et al., 2002; Siddall et al., 2003) display a general fall until the LGM, punctuated by high-frequency changes; these sea-level curves have been constrained in depth by coral reefs studies (Fairbanks, 1989; Bard et al., 1990, 1996) and ice-cap volume estimations (Shackleton, 1977). However, differences in the order of 40 m remain between various data sets, as summarized in Fig. 3. And the last low sea-level (isotopic stage 2) is generally set around 110 and 120 m below present sea-level, but estimates going from 90 to 150 m were proposed (Shackleton, 1977; Fairbanks, 1989; Bard et al., 1990; Lambeck and Bard, 2000; Clark and Mix, 2002).

3. Methods

The study area was surveyed in great detail in preparation of a scientific drilling expedition as part of the European "PROMESS 1" project (Berné et al., 2004). The available data, acquired on board R/V "L'Atalante", R/V "Le Suroît" and R/V "L'Europe", include very precise swath bathymetric data from Simrad EM12D, EM300, and EM1000. Seismic data presented in this paper include Sparker and mud penetrator (Chirp) sources (Figs. 1 and 4). The vertical resolution of the single-channel Sparker (700 Joules, 500 to 2000 Hz) is around 1 m, whereas that of the hull-mounted Chirp system of R/V "Le Suroît" (2000 to 5200 Hz system) is in the range of 50 cm. A long impulse (50 ms) was linearly modulated in time and frequency (Schock et al., 1989). To improve the signal/noise ratio, the raw data

were processed with the Ifremer SITHERE program (Lericolais et al., 1990). The interpretation of seismic profiles was implemented using the general principles of seismic stratigraphy (Mitchum et al., 1977).

Several piston cores, including the "giant" piston corer of *R/V "Marion Dufresne"*, were retrieved from the study area, with penetration reaching more than 20 m in soft sediments or alternating sands and silts, but less than 3 m in massive sands, even with vibro-corers. These cores are located along a transect across the canyon interfluve (Fig. 4). Physical properties were first measured onboard using the MSCL-GEOTEK (Multi Sensor Core Logging system). They were split, described and sampled for multi-proxy studies. Radiometric dates were obtained with accelerator mass spectrometer (AMS) ^{14}C dating of well-preserved shells. AMS measurements were made at Lawrence Livermore National Laboratory (CAMS) and at Poznan Radiocarbon Laboratory (PRL) (Table 1). The ages reported herein are δ^{13}C-normalised conventional ^{14}C years, corrected for an assumed air–sea reservoir effect of 400 yr, then converted into calibrated ages using the Calib. v4.4 version (Stuiver et al., 1998), and the Glacial polynomial (Bard et al., 1998).

4. Results

4.1. Morphology of the study area

The study area is located between 90 and 350 m water depth, in the vicinity of the Bourcart (Aude) and Hérault canyons (Fig. 4). Along the interfluve, the shelf break is positioned at 180 m depth, whereas it is only at about 110 m at the position of canyon heads. Both sides of the canyon interfluve are affected by slump scars. The smooth morphology of this region is disturbed by several pockmarks, often aligned along preferential direction.

4.1.1. Shelf scarps

Besides the shelf break, a major scarp, about 10 m high is observed in the study area. Its average slope is about 4°, compared to the average 0.13° slope of the outer continental shelf. The top of the scarp is at a water depth of 110 to 115 m, except in the vicinity of the Bourcart canyon, where it is at a depth of about 120 m. Another step, best observed on seismic profiles (Fig. 7), has its top at a depth of 98 to 105 m; these two steps can
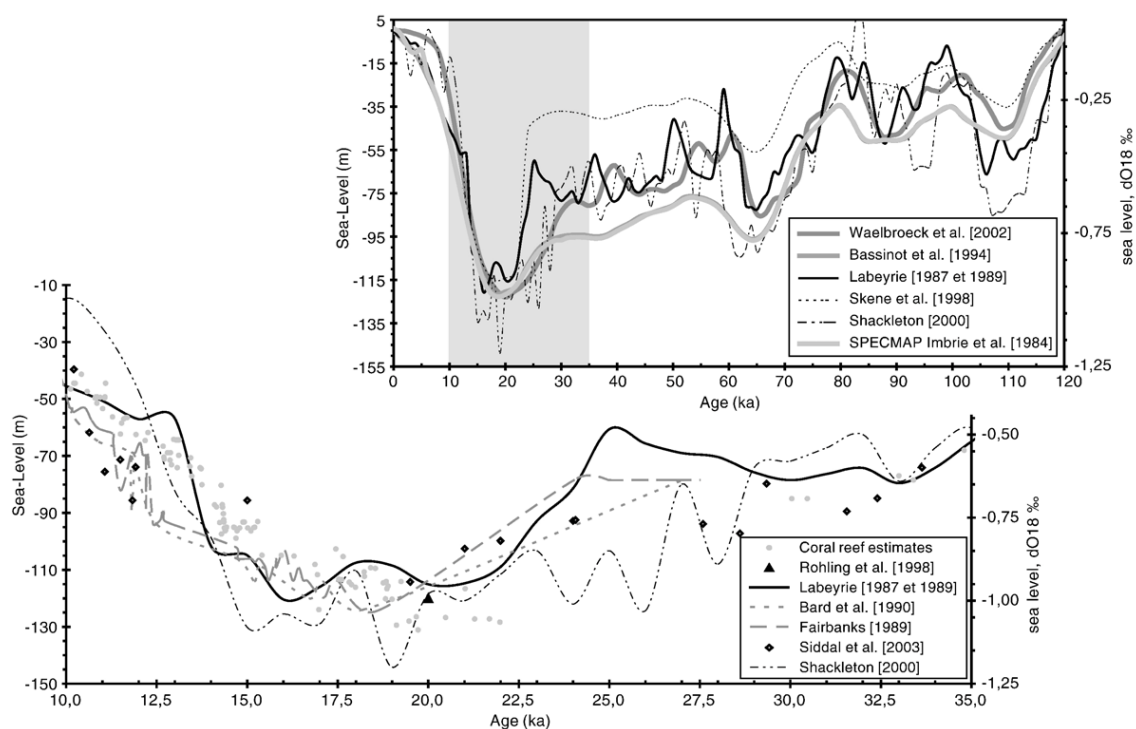

Fig. 3. Global sea-level changes according to different authors for the last 120 kyr, and for the 35–10 kyr period, based on isotopic studies, coral reef studies, or interpretation of paleodelta fronts (Imbrie et al., 1984; Labeyrie, 1987, 1989; Fairbanks, 1989; Bard et al., 1990; Bassinot et al., 1994; Rohling et al., 1998; Skene et al., 1998; Shackleton, 2000; Waelbroeck et al., 2002; Siddall et al., 2003). The right axis represents the mean ocean sea-level derived by Shackleton (2000) from atmospheric δ^{18}O. Note the differences between various curves in the order of 40 m during Marine Isotope Stage 3 and 2.

be observed throughout the Gulf of Lions (Berné et al., 2002; Fig. 1) at similar water depths.

These scarps correspond to the transition between two major sedimentary units:

– "relict offshore sands" that formed during the Last Glacial cycle forced regressions and represent high energy shoreface deposits;
– offshore/prodeltaic muds that represent the distal (seaward) equivalent to the upper shoreface sands (Rabineau et al., 1998; Berné, 1999).

4.1.2. Cemented sands

Another striking morphological feature in the study area corresponds to an area of elongated relief parallel to bathymetric contour lines, culminating at 90 ± 0.5 m water depth (based on very detailed swath bathymetric data), up to 20 m above the surrounding sea-floor (Fig. 5A). It has a lateral extent of more than 7 km and a width of about 300 m. Seismic profiles (Section 4.2) show that it tops the clinoforms of the upper shoreface sand facies, and that erosion occurred, particularly at the bottom of the landward flank of the relief. A sample was dredged at the top of this ridge and shows that it comprises coarse siliciclastic sands cemented by small crystals of high-magnesian calcite during early diagenetic processes. The grain fabric, the petrographic, and geochemical nature of the cement indicate that cementation occurred in the phreatic zone, with a slight influence of brackish water, thus implying a formation in the vicinity of the shoreline with possible lagoonal influence (Bernier et al., 2000). This observation rules out the possibility that these lithified sands could be gresified aeolian dunes as observed in the Eastern Mediterranean (Almagor, 1979) or on the South Florida margin (Locker et al., 1996). A ^{14}C date of the cement extracted and separated from carbonates by density (in order to avoid contamination by carbonate fragments of biogenic or detritic origin) indicates a precise diagenetic age of cementation of $17{,}785 \pm 240$ [14]C yr BP (21 cal. kyr BP). The presence of beach rocks above the shoreface sands, at 90 m below modern sea-level, can only be explained by erosion that would have removed up to 20 m of sediment. This estimate is confirmed by geotechnical measurements around other pinnacles, culminating at the same depth of

90 m and located to the East of the Hérault canyon; they indicate a maximum over-consolidation of muds underlying the eroded shoreface sands of about 30 m (Baztan, 2004).

4.1.3. Fluvial network and canyon incisions

A paleo-network of reliefs, attributed to the retreat path of streams during the deglacial sea-level rise, has already been described all over the continental shelf (Berné et al., 2002), and more specifically on the Bourcart–Hérault interfluve (Rabineau, 2001). The connection between canyon heads and streams during the Last Glacial Maximum is demonstrated by axial incisions within the Bourcart and Hérault-2 and Hérault-3 canyons (Baztan et al., 2005). In fact, the so-called Hérault canyon was connected during LGM to the Rhône (Berné et al., 2004), the Hérault being a tributary of the Rhône at that time; this major stream built a shelf edge delta that can be identified on the basis of bathymetric data, as showed in Fig. 4B (1). Similarly, another stream (Aude or Agly), flowing from the West, reached the western flank of the Bourcart canyon and was at the origin of axial incision within the canyon head (2 in Fig. 4B). Seismic data presented in Section 4.2 indicate that a stream reached the interfluve and fed an eastern branch of the Bourcart canyon head (3 in Fig. 4B), but this is not observable in the present day morphology.

4.1.4. Dunes

All the sandy deposits, interpreted as the result of deglacial and modern processes, are shaped by low amplitude (2–3 m) bedforms (dunes and sand ridges) with a main East–West long axis (Bassetti et al., 2006-this volume).

In summary, all information confirms that the study area was impacted by the outbuilding of a major deltaic/shoreface system during the Last Glacial period.

4.2. Seismic architecture of the last glacial depositional sequence

Within the Last Glacial seismic sequence (S5 in Fig. 2A), several sub-units can be identified thanks to the very dense seismic coverage of the high resolution, newly acquired Sparker and Chirp data (Figs. 4, 6 and 7).

Fig. 4. A) Swath bathymetric map of the Bourcart–Hérault interfluve, based on EM1000 and EM 300 swath bathymetric data. The study area is comprised between 90 and 350 m water depth, in the vicinity of the Bourcart (Aude) and Hérault canyons. Sparker and mud penetrator (Chirp) seismic data include a NW–SE transect along the canyon interfluve sampled by sediment cores. B) Morphological interpretation. The Hérault canyon was connected during LGM to the Rhône (1). Similarly, another stream (Aude, Agly or Hérault), flowing from the West (2), reached the western flank of the Bourcart canyon. Seismic data also indicate that a stream (3) flowed to the interfluve, and fed an eastern branch of the Bourcart canyon head. Besides the shelf break, major scarp are observed at a water depth of 98–105 m and 110–115 m.
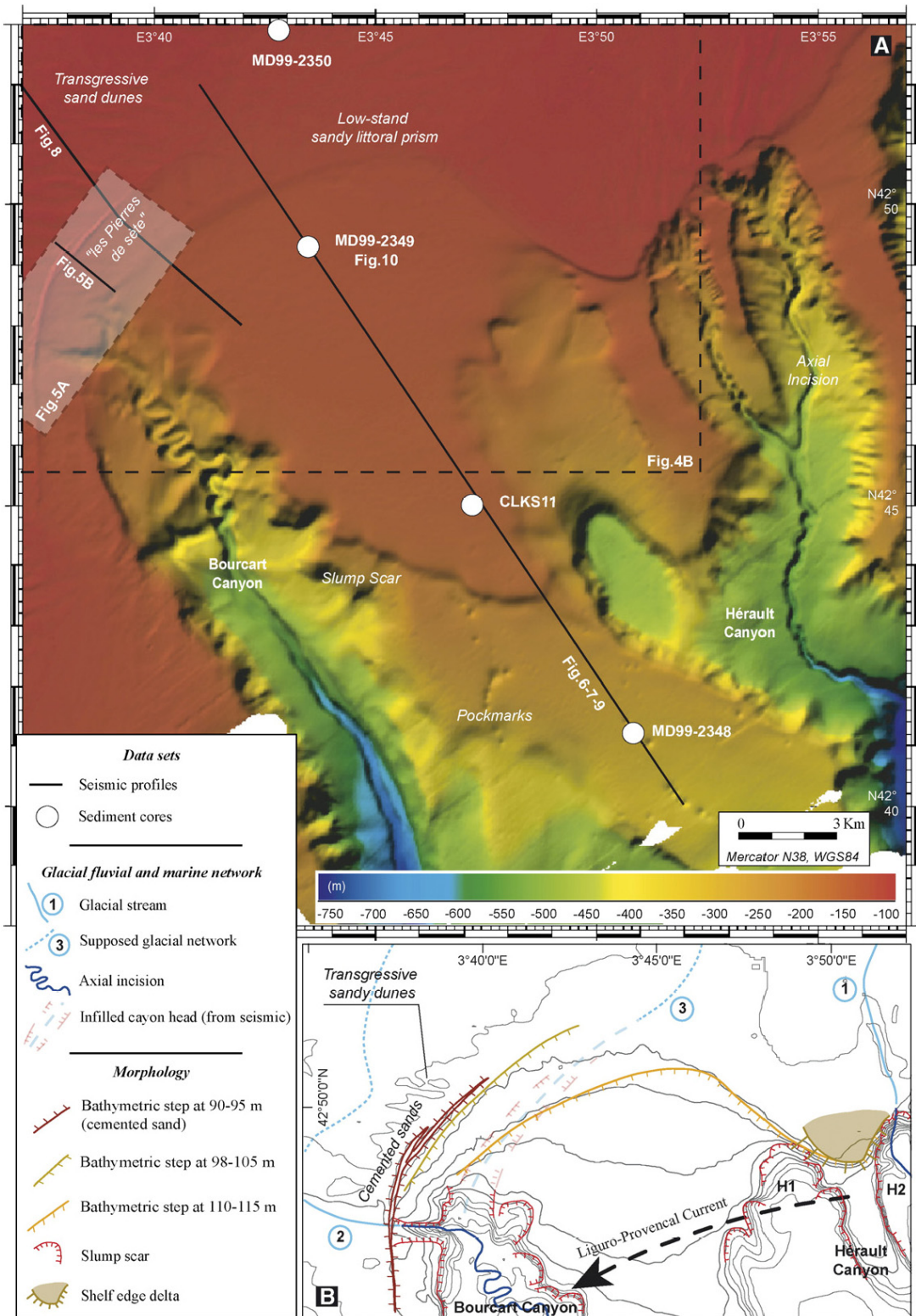
Table 1
Summary of the dated samples used for this study

Depth (cm)	Material	Laboratory #	Dating technique	Corrected C14 ages (yr B.P.)	Calibrated age (yr B.P.)	Calibration reference
MD99-2350			*Depth: 2.57 mbsf–water depth: 98 m–location: 42.91067 N–003.67733 E*			
43	Shell	Ly-11901	Conventional	10,315+/−60	11,683-11,891 (38%) 11,901-12,145 (51%)	Stuiver et al. (1998)
53–54	*Mytilus* spp.	LLNL-98906	AMS	23,770+/−140	28,405 (28,244–28,565)	Bard et al. (1998)
240	*Chlamys opercularis*	Poz-7860	AMS	39,800+/−800	45,549 (44,707–46,386)	Bard et al. (1998)
"Pierres de Sètes" CLDR9701 (Bernier et al., 2000)			*Depth: Sea floor–water depth: 95–108 m–location: north of Bourcart canyon*			
0		Ly-91146	AMS	13,220+/−130	15,499-16,071	Stuiver et al. (1998)
0		Ly-91145	AMS	17,780+/−170	20,645-21,403	Stuiver et al. (1998)
0		Ly-9987	AMS	17,385+/−240	20,148-20,991	Stuiver et al. (1998)
MD99-2349			*Depth: 18.62 mbsf–water depth: 128 m–location: 42.82117 N–003.72383 E*			
397	Benthic Foraminifera +Ostracods	Poz-7851	AMS	17,340+/−90	20,183-20,852	Stuiver et al. (1998)
535–538	*Arctica islandica*	Ly-11900	Conventional	19,235+/−150	22,294-23,104	Stuiver et al. (1998)
902	*Cyclichna* spp.	Poz-7852	AMS	20,570+/−100	24,131 (24,014–24,247)	Bard et al. (1998)
1074	*Corbula Gibba*	LLNL-96163	AMS	20,750+/−70	24,460 (24,376–24,539)	Bard et al. (1998)
1218	*Nucula* spp.	Poz-7854	AMS	21,190+/−100	24,969 (24,853–25,085)	Bard et al. (1998)
1736–1738	*Foraminifera* spp.	LLNL-96165	AMS	35,500+/−800	40,979 (40,117–41,838)	Bard et al. (1998)
CLKS-11 (Rabineau, 2001)			*Depth: 7.04 mbsf–water depth: 157 m–location: 42.74983 N–003.78267 E*			
216–219	Serpulid tubes	LYON-803	Conventional	16,585+/−110	19,318–19,980	Stuiver et al. (1998)
236–239	Serpulid tubes	LYON-804	Conventional	17,045+/−100	19,844–20,513	Stuiver et al. (1998)
MD99-2348			*Depth: 22.77 mbsf–water depth: 296 m–location: 42.69300 N–003.84167 E*			
25	nc.	Univ-Salam.	AMS	12,620	14,497	Stuiver et al. (1998)
80	*Foraminifera* spp.	LLNL-108010	AMS	13,950+/−60	16,377–16,857	Stuiver et al. (1998)
190	*Foraminifera* spp.	LLNL-108011	AMS	14,240+/−60	16,704–17,197	Stuiver et al. (1998)
300	*Foraminifera* spp.	LLNL-108012	AMS	14,980+/−70	17,531–18,074	Stuiver et al. (1998)
518	*Foraminifera* spp.	LLNL-108014	AMS	15,490+/−70	18,101–18,677	Stuiver et al. (1998)
1018	*Foraminifera* spp.	LLNL-108015	AMS	17,510+/−80	20,380–21,047	Stuiver et al. (1998)
1231	nc.	Univ-Salam.	AMS	17,660	20,886	Stuiver et al. (1998)
1498	*Foraminifera* spp.	LLNL-108016	AMS	19,350+/−90	22,447–23,216	Stuiver et al. (1998)
1680–1681	Bulk *Foraminifera* spp.	LLNL-77703	AMS	20,160+/−80	23,763 (23,358–24,193)	Bard et al. (1998)

Absolute dates were obtained with accelerator mass spectrometer (AMS) ^{14}C dating of well-preserved shells and microfauna. AMS measurements were made at Lawrence Livermore National Laboratory (LLNL), and at Poznan Radiocarbon Laboratory (PRL). The conventional radiocarbon datings were done by "Centre de datation par le radiocarbone - Université Claude Bernard Lyon1" (Ly) and "Bureau de Recherches Géologiques et Minières" (BRGM). The ages reported herein are δ^{13}C-normalised conventional ^{14}C years, corrected for an assumed air–sea reservoir effect of −400 yr, and then converted into calibrated ages using the Calib v4.4 version (marine98.14c; Stuiver et al., 1998), and the Glacial polynomial (Bard et al., 1998).

The basal unit (U147) displays sub-parallel, continuous and very gently dipping reflections, with alternating high and low amplitude reflection facies (Fig. 7). Landward, it presents higher angle geometries (Fig. 8). The lower boundary of U147 is the major erosional surface (D60) correlated at the regional scale (Fig. 2) and interpreted as the regressive surface of erosion that formed during Marine Isotope Stage 6 (Rabineau et al., 2005). The upper boundary (D63) is an erosional truncation in the proximal part of the interfluve, down to about 145 m below sea-level, and becomes conformable in the seaward direction (Fig. 7). Consequently, U147 thickens in the offshore direction. The amount of erosion can be estimated on the basis of the truncation of successive reflections up to 10 m in the upper part of the interfluve. The seaward migration of the offlap break and the downlaps within U147 together with the erosion of the topsets in the landward portion demonstrate a general progradation of the depositional system (Figs. 6 and 7).

The upward transition (from U147 to U151) is marked by a dramatic change in clinoform geometries with low angle clinoforms of U147 rapidly passing to high
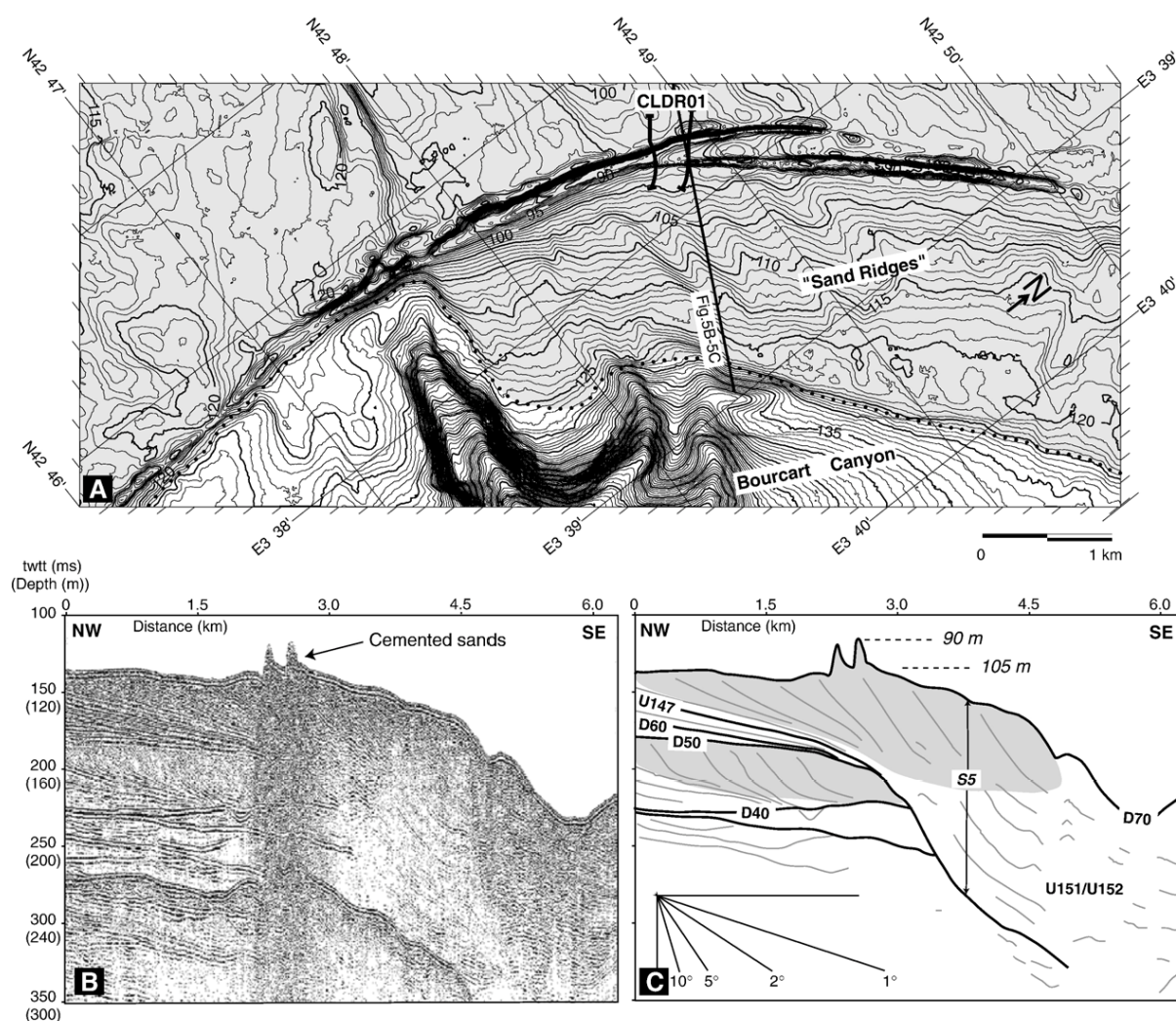
Fig. 5. A) Close-up view of the "Pierres de Sète" zone. This elongated relief (7 km lateral extent and 300 m width) is parallel to bathymetric contour lines, and culminates at 90±0.5 m water depth (20 m above the surrounding sea-floor). B) Seismic profile P-1005 and C) its interpretation show that cemented sands top the clinoforms of the upper shoreface sand facies, and that erosion occurred, especially at the bottom of the landward flank of the relief. A sample was dredged at the top of this ridge (CLDR01) and shows that it is made of coarse silicoclastic sands cemented during early diagenetic processes with an age of cementation of 17,785±240 ^{14}C yr BP (21 cal. kyr BP).

angle clinoforms of the upper sandy shoreface facies (Fig. 8).

Units U151 and U152 have similar seismic facies: they display quasi-parallel internal reflections with important lateral variations in seismic facies and they change from discontinuous wavy reflections in the proximal part (Fig. 7), becoming parallel and continuous in seaward direction. The wavy facies is similar to undulations observed on continental shelves and slopes, interpreted by many authors as bedforms (sediment waves: Migeon et al., 2001; Lee et al., 2002) or deformation structures evolving into depositional bedforms (Cattaneo et al., 2004). They have a spacing of

about 300 m, an average height of 1.5 to 2 m and with a thinning of the seaward dipping limb. U151 is mainly aggradational and the transition to U152 seems to be gradual. It is worth noting that similar bedforms are observed within older sequences, such as sequence S4 in Fig. 6. The very weak slope (<1°) of these bedforms would prevent their recognition in the stratigraphic record.

U152 displays clear seaward migration of the offlap break (progradation). The seaward migration of the wavy facies illustrates this trend, as well as the progressive seaward shift of depocentres creating internal discontinuities within this unit (Fig. 7). The boundary
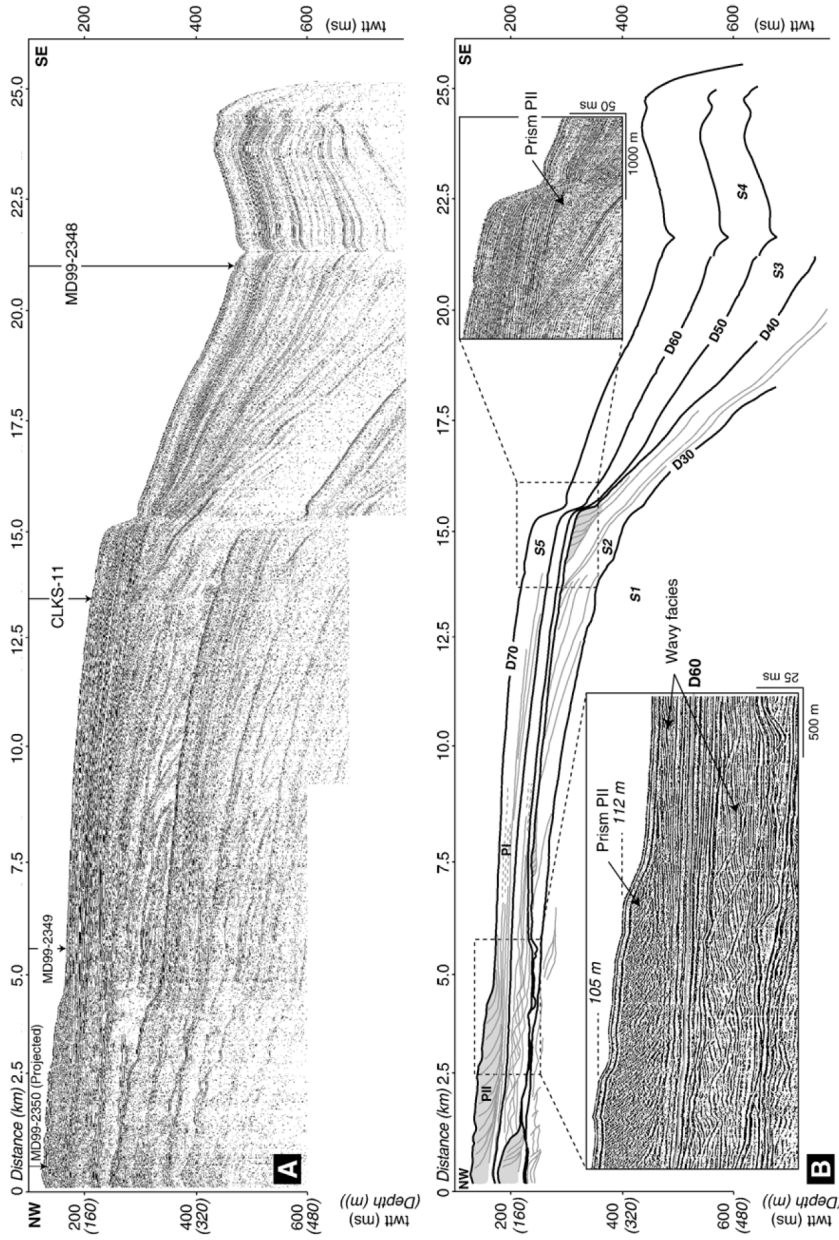
Fig. 6. A) High-resolution seismic Sparker line P-7020 (position in Fig. 4) along the canyon interfluve (dip section). Vwater = 1500 m.s^{-1} and Vsed = 1600 m.s^{-1} are used for the depth conversions. B) Stratigraphic interpretation and close-up views. The five major seismic sequences (S1 to S5) attributed to 100 kyr-cycles are identified. In each major sequence, the high-angle sandy clinoforms often downlap an erosional seismic discontinuity, which affects the underlying low angle clinoforms. A wavy facies, similar to undulations observed on several continental shelves and slopes, is observed within S5 and within other, older sequences, such as sequence S4.
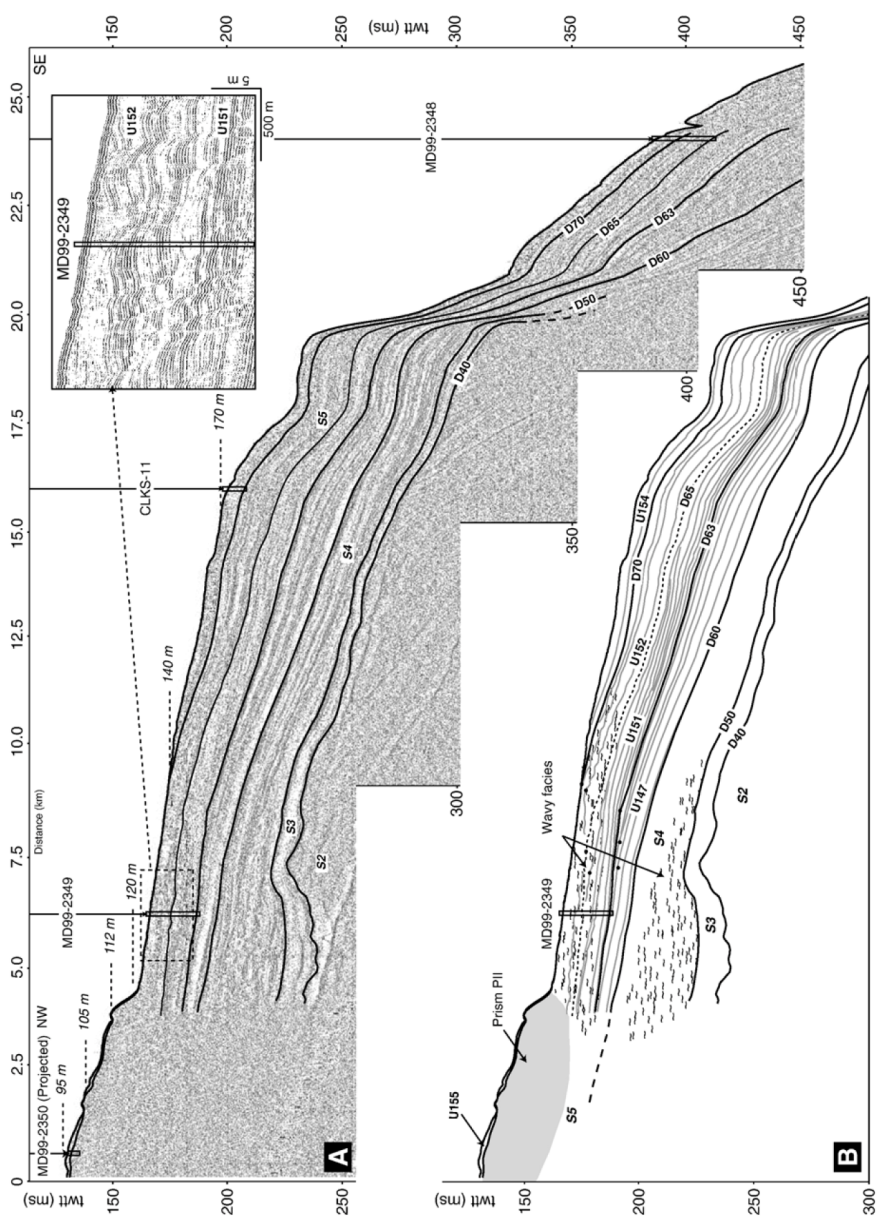
Fig. 7. Very high-resolution seismic Chirp profile P-7020ch (A) (position in Fig. 4) and interpretation (B). The profile is positioned at the same location as Sparker profile of Fig. 6. Steps and terraces identified on bathymetric maps are positioned. Within the Last Glacial cycle sequence (S5), several units (U147, U151, U152, U154 and U155) can be identified throughout the study area. The close-up view shows the position of core MD99-2349 within the wavy facies.
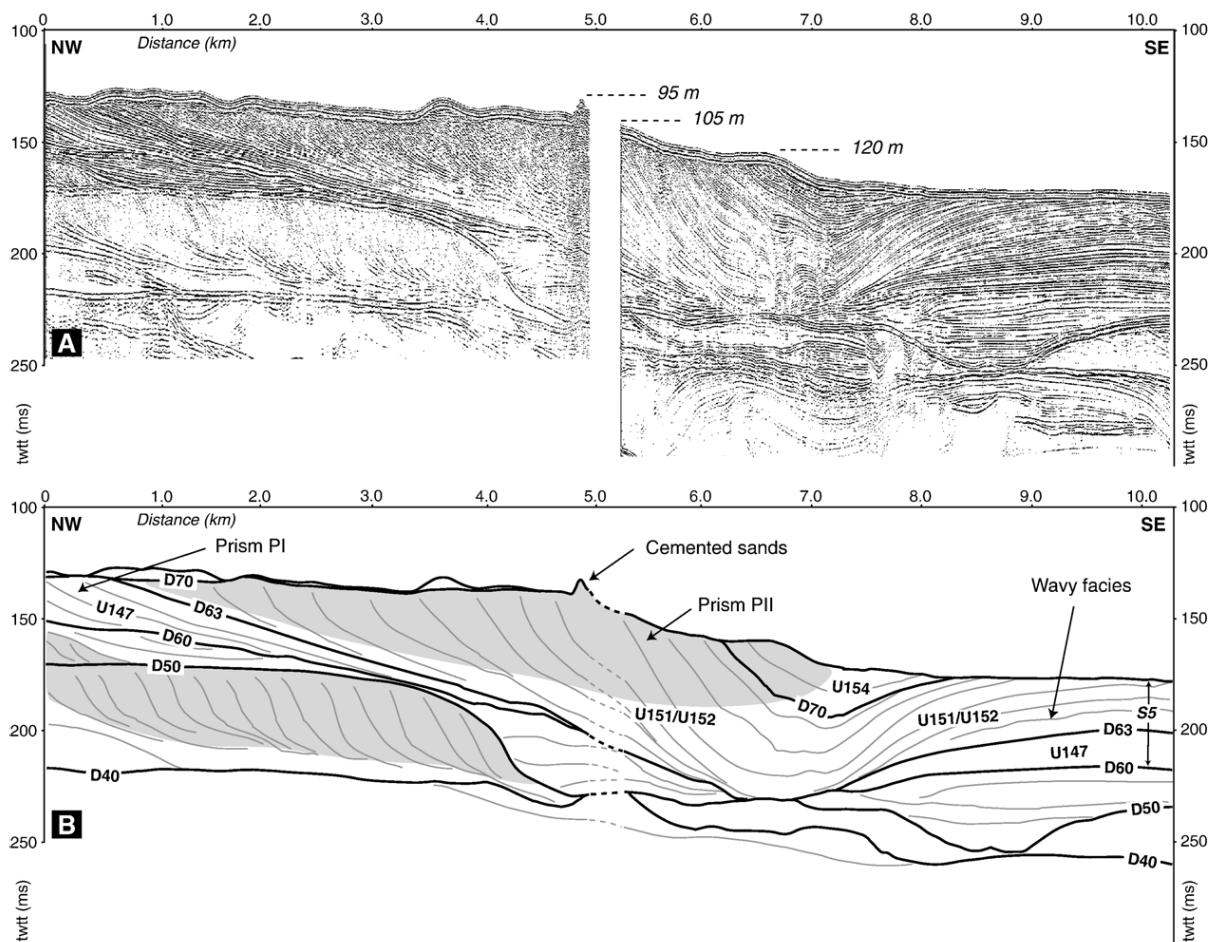
Fig. 8. High-resolution seismic Sparker lines P-7056-7049 (A) and interpretation (B) (position in Fig. 4) across the cemented sands and the easterly Bourcart canyon head. Steps and terraces identified on bathymetric maps are positioned. Note the continuity between high-angle clinoforms of the sandy facies (PII) and low-angle clinoforms of the offshore muds (PI), demonstrating that these deposits formed as forced regressions (see explanation in text). Within U151, U152 and U154, the U-shape of seismic reflections records the infill of a depression incised within U147. This infill runs along a NW–SE direction and connects to the South with the Bourcart canyon head, and to the North to the fluvial drainage network (3 in Fig. 4).

between the two units is locally marked by high-amplitude reflections (D65).

In summary, the stacking pattern of U151 and U152 is characterized by a progressive change from aggradation to progradation of the low-angle clinoforms preserved along the interfluve (Fig. 7). The correlative high-angle reflection clinoforms of the sandy facies (PII) document about 7 km of shoreline progradation (Fig. 8). Despite erosion of the topsets, preservation of the bottomsets can aid estimate the clinoform geometry and does not indicate a major change in sea-level.

Unit U154 is the most distal seismic unit of the prograding wedge. It pinches out at a rather constant depth of about 140 m; its lower boundary (D70) is an erosional discontinuity that truncates the underlying deposits, and progressively becomes conformable sea-

ward. The internal seismic is similar to that of U147, with continuous alternating high and low amplitude reflections (Fig. 7).

Seismic profiles also show, especially within units U151, U152 and U154, a U-shaped morphology of seismic reflections infilling a depression incised in U147. In U151/U152, the reflections are locally discontinuous, recording the instability of the wedge, whereas U154 displays draping facies (Fig. 8A). When mapped in 3D, these depocentres run along a NE–SW direction, and connect to the South with the Bourcart canyon head and to the North to the fluvial network (3 in Fig. 4) described previously.

Unit U155 is only observable on the top of the sandy prism PII and corresponds to a transgressive reworking of underlying deposits (Bassetti et al., 2006-this volume).

4.3. Sedimentary facies

The main lithological and sedimentological characters of 4 piston cores sampled on the Bourcart–Hérault interfluve (Fig. 9), along or very close to a NW–SE Chirp seismic profile shown in Fig. 6, are briefly described here. The ^{14}C dates are summarized in Table 1.

Core MD99-2350 is located at 98 m water depth. It was retrieved from the sandy facies of prism PII, and is therefore only 2.57 m in length (Fig. 9). However, it allows to sample the discontinuity between the fine to medium
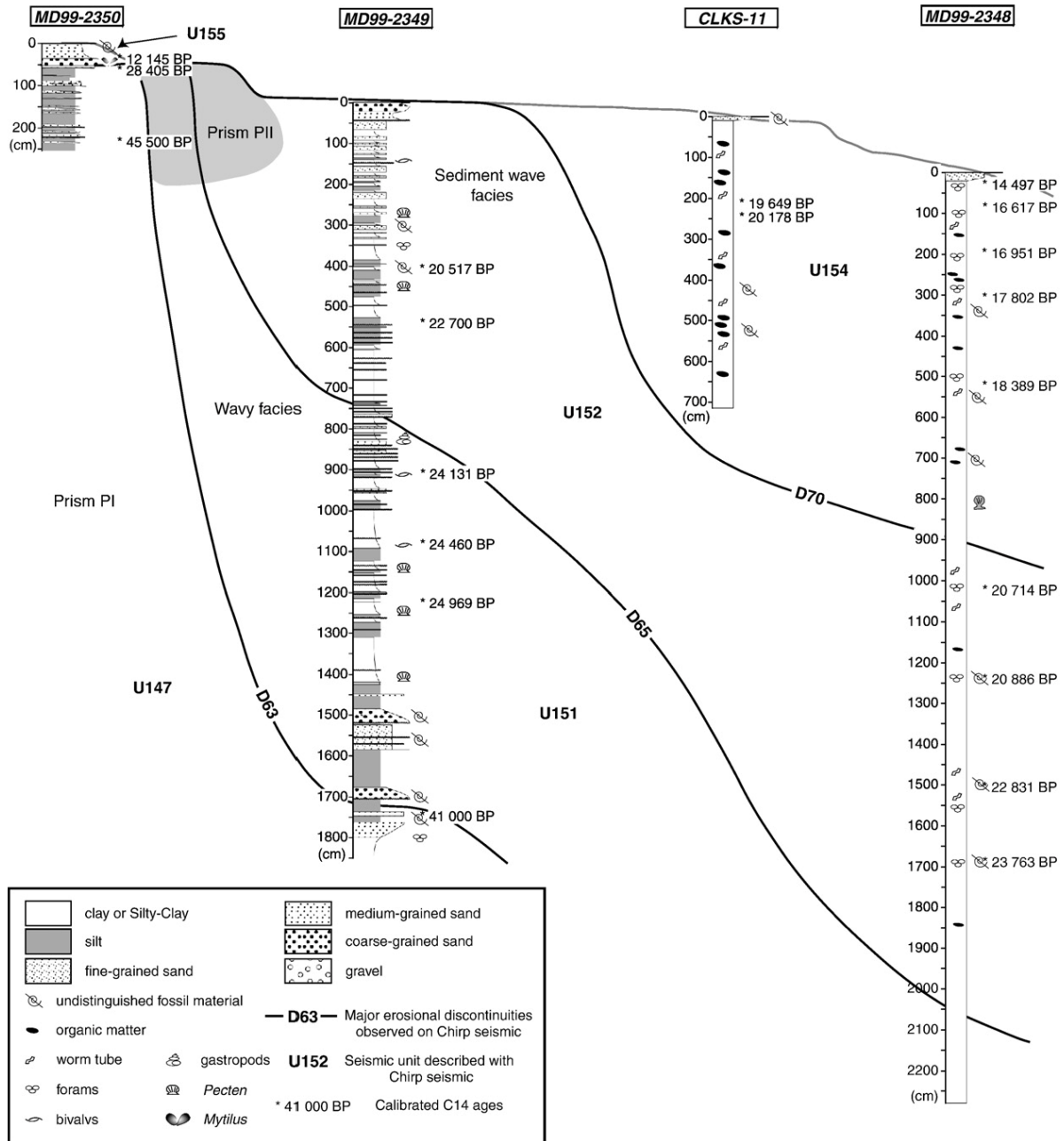

Fig. 9. Correlation between core and seismic data along the Bourcart–Hérault interfluve. Correlations between cores MD99-2350, MD99-2349, CLKS-11 and MD99-2348 are based on seismic reflections and ^{14}C dates, the same time-line corresponding to various sedimentary environments across the shelf edge. The ^{14}C dates are summarized in Table 1.

(median around 200–250 μm) bioclastic, well-sorted sands of unit U155 (50 upper cm in the core) and the alternating sands and silts of the bottomsets of unit U147. The surface bounding the 2 units displays a very coarse lag with shells, pebbles and reworked material (Perez-Belmonte, 2003; Bassetti et al., 2006-this volume). A sample from the top of U147 yields and ages of about 28 cal. kyr BP, and another one from the bottom of U155 gives an age of about 12 cal. kyr BP.

Core MD99-2349 is located at 128 m water depth. It sampled units U147, U151, and U152. U147 consists of clayed silt (mean grain size of 30 μm),

though only 50 cm of this unit were recovered; the unit is dated at about 41 cal. kyr BP (see Table 1 and Figs. 9 and 10) and is overlain by a 3 m thick interval with coarse shelly sands alternating with silts. The boundary between the two intervals likely corresponds to the seismic discontinuity of D63. The upper 15 m of the core show alternating millimetric to centimetric silty clay and silt laminae, with intervals where fine to medium sand beds are more abundant. Sandy or silty beds have sharp or even erosional base and display a clear fining upward trend. Bioturbation is abundant within the fine-grained beds, and generally
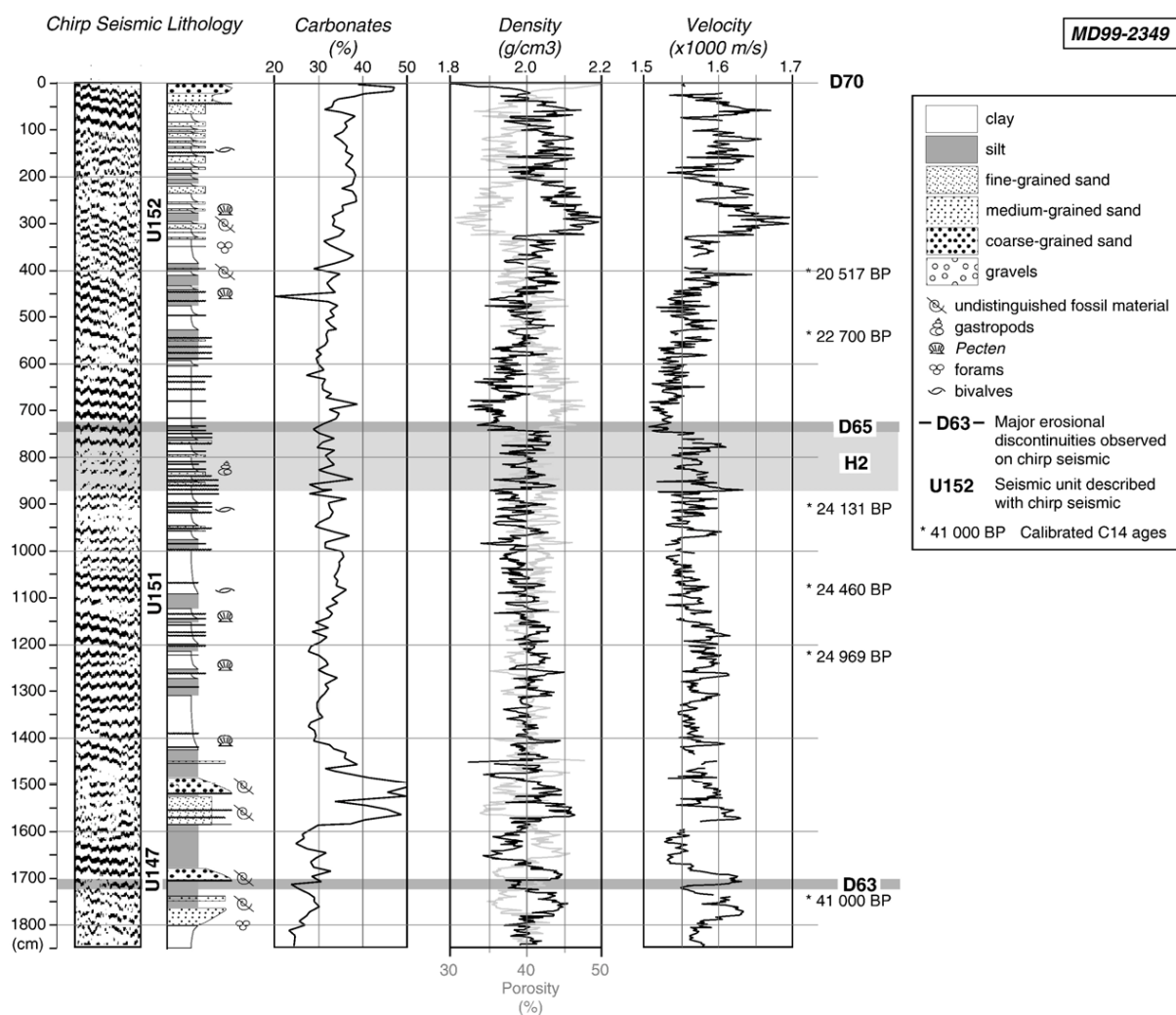

Fig. 10. Chirp seismic section, lithology, carbonate content, density and sonic velocity along core MD99-2349, located at 128 m water depth (position in Fig. 4). This core sampled units U147, U151, and U152, corresponding to a time span estimated to 21 kyr (from 41 to 20 cal. kyr BP; see Table 1 and Fig. 10). The major facies corresponds to alternating millimetric to centimetric silty clay and silt laminae, with intervals where fine to medium sand beds are more abundant. The base of sandy or silty beds is sharp or even erosional, and they display a clear fining upward trend. Note the change in density and sonic velocity below D65 that corresponds to higher sand content (because of increased cascading of cold water during Heinrich Event 2).

incorporates coarser (silty) material from the overlying beds. This pattern is similar to the storm graded beds described by Aigner (1985).

Within the 15–0 m interval, which corresponds to the 28 to 20 cal. kyr BP interval, an overall coarsening upward trend is observed. Between 7.5 and 8.5 m, sand beds are much more abundant and correlate with discontinuity D65 on seismic profiles. This reflection is dated at about 24 cal. kyr BP.

Core MD99-2348 is located at 296 m water depth. It sampled seismic units U154 and U152 (Fig. 9). The core displays homogeneous bioturbated grey silty clay (median of 10 μm at the top of the core, 6 μm at the bottom) with abundant organic matter spots and bioturbation. A thin bed of sand is observed at the top of the core, as on most of other cores sampled around the Bourcart canyon head (Gaudin et al., 2006-this volume). The seismic discontinuity D70, that bounds units U152 and U154, is positioned at about 9 m on the core, and corresponds to a slight change in the density. Sedimentation rate calculated from ^{14}C dates is very high, especially between 21 and 18 cal. kyr BP, where it reaches 2.5 m/kyr. This allows precise dating of the transition between units U152 and U154 (D70) at about 20 cal. kyr BP. The time span represented by U154 ranges from 20 to 15 cal. kyr BP. Holocene deposits are absent in this core.

Core CLKS-11 is located at 157 m water depth and is very similar to core MD99-2348 but only sampled U154 (Fig. 9). The only difference is that organic fragments are more abundant, probably because the core is located in a more proximal position with respect to the MD99-2348. The ^{14}C ages obtained on this core are consistent with those from MD99-2348.

The sedimentary facies, observed on both MD99-2348 and CLKS-11, indicate an offshore environment (Reading and Collinson, 1996) beyond the storm wave base.

4.4. Paleoenvironmental constraints based on fossil content

4.4.1. Temperature

Within the fine-grained fraction of seismic unit U152, cold species of benthic foraminifera (such as *Uvigerina peregrina, Hyalinea baltica*, Cassidulinidae spp.), and planktonic foraminifera (*Globigerina pachyderma* sinistrally coiled, *Globigerina glutinata)* are observed (Bourdillon, 1994). Seismic units U151 and U152 also contain typical cold boreo-celtic guests in the Mediterranean Pleistocene such as the molluscs *Pseudamussium septemradiatum, Chlamys islandica, Arctica islandica, Mya truncata,* and *Buccinum humphreysianum.*

4.4.2. Paleobathymetry

A paleobathymetric reconstruction of core MD99-2349 succession can be proposed. Unit U147 includes mollusc taxa (e.g. the bivalves *Bathyarca grenophia, Kelliella miliaris* and *Venus casina,* the gastropod *Alvania testae* and thecosomatous pteropods), indicative of relatively deep open shelf-upper slope environments (ca. 60–120 m); sandy beds in this same unit contain an assemblage dominated by the serpulid polychaete *Ditrupa arietina* and the bivalve *Corbula gibba,* pointing out a sediment-stressed shelf environment whose bathymetry cannot be established with precision, but hypothesised to be in the range of 30–90 m. Unit U151 between 1700–1500 cm contains mollusc taxa of boreo-celtic significance, such as the gastropod *B. humphreysianum* and the bivalves cf. *Modiolus modiolus, Modiolula phaseolina* (large morphotype), *P. septemradiatum* associated with *Aequipecten opercularis, Astarte sulcata, C. gibba, Turritella* sp. and the bryozoan *Turbicellepora coronopus,* interpreted as indicative of a muddy–silty mid-outer shelf setting comprised between 40–100 m water depth. In the upper part of this unit the macrofossil assemblages still include boreo-celtic (*B. humphreysianum, Arctica islandica, Mya truncata*) and other taxa of lesser climatic significance (e.g., *Nucula* sp., *Yoldia* sp., *Parvicardium minimum, Hiatella arctica* etc.). It documents mid-shelf environments with paleodepth likely in the range of 40–60 m; a pelagic input by Thecosomatous pteropods (*Spiratella* sp.) is a further indication of open marine conditions, while the localised presence of shell layers, serpulid polychaete, minireefs and barnacles (ca. 1450–1460 cm) document times of reduced sediment input. The occurrence of planktonic (e.g., *G. pachyderma* sinistrally coiled, *G. glutinata*) and benthic (*Hyalinea balthica*) foraminifera from units U152 to U147 is a further indication of colder than present (glacial Pleistocene) seawater temperatures at the time of their deposition. Finally the upper part of the succession (U152) has a very important faunal content whereas undetermined bivalve fragments are abundant, together with rotaliid and miliolid foraminifera, and plant remains indicative of active prodeltaic environments.

5. Discussion

We have collected a set of evidence that demonstrate the effect of relative sea-level changes on strata architecture at the shelf edge during the turnaround of LGM. Thanks to the precise ^{14}C dates obtained from cores and cemented beaches along a dip section that allows to identify time-lines, these evidences can be put together into a stratigraphic framework. The detailed stratigraphy

of the Last Glacial Cycle established on the Bourcart–Hérault interfluve (Fig. 7) allows the study of marine accumulation from the shoreface to the upper offshore during the last sea-level lowstand. Taking into consideration both the stratigraphic interpretations and sedimentological information, we evidence rapid fluctuations of
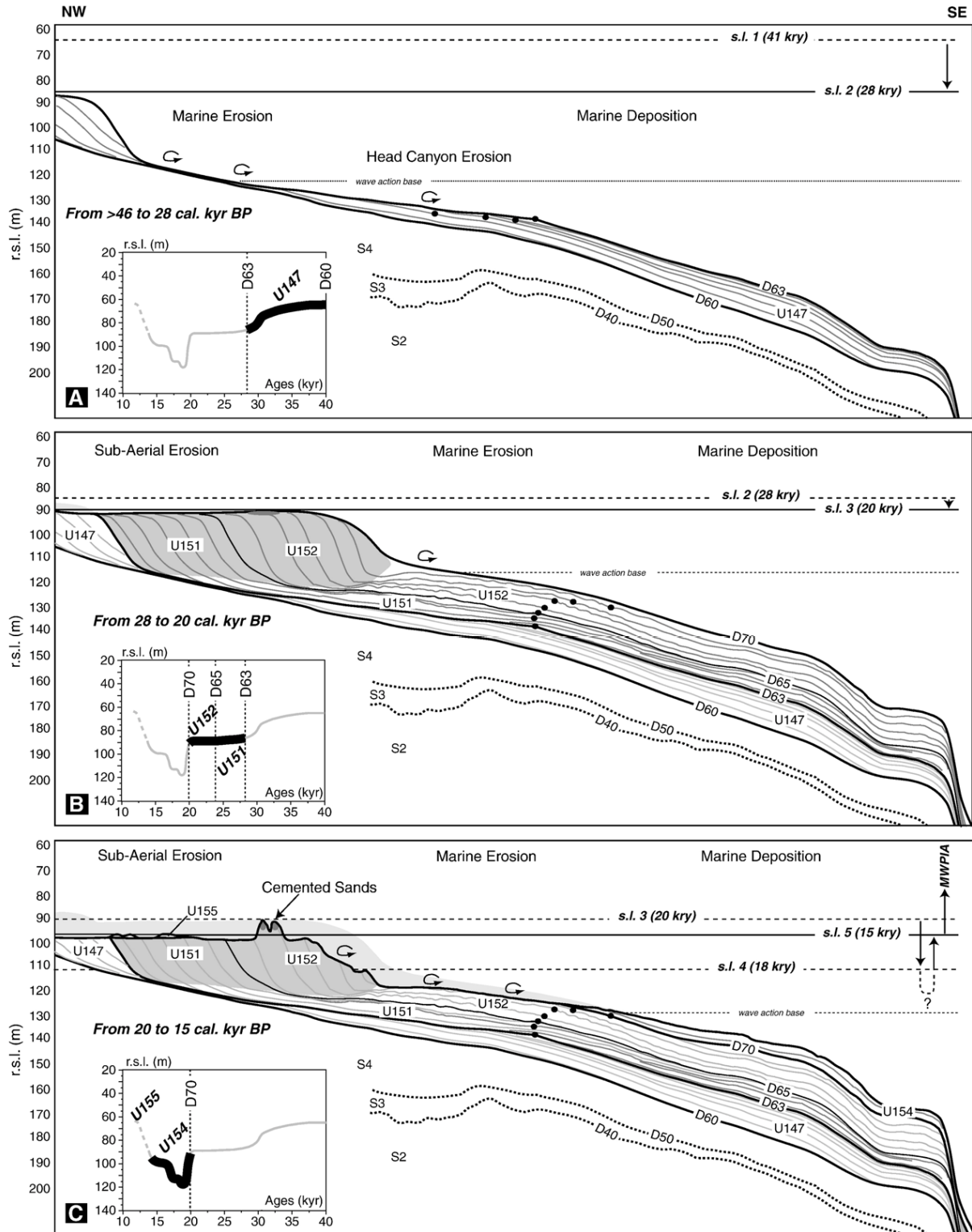
the sedimentary environment (Figs. 7 and 9). Which factors are the causes of the geometric discontinuities that we observe both on the high resolution seismic and inside the sedimentary record described by the cores? These variations in the sedimentation of a beach or prodelta can be explained either by the fast evolution of the paleo-bathymetry, either by changes in the conditions of sedimentation (hydrodynamism) or by fluctuations in sediment supply. What is the relative importance of these processes which variably controlled transport and deposition of sediments from 46 to 15 cal. kyr BP?

5.1. Evidences for regressive processes at the origin of the high-angle clinoforms in S5

On Sparker seismic, the steeply dipping sandy clinoforms often downlap onto an erosional seismic discontinuity which affects the underlying low angle clinoforms (Fig. 6); this geometry led some authors to consider the sandy clinoforms as transgressive para-sequences (Van Wagoner et al., 1990) formed during the overall deglacial sea-level rise (Tesson et al., 2000). In their interpretation, the erosion surface was a ravinement surface separating regressive prodeltaic muds from transgressive overlying sands. However, in places where accommodation was sufficient, such as the Bourcart canyon head (Fig. 8), continuity exists between high-angle (sandy) clinoforms and gently dipping clinoforms, and therefore demonstrates that deposition of the two facies was synchronous. In locations where accommodation was more restricted (Fig. 6), such as the flat outer continental shelf, a zone of erosion and bypass developed between the sandy clinoforms of the shoreface and the muds deposited beyond the storm wave-base (Berné, 1999). Such surfaces, named regressive surfaces of marine erosion (Plint and Nummendal, 2000), form below sea-level under the erosive action of waves and currents. The major erosional surfaces on the interfluve (D60, D63 and D70), located downstream of the sandy prism, formed prior to LGM and bound units showing a shallowing upward trend. They are consequently regressive surfaces of marine erosion linked to downward shifts

of the forced regressive sequence S5, in relation with falls of the wave action base; similar features were described on the Adriatic shelf (Trincardi and Correggiari, 2000; Ridente and Trincardi, 2005). The entire sequence S5 formed during a forced regression, as a seaward and downward shift of the coast line forced by a relative sea-level fall (Posamentier et al., 1992). S5 is topped by transgressive sand bodies and a thin veneer of mobile sands (Bassetti et al., 2006-this volume). The dates obtained in this study allow us to confirm a precise time-frame for the deposition of S5 and overlying deposits. Deposition of units U147 through U152 that compose S5 occurred during the overall sea-level fall, between 46 and 20 cal. kyr BP (Table 1). It should be noted that the deepest evidence of marine erosion detectable on seismic profiles (except around canyon heads where energy is focused) is around 170 m (Fig. 7), far beyond the lowest sea-level scenario for LGM.

The upper part of U147 is dated both at the bottom of cores MD99-2349 and MD99-2350. The time period for the deposition of this unit is estimated older than 41 cal. kyr BP at two different positions on the deposit profile. A date of 28.4 cal. kyr BP is also given at the bottom of U151 within the sandy clinoforms on core MD99-2350 at the erosional surface that corresponds to D63 (analysis performed on complete shell of *Mytilus* sp., indicative of very shallow water environment at the time of deposition). This age post-dates the onset of deposition of U151 and it is consistent with the age of about 25 cal. kyr BP found on core MD99-2349 in the middle part of U151. An age between 20.5 and 20 cal. kyr BP is found for D70 based on dates from cores MD99-2348 and CLKS-11. This is also consistent with an age less than 20,517 cal. kyr BP from core MD99-2349. In addition, cementation of the beach rocks of "Pierres de Sète" occurred at 21 ± 0.4 cal. kyr BP, which corresponds to the end of a regression phase, and therefore to a probable decrease or even stop of the sea-level fall.

In summary, the time-frame for the deposition of units U147, U151 and U152 confirms that they formed between MIS-3 and MIS-2, during a period of sea-level fall.

Fig. 11. Scenario for sedimentation on the Bourcart–Hérault interfluve during the LGM "turnaround". This synthetic NW–SE profile is based on seismic interpretation, lithological and chronological data. A) Evolution *from >46 to 28 cal. kyr BP*: this time interval corresponds to a general decrease of relative sea-level and to the end of deposition of U147. Around 41 cal. kyr BP, rsl is estimated between 45 and 65 m. The best estimate of the interval encompassed by the erosional surface D63 is 41 to 28 cal. kyr BP. This interval corresponds to a major sea-level fall. B) Evolution *from 28 to 20 cal. kyr BP*: this period is interpreted as a phase of stillstand or very slow decrease of sea-level, followed by the onset of renewed sea-level fall (recorded by units U151 and U152). The cementation of beach rocks at 90 m water depth occurred at about 21 cal. kyr BP. C) Evolution *from 20 to 15 cal. kyr BP*. The deposition of seismic unit U154 corresponds to the period of "turnaround" of relative sea-level. Only the fine-grained distal component of the LGM shoreface was preserved, below 140 m water depth. The lowest sea-level is estimated to be at least 110–115 m and the onset of rsl rise between 18 and 17 cal. kyr BP. A slow down of the transgression, between 17 and 15.9 cal. kyr BP, is marked by a bathymetric step at 98–105 m. This period corresponds to the onset of deposition of thin transgressive sand bodies on the outer shelf (U155).

5.2. Scenario for sedimentation on the Bourcart–Hérault interfluve during the LGM turnaround

Geological and chronostratigraphic evidence allow us to propose a scenario for the deposition of seismic units and discontinuities that can be observed throughout the study area (from U147 to U155); this scenario is based on the assumption that the overall subsidence *s.l.* is in the order of 250 m/Myr (Rabineau et al., 2005), equivalent to 5 m for the last 20 kyr. The study area is situated sufficiently far from the former margins of the major ice sheets for sea-level to follow global eustatic changes to a first approximation (Lambeck and Bard, 2000). As to the effect of water loading, a value of about 15 m is proposed for the Gulf of Lions by the same authors. Our scenario, in any event, refers to relative sea-levels (RSL), as measured with respect to the present mean sea-level. It is summarized in Fig. 11.

5.2.1. From >46 to 28 cal. kyr BP

This time interval corresponds to the deposition of the upper part of U147. This unit was sampled at the bottom of cores MD99-2349 and MD99-2350. A paleobathymetry of 80–100 m is indicated by mollusc assemblages at the bottom of core MD99-2349, i.e. at 145 m below present sea-level; it gives a relative sea-level depth of 45 to 65 m at around 41 cal. kyr BP confirmed by the fine-grained composition of sediments. The basinward migration of the offlap break, together with the erosion of topsets in the upper part of the interfluve, suggests a general fall of relative sea-level during the end of deposition of U147.

An early connection of a fluvial system of unknown origin (3 in Fig. 4B) with the Bourcart canyon head was established at the end of this period. This incision is oriented along a NE–SW direction and crosses the interfluve.

Surface D63 corresponds to a major sea-level fall, as evidenced by the abrupt change of sedimentary facies between U147 and U151 in the landward part of the study area (Fig. 8). In the distal part, surface D63 is coeval to the upper most 3 m of U147 on core MD99-2349 (Fig. 10), which correspond to coarse shelly sand, probably reworked and transported seaward from the former shoreline. The best estimate for the time span represented by this surface is 41 to 28 cal. kyr BP.

5.2.2. From 28 to 20 cal. kyr BP

This time interval corresponds to the deposition of U151 and U152 ended by the onset of renewed sea-level fall. This period is interpreted as a phase of stillstand or very slow fall of sea-level for the following reasons:

– the steep clinoforms of the shoreface sands are at a constant depth along a distance of about 7 km (average shoreline progradation of about 0.9 m/yr; Fig. 8);
– the transition from aggradation to progradation of the time-equivalent muddy low-angle clinoforms would result from a progressive decrease of accommodation space (the sediment is progressively bypassed beyond the storm wave-base, when available space is occupied by newly deposited sediment);
– paleobathymetry estimates from macrofauna assemblages within core MD99-2349 indicate a depth of about 50 m in the middle of unit U151 at about 15 m below sea-floor. In unit U152, benthic foraminifera assemblages indicate a depth of about 40 m (see Section 4.4.2. for the details);
– the storm beds observed on core MD99-2349 (Fig. 9) are typically attributed to water depths of 30–40 m (Guillocheau and Hoffer, 1988);
– the overall increase in sand fraction (well illustrated by the upward increase in density and sonic velocity along core MD99-2349; Fig. 10) probably results from progressive infill of available space. Around 20.5 cal. kyr BP, however, the abrupt increase in sand faction is likely related to the onset of sea-level fall;
– cementation of beach rocks (90 m water depth or less if some of the cemented material was eroded) at about 21 cal. kyr BP also requires a fairly stable sea-level. This event would pre-date an episode of renewed sea-level fall.

In the Bourcart canyon head, the end of the 28–20 cal. kyr BP interval is marked by a shift of fluvial connection, from a stream labelled "3" in Fig. 4 to another, labelled "2" and situated further West. The brackish influence observed on the cement of the "Pierres de Sète" beach rocks could result from this fluvial influence.

5.2.3. From 20 to 15 cal. kyr BP

This period corresponds to the deposition of seismic unit U154 and to the period of turnaround of relative sea-level. However, the sediments that could have been deposited between 110 and 140 m during this period were bypassed or eroded, because they were situated above the lowest sea-level, or above the storm wave-base. As a result, only the fine-grained distal component of the LGM shoreface was preserved, below 140 m water depth. The position of the lowest sea-level is difficult to determine precisely, because the topsets of the sandy clinoforms were generally eroded during the ensuing sea-level rise. Consequently, the scarp that occurs at 110–115 m does not represent the position of

the lowest sea-level, but the top of a terrace riser that formed during an ensuing stillstand, as described for instance in lake deposits by Adams and Wesnousky (1998). In any event, it implies that sea-level fell at least down to 110–115 m, and possibly as deep as 140 m rsl Taking into account a subsidence of 5 m and water loading effect of 15 m, the estimation of the corresponding global lowest sea-level would be between 90 −95 and 120 m.The high sedimentation rate between 20 and 18 cal. kyr BP (2.5 m/kyr) can be explained by the vicinity, at that time, of a probable Rhône related shelf-edge delta (1 in Fig. 4), leading to sediment plumes being swept toward the interfluve by the general anti-clockwise circulation.

The timing of the onset of sea-level rise can be estimated from the abrupt decrease in the sedimentation rate, which occurred between 18 and 17 cal. kyr BP. The scarp observed at 98–105 m would represent a decrease in the sea-level rise, which occurred before 15.9 cal. kyr BP (age of the ravinement surface at 99 m water depth, Bassetti et al., 2006-this volume). The progradation of the glacial shoreface (prism PII) which show seaward an upward trend of progressive downlap, is ended by this paleobathymetric step.

The erosion of the "Pierres de Sète" (carving of up to 20 m of sand) took place between 21 and 15 cal. kyr BP, and this age marks the onset of deposition of thin transgressive sand bodies on the outer shelf (U155).

In summary, this scenario requires some variations in the rate of relative sea-level changes, with a drastic drop before 28 cal. kyr BP, a slow-down during the sea-level fall at about 90 m rsl at about 21 cal. kyr BP, a minimum sea-level at least at 110–115 m rsl; the onset of sea-level rise between 18 and 17 cal. kyr BP, and a slow down of sea-level rise at a level of about 98–105 m rsl between 17 and 15.9 cal. kyr BP.

5.3. Heinrich events and seismic reflections

The imprint of Heinrich events was shown in the Alboran Sea (Cacho et al., 2000) and attributed to the intensification of Deep Western Mediterranean Water formation during periods of cooling, in relation with southward displacement of the Polar Front. In the Gulf of Lions, a very distinct cold interval corresponding to Heinrich event 2 (H2) has been evidenced by multi-proxy analysis of core MD99-2348 (Flores et al., 2005). This interval corresponds to an increase in sand fraction along core MD99-2349, between 7.5 m and 8.5 m, dated about at 24 cal. kyr BP; it also corresponds to a seismic reflection (D65) that can be tracked seaward up to the bottom of core MD99-2348. Along this core, there is no clear change in lithology but H2 is marked between 19 and 22.5 m below sea-floor by a peak in abundance of the foraminifer *Neogloboquadrina pachyderma* (*sinistrally coiled*), and in the coccolithophere *Emiliana huxleyi* >4 μm (a cold water morphotype) (Flores et al., 2005).

A similar pattern is observed at the top of this core between 1 and 3.5 m, which corresponds to an age between 16.5 and 18 cal. kyr BP (Berné et al., 2004; Flores et al., 2005). This age matches well with the age of H1 of Bond et al. (1992). Nevertheless, the erosion of unit U152 during relative sea-level rise did not allow preservation of H1 in core MD99-2349.

The process leading to increased sand content must be linked to enhancement of northwesterly winds (Mistral and Tramontane), which control the formation of dense cold water. In the present-day highstand situation, it has been shown that periods of increased northwesterly wind during winter triggers cascading currents (Palanques et al., 2006-this volume); these currents transport sand downslope, as shown by the presence of recent (<100 yr) sand beds buried in muds within the Bourcart canyon head (Gaudin et al., 2006-this volume).

In conclusion, even if there are no IRD (Ice Rafted Debris) in the Gulf of Lions, we can identify a seismic re flection associated to Heinrich event 2, as there are reflections related to IRD in NE Atlantic (Auffret et al., 1998).

6. Conclusion

The new VHR seismic and lithologic data set from the Bourcart–Herault interfluve provide a high-resolution marine sedimentary record of the Last Glacial Maximum at the shelf edge of the Gulf of Lions. Within the last sedimentary sequence S5, which corresponds to the Last Glacial 100 kyr-cycle, several units display a good record of sea-level changes that occurred between 46 and 15 cal kyr BP. This particular interval is only recorded in the critical area constituted by the shelf break (above the major slump scars that cut across the continental slope at about 500 m water depth and deeper). Through time, three zones of connection of fluvial systems with the shelf break can be identified, including a possible distributary of the Rhône.

Because of the high detrital input, sedimentation rate reached a maximum of 2.5 m/kyr between 21–18 kyr. Sediment supply stopped abruptly at 15 kyr, because of the rapid landward shift of fluvial outlets during the deglacial sea-level rise. Geomorphological, sedimentological and paleoenvironmental information

indicate that the fluctuation of sea-level around LGM was punctuated by periods of slowing down and acceleration. Three periods of stillstand are identified and dated at 90 m relative sea-level (21 cal. kyr BP), 110–115 m rsl (18–17 cal. kyr BP), and 98–105 m rsl (before 15.9 cal. kyr BP). The position of relative sea-level during the maximum lowstand is not known, but is at least 115 m. During this time, periods of increased northwesterly winds favoured transport of coarser sediment at the shelf edge, in relation with cascading deep water. This process creates a distinct sandy interval during the period of Heinrich event 2, at the origin of amplitude anomaly on very high resolution seismic data.

Acknowledgements

References

Adams, K.D., Wesnousky, S.G., 1998. Shoreline processes and the age of the Lake Lahontan Highstand in the Jessup embayment, Nevada. Geol. Soc. Amer. Bull. 110, 1318–1332.

Aigner, T., 1985. Storm depositional systems. Lecture Notes in Earth Sciences, vol. 3. Springer Verlag, Berlin. 174 pp.

Almagor, G., 1979. Relict sandstones of Pleistocene age on the continental shelf of Northern Sinai and Israel. Isr. J. Earth-Sci. 28, 70–76.

Aloïsi, J.C., 1986. Sur un modèle de sédimentation deltaïque: contribution à la connaissance des marges passives. Thèse de doctorat d'Etat Thesis, Université de Perpignan, Perpignan, 162 pp.

Aloïsi, J.C., Auffret, G.A., Auffret, J.P., Barusseau, J.P., Hommeril, P., Larsonneur, C., Monaco, A., 1977. Essai de modélisation de la sédimentation actuelle sur les plateaux continentaux français. Bull. Soc. Géol. Fr. 19 (2), 183–195.

Auffret, G., Dennielou, B., Boelaert, A., Bassinot, F., Labeyrie, L., Pujol, C., Loncaric, N., 1998. Physical Properties and Environmental Implications of Thick Heinrich Layers from the Meriadzek Terrace (Bay of Biscay, NE Atlantic Ocean), 6th International Conference on Paleoceanography, Lisbon.

Bard, E., Hamelin, B., Fairbanks, R.G., 1990. U–Th ages obtained by mass spectrometry in corals from Barbados: sea level during the past 130,000 years. Nature 346, 456–458.

Bard, E., Hamelin, B., Arnold, M., Montaggioni, L., Cabioch, G., Faure, G., Rougerie, F., 1996. Deglacial sea-level record from Tahiti corals and the timing of global meltwater discharge. Nature 382, 241–244.

Bard, E., Arnold, M., Hamelin, B., Tisnerat-Laborde, N., Cabioch, G., 1998. Radiocarbon calibration by means of mass spectrometric 230Th/234U and 14C ages of corals. An updated data base including samples from Barbados, Mururoa and Tahiti. Radiocarbon 40 (3), 1085–1092.

Bartov, Y., Stein, M., Enzel, Y., Agnon, A., Reches, Z., 2002. Lake levels and sequence stratigraphy of Lake Lisan, the Late Pleistocene precursor of the Dead Sea. Quat. Res. 57 (1), 9–21.

Bassetti, M.A., Jouët, G., Dufois, F., Berné, S., Rabineau, M., Taviani, M., 2006-this volume. Sand bodies at the shelf edge in the Gulf of Lions (Western Mediterranean): Deglacial history and modern processes. Mar. Geol. 234, 93–109, doi:10.1016/j.margeo.2006.09.010.

Bassinot, F., Labeyrie, L., Vincent, E., Quidelleur, X., Shackleton, N.J., Lancelot, Y., 1994. The astronomical theory of climate and the age of the Brunhes–Matuyama magnetic reversal. Earth Planet. Sci. Lett. 126, 91–108.

Baztan, J., 2004. Formation et évolution des canyons sous-marins du Golfe du Lion: relation avec les cycles glacio-eustatiques. Thèse de Doctorat, UBO-IFREMER, 450 pp.

Baztan, J., Berné, S., Olivet, J.L., Rabineau, M., Aslanian, D., Gaudin, M., Réhault, J.P., Canals, M., 2005. Axial incision: the key to understand submarine canyon evolution (in the western Gulf of Lions). Mar. Pet. Geol. 22 (6–7), 805–826.

Bentounsi, F., 1990. ECORS— Golfe du Lion. Interprétation des profils de sismique réflexion longue écoute-cinématique d'ouverture de la Méditerranée Occidentale. Mémoire de D.E.A. Université de Bretagne Occidentale, Brest. 69 pp.

Berné, S., 1999. Dynamique, architecture et préservation des corps sableux de plateforme. Mémoire d'habilitation à diriger des recherches. Université de Lille 1, Lille. 111 pp.

Berné, S., Gorini, C., 2005. The Gulf of Lions: an overview of recent studies within the French "Margins" Programme. Mar. Pet. Geol. 22 (6–7), 691–693.

Berné, S., Lericolais, G., Marsset, T., Bourillet, J.F., de Batist, M., 1998. Erosional shelf sand ridges and lowstand shorefaces: examples from tide and wave dominated environments of France. J. Sediment. Res. 68 (4), 540–555.

Berné, S., Loubrieu, B., the CALMAR shipboard party, 1999. Canyons and recent sedimentary processes on the western Gulf of Lions margin. First results of the Calmar cruise. C. R. Acad. Sci. Paris 328, 471–477.

Berné, S., Aloïsi, J.C., Baztan, J., Dennielou, B., Droz, L., Dos Reis, T., Lofi, J., Méar, Y., Rabineau, M., 2002. Notice de la carte morpho-

bathymétrique du Golfe du Lion. IFREMER et Région Languedoc Roussillon, Brest. 48 pp.

Berné, S., Rabineau, M., Flores, J.A., Sierro, F.J., 2004. The impact of quaternary global changes on strata formation: exlporation of the shelf edge in the Northwest Mediterranean Sea. Oceanography 17 (4), 92–103.

Bernier, P., Berné, S., Rabineau, M., Baztan, J., 2000. Les Pierres de Sète: un indicateur paléobathymétrique et paléoenvironnemental. In: Berné, S., Guennoc, P., Monaco, A. (Eds.), Atelier Golfe du Lion du GDR Marges, Paris, 8 pp.

Biju-Duval, B., 1984. Les marges continentales françaises de la Méditerranée. In: Boillot, G. (Ed.), Les marges actuelles et fossiles autour de la France. Masson, Paris, pp. 249–334.

Bond, G., Broecker, W., Johnsen, S., McManus, J., Labeyrie, L., Jouzel, J., Bonani, G., 1993. Correlations between climate records from North Atlantic sediments and Greenland ice. Nature 365, 143–147.

Bond, G., Heinrich, H., Broecker, W., Labeyrie, L., McManus, J., Andrews, J., Huon, S., Jantschik, R., Clasen, S., Simet, C., Tedesco, K., Klas, M., Bonani, G., Ivy, S., 1992. Evidence for massive discharges of icebergs into the North Atlantic Ocean during the last glacial period. Nature 360, 245–249.

Bossuet, G., Ruffaldi, P., Magny, M., Richard, H., Mouthon, J., 1996. Dynamique et approche quantitative des remplissages fini-et postwürmiens du bassin lacustre de Cerin (Jura, France). Bull. Soc. Géol. Fr. 167 (4), 483–494.

Bourdillon, C., 1994. Micropaléontologie de sédiments de sondage dans le Golfe du Lion (Mer Méditerranée). BRGM internal report N1864, Orléans. 15 pp.

Cacho, I., Grimalt, J.O., Pelejero, C., Canals, M., Sierro, F.J., Flores, J.A., Shackleton, N., 1999. Dansgaard-Oeschger and Heinrich event imprints in Alboran Sea paleotemperatures. Paleoceanography 14 (6), 698–705.

Cacho, I., Grimalt, J.O., Sierro, F.J., Shackleton, N., Canals, M., 2000. Evidence for enhanced Mediterranean thermohaline circulation during rapid climatic coolings. Earth Planet. Sci. Lett. 183, 417–429.

Cattaneo, A., Correggiari, A., Marsset, T., Thomas, Y., Marsset, B., Trincardi, F., 2004. Seafloor undulation pattern on the Adriatic shelf and comparison to deep-water sediment waves. Mar. Geol. 213 (1–4), 121–148.

Chappell, J., Polach, H., 1991. Post-glacial sea-level rise from a coral record at Huon Peninsula, Papua New Guinea. Nature 349 (10), 147–149.

Clark, P.U., Mix, A.C., 2002. Ice sheets and sea level of the Last Glacial Maximum. Quat. Sci. Rev. 21, 1–7.

Clauzon, G., 1974. L'hypothèse eustatique et le creusement pré-pliocène de la vallée du Rhône. Ann. Géogr. 456, 129–140.

Dansgaard, W., Johnsen, S.J., Clausen, H.B., Dahl-Jensen, D., Gundestrup, N.S., Hammer, C.U., Hvidberg, C.S., Steffensen, J.P., Sveinbjörns-dottir, A.E., Jouzel, J., Bond, G., 1993. Evidence for general instability of past climate from a 250-kyr ice-record. Nature 364, 218–220.

Droz, L., Bellaiche, G., 1985. Rhône deep-sea fan: morphostructure and growth pattern. Am. Assoc. Pet. Geol. Bull. 69, 460–479.

Durrieu de Madron, X., 1992. Hydrography and nepheloid structures in the Grand-Rhône canyon. Cont. Shelf Res. 457–477.

Ehlers, J., 1996. Quaternary and Glacial Geology. Wiley, New York. 578 pp.

Fairbanks, R.G., 1989. A 17,000-year glacio-eustatic sea level record: influence of glacial melting rates on the Younger Dryas event and deep-ocean circulation. Nature 342, 637–642.

Flores, J.A., Sierro, F.J., Pérez-Folgado, M., Colmenero-Hidalgo, E., Gravalosa, J.M., Bárcena, M.A., Grimalt, J., Berné, S., Dennielou, B., Curtis, J.H., Hodell, D.A., 2005. Abrupt climatic changes

during the last climatic cycles in the Gulf of Lions (Western Mediterranean) revealed by micropaleontological and geochemical tools, European Geosciences Union (EGU). Geophys. Res. Abstr. Vienna 02208.

Gaudin, M., Berné, S., Jouanneau, J.-M., Palanques, A., Puig, P., Mulder, T., Cirac, P., Rabineau, M., Imbert, P. 2006-this volume. Massive sand beds attributed to deposition by dense water cascades in the Bourcart canyon head, Gulf of Lions (northwestern Mediterranean Sea). Mar. Geol. 234, 111–128, doi:10.1016/j.margeo.2006.09.020.

Gensous, B., Tesson, M., 1996. Sequence stratigraphy, seismic profiles, and cores of Pleistocene deposits on the Rhône continental shelf. Sediment. Geol. 105, 183–190.

Gensous, B., Williamson, D., Tesson, M., 1993. Late-Quaternary transgressive and highstand deposits of a deltaic shelf (Rhône delta, France). In: Posamentier, H.W., Summerhayes, C.P., Haq, B.A., Allen, G.P. (Eds.), Sequence Stratigraphy and Facies Associations. International Association of Sedimentologists Special Publication, vol. 18. Blackwell, Oxford, pp. 197–212.

Gorini, C., Le Marrec, A., Mauffret, A., 1993. Contribution to the structural and sedimentary history of the Gulf of Lions (Western Mediterranean) from the ECORS profiles, industrial seismic profiles and well data. Bull. Soc. Géol. Fr. 164 (3), 353–363.

Gueguen, E., 1995. La Méditerranée Occidentale: un véritable océan. Exemple de segmentation des marges et de hiatus cinématiques. Implications sur les processus d'amincissement crustal. Thèse de Doctorat, Université de Bretagne Occidentale, Brest, 281 pp.

Guillocheau, F., Hoffer, M., 1988. Zonation des dépôts de tempêtes en milieu de plateforme: le modèle des plateformes nord-gondwanienne et armoricaine à l'Ordovicien et au Dévonien. C. R. Acad. Sci. Paris 307, 1909–1916.

Heinrich, H., 1988. Origin and consequences of cyclic ice rafting in the Northeast Atlantic Ocean during the past 130,000 years. Quat. Res. 29, 142–152.

Hsü, K.J., Cita, M.B., Ryan, W.B.F., 1973. The Origine of the Mediterranean Evaporites, Initial Reports of the Deep Sea Drilling Project. U.S. Government Printing Office, Washington, D.C., pp. 1203–1231.

Imbrie, J., Hays, J.D., Martinson, D.G., McIntyre, A., Mix, A.C., Morley, J.J., Pisias, N.G., Prell, W.L., Shackleton, N.J., 1984. The orbital theory of pleistocene climate: support from a revised chronology of the marine d O^{18} record. In: Berger, A., Imbrie, J., Hays, J., Kukla, G., Saltzman, B. (Eds.), Milankovitch and Climate. Series C: Mathematical and Physical Sciences.

Labeyrie, L.D., 1987. Variations in mode of formation and temperature of oceanic deep waters over the past 125,000 years. Nature 327 (6122), 477–482.

Labeyrie, L.D., 1989. Une courbe du niveau marin sur 150 000 ans. d'après Labeyrie, 1987, pers. com.

Lambeck, K., Bard, E., 2000. Sea-level changes along the French Mediterranean coast for the past 30,000 years. Earth Planet. Sci. Lett. 175, 203–222.

Lee, H.J., Syvitski, J.P.M., Parker, G., Orange, D., Locat, J., Hutton, E.W.H., Imran, J., 2002. Distinguishing sediment waves from slope failure deposits: field examples, including the 'Humboldt slide', and modelling results. Mar. Geol. 192 (1–3), 79–104.

Lericolais, G., Allenou, J.P., Berné, S., Morvan, P., 1990. A new system for acquisition and processing of very high-resolution seismic reflection data. Geophysics 55 (8), 1036–1046.

Lofi, J., Rabineau, M., Gorini, C., Berné, S., Clauzon, G., De Clarens, P., Tadeu Dos Reis, A., Mountain, G.S., Ryan, W.B.F., Steckler, M.S., Fouchet, C., 2003. Plio-Quaternary prograding clinoform

wedges of the western Gulf of Lion continental margin (NW Mediterranean) after the Messinian Salinity Crisis. Mar. Geol. 198 (3–4), 289–317.

Locker, S.D., Hine, A.C., Tedesco, L.P., Shinn, E.A., 1996. Magnitude and timing of episodic sea-level rise during the last deglaciation. Geology 24 (9), 827–830.

Martinson, D.G., Pisias, N.G., Hays, J.D., Imbrie, J., Moore Jr., T.C., Shackleton, N.J., 1987. Age dating and the orbital theory of the ice ages: development of a high-resolution 0 to 300,000-year chrono-stratigraphy. Quat. Res. 27, 1–29.

Migeon, S., Savoye, B., Zanella, E., Mulder, T., Faugères, J.C., Weber, O., 2001. Detailed seismic-reflection and sedimentary study of turbidite sediment waves on the Var Sedimentary Ridge (SE France): significance for sediment transport and deposition and for the mechanisms of sediment-wave construction. Mar. Pet. Geol. 18, 179–208.

Millot, C., 1990. The Gulf of Lions' hydrodynamics. Cont. Shelf Res. 10 (9–11), 885–894.

Millot, C., 1999. Circulation in the Western Mediterranean Sea. J. Mar. Syst. 20, 423–442.

Mitchum, R.M., Vail, P.R., Sangree, J.B., 1977. Seismic stratigraphy and global changes of sea level, part 6: stratigraphic interpretation of seismic reflection patterns in depositional sequences. In: Payton, C.E. (Ed.), Seismic Stratigraphy — Application to Hydrocarbon Exploration. AAPG, vol. 26, pp. 117–133. Tulsa, Oklahoma.

Myers, P.G., Haines, K., Rohling, E.J., 1998. Modelling the paleo-circulation of the Mediterranean: the Last Glacial Maximum and the Holocene with emphasis on the formation of Sapropel. Paleoceanography 13, 586–606.

Palanques, A., Durrieu de Madron, X., Puig, P., Fabres, J., Guillén, J., Calafat, A., Canals, M., Bonnin, J., 2006-this volume. Suspended sediment fluxes and transport processes in the Gulf of Lions submarine canyons. The role of storms and dense water cascading Mar. Geol. 234, 43–61, doi:10.1016/j.margeo.2006.09.002.

Perez-Belmonte, L., 2003. Enregistrement de la dernère transgression dans le Gulf du Lion. Memoire DEA. University of Lille, p. 52.

Plint, A.G., Nummendal, D., 2000. The falling stage systems tract: recognition and importance in sequence stratigraphy. In: Hunt, D., Gawthorpe, R.L. (Eds.), Sedimentary Responses to Forced Regressions. Geological Society, London, pp. 1–17.

Posamentier, H.W., Allen, G.P., James, D.P., Tesson, M., 1992. Forced regressions in a sequence stratigraphic framework: concepts, examples and exploration significance. Am. Assoc. Pet. Geol. Bull. 76, 1687–1709.

Rabineau M., 2001. Un modèle géométrique et stratigraphique des séquences de dépôts quaternaires de la plate-forme du Golfe du Lion : enregistrement des cycles glacioeustatiques de 100 000 ans. Thèse de Doctorat, Université de Rennes 1 and IFREMER, 392–70 pp. (2 vols) http://www.ifremer.fr/docelec.

Rabineau, M., Berné, S., Ledrezen, E., Lericolais, G., Marsset, T., Rotunno, M., 1998. 3D architecture of lowstand and transgressive Quaternary sand bodies on the outer shelf of the Gulf of Lion, France. Mar. Pet. Geol. 15, 439–452.

Rabineau, M., Berné, S., Aslanian, D., Olivet, J.L., Joseph, P., Guillocheau, F., Bourillet, J.F., Le Drezen, E., Grangeaon, D., 2005. Sedimentary sequences in the Gulf of Lion: a record of 100,000 years climatic cycles. Mar. Pet. Geol. 22 (6–7), 775–804.

Reading, H.G., Collinson, J.D., 1996. Clastic coasts. In: Reading, H.G. (Ed.), Sedimentary Environments; Processes, Facies and Stratig-raphy. Blackwell Scientific Publications, Oxford, p. 688.

Ridente, D., Trincardi, F., 2005. Pleistocene "muddy" forced-regression deposits on the Adriatic shelf: a comparison with

prodelta deposits of the late Holocene highstand mud wedge. Mar. Geol. 222–223, 213–233.

Rohling, E.J., Fenton, M., Jorissen, F.J., Bertrand, P., Ganssen, G., Caulet, J.P., 1998. Magnitudes of sea level lowstands of past 500,000 years. Nature 394, 162–165.

Ruddiman, W.F., 1977. North Atlantic ice-rafting: a major change 75000 years before present. Science 196, 1208–1211.

Ruddiman, W.F., McIntyre, A., Raymo, M., 1986. Paleoenvironmental results from North Atlantic sites 607 and 609. In: Orlofsky, S. (Ed.), Initial Reports of the Deep Sea Drilling Project, Washington, pp. 855–878.

Schock, S.G., Leblanc, L.R., Mayer, L.A., 1989. Chirp subbottom profiler for quantitative sediment analysis. Geophysics 54, 445–450.

Shackleton, N.J., 1977. The oxygen isotope stratigraphic record of the Late Pleistocene. Philos. Trans. R. Soc. Lond., B 280, 169–182.

Shackleton, N.J., 1987. Oxygen isotopes, ice volume and sea-level. Quat. Sci. Rev. 6, 183–190.

Shackleton, N.J., 2000. The 100,000-year Ice-Age cycle found to lag temperature, carbon dioxide, and orbital eccentricity. Science 289, 1897–1902.

Siddall, M., Rholing, E.J., Almogi-Labin, A., Hemleben, C., Meischner, D., Schmelzer, I., Smeed, D.A., 2003. Sea-level fluctuations during the last glacial cycle. Nature 423, 853–858.

Sioni, S., 1997. Mer Ionienne et Apulie depuis l'ouverture de l'Océan Alpin. Thèse de Doctorat, Université de Bretagne Occidentale, Brest.

Skene, K.I., Piper, D.J.W., Aksu, A.E., Syvitski, J.P.M., 1998. Evaluation of the global oxygen isotope curve as a proxy for Quaternary sea level by modeling of delta progradation. J. Sediment. Res. 68 (6), 1077–1092.

Stuiver, M., Reimer, P.J., Bard, E., Beck, J.W., Burr, G.S., Hughen, K.A., Kromer, B., McCormac, F.G., Van Der Plicht, J., Spurk, M., 1998. INTCAL98 Radiocarbon age calibration 24,000–0 cal BP. Radiocarbon 40, 1041–1083.

Tesson, M., Allen, G.P., Ravenne, C., 1993. Late Pleistocene shelf-perched lowstand wedges on the Rhône continental shelf. In: Posamentier, H.W., Summerhayes, C.P., Haq, B.A., Allen, G.P. (Eds.), Sequence Stratig-raphy and Facies Associations. . IAS Spec. Pub., vol. 18. Blackwell Sci. Pub., Oxford, pp. 183–196.

Tesson, M., Gensous, B., Ravenne, C., 1994. Architecture of Pleistocene deposits of the Languedoc shelf (Gulf of Lions, France). Relations with Glacio-eustatic Cycles and Stratigraphic Implications, 15th IAS Regional Meeting, Ischia, pp. 401–403.

Tesson, M., Posamentier, H., Gensous, B., 2000. Stratigraphic organisation of Late Pleistocene deposits of the western part of the Rhone shelf (Languedoc shelf) from high resolution seismic and core data. A.A.P.G. Bull. 84 (1), 119–150.

Thunell, R., Rio, D., Sprovieri, R., Vergnaud-Grazzini, C., 1991. An overview of the post-Messinian paleoenvironmental history of the Mediterranean. Paleoceanography 6 (1), 143–164.

Trincardi, F., Correggiari, A., 2000. Quaternary forced regression deposits in the Adriatic Basin and the record of composite sea-level cycles. In: Hunt, D., Gawthorpe, R.L. (Eds.), Sedimentary Responses to Forced Regressions. Geological Society, London, pp. 245–269.

Van Wagoner, J.C., Mitchum, R.M., Campion, K.M., Rahmanian, V.D., 1990. Siliciclastic sequence stratigraphy in well logs, cores and outcrops: Concepts for high resolution correlation of time and facies. Methods in Exploration Series, vol. 7. American Association of Petroleum Geologists. 55 pp.

Waelbroeck, C., Labeyrie, L.D., Michel, E., Duplessy, J.-C., McManus, J., Lambeck, K., Balbon, E., Labracherie, M., 2002. Sea level and deep water changes derived from benthic foraminifera isotopic record. Quat. Sci. Rev. 21 (1–3), 295–305.

Vegetation dynamics in southern France during the last 30 ky BP in the light of marine palynology

Célia Beaudouin[a,b,*], Gwénaël Jouet[c,d], Jean-Pierre Suc[a], Serge Berné[d], Gilles Escarguel[a]

[a]UMR CNRS 5125 Laboratoire PaléoEnvironnements et PaléobioSphère, Université Claude Bernard Lyon 1,
Campus La Doua, Bâtiment Géode, 2 rue Dubois, 69622 Villeurbanne Cédex, France
[b]Department of Earth Sciences, Sun Yat-sen University, 135 Xin Gang Xi Lu, 510275 Guangzhou, China
[c]UMR CNRS 6538 Domaines océaniques, Institut Universitaire Européen de la Mer, 1 Place Copernic, 29280 Plouzané, France
[d]Laboratoire Environnements Sédimentaires, Géosciences Marines, IFREMER, Centre de Brest, BP 70, 29280 Plouzané, France

Abstract

The composition of the glacial vegetation of southern French plains has been a matter of debate for several decades. Vegetation is considered as steppic according to French and Spanish lacustrine pollen records whereas cave deposits suggest the presence of mesothermophilous trees through the Last Glacial Maximum. In our paper, we display new palynological records from marine sediments of the Gulf of Lions. They indicate the presence of *Abies*, *Picea* and deciduous *Quercus* in the Gulf of Lions, certainly located in the drainage basins of the Pyreneo-Languedocian rivers. These populations that were sensitive to short climatic events during Marine Isotopic Stage 2 could have been linked to northeastern Spanish and southeastern French relicts already evidenced by phylogenetic data. These trees were absent from the Rhone drainage basin during the deglaciation and certainly also disappeared from the Pyreneo-Languedocian drainage basins from ca 17 to 15 ky cal BP. Finally, the Last Glacial Maximum does not appear as stable, cold and dry as previously thought.
© 2007 Elsevier Ltd. All rights reserved.

1. Introduction

The composition of West-European vegetation during the Last Glacial and in particular during the Last Glacial Maximum (LGM) has been a matter of debate for several decades (e.g. Tzedakis et al., 2002, 2003; Stewart, 2003). Two models were developed. The first merely suggests the existence of two bioprovinces: most of European vegetation would be represented by steppe while southwards (i.e. in southern Spain, Italy and Balkan Peninsula) mesophilous trees would have survived in favourable climatic areas (e.g. Elenga et al., 2000; Taberlet and Cheddadi, 2002). This model was built on 11 long lacustrine sequences, on several well-dated macroremains and also from the Holocene expansion pathways reconstructed by phyloge-

netic and pollen studies (Huntley and Birks, 1983; Hewitt, 1999; Petit et al., 2002). In this model, the northern tree limit is not well constrained. Several authors suggested that conifers could have survived out of these refugia (e.g. Huntley and Birks, 1983; Bennett et al., 1991). Tzedakis (2004) proposed a tree limit at 45 46°N. But several authors suggested there were no trees (except *Pinus*) in France during the Last Glacial Maximum (Reille and Lowe, 1993). A second model was developed in parallel and suggests the presence of mesophilous trees as well as temperate mammals out of these southern refugia. They would have survived in protected valleys benefiting from a microclimate (Stewart and Lister, 2001; Willis and Van Andel, 2004). It would explain the late-Pleistocene non-analogue mammalian assemblages (i.e. corresponding to a mixture of steppic mammals like *Bison priscus*, *Equus* sp., *Mammuthus primigenius* and also temperate mammals now living under a closed forest canopy like *Cervus elaphus* or *Sus scrofa*). This model is mainly supported by palynological studies made on cave sediments also containing

*Corresponding author. Department of Earth Sciences, Sun Yat-sen University, 135 Xin Gang Xi Lu, 510275 Guangzhou, China.
Tel.: +86 20 84 11 10 68; fax: +86 20 84 11 23 90.
E-mail address: celia.beaudouin@hotmail.com (C. Beaudouin).

mammals. It is often criticized using two arguments: (1) the ecology of mammals and in particular their adaptability for what concerns their ecological niches would be poorly understood, and (2) these occurrences (mammals, pollen or charcoals) would correspond to reworking (see McGarry and Caseldine (2004) for a review). Choosing between the two models has important consequences for our understanding of the climate of Western Europe, the ecology and evolution (Davis and Shaw, 2001). The presence of mammals or plant taxa out of southern refugia would either imply a more temperate climate or their greater capacity of adaptation to the climate. In particular, the reality of non-analogue assemblages has consequences on our understanding of present-day ecosystems, their link with climate and their capacity to face climatic changes.

The composition of southern France vegetation (i.e. between ca 42 and 45°N) during the LGM is a part of this debate. The lacustrine data suggesting the absence of mesothermophilous trees (Fig. 1) are scarce and mainly situated at high altitudes (Beaudouin et al., 2005a). On the contrary, many palynological studies carried out on caves show the presence of mesothermophilous taxa at mid-latitudes such as deciduous *Quercus, Carpinus, Tilia* or *Juglans* during interstadials of Marine Isotopic Stage 2 (MIS) (Lebreton et al., 2004). However, pollen is extracted from different sediment granulometries (from silts to coarse sands) leading to different degradation intensities and to an over-representation of some taxa like the Asteraceae. Furthermore, the chronology is supposed to be particularly discontinuous and not well constrained. For these reasons, many palynologists often consider that pollen assemblages from caves are not suitable to reconstruct palaeovegetation. The recent discussion be-

tween d'Errico and Sánchez-Goñi (2003) and Carrión (2004) illustrates this debate.

In order to reconstruct the palaeovegetation of southern France, new sequences were acquired in marine sediments from the Gulf of Lions. We focussed on the area where sedimentation rate was very high during the Last Glacial in order to acquire high-resolution pollen data. Preliminary records (Acherki, 1997; Beaudouin et al., 2005a) displayed high amounts of pollen of *Picea, Abies* and also deciduous *Quercus* for the MIS 3 and 2 leading to a first interpretation of the presence of a refugium in southern French plains. But this first test was based on short cores not covering the entire MIS 2, with weak chrono-stratigraphic constraints, which did not allow a full interpretation of palynological data. Therefore, we studied three new sequences positioned in well-known palaeogeographic and chrono-stratigraphic contexts (Berné et al., 2004; Rabineau et al., 2005). They almost cover the last 30 ky. The multi-proxy approach applied on these sequences helps to better constrain the palynological signal in order to reconstruct the palaeovegetation dynamics around MIS 2. In particular, we aim at:

(1) precisely determining the location and the vegetation structure in southern France for the LGM,
(2) highlighting the Lateglacial history of this vegetation and discussing the contribution of these refugia to present-day populations of trees,
(3) determining the link between short climatic events and the vegetation of southern France.

2. General settings

2.1. Present-day vegetation, hydrology and sedimentology

The present-day vegetation of the studied area (Noirfalise et al., 1987) covers the northern part of the Mediterranean climatic zone and the temperate climatic zone (Fig. 2). The Mediterranean vegetation belongs to the Meso-Mediterranean belt. It is bounded by coast-line southward and finishes at 500 m in altitude. It corresponds to the development of sclerophyllous forests with evergreen *Quercus* accompanied by *Laurus nobilis*. The degradation of these forests corresponds to mattorals where *Quercus ilex* forests dominate. The Supra-Mediterranean belt is mainly composed of *Quercus pubescens* associated to *Buxus sempervirens*. The temperate zone corresponds to deciduous oak mixed forests in plains (<700 m). The temperate hills and mountains, i.e. the northern part of the Alps as well as the Massif Central is characterized by the development of *Fagus* from 700 to 1000 m high. *Fagus* is mixed with *Abies* in higher reliefs. Mountainous forests of conifers occur from 1450 to 2500 m high. The Alpine belt begins at ca 2000 2300 m being composed of Ericaceae with Poaceae, Fabaceae and Cyperaceae.
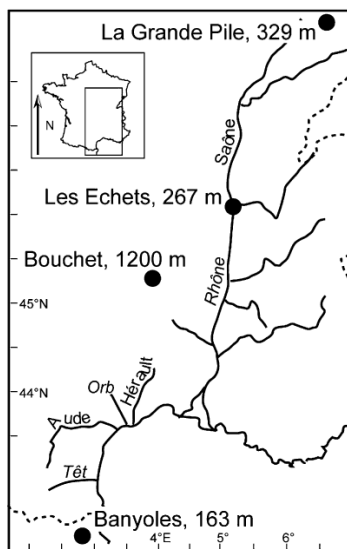

Fig. 1. Location of lacustrine French and Spanish sites covering the last 30 ky and generally used for vegetation reconstructions.
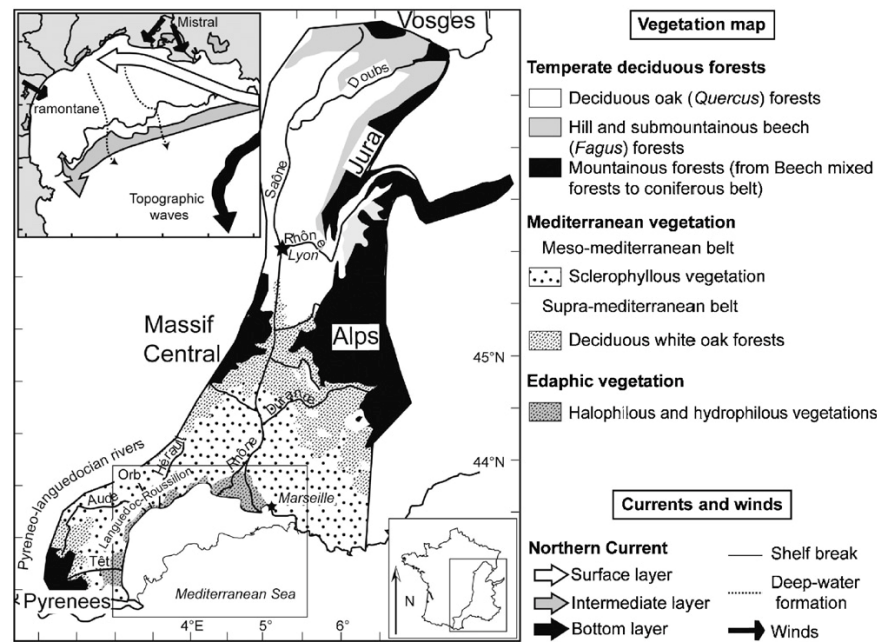
Fig. 2. Simplified vegetation map of the present-day vegetation and main currents and winds in the Gulf of Lions (from Noirfalise et al., 1987; Millot, 1990).

The Mediterranean Sea is characterized by thermohaline circulation: surface water coming from the North Atlantic Ocean enters the Mediterranean basin while Mediterranean deep-water outflows. The circulation in the Gulf of Lions is wind-dependant (Millot, 1990). Two cold winds blowing all year long from the North and the North-west (i.e. Mistral and Tramontane) induce downwellings and deep-water formations (Fig. 2). A secondary wind, coming from the Southeast brings warm air masses sometimes blowing intensely (generally from autumn to spring) and can influence the distribution of sediments down to ten metres of bathymetry. The main surface current of the Gulf of Lions is a gyre called the North-Mediterranean current (Millot, 1999).

The shelf in the Gulf of Lions is maximum 70 km wide. The continental slope is incised by submarine canyons that develop from the shelf break to the rise (Fig. 3). The shelf is made up of terrigenous sediment mainly originating (i.e. 80%) from the Rhone River (Aloïsi et al., 1979). The smaller western rivers (i.e. Tech, Têt, Agly, Aude, Orb and Hérault) deliver the remaining fraction. In contrast, aeolian inputs are negligible (Węgrzynek et al., 1997). At the river mouth, several water layers enriched in particles are formed. The bottom nepheloid layer develops at the mouth near the bottom (Aloïsi et al., 1979; Roussiez et al., 2005). It corresponds to a continuous dense flow, which spreads over the shelf. Its influence weakens from the river mouth to the outer shelf and becomes negligible on the slope (Aloïsi et al., 1979; Monaco et al., 1999). Resuspension from the shelf is the main way to bring terrigenous particles

on the slope and into the canyons (Courp and Monaco, 1990; Durrieu De Madron et al., 1999; Monaco et al., 1999; Frignani et al., 2002).

2.2. Sedimentary history of the Gulf of Lions

The shelf of the Gulf of Lions is made up of Plio-Quaternary sediments (Lofi et al., 2003; Duvail et al., 2005). Rabineau et al. (2005) outlined the depositional pattern of the last 540 ky in the Bourcart-Hérault interfluve, where the upper five sedimentary sequences were assigned to the 100 ky glacio-eustatic cycles, based on stratigraphic modelling (Fig. 4). Within a glacial/inter-glacial cycle, the deposition is maximum at the shelf edge during the end of sea-level fall and lowstand. Whereas most of sedimentation occurs on the inner shelf during deglacial and interglacial conditions, the outer shelf experiences starvation during this interval (Bassetti et al., 2004). The source of sediment at the shelf edge was probably mixed during the last glacial: there is evidence of a connection of the Hérault canyon to a large system including the Rhone and the Hérault rivers, whereas the Bourcart canyon was probably connected both to the Rhone and to a Pyrenean river (Berné et al., 2002) (Fig. 3).

2.3. Reliability of pollen signal

The reliability of marine palynological data has been a matter of debate since the 1950s (see Beaudouin et al., in press; Hooghiemstra et al., 2006 for a review). Especially,
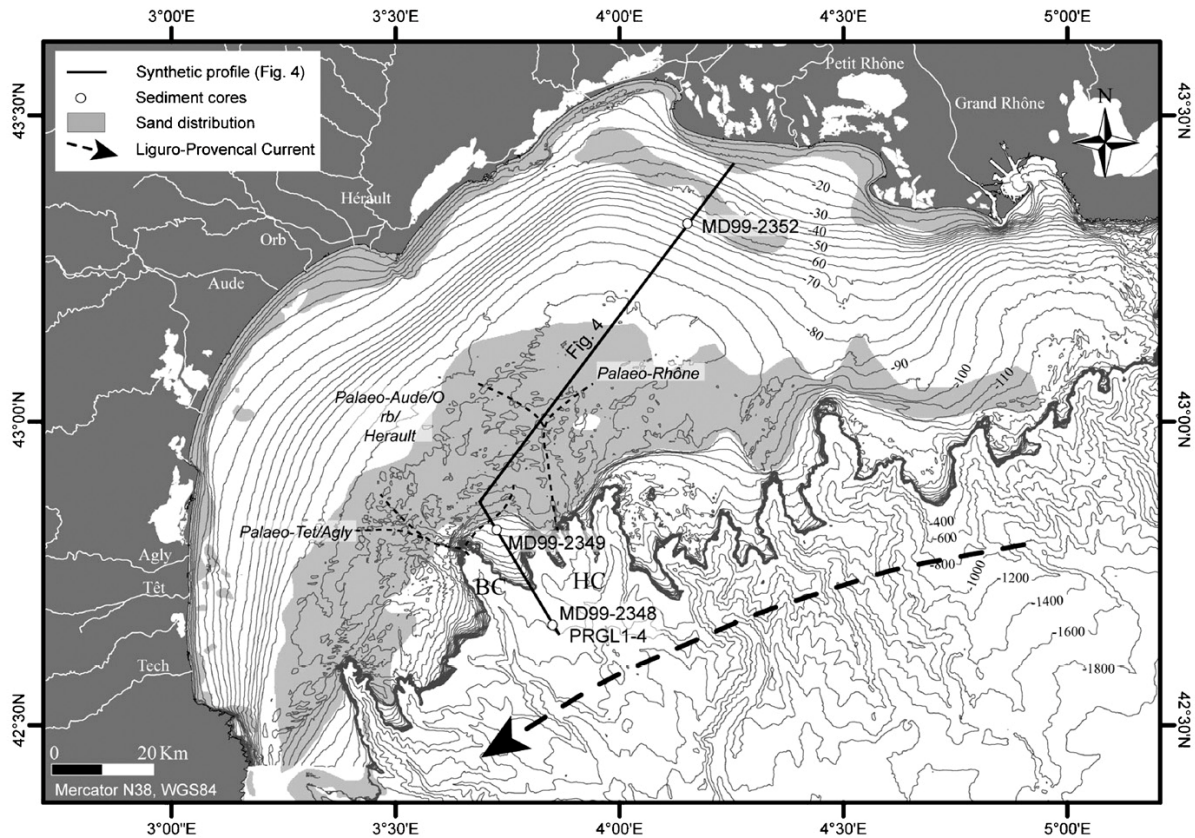
Fig. 3. Location of studied sites and palaeogeography. BC, Bourcart canyon; HC, Hérault canyon.
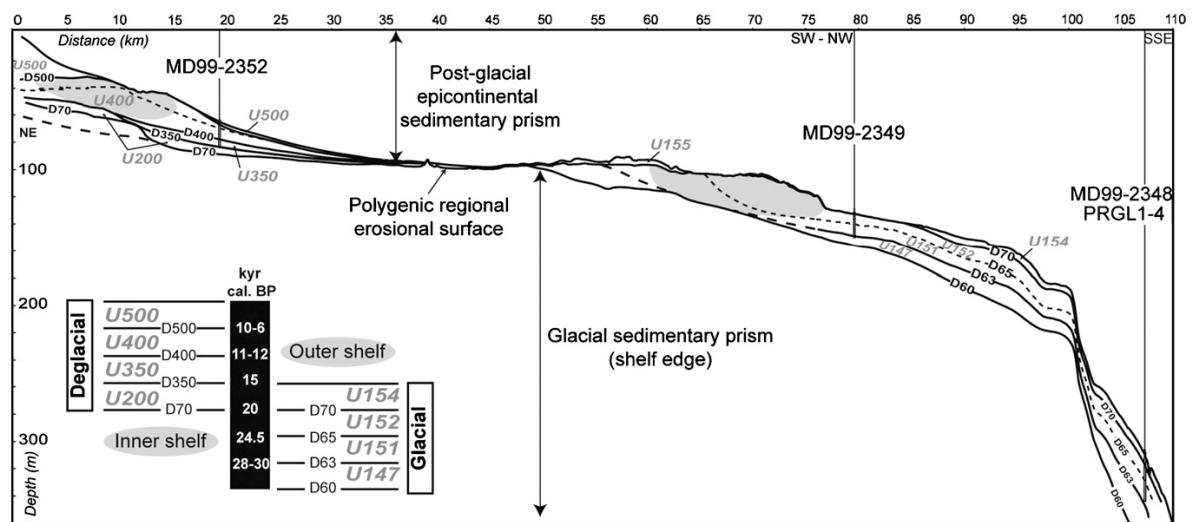

Fig. 4. Interpreted composite line drawing displaying major seismic units of the studied area and location of cores, from Berné et al. (2004) and Jouet et al. (2006).

the presence of reworked palynomorphs in terrigenous sediments was considered as evidence of the unreliability of the whole pollen signal. In contrast, many recent investiga-

tions made on terrigenous and autochthonous sediments in other parts of the world (e.g. Heusser and Balsam, 1977; Sun et al., 1999; Van der Kaars, 2001) and also in the Gulf

of Lions (Beaudouin et al., 2005b, in press) demonstra-
ted the suitability of marine pollen signal to reconstruct
a regional vegetation even if they contain reworked
palynomorphs. In particular, a study carried out on the
present-day prodelta of the Rhone River (i.e. depo-
sited under 40 m of water depth) demonstrated the stability
of the pollen signal during 30 years of sedimentation
despite the occurrence of storms and floods (Beaudouin
et al., 2005b).

Actually, one needs to distinguish between allochtho-
nous (i.e. terrigenous) and autochthonous sediments
to understand the meaning of the marine pollen signal.
Pollen grains contained in autochthonous sediments
are mainly brought by winds (Beaudouin et al., in press).
On the contrary, pollen grains contained in terrige-
nous sediments are mainly brought by rivers and therefore
come from one or several drainage basins (Heusser, 1988).
In the case of the Gulf of Lions, they are incorporated
into the bottom nepheloid layer at the river mouth and
spread all over the shelf (Beaudouin et al., in press).
According to the physiography of the margin, terrige-
nous sediments can reach the sea floor. They carry by
definition reworked particles and therefore reworked
palynomorphs (i.e. identified Pre-Quaternary pollen and
dinoflagellate cysts as well as corroded pollen grains
having totally or partly lost their ektexine) when the
area drained by rivers encounters older sedimentary
basins. Actually, a key question is to know if the amount
of pollen supplied by the erosion of previously depo-
sited sediments is able to balance the contemporaneous
pollen signal (i.e. the contemporaneous amount of
pollen emitted by plants). In present-day sediments of
the Gulf of Lions, reworked palynomorphs reach 5% of
the palynological content while the pollen content is
representative of the vegetation (Beaudouin et al., in
press). Furthermore, several multi-proxy studies made
on Quaternary terrigenous sediments demonstrated that
the pollen signal was sensitive to climatic variations
recorded by oxygen isotopes in the same cores and
therefore definitely evidenced the suitability of terrigenous
marine deposits to reconstruct past vegetation dynamics
(e.g. McGlone, 2001; Sánchez-Goñi et al., 2002). For
example, Sánchez-Goñi et al. (2002) evidenced a clear
correlation between the pollen signal and the oxygen
isotopes in an area located within the Alboran Sea where
88% of sediments are terrigenous (Sánchez-Goñi et al.,
2002), although rivers drain Cenozoic continental basins.
Reworked palynomorphs are not mentioned but more
recent studies evidenced the presence of Pre-Quaternary
palynomorphs in this area within Early Pleistocene
sediments while the pollen signal is once again in
correspondence with oxygen isotopes (Joannin, pers.
com.).

Whatever, we cross-checked the new data with others
based on literature (i.e. palynology, phylogenetic and
botany) to reconstruct the probable history of vegetation
in southern France.

3. Material and method

We provide three long and high-resolution pollen
records extracted from (1) core MD99-2349 (42°49.27′N,
3°43.43′E; 126 m depth), (2) core MD99-2348 (completed
by the upper portion of the PROMESS drillsite PRGL1-4
situated at the same position (42°41.58′N, 3°50.50′E; 296 m
depth) and (3) core MD99-2352 (43°19.15′N, 4°09.64′E;
70 m depth). Core MD99-2349 samples the lowstand
palaeo-lower-shoreface at the interfluve Bourcart-Hérault
on the outer shelf (Figs. 3 and 4). Cores MD99-2349 and
MD9923-48/PRGL1-4 sample units deposited during sea-
level fall, last Glacial and early Deglacial (units 151 154 of
Jouet et al., 2006). These authors provide a detailed
lithological description of both cores. Core MD99-2348 is
situated on the upper slope on the Bourcart-Hérault
interfluve, in a place that was not affected by mass wasting
and where sedimentation rate was very high due to fall of
particles from the plumes of rivers situated in the vicinity
during glacial period (Jouet et al., 2006). Core PRGL1-4 is
made on the same site and samples the last 430 ky on a
thickness of 300 m (Berné et al., 2004). The first analyses
made between 1806 and 3664 cm depth are combined with
the data obtained on core MD99-2348. Core MD99-2352
samples the muddy bottomsets of clinoforms of a
transgressive parasequence that formed during a decrease
in the Deglacial sea-level rise, around the Younger Dryas
(Berné et al., 2003). These authors provide a detailed
lithological interpretation of this core. It was under the
direct influence of the Rhone River.

The general stratigraphy is described by a set of seismic
units defined on mud penetrator chirp signal. Several
radiocarbon datings made on fresh and intact macrofossils
and on foraminifers from numerous cores constrain these
seismic units (Rabineau, 2001; Jouet et al., 2006; Berné
et al., 2003). The radiocarbon datings were calibrated using
Calib 5.0.2 (Stuiver et al., 2005) with the curve of Hughen
et al. (2004). For datings older than 21,786 BP we used the
curve of Bard et al. (1998). We applied a reservoir age of
400 years. The dates are in general coherent. Most of the
chronological inversions evidenced by non-calibrated dates
disappear when taking into account the calibration and its
associated confidence limit (Table 1). However, the radio-
carbon datings on core MD99-2349 are more scattered
because this core corresponds, at the time of deposition, to
a very shallow environment with episodic reworkings by
storms events (Jouet et al., 2006). In order to minimize the
reworking effect on this core, we only take into account the
AMS datings made on microfossils.

This chrono-stratigraphic framework allows a compar-
ison between pollen and climatic data (i.e. $\delta^{18}O$) from
Greenland ice-cores. We chose the signal from the GRIP
ice-core using the time-scale of Johnsen et al. (2001) at a
resolution of 50 years. Indeed, concerning MIS 2, there is a
particularly good correlation between the climatic signal of
the Western Iberian and this core using this chronology
(Roucoux et al., 2005).

Table 1
Radiocarbon datings made on cores MD99-2349, MD99-2348 and MD99-2352

Core	Depth (cm)	Material	C14 ages	Cal ages (Year BP)		Relative area	Technic	Reference	Taken into account
				Lower limit	Upper limit				
MD99-2348	25	Foraminifers	13,020 ± 40	14,633	15,125	1	AMS	Géochron	Yes
MD99-2348	80	Foraminifers	14,350 ± 60	16,230	16,993	1	AMS	CAMS108010	Yes
MD99-2348	190	Foraminifers	14,640 ± 60	16,578	17,414	1	AMS	CAMS108011	Yes
MD99-2348	300	Foraminifers	15,380 ± 70	18,025	18,576	1	AMS	CAMS108012	No
MD99-2348	360	Foraminifers	14,960 ± 70	17,083	17,937	1	AMS	CAMS108013	Yes
MD99-2348	518	Foraminifers	15,890 ± 70	18,678	18,915	1	AMS	CAMS108014	Yes
MD99-2348	1018	Foraminifers	17,910 ± 80	20,395	21,030	1	AMS	CAMS108015	Yes
MD99-2348	1231	Foraminifers	18,060 ± 60	20,535	21,187	1	AMS	Géochron	Yes
MD99-2348	1498	Foraminifers	19,750 ± 90	22,613	23,417	1	AMS	CAMS108016	Yes
MD99-2348	1680	Bulk forams > 200 μm	20,500 ± 80	23,819	24,346	1	AMS	LLNL-L397-77703	Yes
MD99-2348	2058	Foraminifers	21,240 ± 110	24,665	25,455	1	AMS	CAMS108017	Yes
MD99-2348	2218	Foraminifers	21,150 ± 120	24,520	25,410	1	AMS	CAMS108018	Yes
MD99-2349	397	Benthic Foraminifera and Ostracod valves	17,340 ± 90	19,880	20,285	1	AMS	Poz-7851	Yes
MD99-2349	533–538	Shells (Cyprina sp.)	19,635 ± 150	22,528	23,071	1	Classic	LY-11900	No
MD99-2349	902	Shells (Cyclichna sp.)	20,570 ± 100	23,868	24,433	1	AMS	Poz-7852	No
MD99-2349	1074	Shells (Varicorbula Gibba)	21150 ± 70	24,709	25,013	0.72	AMS	LLNL-CAMS-96163	No
MD99-2349	1218	Shell (Nucula sp.)	21190 ± 100	24,617	25,414	1	AMS	Poz-7854	No
MD99-2349	1458	Shells (Chlamys islandica)	19910 ± 480	22,597	23,824	1	Classic	LY-11899	No
MD99-2349	1441	Microshells	24300 ± 140	27,930	28,250	—	AMS	Poz-14903	Yes
MD99-2349	1600	Shells	52400 ± 2900	—	—	—	AMS	LLNL-CAMS-96164	No
MD99-2349	1736–1738	Foraminifers	35900 ± 800	40,120	41,840	—	AMS	LLNL-CAMS-96165	Yes
MD99-2349	1760	Shells	> 54000	—	—	—	AMS	LLNL-CAMS-96166	No
MD99-2352	123	Acanthocardia echinata	4955 ± 45	5173	5443	0.98	Classic	LLNL-95846	Yes
MD99-2352	286	Nucula sp.(nucleus)	9890 ± 60	10,606	11,056	1	AMS	Poz-3842	Yes
MD99-2352	401–403	Turitella communis	10,000 ± 50	10,761	11,136	1	AMS	Poz-3843	Yes
MD99-2352	519–521	small benthic forams (> 63 μm) + few bivalvia, gastropods and ostracods	10,070 ± 60	10,880	11,200	0.96	AMS	Poz-3844	Yes
MD99-2352	731	Turitella communis	10,310 ± 50	11,178	11,422	0.93	AMS	Poz-3845	Yes
MD99-2352	799–801	mixed benthic forams (> 63 μm) + few bivalvia, gastropods and ostracods	11,320 ± 60	12,817	12,955	1	AMS	Poz-3846	Yes
MD99-2352	928–932	Corbula gibba	10,590 ± 50	11,635	12,097	1	AMS	Poz-3848	No
MD99-2352	948	Corbula gibba	10,475 ± 40	11,351	11,766	0.93	Classic	LLNL-95847	Yes
MD99-2352	1105–1107	mixed benthic forams (> 63 μm) + few bivalvia, gastropods and ostracods	11,340 ± 50	12,832	12,953	1	AMS	Poz-3849	Yes
MD99-2352	1305–1307	Ammonia beccarii or Elphidium crispum + few bivalvia	11,820 ± 50	13,184	13,383	1	AMS	Poz-3850	Yes
MD99-2352	1393	Corbula gibba	11,840 ± 40	13,212	13,381	1	Classic	LLNL-95848	Yes
MD99-2352	1494	Turitella communis	12,855 ± 40	14,205	14,865	1	Classic	LLNL-95849	Yes
MD99-2352	1505	Mya truncata	13,245 ± 40	14,945	15,417	1	Classic	LLNL-95850	Yes
MD99-2352	1534–1536	Mytilus sp.	13,090 ± 50	14,716	15,202	1	Classic	LLNL-98908	Yes

A standard chemical treatment was applied to extract palynomorphs, using cold HCl (33%), cold HF (70%), $ZnCl_2$ and sieving at 200 and 10 μm. A minimum of 150 pollen grains (apart from *Pinus*) was counted for each sample. To calculate percentages, we used the sum of pollen grains without *Pinus*. Contrary to continental pollen data (e.g. in lakes) where the pollen of Cyperaceae most probably originates from local herbs and are over-represented, marine terrigenous sediments contains pollen of Cyperaceae that can originate from various environments. We therefore include them as well as other herbs. Dinoflagellate cysts were determined and counted on the same lines as pollen grains. We did not calculate the relative abundance of dinoflagellate cysts because their
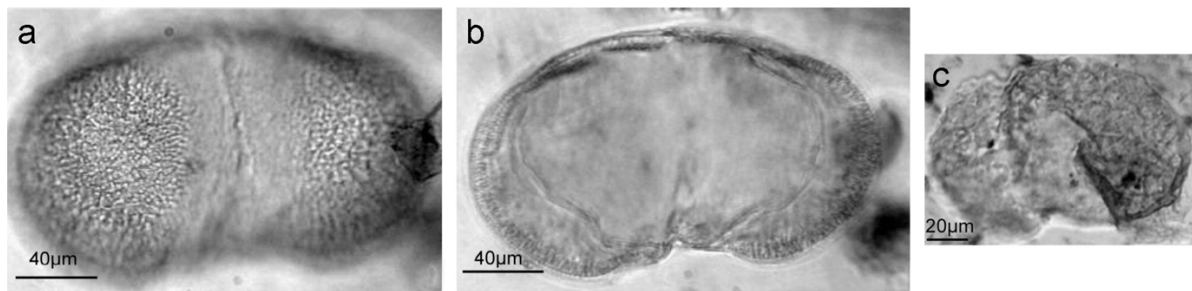
Fig. 5. Example of different state of conservation of pollen grains in core MD99-2349. (a), (b) well-preserved pollen grains of *Picea* displaying a well conserved structure; (c) reworked pollen grain of Pinaceae recognized by its non-structured appearance.

amount was insufficient. Nevertheless, they bring supplementary information about the palaeoenvironment. All corroded and clearly identified pre-Quaternary palynomorphs were classified as reworked (Fig. 5). We distinguished reworked pollen grains from contemporaneous one on the state of the conservation of the ektexine (e.g. Haberle, 1997). A reworked pollen grain should have a partly or totally destroyed ektexine. We used the Cour's Method to calculate concentrations (Cour, 1974). All the palynological data are available in the Cenozoic Pollen Database and Climatic values (http:// cpc.mediasfrance.org/aims/index.php). In terrigenous sediments, the presence of one pollen grain from a taxon cannot be considered as an evidence of the presence of the taxon within the drainage basin because of reworkings. Therefore, we focussed on the main taxa representing more than 5%. We drew a simplified diagram also displaying the confidence limits on each percentage. We did not represent the Cyperaceae and the Poaceae even if they were abundant as their ecological meaning is unconstrained. In order to better constrain the statistical significance of peaks of pollen abundances, binomial confidence limits for proportions were calculated using the program Pro-CI (available on request from G. Escarguel). Given a type I error rate $\alpha = 0.05$, these limits define the 95% confidence intervals associated to each sample percentage, i.e., the range of percentage values within which there is $1-\alpha = 95\%$ of chance to find the unknown true (parametric) percentage (e.g. Sokal and Rohlf, 1995).

Palynozones were defined on the change of the main taxa as well as on the evolution of the abundance or reworked palynomorphs. Indeed, the abundance of reworked palynomorphs in marine sediments is linked to the importance of the erosion of the drainage basins due to (1) sea-level drops (e.g. McGlone, 2001) or (2) melting of glaciers (e.g. Gregory and Hart, 1992; Haberle, 1997). In the case of the Gulf of Lions, major sea-level drops are linked to a great increase of the abundance of reworked particles. It is the case for MIS 6, MIS 4 (J.-P. Suc, pollen study of core PRGL1-4 in progress) and from MIS 3 to 2 in deep-sea terrigenous sediments (Beaudouin et al., 2004). Reworked palynomorphs were also found in

abundance within the drainage basin of the Rhone River in the alpine lake of Annecy at the end of MIS 3 (David et al., 2000).

4. Results

4.1. Palynological content

The palynofacies includes (1) well preserved pollen grains and dinoflagellate cysts, (2) pre-Quaternary destructured dinoflagellate cysts and pollen grains and (3) other debris (charcoals, wood debris, cuticles, stomata, epidermis, etc.). Concentration of pollen grains is generally low (from 40 to 3000 grains/g). Concentration of dinoflagellate cysts and reworked palynomorphs, respectively, reach 0–500 cysts/g and 0–320 grains/g. *Pinus*, Cupressaceae, *Abies*, *Picea*, deciduous *Quercus*, *Hippophae rhamnoides*, Poaceae, *Artemisia* and Cyperaceae constitute the main part of the pollen signal within cores MD99-2348/PRGL1-4 and MD99-2349. One hundred taxa were found in core MD99-2349. Six palynozones were defined (Fig. 6). Twenty-three Dinoflagellate cysts were determined. *Brigantedinium*, *Operculodinium centrocarpum* and *Spiniferites* are relatively frequent. Dinoflagellate cysts adapted to low saline and coastal areas (*Lingulodinium machaerophorum*) and found at river mouths and in lagoons (*Polysphaeridium zoharyi*) or in freshwater (*Concentricystes*) are relatively well represented and confirm that sediments were deposited in the lower-shoreface. Dinoflagellate cysts characterizing cold waters are present only sporadically (*Nematosphaeropsis labyrinthus*, Cf. *Pentapharsodinium dalei* and *Bitectatodinium tepikiense*). Eighty-eight taxa were found in the sequence MD99-2348/PRGL1-4. Seven palynozones were built (Fig. 7). The same dinoflagellate cysts as in core MD99-2349 were found. Freshwater or lagoon dinoflagellates are not as frequent as in core MD99-2349. Seventy-six taxa were found in core MD99-2352. The dominant taxa are *Pinus*, deciduous *Quercus*, evergreen *Quercus*, Cupressaceae, *Corylus*, *Ulmus*, *Betula*, Poaceae, Cyperaceae and *Artemisia*. Three palynozones were created (Fig. 8). Dinoflagellate cysts are relatively abundant representing 25% of the palynomorphs from 1515 to 290 cm depth: they are mainly represented by
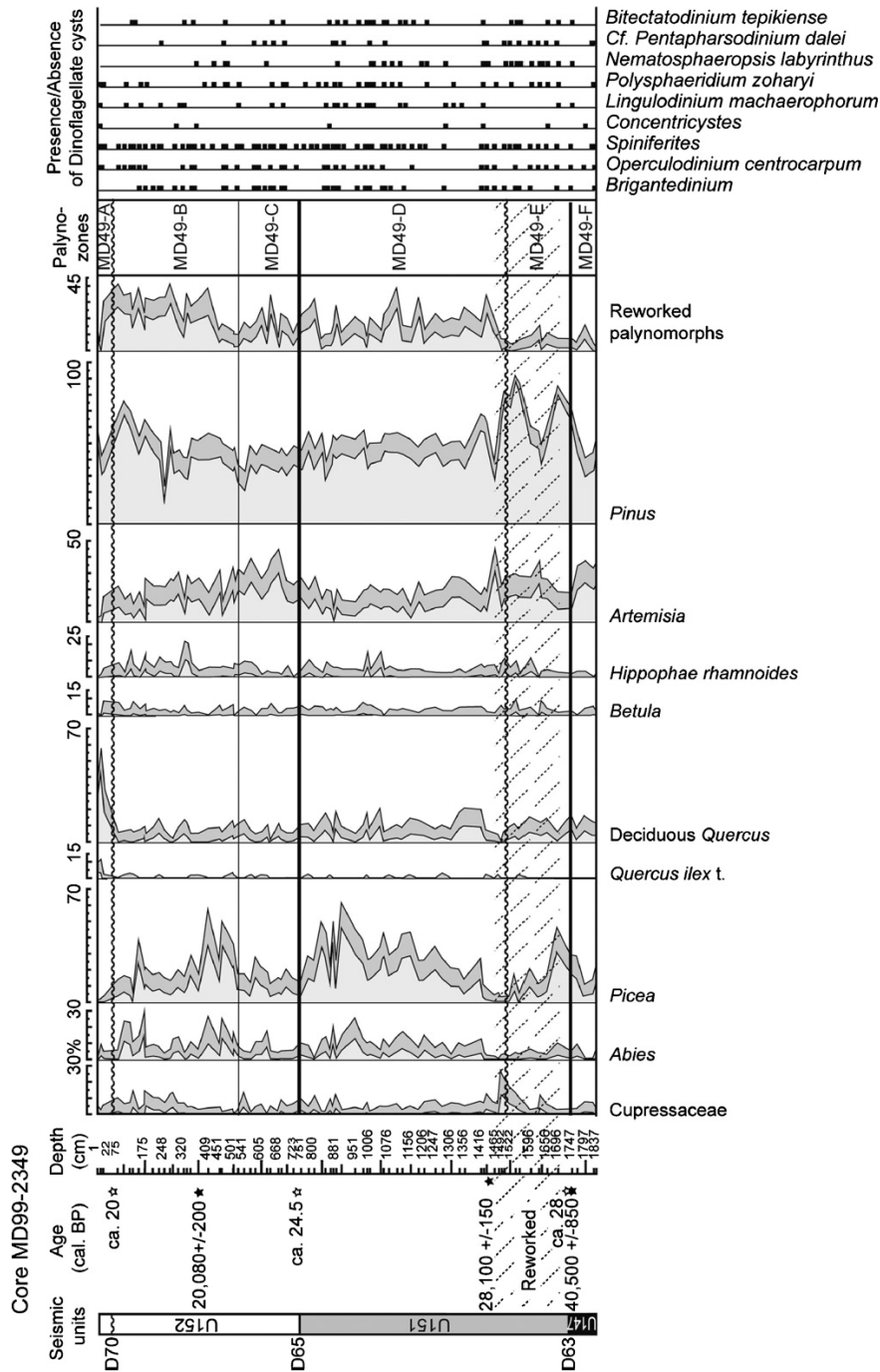
Fig. 6. Simplified pollen diagram of core MD99-2349 and corresponding seismic units. For each taxon, the grey area delimited by the two continuous curves corresponds to the 95% confidence belt associated to the observed (sampled) percentage of pollen. Black and white stars correspond to levels dated by radiocarbon and seismic correlations, respectively. Thick lines correspond to the seismic limits. Wavy lines correspond to discontinuities visible on the sediment.

Brigantedinium, *Spiniferites*, Cf. *Pentapharsodinium dalei* and *Operculodinium centrocarpum*. From 290 to 152 cm depth, dinoflagellate cysts are rare and only represented by some *Spiniferites*. In the upper part of the core (from 90 to 10 cm depth), *Concentricystes* is the only taxon to be represented: it may characterize the influence of the Rhone River.

In all sequences, the evolution of the abundance of pollen from the main taxa does not follow the evolution of reworked palynomorphs (Figs. 6 8).
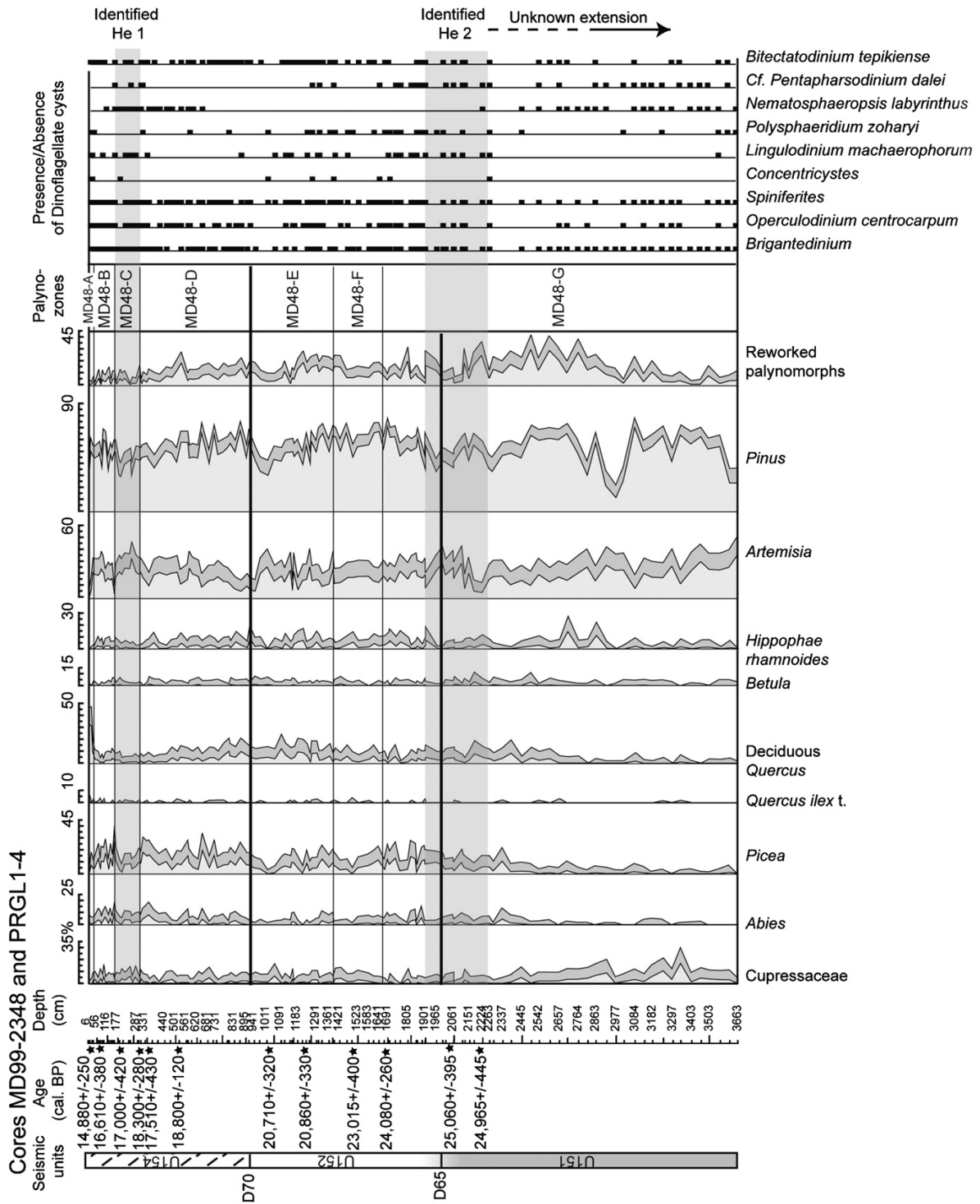
Fig. 7. Simplified pollen diagram of core MD99-2348/PRGL1-4 and corresponding seismic units. For each taxon, the grey area delimited by the two continuous curves corresponds to the 95% confidence belt associated to the observed (sampled) percentage of pollen. Black stars correspond to levels dated by radiocarbon. Thick lines correspond to the seismic limits.
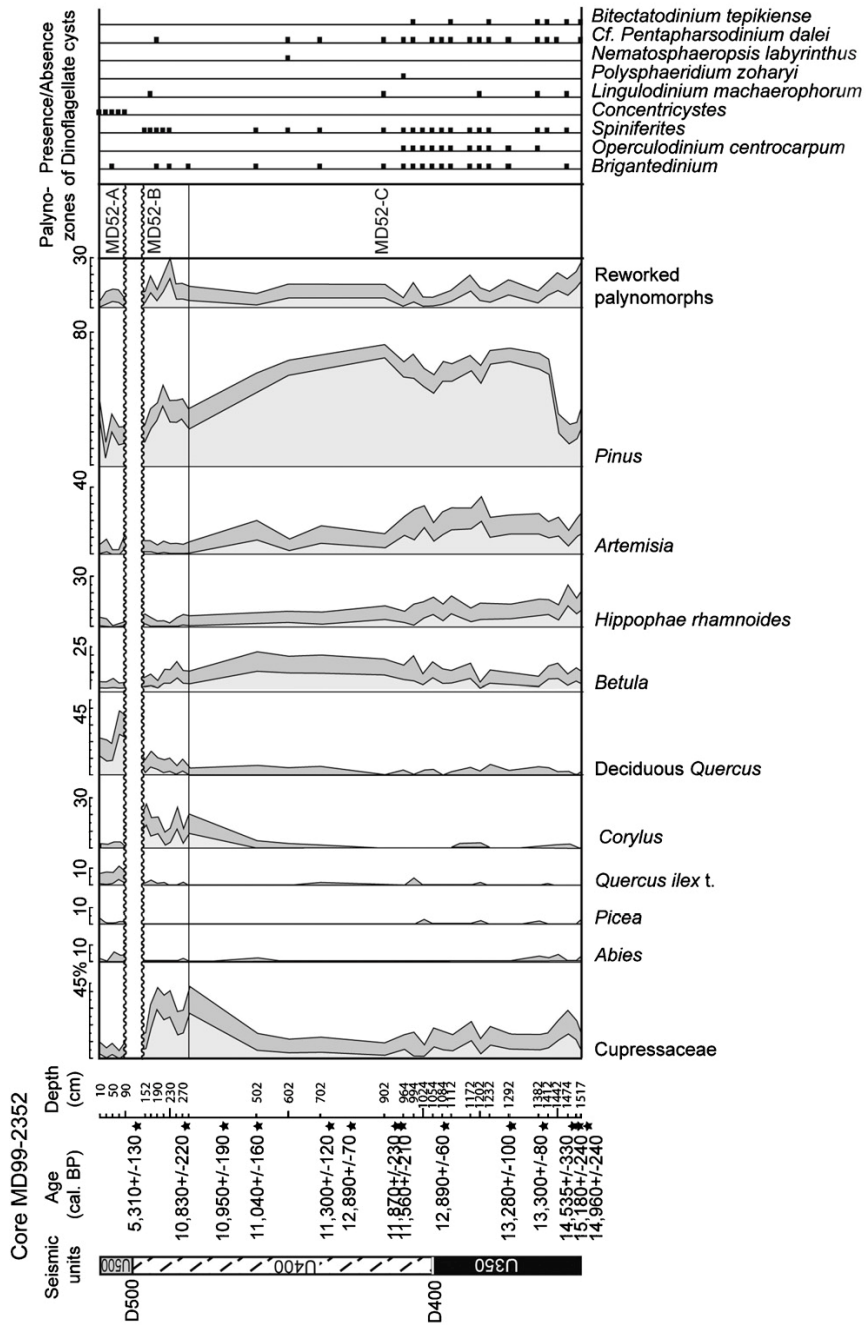
Fig. 8. Simplified pollen diagram of core MD99-2352 and corresponding seismic units. For each taxon, the grey area delimited by the two continuous curves corresponds to the 95% confidence belt associated to the observed (sampled) percentage of pollen. Black stars correspond to levels dated by radiocarbon. Wavy lines correspond to discontinuities visible on the sediment.

4.2. Correlation of cores and comparison with global climatic changes

The cores display comparable pollen fluctuations in terms of variation but not abundance (Fig. 9). We therefore propose a correlation based on seismic stratigraphy and radiocarbon datings. The time-window recorded by our cores is small and consequently, the resolution of pollen data is high, reaching ca 70 years in core MD99-2349 and 100 years in core MD99-2348. Pollen curves in the latter core shows slight fluctuations difficult to correlate with the pollen signal from core MD99-2349. The cause of this
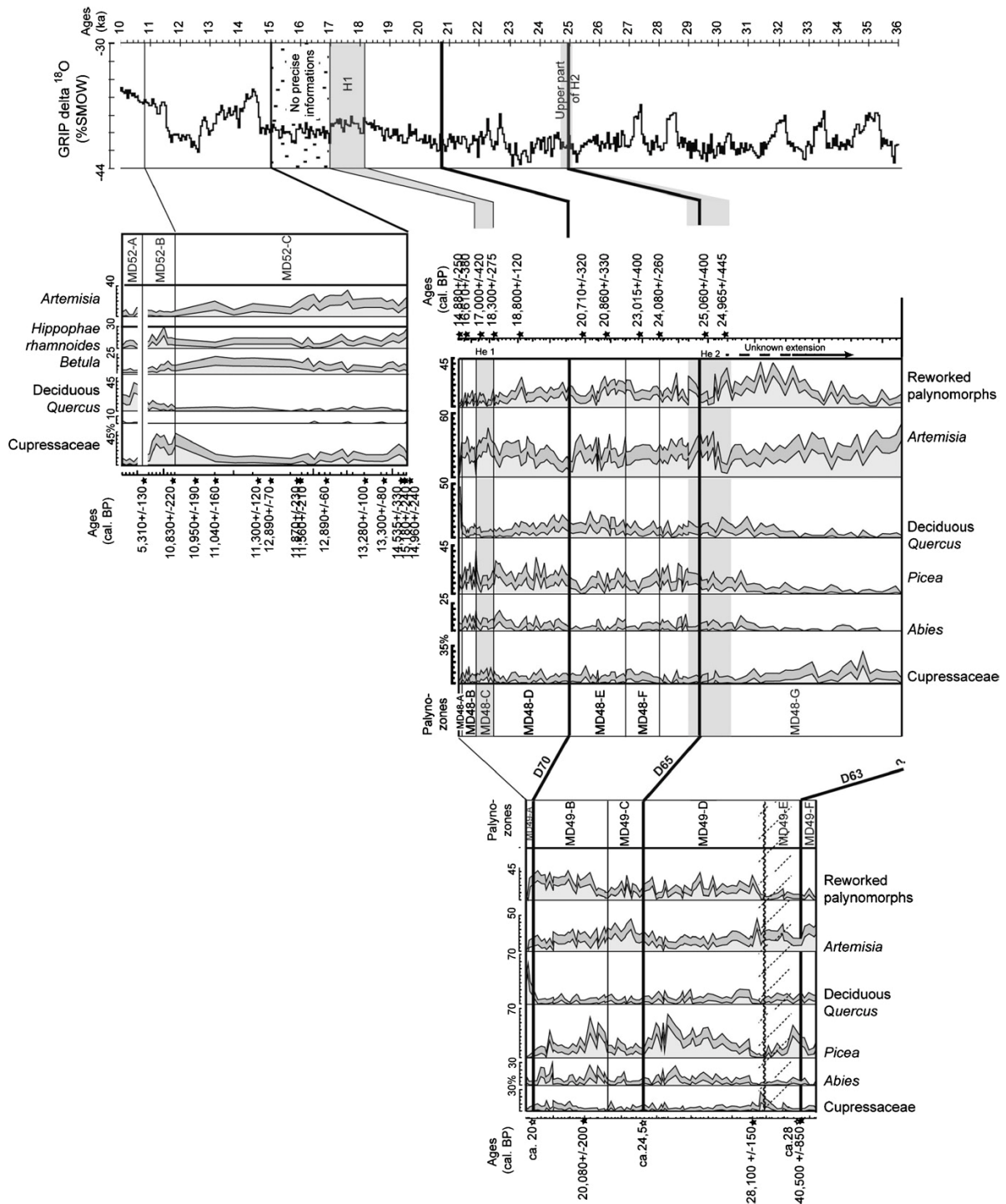
Fig. 9. Synthetic view of the correlations between palynological signals of cores and isotopic records from GRIP ice-core.

characteristic will be explained further. The variations of abundances of the main taxa match relatively well with the GRIP δ18O record for such a short time-window. Two synchronous common pollen features shared by two or all

cores are noteworthy. The first feature corresponds to the great increase of deciduous *Quercus* and *Quercus ilex* t. associated with the decrease of *Artemisia* and reworked elements correlated with the Holocene (palynozones

MD48-A, MD49-A and MD52-A). In the sequence MD99-2348/PRGL1-4, the apparent Holocene increase of decid-uous *Quercus* from 2% reaching 14% is dated at 14,880±250 cal BP at 25 cm depth. The highest sample carries a similar signal to present-day sediments from the Gulf of Lions (Beaudouin et al., in press). In fact, the upper 25 cm (i.e. only 3 samples) correspond to condensed levels recording the Interstade 1 (IS1), the Younger Dryas and the Holocene, the pollen signal representing a mean of the vegetation changes through these climatic changes. The second main feature is found at the base of sequences MD99-2349 and MD99-2348/PRGL1-4. It corresponds to the development of the curve of reworked palynomorphs followed by the increase of *Picea*, *Abies* and deciduous *Quercus* to the detriment of the Cupressaceae (palynozone MD49-E, MD49-D and MD48-G). In core MD99-2349, the bottom part of the pollen signal (i.e. zone MD49-E) is reworked according to the sedimentary facies. Never-theless, reworkings do not affect levels situated above 1442 cm also containing a low amount of *Picea* and *Abies*. The radiocarbon datings confirm that the great increase of reworked palynomorphs corresponds to the sea-level drop between MIS 3 and 2. The associated and following vegetation pattern (i.e. the decrease of Cupressaceae and the increase of *Picea* and *Abies*) is situated within the same sedimentary unit (U151) in both cores and is dated at ca 28 ky cal BP in core MD99-2349 and up to ca 25 24.5 ky cal BP according to core MD99-2348/PRGL1-4. The H2 event is partly identified (with the presence of *Neogloboquadrina pachyderma* sinistra) in the upper part of zone MD48-G corresponding to the base of core MD99-2348 (Flores et al., 2005). The H2 event could correspond to the palynozone MD49-C in core MD99-2349 according to the chrono-stratigraphy and would be characterized by the development of *Artemisia* and the decrease of temperate taxa. From ca 28 to 25.5 ky cal BP, the Gulf of Lions seems to experience an increase of dryness at the end of which the H2 event is identified. But the effect of the latter is not clearly recorded by vegetation. The same pattern occurs in the Western Mediterranean. In western Iberia (between 40°N and 43°N), the MIS 3 vegetation was made up of *Pinus*, deciduous *Quercus*, *Betula* and Cupressaceae asso-ciated with Ericaceae, Poaceae and *Artemisia* (Roucoux et al., 2005). In detail, from ca 27.5 to 24 ky cal BP deciduous *Quercus* disappears (Roucoux et al., 2005). This phase is followed by the H2 event recorded by ice-rafted debris. But the response of the vegetation is not clear for this event. On the southern part of the Portuguese Margin, the response of the vegetation to H2 event is characterized by a slight decrease of Ericaceae and fluctuations of *Artemisia* (Turon et al., 2003). In the Alboran Sea, H2 event is found within a succession of peaks of semidesert taxa beginning at 27 ka cal BP and finishing at 24 ka cal BP (Combourieu-Nebout et al., 2002). In Italy at Lago di Monticchio (Allen et al., 2000), the pollen of *Quercus* also experiences a strong decrease at 26 ky cal BP. The phase of *Picea* and *Abies* in MD99-2349 (i.e. zone MD49-D) could correspond to the

peak of temperate taxa found in the Alboran Sea around ca 25.5 cal BP (Combourieu-Nebout et al., 2002). But it does not correspond to any vegetation change in core MD9923-48/PRGL1-4 as well as in North West Iberia (Roucoux et al., 2005). This correlation hypothesis implies that the IS3 is not well-recorded in the Gulf of Lions like in North West Iberia (Roucoux et al., 2005). According to the seismic data, zones MD48-B to MD48-D corresponding to U154 (above the discontinuity D70) are not recorded in core MD99-2349 where it should be represented by a condensed interval. Zone MD48-D (from ca 20.5 to 18.3 ky cal BP) corresponds to a high amount of *Picea*, deciduous *Quercus* and *Artemisia*. Deciduous *Quercus* is more abundant at the bottom of the zone while *Artemisia* increases upward. MD48-C is characterized by a decrease in *Picea*, *Abies* and *Pinus*, while Cupressaceae and *Artemisia* increase. Flores et al. (2005) attribute these levels to the H1 event (from foraminifer's assemblages). Zone MD48-B records a slight increase of *Picea* and deciduous *Quercus* and could correspond to IS2 according to the chrono-stratigraphy. H1 is also well-marked in other Mediterranean sites. It is characterized by a well-marked development of the curve of semidesert taxa (including *Artemisia*) in the Alboran Sea (Combourieu-Nebout et al., 2002) and by a severe decrease of Ericaceae on the Portuguese Margin (Turon et al., 2003; Roucoux et al., 2005). Core MD99-2352 records the last 15 ky and should record IS1 and the following Younger Dryas. It cannot be correlated to core MD99-2348 as this period corresponds to three samples in the latter core (i.e. the first 25 cm of sediments). Zone MD52-C is characterized by the dom-inance of *Artemisia*, *Hippophae rhamnoides* and Cupressa-ceae (from 14,960±240 to 11,870±230 cal BP) except from 11,870±230 to 10,950±190 cal BP corresponding to an increase of *Betula*. The bottom part of the core is characterized by the low amount of *Pinus* associated with a high percentage of reworked palynomorphs. Zone MD52-B (from 10,830±220 cal BP up to the upper discontinuity) is characterized by the development of *Corylus* and Cupressa-ceae. *Pinus* as well as reworked elements increase in this zone. In core MD99-2352, the Holocene is represented by a condensed interval dated at ca 5310±130 cal BP likely formed during a sudden sea-level rise after the Younger Dryas (Berné et al., 2003).

5. Discussion

5.1. Location and structure of the populations of trees

In the Gulf of Lions, (1) the high amount of pollen of Cupressaceae, *Abies*, *Picea*, and deciduous *Quercus*, (2) their reaction fitting climatic changes (at least evidenced for the 28 26 ky cal BP event and the H1 event) and (3) the fact that their abundance does not follow the evolution of the abundance of reworked particles suggest the presence of these trees in the basins drained by the Rhone and the Pyreneo-Languedocian rivers during the MIS 3 and

through the LGM. *Pinus* was also present. The signal of *Pinus* is known to be difficult to interpret in marine sediments because it is sorted by currents unlike other bisaccate pollen grains (Heusser, 1988). The abundance of *Pinus* is modulated by pollen production and also by the fluctuation of sea-level through sedimentary supplies or sea-level changes. We can attest that *Pinus* was present in the Rhone and the Pyreneo-Languedocian drainage basins although we cannot give any further conclusions concerning its percentage evolution. This conclusion is in agreement with other studies carried out in the area (de Beaulieu and Reille, 1984; Cheddadi et al., 2006).

Even if the evolution of pollen curves can be compared for what concerns long-term changes between core MD99-2348 and MD99-2349, the abundance of each taxon is different in each core. Core MD99-2349 shows an amount of *Abies* and *Picea* higher than core MD99-2348 for the same time-window. This difference cannot be linked to a sorting of pollen grains: a study made on present-day sediments from the Gulf of Lions demonstrated that pollen content was similar from the coast to the edge of the shelf (Beaudouin et al., in press). This difference may be more likely due to a double origin of the sediments, i.e. coming on the one hand from the Pyreneo-Languedocian Rivers and on the other hand from the Rhone River according to the palaeogeography (Fig. 3). This phenomenon is found in present-day sediments of the Gulf of Lions: the pollen signal in the western part of the shelf is different from that of the eastern part. This reflects the different vegetation within the areas drained by the Rhone River and the Pyreneo-Languedocian Rivers. From this point of view, the pollen contained within seismic units U151 and U152 in core MD99-2349 has been brought by the Agly/Aude/Orb/Hérault palaeoriver draining the Pyrenean Mountains and the plains of the Languedoc-Roussillon. It is the closest channel from the sampled area (Fig. 3). Sediments of sequence MD99-2348/PRGL1-4 were deposited at a deeper bathymetry (i.e. at 130 m depth during the lowstand) and have also received abundant inputs from the Rhone River connected to the Hérault canyon, i.e. 20 m above and 30 km eastwards. The area drilled by core MD99-2349 has been relatively protected from these Rhone River inputs because the Agly/Aude/Orb/Hérault palaeoriver was the most important flow (Rabineau, 2001). Furthermore, the Rhone River was connected to several canyons at the same time, i.e. at least to the Petit-Rhone (Beaudouin et al., 2004) and the Hérault canyons certainly dividing the power of its tributaries. This scheme also explains the difference between the curves of reworked palynomorphs in cores MD99-2349 and MD99-2348/PRGL1-4 for what concerns short-term variations. We therefore suggest a difference of vegetation between the eastern and the western part of the Gulf of Lions, the Rhone drainage basin having less *Picea*, *Abies* and deciduous *Quercus* and more herbs and shrubs (Poaceae, Cyperaceae, *Artemisia* and *Hippophae rhamnoides*).

The significance of pollen signal in terrigenous sediments cannot be interpreted like a signal extracted from hemi-pelagic sediments or from continental sediments (peat and little lakes) constituting the main source of palynological data in the literature. The high amount of pollen grains of a taxon (here *Picea*, *Abies* or deciduous *Quercus*) cannot be taken as an evidence for a forest. According to studies carried out on present-day sediments of the Gulf of Lions, the most abundant pollen taxa are found close to the river (riparian woodland) and in the southern part of the drainage basin (Beaudouin et al., 2005b, in press). During the Glacial, populations of trees could have lived on the emerged shelf of the Gulf of Lions. Faure et al. (2002) suggested that during lowstands, shelves constitute a source of freshwater and would represent "coastal oasis" while continental interior would desiccate. The shelf of the Gulf of Lions, relatively flat and made of clays could have favoured the installation of trees.

5.2. Other evidences for the presence of high latitude populations of trees

According to the long French and Spanish lacustrine sites [Les Echets near Lyon, Bouchet lake (Massif Central) and La Grande Pile (Vosges)] (Fig. 1), *Picea* would have been totally absent from France since 30 ky cal BP (Woillard, 1978; de Beaulieu and Reille, 1984, 1992; Reille and de Beaulieu, 1988). Its recolonization would have occurred at 4.5 ky cal BP from eastern Europe through the Alps (Huntley and Birks, 1983). This route was confirmed by phylogenetic studies (Collignon and Favre, 2000; Gugerli et al., 2001). Nevertheless, Collignon and Favre (2000) also identified a genetically different population of *Picea* living in the Southern Alps while the populations encountered in the northern Alps, Jura and Vosges mountains are similar. Southern populations of *Picea*, *Abies* are particularly well adapted to Mediterranean climatic conditions (i.e. to droughts). Collignon and Favre (2000) combining their phylogenetic data with palynological data hypothesized that these trees would originate from a refugium situated in northern Apennines. However, according to Ravazzi (2002) and Scotti et al. (2000), the population from Southern Alps would be a relict. Therefore, the pollen signal found in the Gulf of Lions is not surprising: *Picea* was present at relatively high latitudes from at least 30 ky cal BP and through the LGM. The results found in the present study suggest that their area restricted later (i.e. between ca 16 and 14.5 cal BP). However, it is not possible to deduce if the population of *Picea* of the Gulf of Lions contributed genetically to the southeastern present-day relict. Actually, the absence of pollen from *Picea* in lacustrine sequences is due to the fact that they record a local vegetation and to the fact that *Picea* pollen grains are heavy and do not spread regionally (Triat-Laval, 1978).

The history of *Abies* was a matter of debate for several years in particular in the Pyrenees (Jalut et al., 1982; Huntley and Birks, 1983; de Beaulieu and Reille, 1984; Reille, 1991; Reille and Lowe, 1993). Terhürne-Berson et al. (2004) recently clarified its history. They found

evidences for an important refugium of *Abies* in the Pyrenean Mountains as well as in northwestern Italy from macrorests and pollen data. In detail, the Pyrenean refugium is not documented by the Spanish low altitude site of Banyoles (Pérez-Obiol and Julià, 1994) as first suggested by Terhürne-Berson et al. (2004) but instead the site of La Borde situated northward at 1660 m (Reille, 1991; Terhürne-Berson, pers. com). *Abies* was present in Greece and in Italy from the Glacial and during the Lateglacial (Tzedakis, 1993; Tzedakis et al., 2002). It started to spread in France since 9–8.5 ky cal BP in the Alps and in the Pyrenees and finally reached the Massif Central at ca 5.5 ky cal BP. The populations of the Massif Central and the Alps share the same genetic imprint and would originate from southeastern France and/or northern Italy (Terhürne-Berson et al., 2004). The presence of a Pyrenean refugium would explain the genetic singularity of the Pyrenean populations of *Abies alba* compared with the other European populations. The presence of *Abies* in southern France is also attested by marine pollen data from the Gulf of Lions. Once again, the absence of *Abies* pollen grains in French and Spanish lacustrine sites can be explained by the fact that this pollen cannot be transported very far (Triat-Laval, 1978).

The European history of deciduous *Quercus* is now considered to be well constrained. According to the most recent study based on the European Pollen Database (Brewer et al., 2002), deciduous *Quercus* might be absent from France, northern Italy and northern Spain during the Last Glacial. The trace of pollen found in these countries would be an echo of southern refugia situated in southern Spain, southern Italy, southern Balkan Peninsula and Black Sea. Deciduous *Quercus* spreads from these refugia northwards during the Lateglacial. It was severely affected by the cooling and the drying of the Younger Dryas (11.5–12.5 ky cal BP). Populations would have persisted in secondary refugia southward to a line from the Pyrenees to the Balkan. Then, deciduous *Quercus* re-expanded from 11.5 ky cal BP to reach Scandinavia at ca 6.5 ky cal BP. The presence of deciduous *Quercus* in plains of southern France during the Last Glacial (as suggested by our data) is a particularly controversial point. Concerning southern France, northern Spain and northern Italy at the LGM and the deglaciation, available sites of the European Pollen database are scarce and mostly situated in mountains: in the Pyrenees, they are at least 1600 m-high (except one site situated at 880 m of altitude), in the Massif Central there are at least 1000 m-high and in the Alps they are at least 1900 m-high. Closed lakes record relatively local vegetation compared with marine sediments. Even if these pollen grains are transported from plains to higher altitudes in open environments, the absence of pollen grains of deciduous *Quercus* at high altitudes does not mean that the tree was not present in plains. The site of Banyoles is the only one to be situated in plains at 173 m of altitude (Pérez-Obiol and Julià, 1994). It contains a small amount of pollen of deciduous *Quercus* at ca 27 ky BP. Then, pollen

of deciduous *Quercus* regularly but not frequently occur (15 occurrences are recorded in 27 spectra at a constant pollen concentration). The frequency starts to increase before 15 ky cal BP (11 occurrences are recorded in 12 spectra) but may be correlated to the general decrease in pollen fluxes. This small amount of pollen may be an echo of regional refugia. Phylogenetic studies (Petit et al., 2002) identified the three refugia (Balkan Peninsula, Italy and Spain). But, they also evidenced a genetically different population of trees spread on the western side of Spain. They suggest that it could originate from a refugium situated in the Ebro Valley, i.e. a few hundred km southward to Banyoles. Our data suggesting the presence of deciduous *Quercus* in plains of southern France up to ca 16 ky cal BP is not in contradiction with such a high latitude refugium. However, the population of southern France was certainly very fragile according to the low amount of its pollen in the sediments. It was not present in the Rhone drainage basin during the deglaciation (from at least 14.5 ky cal BP). The increase of deciduous *Quercus* in the Rhone drainage basin begins between 11 and 10.7 ky cal BP corresponding to the second expansion of deciduous *Quercus* (Brewer et al., 2002) linked to the warming of the Holocene. This increase of pollen abundances in the Gulf of Lions is also synchronous with the increase of pollen abundances in northwestern Spain.

The Lateglacial history of *Picea*, *Abies* and deciduous *Quercus* in plains is still difficult to reconstruct from our marine data, due to the presence of hiatuses and to the weak thickness of the Holocene recorded in the studied sites. In the Rhone drainage basin, the pollen of *Pinus*, *Betula*, Cupressaceae, *Hippophae rhamnoides* and herbs constitute the main part of the pollen signal during the Lateglacial (Triat-Laval, 1978) confirming the signal of core MD99-2352. The charcoal analyses of caves from the plain of Roussillon show the local presence of *Pinus sylvestris* and Juniperus but neither *Abies* nor *Picea* at ca 12.5 ky cal BP (Heinz and Thiébault, 1998). Deciduous *Quercus* could have been present. It seems that *Abies*, *Picea* and deciduous *Quercus* also disappeared from the Pyreneo-Languedocian river drainage basins during the deglaciation. But this hypothesis has to be tested. The existence of southern France relicts during the Last Glacial Maximum is also attested for another mesophilous tree, i.e. *Fagus sylvatica* (Magri et al., 2006) while its echo is not well-recorded in cores from the Gulf of Lions. This could be due to the low density of the population or to its situation, i.e. far from rivers.

The fact that these populations of trees did not spread during the deglaciation is in favour of the existence of relicts rather than refugia s.s. A refugium is considered in our point of view as a population which spreads out of its area while a relict does not spread even if it can survive. The data from the Gulf of Lions are therefore in favour of the first model for what concerns the location of refugia (i.e. situated in southern Mediterranean peninsula) and in favour of Tzedakis (2004) for what concerns the northern

tree limit of southern France during the Last Glacial Maximum.

It is worth noting that the ultimate northern relicts attested by phylogenetic studies (i.e. in north-eastern Spain and south-eastern France) even if going through rapid climatic deteriorations, did not expand during the climatic amelioration of the post-glacial while populations from Southern Spain, Italy, Balkan and Eastern Europe started to spread. Their non-expansion could be linked to their physiology and/or an effect of competition with other trees like *Pinus*. The impact of mammals (i.e. grazing) is also a factor to take into account. The ground competition of seeds with other plants is also particularly important for what concerns colonization. But, the spatial colonization of several taxa competing in a context of climate change is not yet understood. The study of cores situated in front of the Pyreneo-languedocian Rivers, northern Spain margin, eastern part of the Gulf of Lions and covering the Lateglacial and the Holocene would help to clarify this point.

5.3. Climatic implications

MIS 2 climate is known to be less variable than the MIS 3's even if millennial-scale fluctuations still occur. Therefore, it is considered as almost constant during the LGM and generally treated as such in a time-window ranging from 24 to 19 ky cal BP (i.e. 18 ± 2 ky 14C BP) (e.g. Elenga et al., 2000). However, the apparent climatic stability of the LGM is purely relative compared to the high variability of MIS 3. In fact, the variability of the δ18O recorded in GRIP ice-core is higher than the 8.2 ky event which had an effect on vegetation dynamics (Alley and Ágústsdóttir, 2005). Recent studies documented the effect of short-climatic changes from ca 30 ky to 16 ky cal BP on the western European climate (Chondrogianni et al., 2004) and vegetation (Combourieu-Nebout et al., 2002; Roucoux et al., 2005). The data from the Gulf of Lions also suggest a high variability of climatic parameters during the LGM. The response of the vegetation follows the same pattern as in western Iberia although its composition differs. In the Gulf of Lions, cold and arid episodes (including Heinrich events) are characterized by the decrease of *Abies*, *Picea* and deciduous *Quercus* and the increase of *Artemisia*. These trees were probably at the limit of their tolerance in terms of temperature and precipitations during the Glacial. During the most severe event (from 28 to 26 ky cal BP) they may have disappeared from the area (less than 5% of their pollen is found in the sediment) whereas the Cupressaceae were more abundant. The latter are actually more tolerant to low temperatures and low Growing Degree Day values (Laurent et al., 2004). The response of vegetation in the Gulf of Lions supports the hypothesis of strengthened cold and arid winds in the region during Heinrich events maybe due to the strengthening of the Scandinavian Polar Highs (Cacho et al., 2002; Moreno et al., 2005; Sánchez-Goñi et al., 2002).

6. Conclusions

Sediments of the Gulf of Lions suggest the presence of *Pinus*, Cupressaceae, Betula, *Abies*, *Picea* and also deciduous *Quercus* in plains. *Abies*, *Picea* and deciduous *Quercus* would have more certainly been located in the drainage basins of the Pyreneo-Languedocian Rivers. A relict of trees in the Gulf of Lions is strongly probable as other studies, like phylogenetics combined with pollen data suggested the presence of relicts of *Picea* in South-Eastern France (Ravazzi, 2002), *Abies* in the Pyrenees (Terhürne-Berson et al., 2004) and deciduous *Quercus* in Northern Spain (Petit et al., 2002). We cannot affirm that the populations of *Abies*, *Picea* and deciduous *Quercus* in the Gulf of Lions were still genetically linked to these relicts during the LGM. These certainly fragile populations were very sensitive to short climatic events (i.e. Heinrich events or not) and may have disappeared from the Gulf of Lions during the Lateglacial. The presence of trees at such high latitudes during the late MIS 3 and the LGM may explain a part of discrepancies between models and the pollen data sets usually used for comparisons (Alfano et al., 2003; Huntley et al., 2003). Finally, the south-eastern France and the north-eastern Spain areas may represent the ultimate and smallest relicts that had descendants. The non-expansion or weak expansion of these trees during the deglaciation could be due to an effect of local competition for resources as climate warmed up. To clarify this point, we suggest studying cores from the Lateglacial of south-eastern, south-western France and north-eastern Spain.

References

Acherki, N., 1997. Analyse palynologique de quatre carottes du golfe du Lion. Application à la restitution de la végétation et du climat du midi de la France pendant le dernier cycle climatique et à la stratigraphie marine. Unpublished Ph.D. Thesis, University of Montpellier 2, 157pp.

Alfano, M.J., Barron, E.J., Pollard, D., Huntley, B., Allen, J.R.M., 2003. Comparison of climate model results with European vegetation and permafrost during oxygen isotope stage three. Quaternary Research 59, 97–107.

Allen, J.R.M., Watts, W.A., Huntley, B., 2000. Weichselian palynostratigraphy, palaeovegetation and palaeoenvironment: the record from Lago Grande di Monticchio, southern Italy. Quaternary International 73–74, 91–110.

Alley, R.B., Ágústsdóttir, A.M., 2005. The 8 k event: cause and consequences of a major Holocene abrupt climate change. Quaternary Science Reviews 24, 1123–1149.

Aloïsi, J.-C., Millot, C., Monaco, A., Pauc, H., 1979. Dynamique des suspensions et mécanismes sédimentologiques sur le plateau continental du golfe du Lion. Comptes Rendus de l'Académie des Sciences de Paris D 289 (13), 879–882.

Bard, E., Arnold, M., Hamelin, B., Tisnerat-Laborde, N., Cabioch, G., 1998. Radiocarbon calibration by means of mass spectrometric 230Th/234U and 14C ages of corals. An updated data base including samples from Barbados, Mururoa and Tahiti. Radiocarbon 40 (3), 1085–1092.

Bassetti, M.A., Jouet, G., Berné, S., Taviani, M., Leroux, E., Perez-Belmonte, L., 2004. Depositional history of the post-glacial transgression on the outer continental shelf of the Gulf of Lions (Western Mediterranean). American Geophysical Union, Fall Meeting, 1329.

Beaudouin, C., Dennielou, B., Melki, T., Guichard, F., Kallel, N., Berné, S., Huchon, A., 2004. The Late-Quaternary climatic signal according to palynology in a deep-sea turbiditic levee (Rhône Neofan, Gulf of Lions, NW Mediterranean). Sedimentary Geology 172 (1–2), 85–97.

Beaudouin, C., Suc, J.-P., Acherki, N., Courtois, L., Rabineau, M., Aloïsi, J.-C., Sierro, F.J., Oberlin, C., 2005a. Palynology of the Northwestern Mediterranean shelf (Gulf of Lions): first vegetational record for the last climatic cycle. Marine and Petroleum Geology 22, 845–863.

Beaudouin, C., Suc, J.-P., Cambon, G., Touzali, A., Giresse, P., Pont, D., Aloïsi, J.-C., Marsset, T., Cochonat, P., Duzer, D., Ferrier, J., 2005b. Present-day rhythmic deposition in the Grand Rhone prodelta (NW Mediterranean) according to high-resolution pollen analyses. Journal of Coastal Research 21 (2), 292–306.

Beaudouin, C., Suc, J.-P., Escarguel, G., Arnaud, M., Charmasson, S., in press. The significance of pollen signal in present-day marine terrigenous sediments: the example of the Gulf of Lions (western Mediterranean Sea). Geobios.

Bennett, K.D., Tzedakis, P.C., Willis, K.J., 1991. Quaternary refugia of North European trees. Journal of Biogeography 18, 103–115.

Berné, S., Aloïsi, J.C., Baztan, J., Dennielou, B., Droz, L., Dos Reis, T., Lofi, J., Méar, Y., Rabineau, M., 2002. Notice de la carte morphobathymétrique du Golfe du Lion. IFREMER et Région Languedoc Roussillon, Brest, 48.

Berné, S., Baton, J.M., Delpeint, A., Dennielou, B., Duval, F., Field, M.E., Lericolais, G., Le Roux, E., Satra, C., Taviani, M., 2003. Deglacial history of the Rhone prodelta from detailed morphology and preliminary stratigraphic data. In: Trincardi, F. (Ed.), Comdelta. ISMAR-CNR, Bologna, Italy, Aix en Provence, France, pp. 7–8.

Berné, S., Rabineau, M., Flores, J.A., Sierro, F.J., 2004. The impact of Quaternary global changes on Strata formation. Oceanography 17 (4), 93–103.

Brewer, S., Cheddadi, R., de Beaulieu, J.-L., Reille, M., contributors, 2002. The spread of deciduous *Quercus* throughout Europe since the last glacial period. Forest Ecology and Management 156, 27–48.

Cacho, I., Grimaalt, J.O., Sierro, F.J., Shackleton, N., Canals, M., 2002. Evidence for enhanced Mediterranean thermohaline circulation during rapid climatic cooling. Earth and Planetary Science Letters 183, 417–429.

Carrión, J.S., 2004. The use of two pollen records from deep-sea cores to frame adaptative evolutionary change for humans: a comment on "Neanderthal extinction and the millennial-scale climate variability of OIS 3" by F. d'Errico and M.F. Sánchez-Goñi. Quaternary Science Reviews 23 (9–10), 1217–1219.

Cheddadi, R., Vendramin, G.G., Litt, T., François, L., Kageyama, M., Lorentz, S., Laurent, J.-M., Beaulieu, J.-L., Sadori, L., Jost, A., Lunt, D., 2006. Imprints of glacial refugia in the modern genetic diversity of *Pinus sylvestris*. Global Change Biology 15 (3), 271–282.

Chondrogianni, C., Aritzegui, D., Rolph, T., Juggins, S., Shemesh, A., Rietti-Shati, M., Niessen, F., Guilizzoni, P., Lami, A., McKenzie, J.A., Oldfield, F., 2004. Millenial to interannual climate variability in the Mediterranean during the Last Glacial Maximun. Quaternary International 122, 31–41.

Collignon, A.M., Favre, J.M., 2000. Contribution to the postglacial history at the Western Margin of *Picea Abies*' natural area using RAPD markers. Annals of Botany 85, 713–722.

Combourieu-Nebout, N., Turon, J.-L., Zahn, R., Capotondi, L., Londeix, L., Pahnke, K., 2002. Enhanced aridity and atmospheric high-pressure stability over the western Mediterranean during the North Atlantic cold events of the past 50 ky. Geology 30 (10), 863–866.

Cour, P., 1974. Nouvelles techniques de détection des flux et des retombées polliniques: études de la sédimentation des pollens et des spores à la surface du sol. Pollen et Spores 16 (1), 103–141.

Courp, T., Monaco, A., 1990. Sediment dispersal and accumulation on the continental margin of the Gulf of Lions: sedimentary budget. Continental Shelf Research 10 (9–11), 1063–1087.

David, F., Farjanel, G., Jolly, M.-P., 2000. Enregistrement de l'histoire de la vegetation tardiglaciaire et holocène dans un grand lac: le lac d'Annecy, France.

Davis, M.B., Shaw, R.G., 2001. Range shifts and adaptative responses to Quaternary climate change. Science 292, 673–679.

de Beaulieu, J.-L., Reille, M., 1984. A long upper Pleistocene pollen record from Les Echets, near Lyon, France. Boreas 13, 111–132.

de Beaulieu, J.-L., Reille, M., 1992. The last climatic cycle at La Grande Pile (Vosges, France)—a new pollen profile. Quaternary Science Reviews 11, 431–438.

D'Errico, F., Sánchez-Goñi, M.F., 2003. Neanderthal extinction and the millennial-scale climatic variability of OIS 3. Quaternary Science Reviews 22, 769–788.

Durrieu De Madron, X., Castaing, P., Nyffeler, F., Courp, T., 1999. Slope transport of suspended particulate matter on the Aquitanian margin of the Bay of Biscay. Deep-Sea Research II 46, 2003–2027.

Duvail, C., Gorini, C., Lofi, J., Le Strat, P., Clauzon, G., Tadeu dos Reis, A., 2005. Correlation between onshore and offshore Pliocene—Quaternary systems tracts below the Roussillon Basin (eastern Pyrenees, France). Marine and Petroleum Geology 22 (6–7), 747–756.

Elenga, H., Peyron, O., Bonnefille, R., Jolly, D., Cheddadi, R., Guiot, J., Andrieu, V., Bottema, S., Buchet, G., de Beaulieu, J.-L., Hamilton, A., Maley, J., Marchant, R., Pérez-Obiol, R., Reille, M., Riollet, G., Scott, L., Straka, H., Taylor, D., Van Campo, E., Vincens, A., Laarif, F., Jonson, H., 2000. Pollen-based biome reconstruction for southern Europe and Africa 18,000 yr BP. Journal of Biogeography 27, 221–234.

Faure, H., Walter, R.C., Grant, D.R., 2002. The coastal oasis: ice age springs on emerged continental shelves. Global and Planetary Change 33, 47–56.

Flores, J.A., Sierro, F.J., Pérez-Folgado, M., Colmenero-Hidalgo, E., Gravalosa, J.M., Bárcena, M.A., Grimalt, J., Berné, S., Dennielou, B., Curtis, J.H., Hodell, D.A., PROMESS 1 Scientific Party members. 2005. Abrupt climatic changes during the last climatic cycles in the Gulf of Lions (Western Mediterranean) revealed by micropaleontological and geochemical tools. European Geosciences Union (EGU). Geophysical Research Abstract, Vienna, p. 02208.

Frignani, M., Courp, T., Cochran, J.K., Hirschberg, D., Vitoria i Codina, L., 2002. Scavenging rates and particle characteristics in and near the

Lacaze-Duthiers submarine canyon, northwest Mediterranean. Continental Shelf Research 2, 2175–2190.

Gregory, W.A., Hart, G.F., 1992. Toward a predictive model for the palynological response to sea-level changes. Palaios 7 (1), 3–33.

Gugerli, F., Sperisen, C., Büchler, U., Magni, F., Geburek, T., Jeandroz, S., Senn, J., 2001. Haplotype variation in a mitochondrial tandem repeat of Norway spruce (*Picea Abies*) populations suggests a serious founder effect during postglacial re-colonization of the western Alps. Molecular Ecology 10, 1255–1263.

Haberle, S., 1997. Upper Quaternary vegetation and climate history of the Amazon Basin: correlating marine and continental pollen record. In: Flood, R.D., Piper, D.J.W., Klaus, A., Peterson, L.C. (Eds.), Proceedings of the Ocean Drilling Program, Scientific Results, vol. 155, pp. 381–396.

Heinz, C., Thiébault, S., 1998. Characterization and palaeoecological significance of archaeological charcoal assemblages during Late-Glacial and Post-Glacial phases in southern France. Quaternary Research 50, 56–68.

Heusser, L.E., 1988. Pollen distribution in marine sediments on the continental margin off northern California. Marine Geology 80, 131–147.

Heusser, L.E., Balsam, W.L., 1977. Pollen distribution in the Northeast Pacific Ocean. Quaternary Research 7, 45–62.

Hewitt, G.M., 1999. Post-glacial re-colonization of European biota. Biological Journal of the Linnean Society 68, 87–112.

Hooghiemstra, H., Lézine, A.-M., Leroy, S.A.G., Dupont, L., Marret, F., 2006. Late Quaternary palynology in marine sediments: a synthesis of the understanding of pollen distribution patterns in NW African settings. Quaternary International 148 (1), 29–44.

Hughen, K.A., Baillie, M.G.L., Bard, E., Bayliss, A., Beck, J.W., Bertrand, C.J.H., Blackwell, P.G., Buck, C.E., Burr, G.S., Cutler, K.B., Damon, P.E., Edwards, R.L., Fairbanks, R.G., Friedrich, M., Guilderson, T.P., Kromer, B., McCormac, F.G., Manning, S.W., Bronk Ramsey, C., Reimer, P.J., Reimer, R.W., Remmele, S., Southon, J.R., Stuiver, M., Talamo, S., Taylor, F.W., van der Plicht, J., Weyhenmeyer, C.E., 2004. Marine radiocarbon age calibration, 26–0 ka BP. Radiocarbon 46, 1059–1086.

Huntley, B., Birks, H.B.J., 1983. An Atlas of Past and Present Pollen Maps for Europe: 0–13,000 years ago. Cambridge University Press, Cambridge, 667pp.

Huntley, B., Alfano, M.J., Allen, J.R.M., Pollard, D., Tzedakis, P.C., Beaulieu de, J.-L., Grüger, E., Watts, B., 2003. European vegetation during marine oxygen isotope stage-3. Quaternary Research 59, 195–212.

Jalut, G., Delibrias, G., Dagnac, J., Mardones, M., Bouhours, M., 1982. A palaeoecological approach to the last 21,000 years in the Pyrénées: the peat bog of Freychinède (alt. 1350 m, Ariège, South France). Palaeogeography, Palaeoclimatology, Palaeoecology 40, 321–359.

Johnsen, S.J., Dahl-Jensen, D., Gundestrup, N., Steffensen, J.P., Clausen, H.B., Miller, H., Masson-Delmotte, V., Sveinbjornsdottir, A.E., White, J., 2001. Oxygen isotope and palaeotemperature records from six Greenland ice-core stations: camp century, dye-3, GRIP, GISP2, Renland and NorthGRIP. Journal of Quaternary Science 14, 299–307.

Jouet, G., Berné, S., Rabineau, M., Bassetti, M.A., Bernier, P., Dennielou, B., 2006. Shoreface migration at the shelf edge and sea-level changes around the Last Glacial Maximum (Gulf of Lions, NW Mediterranean). Marine Geology 234 (1–4), 21–42.

Laurent, J.-M., Bar-Hen, A., François, L., Ghislain, M., Cheddadi, R., 2004. Refining vegetation simulation models: from plant functional types to bioclimatic affinity groups of plants. Journal of Vegetation Science 15, 739–746.

Lebreton, V., Renault-Miskovsky, J., Sémah, A.-M., 2004. La chronologie pollinique de la fin du Pliocène, du Pléistocène et de l'Holocène en Europe. Stations éponymes et historiques; nouvelles données. In: Sémah, A.-M., Renault-Miskovski, J. (Eds.), L'Evolution de la Végétation Depuis Deux Millions D'années. Saint-Etienne, Errance, pp. 30–52.

Lofi, J., Rabineau, M., Gorini, C., Berné, S., Clauzon, G., de Clarens, P., Dos Reis, T., Mountain, G.S., Ryan, W.B.F., Steckler, M., Fouchet, C., 2003. Plio-Quaternary prograding clinoform wedges of the Western Gulf of Lions continental margin (NW Mediterranean) after the Messinian Salinity crisis. Marine Geology 198, 289–317.

Magri, D., Vendramin, G.G., Comps, B., Dupanloup, I., Geburek, T., Dušan, G., Malgorzata, L., Litt, T., Ladislav, P., Roure, J.-M., Tantau, I., van der Knapp, W.O., Petit, R.-J., de Beaulieu, J.-L., 2006. A new scenario for the Quaternary history of European beech populations: palaeobotanical evidences and genetic consequences. New Phytologist 171 (1), 199–221.

McGarry, S.F., Caseldine, C., 2004. Speleothem palynology: an under-valued tool in Quaternary studies. Quaternary Science Reviews 23, 2389–2404.

McGlone, M.S., 2001. A late Quaternary pollen record from marine core P69, southeastern north island, New Zealand. New Zealand Journal of Geology and Geophysics 44, 69–77.

Millot, C., 1990. The Gulf of Lions' hydrodynamics. Continental Shelf Research 10 (9–11), 885–894.

Millot, C., 1999. Circulation in the western Mediterranean sea. Journal of Marine Systems 20, 423–442.

Monaco, A., Durrieu De Madron, X., Radakovitch, O., Heussner, S., Carbonne, J., 1999. Origin and variability of downward biogeochemical fluxes on the Rhone continental margin (NW Mediterrean). Deep-Sea Research I 46, 1483–1511.

Moreno, A., Cacho, I., Canals, M., Grimalt, J.O., Sánchez-Goñi, M.F., Shakleton, N., Sierro, F.J., 2005. Links between marine and atmospheric processes oscillating on a millennial time-scale. A multi-proxy study of the last 50,000 yr from the Alboran Sea (Western Mediterranean Sea). Quaternary Science Reviews 24, 1623–1636.

Noirfalise, A., Dahl, E., Ozenda, P., Quézel, P., 1987. Carte de la Végétation Naturelle des états Membres des Communautés Européennes et du Conseil de l'Europe. 2nd ed. Office des Publications Officielles des Communautés Européennes, Luxembourg, 78pp.

Pérez-Obiol, R., Juliá, R., 1994. Climatic change on the Iberian Peninsula recorded in a 30,000-yr pollen record from Lake Banyoles. Quaternary Research 41, 91–98.

Petit, R.J., Brewer, S., Bordacs, S., Burg, K., Cheddadi, R., Coart, E., Cottrell, J., Csaikl, U.M., Van Dam, B., Deans, J.D., Espinel, S., Fineschi, S., Finkeldey, R., Glaz, I., Goicoechea, P.G., Svejgaard Jensen, J., König, A.O., Lowe, A.J., Flemming Madsen, S., Matyas, G., Munro, R.C., Popescu, F., Slade, D., Tabbener, H., de Vries, S.G.M., Ziegenhagen, B., de Beaulieu, J.-L., Kremer, A., 2002. Identification of refugia and post-glacial colonisation routes of European white oaks based on chloroplast DNA and fossil pollen evidence. Forest Ecology and Management 156, 49–74.

Rabineau, M., 2001. Un modèle géométrique et stratigraphique des séquences de dépôts quaternaires sur la marge du golfe du Lion: enregistrement des cycles climatiques de 100,000 ans. Unpublished Thesis, University of Rennes, France, 445pp.

Rabineau, M., Berné, S., Aslanian, D., Olivet, J.-C., Joseph, P., Guillocheau, F., Bourillet, J.-F., Ledrezen, E., Granjon, A., 2005. Sedimentary processes in the Gulf of Lion: a record of 100,000 years climatic cycles. Marine and Petroleum Geology 22 (6–7), 775–804.

Ravazzi, C., 2002. Late Quaternary history of spruce in southern Europe. Review of Palaeobotany and Palynology 120, 131–177.

Reille, M., 1991. Quelques exemples de séquences polliniques polluées par de la matière organique intruse: conséquences pour l'histoire de la végétation des Pyrénées (France). Palynosciences 1, 113–138.

Reille, M., de Beaulieu, J.-L., 1988. History of the Würm and Holocene vegetation in Western Velay (Massif Central, France): a comparison of pollen analysis from three corings at the lac du Bouchet. Review of Palaeobotany and Palynology 54, 233–248.

Reille, M., Lowe, J.J., 1993. A re-evaluation of the vegetation history of the eastern Pyrenees (France) from the end of the last glacial to the present. Quaternary Science Reviews 12, 47–77.

Roucoux, K.H., Abreu de, L., Shakleton, N.J., Tzedakis, P.C., 2005. The response of NW Iberian vegetation to North Atlantic climate

oscillations during the last 65 ky. Quaternary Science Reviews 24, 1637–1653.

Roussiez, V., Aloïsi, J.-C., Monaco, A., Ludwig, W., 2005. Early muddy deposits along the Gulf of Lions shoreline: a key for a better understanding of land-to-sea transfer of sediment and associated pollutant fluxes. Marine Geology 222–223, 345–358.

Sánchez-Goñi, M.F., Cacho, I., Turon, J.-L., Guiot, J., Sierro, F.J., Peypouquet, J.-P., Grimalt, J.O., Shackleton, N.J., 2002. Synchroneity between marine and terrestrial responses to millennial scale climatic variability during the last glacial period in the Mediterranean region. Climate Dynamics 19, 95–105.

Scotti, I., Vendramin, G.C., Matteotti, L.S., Scarponi, C., Sari-Gorla, M., Binelli, G., 2000. Postglacial recolonization routes for *Picea Abies* K. in Italy as suggested by the analysis of sequence-characterized amplified region (SCAR) markers. Molecular Ecology 9, 699–708.

Stewart, J.R., 2003. Comment on "Buffered tree population changes in a Quaternary Refugium: evolutionary implications". Science 299, 825a.

Sokal, R.R., Rohlf, F.J., 1995. Biometry, third ed. Freeman and Co., New York, 887pp.

Stewart, J.R., Lister, A.M., 2001. Cryptic northern refugia and the origin of the modern biota. Trends in Ecology and Evolution 16 (11), 608–613.

Stuiver, M., Reimer, P.J., Reimer, R.W., 2005. CALIB 5.0. ⟨http://radiocarbon.pa.qub.ac.uk/calib/⟩.

Sun, X., Li, X., Beug, H.-J., 1999. Pollen distribution in hemipelagic surface sediments of the South China Sea and its relation to modern vegetation distribution. Marine Geology 156, 211–226.

Taberlet, P., Cheddadi, R., 2002. Quaternary Refugia and persistence of biodiversity. Science 297, 2009–2010.

Terhürne-Berson, R., Litt, T., Cheddadi, R., 2004. The spread of *Abies* throughout Europe since the last glacial period: combined macrofossil and pollen data. Vegetation History and Archaeobotany 13, 257–268.

Triat-Laval, H., 1978. Contribution pollenanalytique à l'histoire tardigla-ciaire de la végétation de la basse vallée du Rhône. Unpublished Thesis, University of Aix-Marseille 3, France, 343pp.

Turon, J.-L., Lézine, A.-M., Denèfle, M., 2003. Land–sea correlations for the last glaciation inferred from a pollen and dinocyst record from the Portuguese margin. Quaternary Research 59, 88–96.

Tzedakis, C., 1993. Long-term tree populations in northwest Greece through multiple Quaternary climatic cycles. Nature 364, 437–440.

Tzedakis, P.C., 2004. The Balkans as prime glacial refugial territory of European temperate trees. In: Griffiths, H.I., Krystufek, B., Reed, J.M. (Eds.), Balkan Biodiversity. Pattern and Process in the European Hotspot. Kluwer Academic Publishers, Dordrecht, pp. 49–68.

Tzedakis, P.C., Lawson, I.T., Frogley, M.R., Hewitt, G.M., Preece, R.C., 2002. Buffered tree population changes in a Quaternary refugium: evolutionary implications. Science 297, 2044–2047.

Tzedakis, P.C., Lawson, I.T., Frogley, M.R., Hewitt, G.M., Preece, R.C., 2003. Comment on "buffered tree population changes in a Quaternary refugium: evolutionary implications". Science 299, 825b.

Van der Kaars, S., 2001. Pollen distribution in marine sediments from the south-eastern Indonesian waters. Palaeogeography, Palaeoclimato-logy, Palaeoecology 171, 341–361.

Węgrzynek, D., Jambers, W., Van Grieken, R., Eisma, D., 1997. Individual particles analysis of western Mediterranean sediments cores, Rhône suspended matter and Sahara aerosols, investigation of inputs to the sediments. Marine Chemistry 57, 41–53.

Willis, K.J., Van Andel, T.H., 2004. Trees or not trees: the environments of central and eastern Europe during the last Glaciation. Quaternary Science Reviews 23, 2369–2387.

Woillard, G.M., 1978. Grande pile peat bog: a continuous pollen record for the last 140,000 Years. Quaternary Research 9, 1–21.

RESPONSE OF THE RHÔNE DELTAIC MARGIN TO LOADING AND SUBSIDENCE DURING THE LAST CLIMATIC CYCLE

Gwenael Jouet, Eric W.H. Hutton, James P.M. Syvitski and Serge Berné.

Corresponding author: Gwenael Jouet

(gwenael.jouet@ifremer.fr)

Response of the Rhône deltaic margin to loading and subsidence during the last climatic cycle.

Gwenael Jouet[a,b,*], Eric W.H. Hutton[c], James P.M. Syvitski[c] and Serge Berné[b].

[a]Géosciences Marines, IFREMER - French Research Institute for Exploitation of the Sea, Technopôle Brest-Iroise, BP 70, 29280 Plouzané, France.
[b]Laboratoire CNRS UMR6538 Domaines Oceaniques, Université de Bretagne Occidentale, IUEM, place N. Copernic, Technopôle Brest-Iroise, 29280 Plouzane, France,
[c]Environmental Computation and Imaging Facility, INSTAAR, University of Colorado, 1560 30th Street, Boulder, CO 80309-0450, USA.

Abstract:

Passive continental margin subsidence is initiated by the synrift mechanical stretching of the lithospheric upper brittle layer and continues during the postrift phase; the thermal cooling and contraction of the upwelled asthenosphere forces the margin to subside in addition to the overloads from sea water and sediments. Therefore, the total subsidence in stretched basins includes fault-controlled initial sinking, thermal subsidence and flexural isostatic compensations. Decoupling and estimating the different components of this subsidence from stratigraphic analysis and restricted geophysical and sedimentological databases remains problematic. In particular, backstripping the sediment layers requires a well-constrained geological framework. A method is proposed here to investigate the subsidence history of a margin based on forward stratigraphic modelling. Using the *Sedflux* model, several experiments are done using generally agreed upon assumptions on the parameters describing lithospheric rheology and isostatic behaviour of a margin. The stratigraphic modelling of the Rhône deltaic margin during the last climatic cycle (125 ky) provides an assessment of these parameter-estimates and their influence on geohistory (tectonic/thermal subsidence and sediment loading). The model results confirm the important impact of water loading on vertical deflection along the platform between glacial low sea level and interglacial high sea level. Based on Gulf of Lions (NW Mediterranean) observations, a conceptual method that uses the stratigraphic simulations is produced in order to evaluate the different components of the total subsidence of a margin, and in particular, the relative impact of tectonic subsidence and sediment load.

* Corresponding author. *E-mail address: gjouet@ifremer.fr*

Tel: +33 (0)2 98 22 48 19 or +33 (0)2 98 49 87 17

Fax: +33 (0)2 98 22 45 70

1. Introduction

Present-day stratigraphic organisation and sedimentary thickness on a platform are products of cumulative changes in sedimentary systems through time. The location and preservation of depocentres, as shown by seismic profiles from the shelf, result from changes in accommodation. A significant subsidence rate of the margin is necessary to permit a continuous record and preservation of a depositional sequence. On passive margins, accommodation is most important at the shelf edge. The location and magnitude of the sediment sources, together with eustatic controls, may result in erosion of the sediment wedge on the inner shelf. Studying basin subsidence and sedimentary filling is essential for understanding the tectonic and thermal history of passive continental margins. Therefore, subsidence rate, together with sediment flux and global sea-level variations have to be taken into account in order to investigate the origin of vertical motions of marine continental shelves. Total subsidence, which contributes to accommodation, corresponds to medium to long-term Earth processes that involve constraints from lithospheric structure and asthenospheric cooling. The overloads of sediments and water amplify vertical movements, according to the laws of isostatic compensation. Numerous parameters are implied for this process. It is therefore difficult to disentangle and quantify the different components that contribute to the subsidence of the platform.

Geohistory analysis (Van Hinte, 1978), based on seismic stratigraphy and lithological information from boreholes or sediments cores, provides important constraints on the tectonic and/or thermal subsidence and sediment accumulation rates through time. Decompaction of the present-day sedimentary thicknesses, paleobathymetry and paleosealevel helps to evaluate the vertical evolution of a continental margin. Using this method, amounts of total and tectonic subsidence can be determined through decompaction of stratigraphy and backstripping of sediment load. This technique has been applied to investigate several margins worldwide (Ceramicola *et al.*, 2005, Steckler *et al.*, 1999). Watts and Ryan (1976) proposed the isolation of the tectonic driving force by removal of the isostatic effects of sediment load (i.e the Backstripping technique). Unfortunately, the validity of the method

requires a well-known sedimentary and structural system and precise estimates of specific parameters like compaction, paleobathymetry and absolute sea-level fluctuations. A quantitative analysis of subsidence rate through time relies on knowledge of basin formation and evolution.

There are two conceptual approaches to model a basin and to determine the factors that affect its formation and its infilling. The first is the backstripping method, which successively removes strata to recover a margin's geohistory. Most of the time, it is not simple to estimate each of the parameters required by this method. This leads to under- or over-estimation of the subsidence components. In particular, determination of paleobathymetry from observational data cannot generally be estimated with enough accuracy. In addition, the sediment record is discontinuous because of non-deposition and erosional events, and the complete geodynamic evolution of margins cannot be reconstructed (i.e. Bessis, 1986; Ceramicola *et al.*, 2005, Steckler *et al.*, 1999). Thus, backstripping implies assumptions about the geological evolution of the studied margin, without possibility for testing the validity of these hypotheses. The second approach, described here, uses forward stratigraphic modelling to simulate the delivery of sediment and its accumulation in a sedimentary basin (e.g. Syvitski and Hutton, 2001), and takes into account variations in the various controls on sedimentation. In conjunction with the backstripping method, the stratigraphic simulation is useful for investigating the boundary conditions of the evolution of a basin and its changes in accommodation.

This paper demonstrates the use of stratigraphic simulations to validate and extrapolate different hypotheses on basin dynamics and the formation of shelf sedimentary wedges. An estimate of subsidence and sediment thickness from seismic stratigraphic analysis is tested and refined during a simulation of the basin evolution. The method is applied to the Gulf of Lions as a case study. Next, a conceptual method using the stratigraphic simulations is produced to isolate the different components of total subsidence of a margin (tectonic/thermal subsidence, sediment and water loading) during a relatively short geological interval.

2. Subsidence and Isostasy

Sediment dispersion and deposition in a sedimentary basin is the product of the interplay between the generation of accommodation and sediment supply. Sediment accumulations and their internal geometries are therefore controlled largely by the tectonic/thermal and isostatic

mechanisms that cause subsidence (Fig. 1). Change in accommodation is thus an important part of the driving mechanisms responsible for the stratigraphic pattern in basin-fill. If we consider a theoretical lithological column, these mechanisms can be subdivided into: 1- tectonic forcing controlling the spatial and temporal pattern of subsidence and the evolution of the sediment routing system, and 2- eustasy that essentially controls accommodation and sets base level (Allen and Allen, 2005). As a consequence, several vertical motions of the reference level can be observed (Fig. 1). Motions can be inferred from the evolution of each lithological unit and lead us to define the different components of the total subsidence (S). The lithospheric structural processes of margin formation and evolution through time are involved in the tectonic/thermal subsidence (TS), whereas global eustasy and sedimentation are associated and have an important impact on the isostatic response of this margin. Sea water defines the water loading (WL), which relies on sea-level variations. The thickness of sedimentary accretion is the result of erosion/deposition processes; it contributes to the sediment load (SL). We define "geohistory" subsidence (GS) as the combination of TS and SL. Seismic stratigraphy is one way to evaluate GS through time, often between two successive interglacial high sea-levels in order to remove the effects of sea-level variations. Below we discuss each component of the total subsidence and, in particular, the proportion of tectonic subsidence and sediment load in the geohistory subsidence (Fig. 2).

2.1 Tectonic/thermal subsidence: basin formation

Our study focuses on the shelf area of passive continental margins (i.e. seismically inactive). In a uniform stretching model (McKenzie, 1978), the formation of a passive margin can be divided into two major phases of structural adjustments. During continental rifting, there is a brittle extension of the crust that produces the stretching of the continental lithosphere and a rapid synrift subsidence. After lithospheric thinning, a postrift phase is mainly governed by the cooling and contraction of the upwelled asthenosphere. The thermal relaxation is at the origin of an exponentially decreasing postrift subsidence. Synrift tectonic subsidence rates are typically <0.2 mm/y (200 m/My) and postrift tectonic subsidence rates are about <0.05 mm/y (50 m/My) (Allen and Allen, 2005). The amount of synrift and postrift subsidence depends essentially on the initial crustal to lithospheric thickness ratio and on the amount of stretching. The present-day tectonic/thermal subsidence of a margin is a long-term geological process that directly results from its structural and thermal context and history, and from its age (Fig. 1).

2.2 Isostatic subsidence

Increases in sediment load and water load causes additional subsidence of the sedimentary basin through the isostatic response of the lithosphere.

2.2.1 Subsidence from overload

Passive margins are characterized by seaward thickening prisms of marine sediments overlying a faulted basement of synrift sedimentary sequences. The postrift seaward-thickening sediment prisms consist predominantly of shallower marine deposits (Allen and Allen, 2005). This sedimentary wedge, together with the overlying sea water column modifies long-term tectonic subsidence. The weight of sediment deposited on a particular area of the shelf may cause the underlying crust to sink. Sediment erosion may cause the margin to rise.

A change in global sea-level relative to a reference datum is known as eustasy (Lisitzin, 1974). Eustasy in turn is one of the major causes of relative sea-level changes through hydro-isostasy (Johnston, 1995; Lambeck, 1997, 2000; Peltier, 2002; Posamentier et al., 1988), and thus impacts accommodation. Any increase (or decrease) of ocean volume must be compensated isostatically. Global sea-level changes are largely due to global climatic changes. As the earth's climate cools, the ocean surface cools and ocean volume decreases (the steric effect). Additionally ice-sheets may form, storing water on land and reducing the ocean volume. During a warming period, ocean volume changes will move in the opposite direction. The major consequences of sea-level rise are observed at the glacial/interglacial transition, with differences between low and high sea-level positions of more than 120 m; between successive interglacial sea-level positions, the differences are minor.

2.2.2 Flexure of the lithosphere: isostatic compensation

Below some depth, there is no density contrast between two adjacent columns. The weight of the columns above this depth of compensation must be equal. This is a local isostatic balance (Airy, 1855; Pratt, 1855); the deflection of the crust at any location depends only on the local overload at that location (Airy and Pratt models of compensation). But the local isostatic balance neglects the lateral strength of the lithosphere and its relative rigidity. A more realistic model assumes that the lithosphere responds to loads like an elastic plate overlying an inviscid fluid (Kirby, 1983). Application of Archimedes principle suggests that bent continental plates are buoyed up by a force equal to the weight of the displaced mantle (Turcotte and Schubert, 1982). The net effect is for the entire region affected by flexure to be

in regional isostatic balance. The lithosphere behaves approximately as an elastic beam of some assumed rigidity. A more rigid beam produces a broader and shallower deflection. A less rigid beam results in a deeper and narrower deflection.

A quantitative way to estimate the rigidity of the lithosphere is its effective elastic thickness (*EET*) (Burov and Diament, 1995; Watts, 1992).

$$EET = \sqrt[3]{\frac{12(1 - v^2)D}{E}}$$ (1)

Two constants, the Poisson's ratio ($v = 0.25$) and the Young's modulus ($E = 7.10^{10}$ N/m^2), characterize the rheology (the stress/strain relationship) of the elastic portion of the crust and mantle lithosphere. D is the flexural rigidity in N/m. *EET* appears to be independent of the age of the load (Watts *et al.*, 1982), which suggests that the elastic stresses that cause deflection, do not relax on a geological time scale. Adding a sediment and/or water load to the deflection causes the amount of deflection to increase. The most complete dataset currently available (Watts, 2001) describes values of *EET* between 5 and 110 km. For the specific application in the Gulf of Lions, Lambeck and Bard (2000) use an *EET* of 65 km in order to model the last deglacial isostatic rebound.

Using a simple model for bending a visco-elastic slab under a distributed load permits us to explore the effects of the isostatic components within a single-layer lithosphere. In the case of a glaciated margin, Huybrechts and De Wolde (1999) propose an isostatic ice-dynamic reconstruction model that assumes a rigid elastic lithosphere overlies a viscous asthenosphere. In this model bedrock adjustments are described by a single isostatic relaxation time. In this way, the isostatic compensation takes into account the effects of loading changes within an area several hundred kilometres wide. From this example, we obtain a value for the flexural rigidity (10^{25} Nm) corresponding to a lithospheric thickness of 115 km; the characteristic relaxation time for the asthenosphere is about 3,000 years (Huybrechts, 2002). The relaxation time is characteristic of the time dependence of the isostatic rebound process; it depends almost entirely upon the viscosity of the mantle. Relaxation times vary from approximately 3,400 years in SE Hudson Bay (Canada) to 4,200 years in the Gulf of Bothnia (Sweden) for postglacial rebound modelling (Peltier, 1998).

Thus, investigating the present-day stratigraphy should help us to estimate the accommodation history and evaluate the different components of subsidence that contribute to

its changes. The typical response of continental stretching is early, rapid, fault-controlled subsidence followed by lithosphere cooling dominated by gravity-controlled deformation. Sediment accumulation and water load in a sedimentary basin causes extra-subsidence of the basement corresponding to a general basinward tilt in a long-term postrift tectonic and thermal subsiding context. The isostatic flexure of the lithosphere undergoing additional sedimentary load, such as a prograding sedimentary wedge, produces a regional deflection that is controlled by the effective elastic thickness of the lithosphere and the properties of the mantle viscosity (modelled by the relaxation time parameter). However, if the lithosphere reacts to the sediment load through regional flexure, the separation of the tectonic and sediment contributions is complex. The flexural loading of the sedimentary basin can be accounted for if the flexural rigidity and spatial distribution of the sediment load is known.

3. Methods for estimating subsidence

This study defines a method to better constrain the environmental and structural settings of a study area (Fig. 2), especially the isostatic behaviour of a continental shelf under different loading conditions (variations in sediment and water loads). There are different ways to estimate components of subsidence and to approach a margin's isostatic characteristics. The weakness of methods, such as "backstripping", is that they often require much knowledge about general settings that lead to many assumptions. In order to fix the isostatic parameters, one solution is to test them in their context and take advantage of stratigraphic simulations. Different hypothesis can be tested. Numerical stratigraphic models are useful for understanding the time-varying impact of sedimentary processes on the stratigraphic organisation. Stratigraphic simulation models are based on algorithms that conceptually or dynamically simulate the important input, boundary conditions and processes that define a sedimentary system (Syvitski, 1989). Subsidence, sea-level and isostasy combine to create accommodation in the basin, which controls sedimentation on the shelf. They also correspond to the main input values required for the simulations. In this way the different components of subsidence, measured during geohistory analysis, can be tested and estimated through numerical modelling.

3.1 *Sedflux*: eustasy and subsidence modelling

Here, we apply the model *Sedflux (Hutton & Syvitski, this volume)* to simulate the delivery and accumulation of sediment within a basin through time. *Sedflux* includes the effects of sea-level and sediment supply fluctuations over time scales of tens of thousands of years. The

basin-fill model allows for the continental margin to undergo tectonic processes (subsidence and uplift) and isostatic effects from sediment and water loads. The model architecture has a typical vertical resolution of 1 to 25 cm, and a typical horizontal resolution of 10 to 100 m. Various processes are modelled at a time step (days to years) that is sensitive to median-term variations of the seafloor (Syvitski and Hutton, 2001). A major subroutine of *Sedflux* corresponds to a momentum-driven hypopycnal plume, based on the Albertson *et al.* (1950) model of a submerged and steady, two-dimentional surface jet emanating out of a river mouth (Syvitski *et al.*, 1998). This advection-diffusion subroutine introduces a time-varying sediment flux into the modelled basin to allow the stratigraphic organisation of sediment on a shelf. *Sedflux* requires as inputs an initial bathymetry of the basin at the simulation onset, and time-varying sediment flux and sea-level history. Of importance to this study are parameters related to subsidence and flexural response. In *Sedflux*, two different types of subsidence are considered: isostasy and tectonic subsidence. For isostatic subsidence, the lithosphere is treated as an elastic beam that is allowed to flex under the load of added sediment and water. For tectonic subsidence the user specifies subsidence rates at various positions and times (Syvitski and Hutton, 2001).

3.1.1 Tectonic subsidence

The physics of the processes that lead to tectonic or thermal movements are not modelled in *Sedflux*. Instead the results of these processes are incorporated as input to the model domain; vertical displacements for the modelled basin are specified in an input file, and these are allowed to vary both spatially and temporally. Subsidence and uplift rates are defined in meters per year at particular point along a basin for a specific instant in time. *Sedflux* interpolates these data to the defined temporal and spatial resolution of the particular model run. Results of the modelling provide confirmation of the range of subsidence rates used for it.

3.1.2 Isostatic subsidence

The changes in water and sediment load in a basin cause vertical lithospheric deflections (Fig. 1). In the case of a thick sedimentary wedge, subsidence becomes a leading process. *Sedflux* models subsidence due to loading using an elastic flexure model (Syvitski and Hutton, 2001). The elastic flexure model applied to Earth's crust makes four basic assumptions; 1- the lithosphere is assumed to have a linear elastic rheology, 2- the deflections are assumed to be small, 3- the elastic lithosphere is assumed to be thin compared to the horizontal dimensions of the plate, 4- planar sections within the plate are assumed to remain planar after deflection.

For a single vertical load applied to the Earth's crust, the resulting displacements are given by:

$$w(x) = \frac{p(x)\alpha^3}{8D} \exp\left(-\frac{|x|}{\alpha}\right)\left(\cos\left(\frac{|x|}{\alpha}\right) + \sin\left(\frac{|x|}{\alpha}\right)\right) \tag{2}$$

with α defined as

$$\alpha \equiv \sqrt[4]{\frac{4D}{\rho_m g}} \tag{3}$$

and w is the displacement of crust due to sediment loading, D the flexural rigidity of the Earth's crust (i.e. Equ.1), ρ_m the density of the overlying sediment, and x the horizontal position. Because of our assumption of the linearity of our system, the resulting displacement due to multiple columns of sediment is simply the sum of the displacements due to each individual column.

After a load is applied, the viscous asthenosphere must flow out of the way before the lithosphere can deflect; causing a time delay between the addition of load and the lithosphere's response. Although models exist that predict the crustal response given a series of viscosity layers (Paulson *et al.*, 2005), this is beyond the scope of *Sedflux*. Instead, *Sedflux* assumes that the crustal response is exponential with time,

$$w(t) = w_0\left(1 - \exp\left(-\frac{t}{t_0}\right)\right) \tag{4}$$

where w_0 is the equilibrium deflection as determined by Equation (2), t is the time since the load was applied, and t_0 is the response time of the lithosphere. The elastic flexure model in *Sedflux* only needs values for the effective elastic thickness (Equ.1) and the relaxation time (Equ.4) in order to calculate lithospheric deflections.

3.2 Method strategy

Based on the results from geohistory analysis (1 in Fig. 2), different parameters are used for several numerical runs of the stratigraphic model to estimate the different components of the total subsidence (S). The interpretation of seismic and lithological data allows the definition of the geohistory subsidence (GS) (2 in Fig. 2). The identification of dated erosion paleosurfaces permits us to quantify their vertical evolution through time and to estimate the GS subsidence. This value takes into account both the tectonic subsidence (TS) and the loads

due to sediment deposition (SL). Using the GS estimation and the sea-level variations as input parameters, the stratigraphic modelling can be realized with *Sedflux* (3 in Fig. 2).

The first stage of modelling is to experiment with different ranges of parameters that set the isostatic adjustment, in order to define of the best effective elastic thickness and relaxation time. The first model is run only with the GS subsidence (4 in Fig. 2), and provides a view of the tectonic subsidence added to the sediment load effect on the margin during the simulated time. The second model run does the same with eustasy (5 in Fig. 2). Therefore the margin responds to changing water load due to sea-level variations and consequently water column thickness fluctuates (WL). The combination of GS and eustasy is used for the third simulation (6 in Fig. 2), and corresponds to the modelling of the total subsidence (S) as all components are considered. These results are compared to the stratigraphic pattern observed on seismic profiles and parameters are adjusted in order to minimize the differences between model results and field observations (7 in Fig. 2).

The final stage of this method is to quantify the fraction of tectonic subsidence (TS) relative to the sediment load (SL) within the GS subsidence. For this simulation, a constant sediment flux is added to the GS subsidence and the eustasy, with the objective to reproduce the sedimentary thicknesses observed on seismic analysis (8 in Fig. 2). We call the resulting simulated subsidence S', as it corresponds to the addition of total subsidence (S) with the sediment load (SL) (9 in Fig. 2). The comparison between S and S' allows us to estimate the effect of sediment load (SL) (10 in Fig. 2). Finally, the values of SL serve to partition GS subsidence into sediment load (SL) and tectonic/thermal subsidence (TS). Therefore, the suite of stratigraphic simulation provides an estimate of all the components controlling the vertical motion of the margin.

4. Application: Stratigraphic modelling of the Gulf of Lions margin

The subsidence history of the Gulf of Lions margin (Fig. 3) is investigated using stratigraphic simulations to calibrate our subsidence study. The available geophysical and lithological datasets provide an ideal well-constrained domain of application. Subsidence was historically explored on the basis of petroleum boreholes (Watts and Ryan, 1976) and multichannel seismic (Bessis, 1986; Bessis and Burrus, 1986). More recently, subsidence rate was established from high resolution seismic, constrained by modelling of the last 500 ky

(Rabineau, 2001). Our method, using the *Sedflux* model, has been assessed for the last climatic cycle, and subsidence components have been estimated.

4.1 Geological settings

The Palaeozoic and Mesozoic basement of the Gulf of Lions continental margin has undergone several phases of stretches and strains since the Hercynian orogeneses (Biju-Duval, 1984). The passive margin was shaped following the combined Oligo-Aquitanian rifting phase between continent and the Corsica-Sardinia microplate, and the Burdigalian crustal opening (Gueguen, 1995; Sioni, 1997). This margin is covered by sedimentary series dated from Oligocene to Quaternary (Bentounsi, 1990; Gorini *et al.*, 1993). The synrift series (30-24 My) is topped by a Middle Aquitanian to Middle Burdigalian ravinement surface, which marked the onset of clastic postrift deposits. This depositional sequence (24-6.3 My) corresponds to the Miocene prograding wedge, largely eroded on the shelf and upper slope during the Messinian crisis (6.3-5.2 My) (Lofi *et al.*, 2003). The upper Plio-Quaternary deposits have recorded the sedimentary structures associated with the increasing sea-level fluctuations during that time (Berné *et al.*, 2002).

The Quaternary stratigraphic organisation of the Gulf of Lions is described by several conceptual models (Aloisi, 1986; Got, 1973; Monaco, 1971). High-resolution seismic data show, within the Middle and Late Quaternary, the repetition of several prograding wedges bounded by high amplitude seismic discontinuities (Fig. 4). These surfaces pinch out landward at about 80 m water depth. Within each seismic sequence, two major types of seismic facies are identified. Gently dipping clinoforms (PI) were interpreted as the product of mud deposition in a relatively low-energy environment whereas relatively high-angle clinoforms (PII, from 3° to 7°) were considered as corresponding to sandy upper shoreface facies (Berné *et al.*, 1998; Gensous and Tesson, 1996; Rabineau, 2001; Rabineau *et al.* 2005; Tesson *et al.*, 1990; Tesson *et al.*, 2000). The major shelf sequences are associated with the Middle and Late Quaternary glacial/interglacial climatic and eustatic fluctuations. Regressive deposits constitute the majority of preserved sediments. Using stratigraphic modelling, Rabineau (2001) demonstrated that these sequences are linked to 100 ky orbital cycles.

The present-day bathymetric configuration (Fig. 3) of the Gulf of Lions illustrates the present highstand situation with distinct lowstand, forced regressed and highstand systems tracts. The Holocene Rhône prodeltaic lobes and the last transgressive units, form the post-glacial

subaqueous delta on the inner shelf, and sediment accumulations along the coast. From the middle to outer shelf, the majority of the prograding wedges correspond to regressive deposits. Parts of the wedges consist of muddy sedimentary bodies with gently dipping clinoforms while others form sandy shorefaces with high-angle clinoforms that settle on the outer shelf (Berné *et al.*, 1998) (Fig. 5). This major seismic sequence, formed as a forced regression during the overall sea-level fall between MIS-3 and MIS-2, corresponds to a falling stage systems tract in the sense of Plint and Nummedal (2000). It can be sub-divided into several prograding units, which indicate that this relative sea-level fall was punctuated by intervals of increased or decreased falls, or even stillstand (Jouet *et al.*, 2006). Major polygenetic regional erosion surfaces top the last two glacial sedimentary prisms. They formed both as subaerial and marine erosion surfaces during sea-level fall (sequence boundaries), and then were reworked (as a ravinement surface) during the ensuing transgression (Bassetti et al., 2006).

The sequence deposited during the last climatic cycle is shown by a very-high resolution Chirp seismic profile (Fig. 5). It is located between the erosion surface *D60*, attributed to the penultimate glacial period (Marine Isotopic Stage 6 or MIS-6), and the erosion surface *D70*, formed during MIS-2 (Fig. 6). During glacial periods, sea-level was at a relatively low position, and favoured erosion. Although *D70* is defined as the last glacial erosion surface, we can observe it within an interglacial (highstand of sea-level, MIS-1) situation. Later in this paper, we will compare the present-day position (MIS-1) of *D70* to the position of *D60* (dated to MIS-6) at its subsequent interglacial position (MIS-5). For each case, it corresponds to the position of a glacial erosional surface at the following interglacial highstand.

4.2 Subsidence in the Gulf of Lions

During the Late Quaternary, the Gulf of Lions margin underwent postrift deformations. The amount of well-preserved sediment accumulation on the shelf attests to a considerable geohistory subsidence, which is the result of the combination of thermal subsidence and sediment load effects. The quantitative estimation of the geohistory subsidence in the Gulf of Lions was typically realised by the "Backstripping" method on depth converted seismic sections crossing the margin, and using several petroleum exploration boreholes (Bessis, 1986; Watts and Ryan, 1976). The variations of subsidence from the internal platform to the deep basin confirm the rapid initial burying of the margin between 30 to 23 My associated with crustal stretching during rifting (mechanic tectonic subsidence). The curves illustrate the

exponential slowdown in postrift subsidence rate in response to the cooling of the lithosphere (thermal tectonic subsidence) without any significant tectonic activity. The cumulative subsidence of the basin (reaching 10 km in the deep basin) since the Oligocene would be equivalent to that calculated for older Atlantic margins (Bessis and Burrus, 1986; Burrus, 1984) although its age is only 30 My. Such magnitudes cannot be explained by an extensional model alone. The Gulf of Lions margin has the physiography of an Atlantic-type margin with the subsidence rate of an active margin (100-200 m/My) (Steckler and Watts, 1980). For the Upper Quaternary, Rabineau *et al.* (2005) estimates the geohistory subsidence rate at around 255 m/My at the shelf edge from the stratigraphic analysis of different seismic data sets and the modelling of cyclic stratigraphic sequences. It is based on the identification of dated erosion paleosurfaces that are interpreted as representing 100 ky glacial cycles (Fig. 5). The present position of the Messinian erosion surface is consistent with this value, and this work was used as a reference for estimating the vertical evolution of the margin (Fig. 6).

For the same period, Burrus and Audebert (1990) estimate the tectonic subsidence from about 20 m/My on the continental platform to about 180 m/My in the deep basin. The basic mechanism for postrift subsidence is thermal relaxation. However, according to Bessis and Burrus (1986), the loading effect of the sediment would contribute by 40 to 50 % to the total subsidence of the margin. Consequently, part of the high increase in accommodation could be due to the loading effect of sediments. The water loading effect was investigated by Lambeck and Bard (2000) on the basis of a comparison between observational evidence for sea-level changes along the French Mediterranean coast and the prediction from a glacio-hydro-isostatic model. From the last glacial period to present-day (Fig. 6), they tested the impact of the sea-level rise on the margin. A difference of 15 m between the position of sea-level during LGM and the present-day position of this paleoshoreline, confirms the importance of the isostatic rebound due to decreasing water column (Lambeck and Bard, 2000).

4.3 Results

Based on these estimates of the geohistory subsidence and using a compilation of global sea level from Waelbroeck *et al.* (2002) (Fig. 6), we ran several isostatic models with *Sedflux* for the last climatic cycle from 125 ky (MIS-5) to present-day (MIS-1) (Fig. 2). Models R1-R5 (Table 1) represent different isostatic adjustments obtained from the range of parameters tested and are broadly consistent with isostatic effective elastic thickness (*EET*) and relaxation time (*RT*), described in similar studies (sect. 4.2). The *EET* allows us to set local to regional

flexural isostatic compensation and RT to fix slow to fast margin adjustments (Table 1). The geohistory subsidence (GS), used for simulation input, was defined as a progressive seaward tilt, taking into account the measured values of 255 m/My at 70 km from the coast (Rabineau, 2001). The convergence point of major seismic discontinuities roughly corresponds to the present shoreline (50 km on the simulated section). In a first approximation, this convergence point represents the position of the tectonic hinge point. However, its precise location cannot be determined geometrically because the magnitude of erosion affecting each surface is unknown. The sediment load (SL) effect is included in GS. Therefore, the R1-R5 Models were run without sediment input. Only the sea-level variations (WL) were added to GS in order to simulate the total subsidence (S). The simulation duration corresponds to the last 125 ky from the last interglacial and high sea-level to present warm period and highstand (Fig. 6). The strategy for these simulations is to compare the interglacial position of two successive erosional surfaces formed during two successive glacial low sea-levels.

The seismic discontinuity $D70$ (formed during MIS-2) is presently observed at the position that corresponds to interglacial MIS-1. $D70$ is used as the initial surface for the simulation. We make the assumption that this surface represents the closest position that was occupied by the previous seismic discontinuity $D60$ (formed at the penultimate glacial period MIS-6) during the last interglacial MIS-5 (125 ky). The final surface at the simulation end is compared with the present-day position of $D60$ on seismic profiles. Otherwise, as described on seismic profiles, sandy wedges with high-angle clinoforms are preserved on the outer shelf and represent successive glacial shorefaces that can be used as a "dipstick" for sea-levels. It must be noted that the magnitude of erosion of these deposits was different during the last two glacial cycles; the last glacial sandy shoreface being better preserved compared to the shoreface formed during MIS-6 (Fig. 6). Nevertheless, the adjustment of the final simulated surface, based on these features, is feasible.

4.3.1 Test of rheology

The results of different tests on the lithosperic and asthenospheric behaviour are presented in figure 7. For each isostatic parameter (EET and RT) and for different values of them, the initial and final surfaces are plotted. Figure 7 shows, successively, the initial surface at the high sea-level of simulation onset (125 ky), the position of this surface during glacial low sea level, and finally, the simulated final surface at present-day position. The last erosional

surface is compared with the present-day position of *D60* observed on the seismic profile (Fig. 5) and reported in this graph.

We tested *EET* ranging from 50 to 100 km. Our results show that this value has relatively limited impact on the position of the final observed surface (Fig. 7). Only a difference in the isostatic response during the glacial period can be observed. In contrast, large variations of the position of final surfaces on the basis of different *RT* confirm the importance of this semi-empirical parameter, controlled by upper mantle cooling (sect. 2.2.2). The difference between the simulated and observed final position of *D60* is associated with the morphological difference between *D70*, used as the initial surface, and *D60*, the modelled surface (Fig. 7). The comparison is made to sandy paleoshorefaces that mark the paleoshoreline position through time. There is a good match between the simulated and observed paleoshoreline, except for differences in erosion. At this stage, the simulations do not take this erosion into account. From these tests, the preferred isostatic adjustment R8, for the following simulations, use an effective elastic thickness of 65 km and a relaxation time of 3,500 years (Table 1). The seismic interpretation otherwise leads us to run different scenarios of the geohistory subsidence. In particular, the seaward migration of the convergence point between *D70* and *D60* from 50 to 80 km provides a best fit between simulated and observed final surfaces between 70 and 90 km on the working section. Note that above this point, simulations are not precisely constrained. Only the marine part of the model is accurate enough for simulating the vertical motions.

4.3.2 Evolution of the total subsidence through time

Stratigraphic modelling points to a specific position along the section through the 125 ky of simulations. We observed, in particular, the evolution of the elevation at 100 km, where the total subsidence (*S*) variations can be quantified (Fig. 8). Simulations have taken into account only the geohistory subsidence (*GS*) or the water loading (*WL*) effect. Therefore, *S*, *WL* and *GS* are plotted as a function of simulated time and the difference of evolutions can be monitored (Fig. 8). The modelling confirms that the simple addition of *WL* and *GS* is not sufficient to reproduce the total subsidence. The evolution of each component of subsidence is dependant on the others. In particular, the water loading is mainly the consequence of relative sea-level, which is partly dependant on the geohistory subsidence (Fig. 1). The second aspect, deduced from these observations, is to consider the rapid total subsidence variations as the results of the water loading fluctuations. The *GS* is assumed to be constant along the

simulations; the sea-level oscillations are the only parameter that can modify the load on the shelf. As a result, total subsidence mimics the seal-level variations of the last climatic cycle (Fig. 8.2).

4.3.3 The geohistory subsidence and water loading effect

We estimate the importance of water loading on the vertical evolution of the shelf. From the tests described in figure 7, the platform is uplifted as sea-level falls until the glacial period (21 ky) even with geohistory subsidence active. Confirmation is seen in the results from the adapted isostatic model R8 (Fig. 8); the elevation, which only takes into account water loading, rises between 125 and 21 ky and then rapidly drops after the Glacial period when relatively low sea-level unloads the shelf. The impact of the WL on the shelf, between the glacial sea-level lowstand (21 ky) and the present-day highstand, can cause isostatic sinking of about 20 m at 100 km on the simulated section (Fig. 8).

Similarly the progressive sinking of the margin due to the combination of the tectonic/thermal subsidence and the sediment loading (GS) is estimated to be about 15 m for the last climatic cycle and about 5 m for the last deglaciation (from 21 ky to present-day).

4.3.4 Estimation of the sediment loading effect

Tectonic/thermal subsidence and sediment loading both contribute to the GS, which has been evaluated as 15 m of subsidence during the last climatic cycle (Fig. 8). During the stratigraphic model simulation R8, the sediment load contribution is taken into account in the GS, as we did not add sediment into the model domain. In order to estimate the contribution of sediment load into the GS, the model R9 was run with a sediment source (Table 1). The amount of sediment input was determined in order to obtain a sedimentary thickness equivalent to that measured on the seismic interpretation.

For this study, we considered the sediment influx as a constant parameter during the 125 ky; locally, the change in accommodation and the sediment load could suffer from this hypothesis, but the isostatic model, used to simulate the behaviour of the margin, is a regional flexural model and local loads do not have a significant impact on the isostatic response. Moreover, the modelled sedimentary thickness allows us to compare and to adjust the seafloor from seismic data and simulations at the top of this wedge.

Because sediment load is already included in the *GS*, model R9 calculates the final position of the erosion surface with twice the sediment load; one with the *GS* estimate and one with an imposed sediment flux. The final result allows us to present the simulated *D60* (with 2.*SL*) and the simulated *D70*, as we modelled the sedimentary thickness between these two major erosion surfaces (Fig. 9). The difference between simulated *D60* from R8 (*SL* is comprised in *GS*) and from R9 (2x*SL*) provides about 5 more meters of total subsidence (*S*+*SL*) at the end of the last climatic cycle simulation (Fig. 9), compared to the previous R8 total subsidence (*S*). It is mainly from the added *SL* contribution. If we now consider the 15 m of *GS* for the last climatic cycle, we can infer about 10 m of sinking related to the tectonic and thermal subsidence. Consequently, and from these 125 ky simulations, about 1/3 of GS is a result of sediment load (*SL*), while the remaining 2/3 is due to thermal subsidence (*TS*).

4.4 Discussion

Successive low sea-level during glacial periods and their corresponding erosional surfaces have a cyclic repetition through time in the Gulf of Lions. Using these surfaces as chrono-stratigraphic indicators, it is possible to estimate the geohistory subsidence (*GS*) and the stratigraphic simulations of the last climatic cycle. In the *Sedflux* model, the flexural isostatic adjustments and compensation were simulated using parameters that are broadly consistent with isostatic effective elastic thickness (*EET*) and relaxation time (*RT*) described in similar studies (Huybrechts, 2002; Lambeck and Bard, 2000; Peltier, 1998; Watts, 2001). The high values of *EET* used for these experiments can be compared to the global bi-modal distribution of continental *EET* values established by Watts (1992). The 65 km effective elastic thickness corresponds to the lower part of Watts' distribution, that describes basins generally developed on high *EET* cratonic interiors. This value is in agreement with the geological setting of the structural region; the Gulf of Lions is a passive margin originating from Alpine thrust and its lithospheric thickness results from a long and complex marine and continental geological history.

From the simulations, we estimate each component of the total subsidence (*S*) (Table 2 and Fig. 9). First, the water loading (*WL*), associated with relative sea-level variations, can impact the vertical evolution of the margin between glacial lowstand and interglacial highstand. The range of *WL* effect can reach about 20 m. As a consequence, the position of glacial sedimentary features, observed at the present-day outer shelf, have to be corrected from this subsidence in order to approach the real water depth of their formation. For instance,

Lambeck and Bard. (2000) determined a 15 m isostatic rebound for the last deglaciation period in the Gulf of Lions, as compared to our value of 20 m. Second, the geohistory subsidence (*GS*) measured on seismic is confirmed. The thermal cooling effect (*TS*) of the margin would contribute to about 60 to 65 % of the *GS*; the remaining fraction being represented by the sediment load (*SL*). These estimates are similar to those defined by Bessis and Burrus (1986). They are in the same range as estimates for other areas found in the literature (sect. 4.2) (Fig. 2). These comparisons demonstrate that our method provides, for short time-periods, results in the same range as those obtained through traditional approaches for longer time-scales. It allows one to take into account the hydro-isostatic effect, which is a key parameter for studying the impact of Quaternary glacial-interglacial sea-level changes. Moreover, our simulations confirm that the first order controls on depositional patterns are sea-level change and sediment supply, but that accommodation determines what is preserved in the Quaternary stratigraphic record.

5. Conclusion

Subsidence corresponds to the movement of the Earth's surface with respect to a reference level. Total subsidence has two major components: a tectonic part (mechanic and thermal) and a gravity part (sedimentary and hydrostatic loading). The aim of our method allows each of these components to be evaluated from a combined field stratigraphic and modelling approach. One application of the method is to estimate the impacts of global sea-level changes for a site where relative sea-level changes are stratigraphically well-constrained. The amplitudes of global Quaternary sea-level oscillations, derived from paleoclimatic proxies obtained from ice or sediment cores, need to be calibrated by independent geological measurements. On passive margins, the shelf edge is the place where accommodation is most important and direct measurement of successive relative sea-level positions is possible from the stratigraphic record (Jouet *et al.*, 2006; Rabineau *et al.*, 2005; Skene et al., 1998).

The only way to evaluate absolute sea-level positions is to estimate the subsidence and correct the local eustatic curve. With new estimates of geohistory subsidence (*GS*) and global sea-level variations, stratigraphic simulations are adapted to understand the impact of water and sediment loading (*WL* and *SL*) on the shelf. Their rapid fluctuations (100 ky cycles) are superimposed on an overall trend corresponding to thermal cooling (*TS*) of the continental margin. This tectonic subsidence is a portion of the vertical deflection of the Earth's surface through time due to basin formation.

The stratigraphic modelling of the Rhône deltaic margin during the last climatic cycle (125 ky) allows the assessment of parameters estimated with the geohistory analysis (tectonic/thermal subsidence and sediment loading). Global eustasy fluctuations using the *Sedflux* model provides confirmation of the important impact of water loading on vertical motions of the platform between glacial low sea level and interglacial high sea level. Finally, the thermal subsidence and the sediment load both contribute to the geohistory subsidence, defined from stratigraphic analysis, with a relative impact of 60-65 % and 35-40 %, respectively.

From seismic profiles and their interpretation, stratigraphic modelling provides a way to either confirm or discard different hypothesis on subsidence. This method permits us to test hypothesis without some of the information needed for the "backstripping" method; for example lithological information is unnecessary. However, several assumptions, considered as reasonable in the case of our study area, have to be made, especially about the repetition of the sedimentary features (glacial erosion surfaces) through each glacial cycle. A future application of this technique will be to better constrain sediment supply. The European project PROMESS, which cored two boreholes on the outer shelf in 2004, will provide lithological and geochronological information for the last 500 ky sedimentary record. A new analysis at this time-scale will soon be undergone, taking into account the entire Gulf of Lions platform, in order to assess the space and time variability of the different components of subsidence.

7. References

Airy, G.B., 1855. On the computation of the effect of the attraction of mountain-masses as disturbing the apparent astronomical latitude of stations of geodetic surveys. Philosophical Transaction of the Royal Society of London, 145: 101-104.

Albertson, M.L., Dai, Y.B., Jensen, R.A. and Hunter, R., 1950. Diffusion of submerged jets. American Society of Civil Engineers Transactions, 115: 639-697.

Allen, P.A. and Allen, J.R., 2005. Basin analysis; principles and applications. Blackwell Publishing Ltd, Malden-Oxford-Victoria, 549 pp.

Aloïsi, J.C., 1986. Sur un modèle de sédimentation deltaïque: contribution à la connaissance des marges passives. Thèse de doctorat d'Etat, Université de Perpignan, Perpignan, 162 pp.

Bassetti, M.A., Jouet, G., Dufois, F., Berné, S., Rabineau, M. and Taviani, M., 2006. Sand bodies at the shelf edge in the Gulf of Lions (Western Mediterranean): deglacial history and modern processes. Marine Geology, 234: 93-109.

Bentounsi, F., 1990. ECORS - Golfe du Lion. Interprétation des profils de sismique réflexion longue écoute - cinématique d'ouverture de la Méditerranée Occidentale. Mémoire de D.E.A., Université de Bretagne Occidentale, Brest, 69 pp.

Berné, S., Aloïsi, J.C., Baztan, J., Dennielou, B., Droz, L., Dos Reis, T., Lofi, J., Méar, Y. and Rabineau, M., 2002. Notice de la carte morpho-bathymétrique du Golfe du Lion. IFREMER et Région Languedoc Roussillon, Brest, pp. 48.

Berné, S., Lericolais, G., Marsset, T., Bourillet, J.F. and de Batist, M., 1998. Erosional shelf sand ridges and lowstand shorefaces: examples from tide and wave dominated environments of France. Journal of Sedimentary Research, 68(4): 540-555.

Bessis, F., 1986. Some remarks on the subsidence of sedimentary basins; application to the Gulf of Lions margin (western Mediterranean). Marine and Petroleum Geology, 3(1): 37-63.

Bessis, F. and Burrus, J., 1986. Etude de la subsidence de la marge du Golfe du Lion (Méditerranée occidentale). Bulletin Centre de Recherche Exploration-Production Elf Aquitaine, 10: 123-141.

Biju-Duval, B., 1984. Les marges continentales françaises de la Méditerranée. In: G. Boillot (Editor), Les marges actuelles et fossiles autour de la France. Masson, Paris, pp. 249-334.

Burov, E.B. and Diament, M., 1995. The effective elastic thickness (Te) of continental lithosphere: what does it really mean? Journal of Geophysical Research, 100: 3905–3927.

Burrus, J. and Audebert, F., 1990. Thermal and Compaction processes in a young rifted Basin containing Evaporites: Gulf of Lions, France. American Association of Petroleum Geologists Bulletin, 74(9): 1420-1440.

Burrus, J., 1984. Contribution to a geodynamic synthesis of the Provençal basin (North Western Mediterranean). Marine Geology, 55: 247-269.

Ceramicola, S., Stoker, M., Praeg, D., Shannon, P.M., De Santis, L., Hoult, R., Hjelstuen, B.O., Laberg, S. and Mathiesen, A., 2005. Anomalous Cenozoic subsidence along the `passive' continental margin from Ireland to mid-Norway. Marine and Petroleum Geology, 22(9-10): 1045-1067.

Gensous, B. and Tesson, M., 1996. Sequence stratigraphy, seismic profiles, and cores of Pleistocene deposits on the Rhône continental shelf. Sedimentary Geology, 105: 183-190.

Gorini, C., Le Marrec, A. and Mauffret, A., 1993. Contribution to the structural and sedimentary history of the Gulf of Lions (Western Mediterranean) from the ECORS profiles, industrial seismic profiles and well data. Bulletin de la Société Géologique de France, 164(3): 353-363.

Got, H., 1973. Etude des corrélations tectonique-sédimentation au cours de l'histoire quaternaire du précontinent pyrénéo-catalan. Thèse de Docorat d'Etat, Université de Perpignan, Université de Perpignan, 294 pp.

Gueguen, E., 1995. La Méditerranée Occidentale: un véritable océan. Exemple de segmentation des marges et de hiatus cinématiques. Implications sur les processus d'amincissement crustal. Thèse de Doctorat, Université de Bretagne Occidentale, Brest, 281 pp.

Huybrechts, P., 2002. Sea-level changes at the LGM from ice-dynamic reconstructions of the Greenland and Antarctic ice sheets during the glacial cycles. Quaternary Science Reviews, 21: 203-231.

Huybrechts, P. and De Wolde, J., 1999. The dynamic response of the Greenland and Antarctic ice sheets to multiple-century climatic warming. Journal of Climate, 12: 2169-2188.

Johnston, P., 1995. The role of hydro-isostasy for Holocene sea-level changes in the British Isles. Marine Geology, 124(1-4): 61-70.

Jouet, G., Berné, S., Rabineau, M., Bassetti, M.A., Bernier, P., Dennielou, B., Flores, J.A., Sierro, F.J. and Taviani, M., 2006. Shoreface migrations at the shelf edge and sea-level changes around the Last Glacial Maximum (Gulf of Lions, NW Mediterranean). Marine Geology, 234: 21-42.

Kirby, S.H., 1983. Rheology of the lithosphere. Reviews Geophysics and Space Physics, 21: 1458-1487.

Lambeck, K. and Bard, E., 2000. Sea-level changes along the French Mediterranean coast for the past 30,000 years. Earth and Planetary Science Letters, 175: 203-222.

Lambeck, K., 1997. Sea-level change along the French Atlantic and Channel coasts since the time of the Last Glacial Maximum. Palaeogeography, Palaeoclimatology, Palaeoecology, 129(1-2): 1-22.

Lisitzin, E., 1974. Sea-level changes. Elsevier Oceanography Series, 8, Amsterdam-Oxford-New York.

Lofi, J., Rabineau, M., Gorini, C., Berné, S., Clauzon, G., De Clarens, P., Tadeu Dos Reis, A., Mountain, G.S., Ryan, W.B.F., Steckler, M.S. and Fouchet, C., 2003. Plio-Quaternary prograding clinoform wedges of the western Gulf of Lion continental margin (NW Mediterranean) after the Messinian Salinity Crisis. Marine Geology, 198(3-4): 289-317.

McKenzie, D.P., 1978. Some remarks on the development of sedimentary basins. Earth and Planetary Science Letters, 40: 25-32.

Monaco, A., 1971. Contribution à l'étude géologique et sédimentologique du plateau continental du Roussillon. Thèse de Doctorat d'Etat, Université de Perpignan, Perpignan, 295 pp.

Paulson, A., Zhong, S. and Wahr, J., 2005. Modelling post-glacial rebound with lateral viscosity variations. Geophysical Journal International, 163: 357-371.

Peltier, W.R., 2004. Global glacial Isostasy and the surface of the ice-age earth: the ICE-5G (VM2) model and GRACE. Annual Review of Earth and Planetary Sciences, 32: 111-149.

Peltier, W.R., 2002. On eustatic sea level history: Last Glacial Maximum to Holocene. Quaternary Science Reviews, 21(1-3): 377-396.

Peltier, W.R., 1998. Postglacial variations in the level of the sea: implications for climate dynamics and solid-earth geophysics. Reviews of Geophysics, 36: 603-689.

Plint, G.A. and Nummendal, D., 2000. The falling stage systems tract: recognition and importance in sequence stratigraphic analysis. In: D. Hunt and R.L. Gawthorpe

(Editors), Sedimentary responses to forced regressions. The Geological Society, London, pp. 1-17.

Posamentier, H.W., Jervey, M.T. and Vail, P.R., 1988. Eustatic controls on clastic deposition I. Conceptual framework. In: C.K. Wilgus, B.S. Hastings, C.G.S.C. Kendall, H.W. Posamentier, C.A. Ross and J.C. Van Wagoner (Editors), Sea-Level Changes- an Integrated Approach. SEPM Spec. Pub. 42, Tulsa, pp. 102-124.

Pratt, J.H., 1855. On the attraction of the Himalaya Mountains and of the elevated regions beyond them, upon the plumb line in India. Philosophical Transaction of the Royal Society of London, 145: 53-100.

Rabineau, M., Berné, S., Aslanian, D., Olivet, J.L., Joseph, P., Guillocheau, F., Bourillet, J.F., Le Drezen, E. and Granjeon, D., 2005. Sedimentary sequences in the Gulf of Lion: a record of 100,000 years climatic cycles. Marine and Petroleum Geology, 22: 775-804.

Rabineau, M., 2001. Un modèle géométrique et stratigraphique des séquences de dépôts quaternaires de la plateforme du Golfe du Lion: enregistrement des cycles glacioeustatiques de 100 000 ans. Thèse de Doctorat, Université de Rennes 1, Rennes, (2 vols) 392 + 70 pp.

Sioni, S., 1997. Mer Ionienne et Apulie depuis l'ouverture de l'Océan Alpin. Thèse de Doctorat, Université de Bretagne Occidentale, Brest.

Skene, K.I., Piper, D.J.W., Aksu, A.E. and Syvitski, J.P.M., 1998. Evaluation of the global oxygen isotope curve as a proxy for Quaternary sea level by modeling of delta progradation. Journal of Sedimentary Research, 68(6): 1077-1092.

Steckler, M.S., Mountain, G.S., Miller, K.G. and Christie-Blick, N., 1999. Reconstruction of Tertiary progradation and clinoform development on the New Jersey passive margin by 2-D backstripping. Marine Geology, 154(1-4): 399-420.

Steckler, M.S. and Watts, A.B., 1980. The Gulf of Lion: subsidence of a young continental margin. Nature, 287: 425-429.

Syvitski, J.P. and Hutton, E.W.H., 2001. 2D SEDFLUX 1.0C: an advanced process-response numerical model for the fill of marine sedimentary basins. Computers & Geosciences, 27(6): 731-753.

Syvitski, J.P.M., Nicholson, M., Skene, K. and Morehead, M.D., 1998. PLUME1.1: Deposition of sediment from a fluvial plume. Computers & Geosciences, 24(2): 159-171.

Syvitski, J.P.M., 1989. The process-response model in Quantitative Dynamic Stratigraphy. In: T.A. Cross (Editor), Quantitative Dynamic Stratigraphy. Prentice-Hall, New York, pp. 309-334.

Tesson, M., Posamentier, H. and Gensous, B., 2000. Stratigraphic organisation of Late Pleistocene deposits of the western part of the Rhone shelf (Languedoc shelf) from high resolution seismic and core data. A.A.P.G. Bull., 84(1): 119-150.

Tesson, M., Gensous, B., Allen, G.P. and Ravenne, C., 1990. Late Quaternary lowstand wedges on the Rhône Continental Shelf, France. Marine Geology, 91: 325-332.

Turcotte, D.L. and Schubert, G., 1982. Geodynamics, applications of continuum physics to geological problems. John Wiley & sons, New York, 450 pp.

Van Hinte, J.E., 1978. Geohistory analysis: application of micropaleontology in exploration geology. Bulletin American Association of Petroleum Geologists, 62: 201-222.

Waelbroeck, C., Labeyrie, L.D., Michel, E., Duplessy, J.-C., McManus, J., Lambeck, K., Balbon, E. and Labracherie, M., 2002. Sea-level and deep water changes derived from benthic Foraminifera isotopic record. Quaternary Science Reviews, 21(1-3): 295-305.

Watts, A.B., 2001. Isostasy and Flexure of the Lithosphere, Cambridge University Press, Cambridge.

Watts, A.B., 1992. The effective elastic thickness of the lithosphere and the evolution of foreland basin. Basin Research, 4: 169–178.

Watts, A.B., Karner, G.D. and Steckler, M.S., 1982. Lithospheric flexure and the evolution of sedimentary basins. Philosophical Transaction of the Royal Society of London, 305 Series A: 249-281.

Watts, A.B. and Ryan, W.B.F., 1976. Flexure of the lithosphere and continental margin basins, Tectonophysics, pp. 25-44.

8. Figure captions

Fig. 1: Definition of the mechanisms causing subsidence on a passive continental margin. The total subsidence (S) results from vertical motions that are specific for each lithology. Different subsidence components can be determined by the mechanisms that cause these motions. Note the term geohistory subsidence (GS) that corresponds to the subsidence measured from seismic stratigraphy and associated to the combination of the tectonic/thermal subsidence (TS) and the sediment load (SL).

Fig. 2: Flow chart of the method defined in this paper and aimed at investigating the different components of the total subsidence (S). The strategy uses stratigraphic modelling along with the *Sedflux* program and input parameters from the geohistory and stratigraphic analysis.

Fig. 3: The Gulf of Lions continental margin (North-Western Mediterranean); Geographic, morpho-bathymetric (from Berné *et al.*, 2002) and hydrographic settings. The dotted line indicates the position of the NE–SW seismic synthesis shown on the figure 4. The location of the North-South simulated profile on the map shows that the marine section presented here is between 50 and 130 km. Note that the simulations take into account the entire profile (including the onshore section).

Fig. 4: Stratigraphic interpretation from composite high-resolution Sparker seismic lines (position in Fig. 3). The NE–SW transect across the platform illustrates the stacking of the last five sedimentary sequences (S1 to S5) bounded by major discontinuities (D40 to D70). Within these sequences, the deposits are organized in a vertically stacked sedimentary motif consisting of prisms (PI) with gently dipping clinoforms, and prisms (PII) with relatively high-angle clinoforms (from 3 to 7°) (Rabineau *et al*, 2005). The highest amplitude seismic reflections reveal major erosional surfaces that formed during the overall sea-level fall and lowstands.

Fig. 5: Chirp seismic profile across the continental shelf (position in Fig. 3). Major seismic surfaces correspond to cyclic erosion surfaces formed during forced regressions (see text for detailed explanation).

Fig. 6: Definition of geohistory subsidence (GS) and water loading (WL) as they are input in the numerical stratigraphic model *Sedflux*. The identification of dated erosion paleosurfaces

permits one to quantify their vertical evolution through time, and to estimate the GS subsidence. This value takes into account both the tectonic subsidence (TS) and the loads due to sediment deposition (SL). The water loading (WL) results from relative sea-level fluctuations and reaches its maximum between glacial and interglacial periods.

Fig. 7: Test of the isostatic parameters used in the numerical stratigraphic model *Sedflux*. The total subsidence (S) is modelled using different values of **1**- effective elastic thickness (EET) and **2**- relaxation time (RT).

Fig. 8: 1- Modelling of the total subsidence (S) with the best adapted isostatic parameters (Model R8: EET = 65 km; RT = 3,500 years). **2**- Evolution through time of the GS, S and WL subsidence from this simulation R8.

Fig. 9: Modelling of the total subsidence (S) and (S'). (S') is the results of Model R9 with sediment flux turned on. The comparison of these models permits the estimation of the different components of the total subsidence (S) at 100 km of the simulated section (outer shelf).

Table 1: Description of the different numerical stratigraphic models (R1 to R9) and their input parameters.

Table 2: Quantification of the different components of the total subsidence (S) at 100 and 120 km of the simulated section.
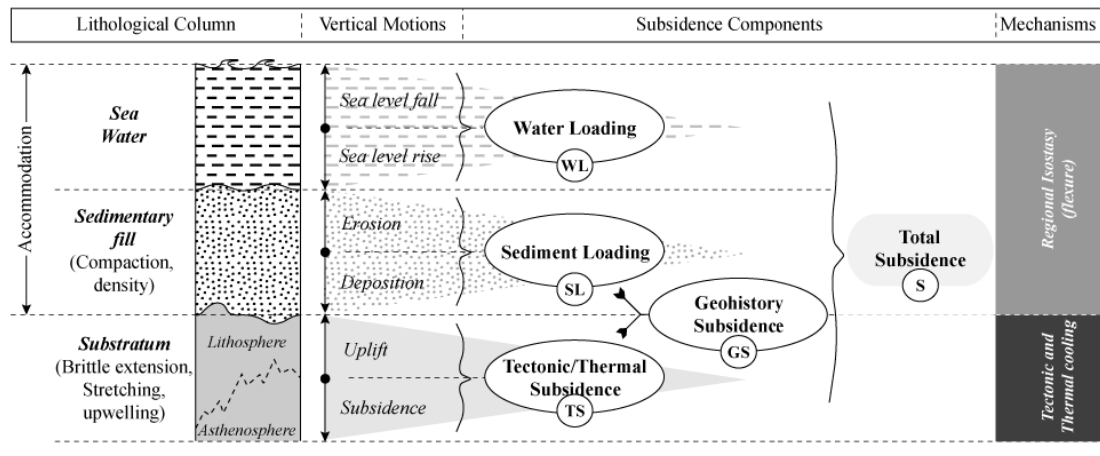
PASSIVE CONTINENTAL MARGIN

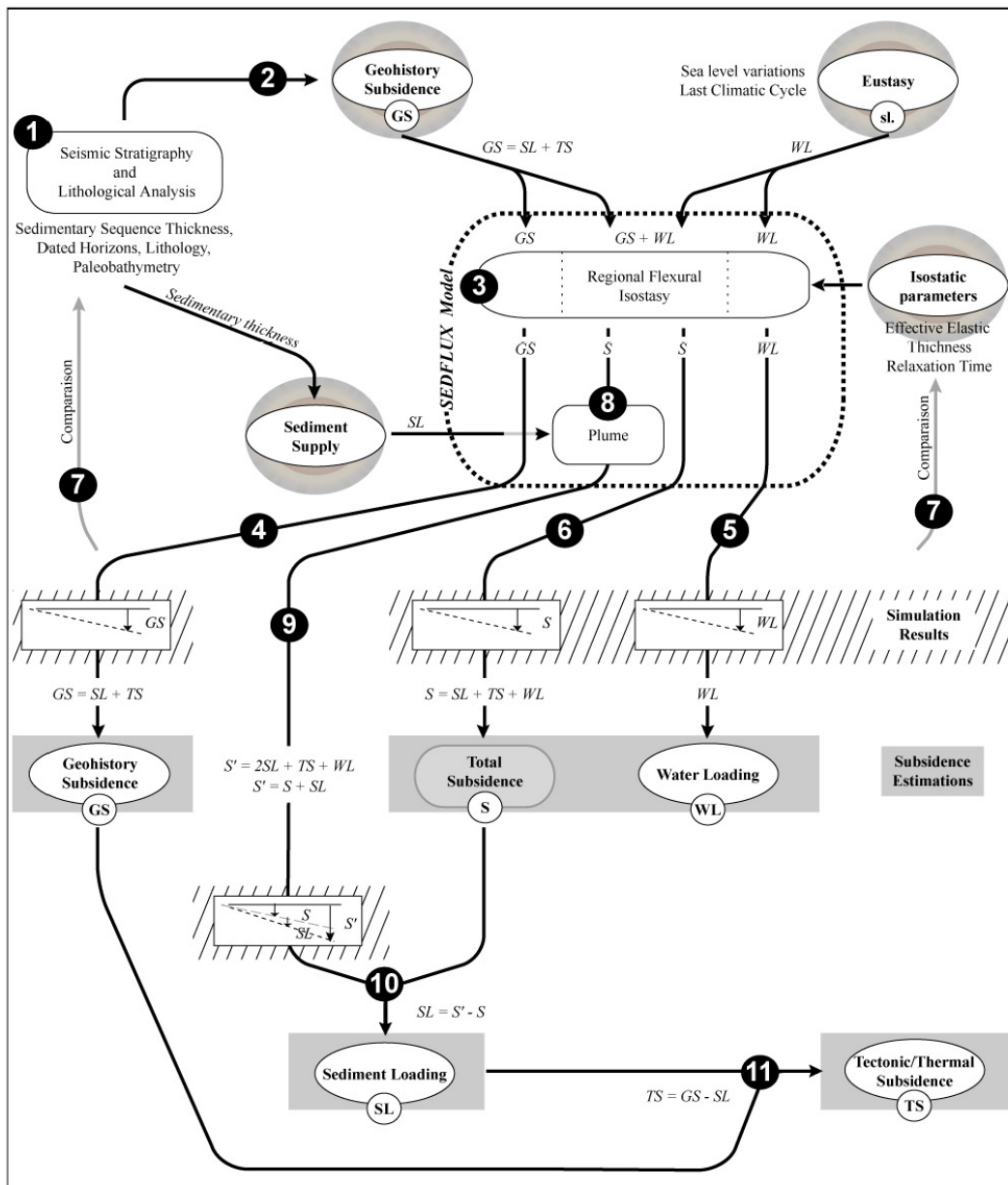| Lithological Column | Vertical Motions | Subsidence Components | Mechanisms |

Figure. 1 - Jouet *et al.*
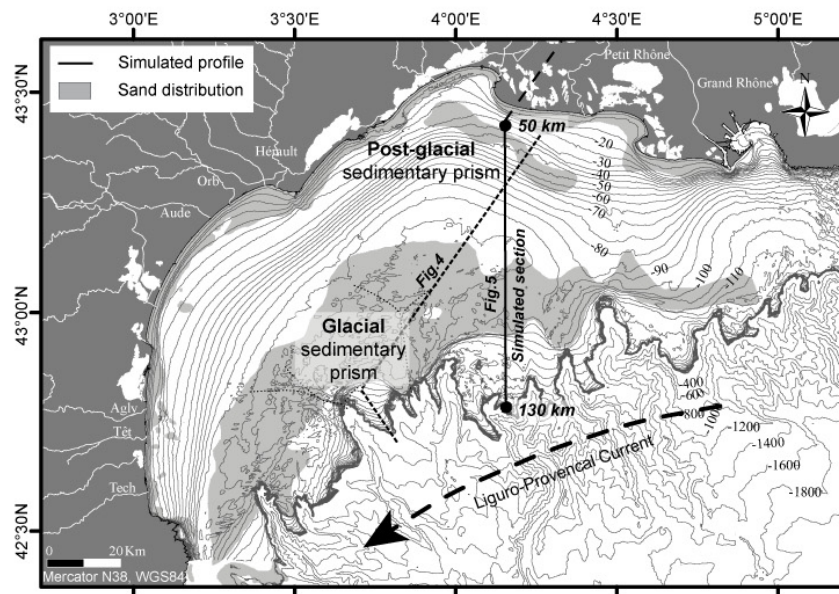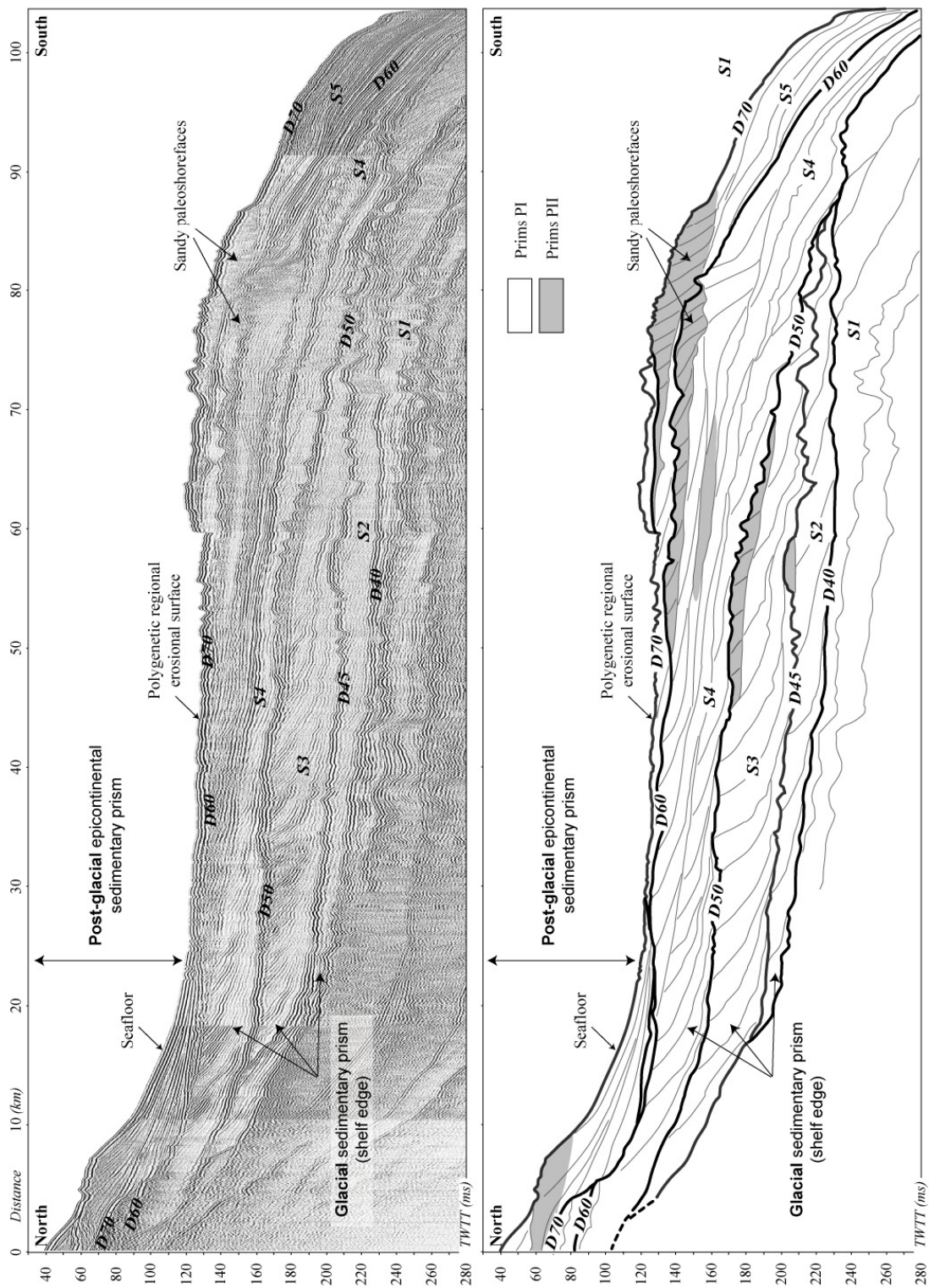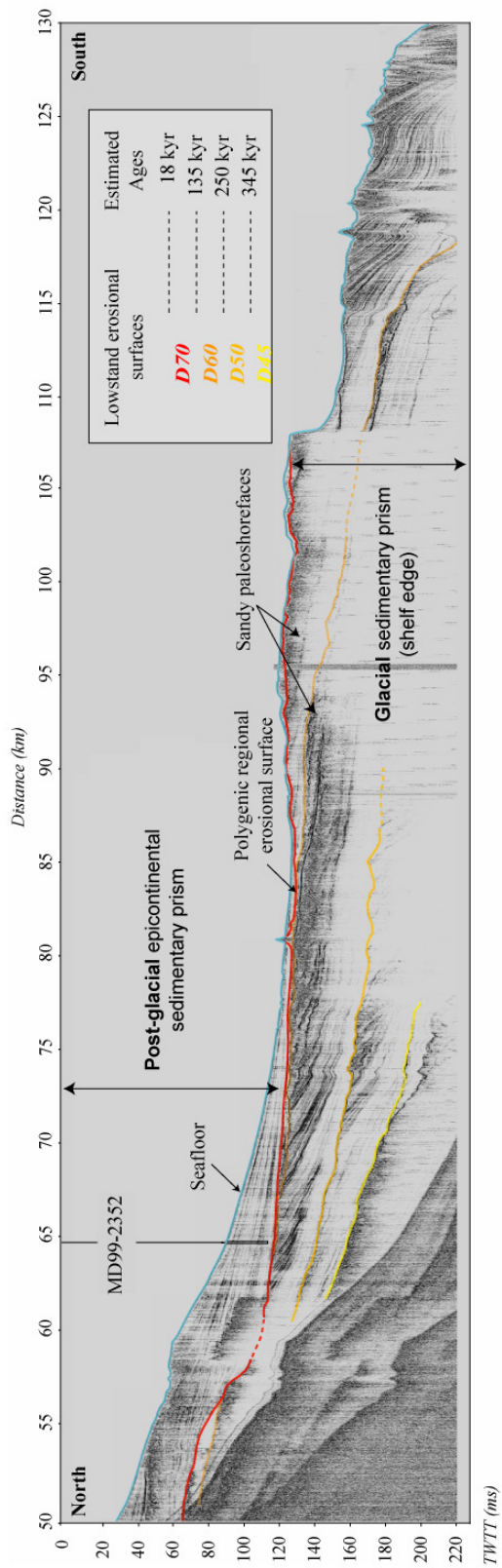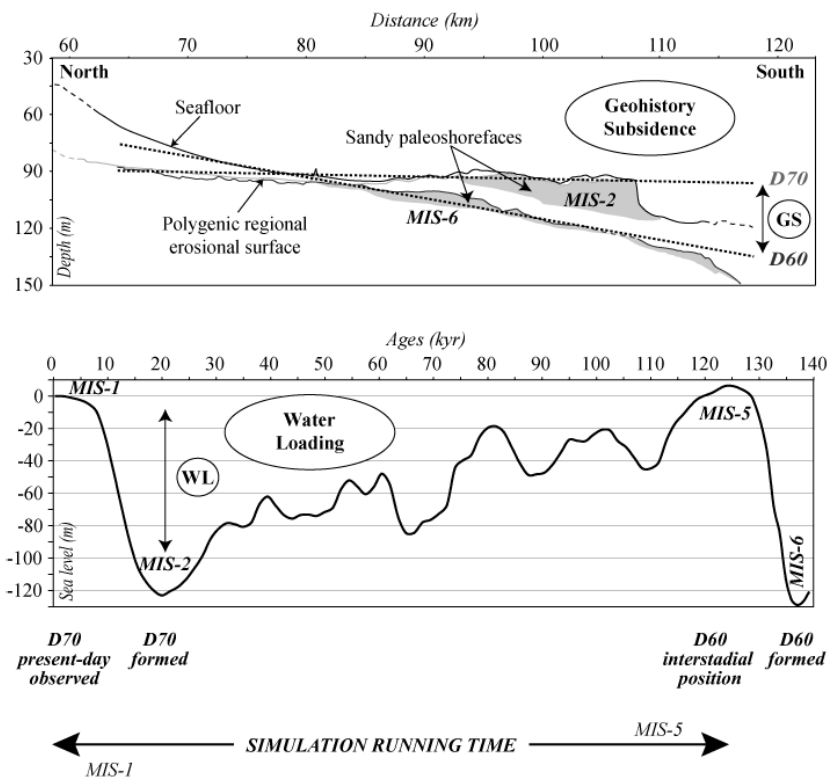
Figure. 2 - Jouet *et al.*

Figure. 3 - Jouet *et al.*

Figure. 4 - Jouet *et al.*

135

Figure. 5 - Jouet *et al.*

136

Figure. 6 - Jouet *et al.*
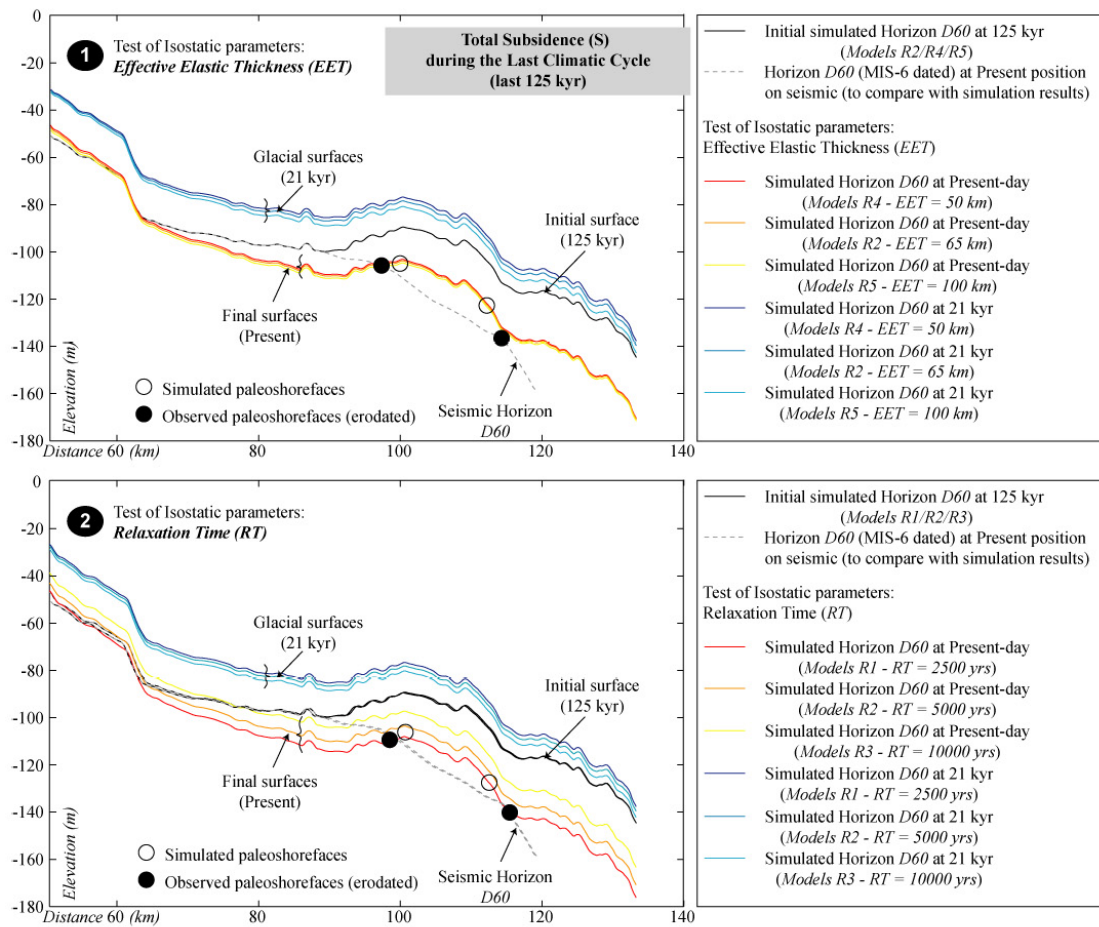
Figure. 7 - **Jouet** *et al.*
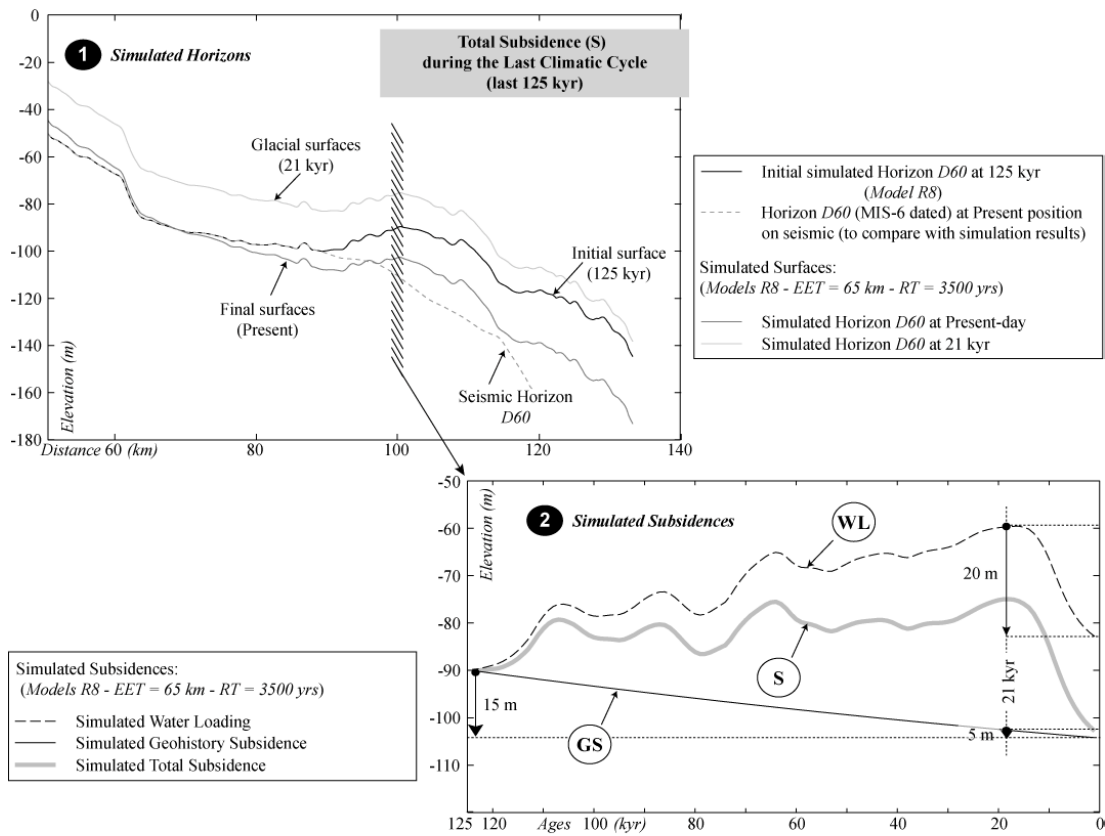
Figure. 8 - Jouet *et al.*
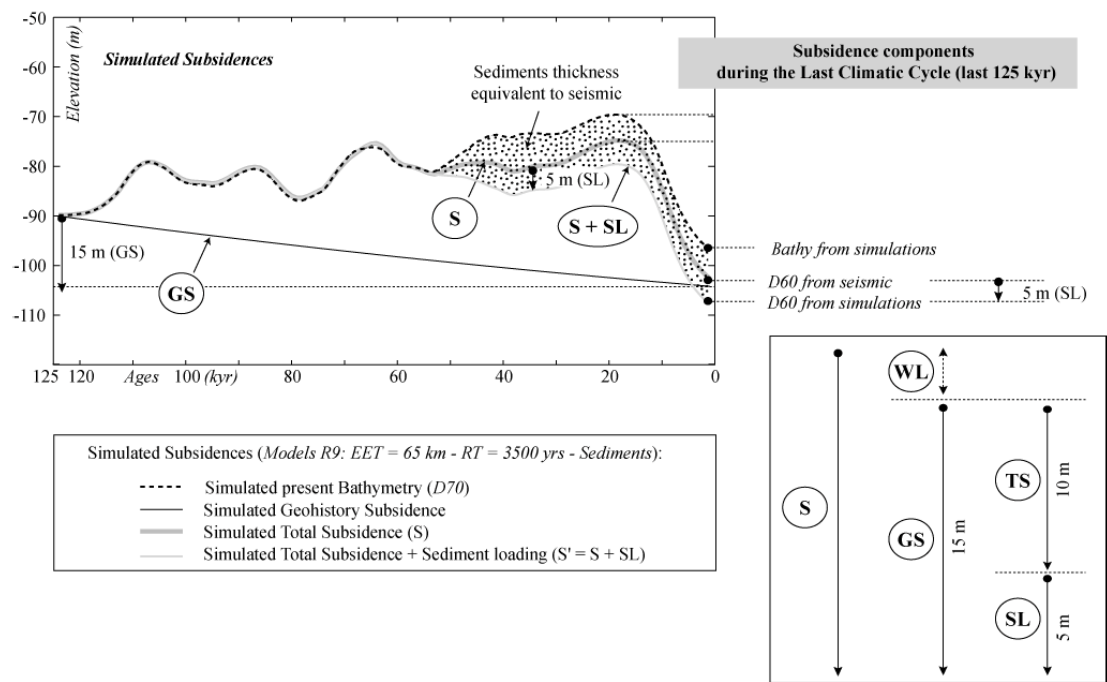
Figure. 9 - Jouet *et al.*

MODELS	DESCRIPTION	ISOSTASY		SUBSIDENCE		SEDIMENT	DURATION
		Isostatic Effective Elastic Thickness (km)	Isostatic Relaxation Time (yrs)	Inner shelf (m/yrs)	Outer shelf (m/yrs)		
R1	Fast margin adjustment	65	2 500	0 (50 km)	2,5E-04	No	LCC (125 kyr)
R2	Medium margin adjustment	65	5 000	0 (50 km)	2,5E-04	No	LCC (125 kyr)
R3	Slow margin adjustment	65	10 000	0 (50 km)	2,5E-04	No	LCC (125 kyr)
R4	Local margin adjustment	50	5 000	0 (50 km)	2,5E-04	No	LCC (125 kyr)
R5	Regional margin adjustment	100	5 000	0 (50 km)	2,5E-04	No	LCC (125 kyr)
R6	Conv. point migration, fast adjustment	65	2 500	0 (50-80 km)	2,5E-04	No	LCC (125 kyr)
R7	Conv. point migration, medium adjustment	65	5 000	0 (50-80 km)	2,5E-04	No	LCC (125 kyr)
R8	Adapted eath model (LCC)	65	3 500	0 (50-80 km)	2,5E-04	No	LCC (125 kyr)
R9	Estimation of the Sediment load	65	3 500	0 (50-80 km)	2,5E-04	Yes	LCC (125 kyr)

Table. 1 - Jouet *et al.*

MODELS	DESCRIPTION	POSITION 100 km						
		Total Subsidence LCC D60 (m)	Sediment Thickness D60-D70 (m)	Total Subsidence LD D70 (m)	Subsidence (Sed. Load. + Teconics) (m)	Hydo-Isostasy (Water Load.) (m)	Sediment Loading (m)	Tectonic Subsidence (m)
	- At position 100 km -							
R8	Adapted eath model (LCC)	+15	+10	+25	+4,5	+20,5		
R9	Estimation of the Sediment load						1/3 Subsid	2/3 Subsid
	- At position 120 km -							
R8	Adapted eath model (LCC)	+10	+15	+25	+5,5	+19,5		
R9	Estimation of the Sediment load						1/3 Subsid	2/3 Subsid

Table. 2 - Jouet *et al.*

SEDIMENTARY RESPONSES TO MILLENNIAL-SCALE SEA-LEVEL CHANGES IN THE NW MEDITERRANEAN

Gwenael Jouet, Serge Berné, Francisco J. Sierro,

Maria-Angela Bassetti, Miquel Canals, Bernard Dennielou,

José-Abel Flores & the PROMESS-1 Team

Corresponding author: Gwenael Jouet

(gwenael.jouet@ifremer.fr)

Length of the paper:	4 pages *(1,300 words per page)*
Summary:	228 words *(~200-250 words)*
Text:	1,653 words *(~1,500 words)*
References:	30 refs *(<30 refs)*
Figure legends:	527 words *(<300 words each;<800 words)*

Sedimentary responses to millennial-scale sea-level changes in the NW Mediterranean

Gwenael Jouet[1,2,*], Serge Berné[1], Francisco J. Sierro[3], Maria-Angela Bassetti[1], Miquel Canals[4], Bernard Dennielou[1], José-Abel Flores[3] & the PROMESS-1 team

[1] Géosciences Marines, IFREMER, Plouzané, France.

[2] UMR-CNRS 6538 Domaines Océaniques, IUEM, Université de Bretagne Occidentale, Plouzané, France.

[3] Departamento de Geología, Universidad de Salamanca, Salamanca, Spain.

[4] CRG Marine Geosciences, University of Barcelona, Barcelona, Spain.

* Corresponding author. *E-mail address: gjouet@ifremer.fr*

Tel: +33 (0)2 98 22 48 19 or +33 (0)2 98 49 87 17

Fax: +33 (0)2 98 22 45 70

1. Summary

Millennial-scale changes of Earth climate during the last 130,000 years have been described in ice cores[1,2] and in deep marine sedimentary archives[3,4]. Related sea-level changes, more than 10 m in magnitude, are reported worldwide[5-7]. These sea-level oscillations are in the same order as those that occurred during some geological periods when no large ice sheet existed[8]. However, the impact of these short-term events on the Quaternary stratal geometry of continental margins has never been documented. In this paper, we describe in the Gulf of Lions a set of prograding sedimentary units that correspond to rapid sea-level fluctuations linked to climatic Bond cycles[3]. Very-high resolution seismic profiles and borehole data from the European PROMESS-1 Project show on the upper slope coarse-grained condensed level that formed during highstand periods and coincides with the longest Dansgaard-Oeschger interstadials[9]. Each unit, up to 20 m thick, is bounded on the outer shelf by an erosional surface that formed in response to sea-level falls just prior to Atlantic Heinrich events, and its seaward correlative conformity. Our precisely dated stratigraphic data provide independent sedimentary evidences for the effect of Bond climatic oscillations on sea-level changes. They show that, in favourable deltaic margins where subsidence provides space for deposition and where sedimentation rate is high, relatively minor eustatic changes have a distinct sedimentary signature that can be preserved and identified in the stratigraphic record.

144

2. Text

Late Pleistocene glacial-interglacial cycles are described from multi-proxy analysis of ice records[1,2] and from worldwide hemipelagic sediments[10,11]. The associated sea-level changes, in the order of 100 m, were much larger than during other geological periods; they had a strong influence on continental margin architecture. The advent of sequence stratigraphy[12] offered a paradigm for interpreting major depositional sequences, that are generally considered as linked to 100 kyr (5th order) cycles[13-16]. More precisely, for the last glacial cycle, these studies demonstrated that, despite very distinct tectonic and sedimentary settings, the overall sea-level fall occurring between MIS-5 and MIS-2 corresponds to the deposition, on the outer continental shelf, of a major prograding sedimentary sequence, several meters to tenths of meters thick. During this period, the climate was subject to abrupt millennial-scale changes (stadial-interstadials) of up to one-half of the glacial-interglacial amplitude, affecting both marine and continental records[17]. These fluctuations are referred to as Dansgaard-Oeschger (DO) oscillations[1]. The coldest stadials correspond to Heinrich events (HE). They are associated to massive ice discharge in North Atlantic region[3,18]. A complete sequence through several DO, with a progressive cooling until HE followed by an abrupt shift to a particularly warm interstadial, defines the lower-frequency Bond cycle[3]. The bipolar see-saw effect[19] implies that HE always occurred during North hemisphere cold stadials and synchronous South hemisphere warming[2,20]. If these millennial scale climate changes are now well recognized, associated changes in global sea-level are not fully established. However, several multi-proxy studies suggest that rapid sea-level rises, in the order of 10-15 m[5,6] or up to 35 m[7] occurred before and at the onset of the transition between HE and the following DO interstadial. Limitation in seismic resolution and the lack of deep borehole data did not allow, so far, to explore how these sea-level changes impacted the architecture of sedimentary sequences deposited on continental margins. The continuous and expanded sedimentary record recovered during the PROMESS-1 European drilling project gives us a first opportunity to link ultra-high resolution seismic stratigraphy and multi-proxy record of millennial-scale climate changes at the shelf edge in the Gulf of Lions.

In the Western Mediterranean area (Fig. 1A), DO oscillations resulted in the modification of the intensity of cold and dry polar north-westerlies winds (Mistral and Tramontane)[4,21-23]. Recent studies support the theory of reduced precipitation[24] associated to increased evaporation[21] that caused the decrease in the amount of sediment flux from Mediterranean watersheds during the cold and arid HE[22]. On the contrary, during the return to warm interstadials, precipitation and floods drastically increased, and vegetation developed

accordingly. In the Meditteranean, the central Gulf of Lions is one of the major areas of deep water formation. During the last glacial period, increased northwesterly winds during HE and stadials resulted in increased deep water formation and circulation compared to warm interstadials[21]. Nowadays, dense cold water also forms on the wide continental shelf and episodically cascades along the continental slope during periods of strong northwesterly winter winds[25]. It is not clear if similar conditions may have occurred during HE/stadials of the glacial period, or if reduced shelf width (due to low sea-level) prevented cascading at the shelf edge.

The last climatic cycle has a very distinct stratigraphic expression throughout the Gulf of Lions continental margin (Fig. 1). It corresponds to a major seismic sequence S5, bounded by two regional high-amplitude seismic reflections (D60 and D70). Due to sea-level changes, last deglacial sediments are mainly deposited on the inner shelf whereas outer shelf/upper slope are mainly composed of sediments deposited during the last glacial period. On the outer shelf/upper continental slope, the bulk 130,000 years of marine sedimentation is preserved as a regressive sequence pinching out landward and thickening seaward, 20 to 90 m thick. Within the sequence, very-high resolution Chirp seismic profiles unveil internal discontinuities (outer shelf) and their correlative conformities (upper slope) that can be correlated on the 149 profiles that cover the entire canyon interfluve, as well as the nearest Bourcart canyon. Therefore these surfaces have a regional significance. **On the upper continental slope**, the conformable surfaces bound 12 elementary units with a different stacking pattern from bottom to top (Fig. 2). Below seismic surface labelled D63, the 6 lower units pinch out in a landward direction whereas above D63, the 6 overlying units display an overall aggrading pattern. The comparison of seismic reflections with multi-proxy data from borehole PRGL1-4 shows a very good match between amplitude of seismic reflections and the sand content of sediment (Fig. 2). The very high sedimentation rate at this drill site (over 200 cm/kyr) allows a precise correlation with abrupt climatic events during the last glacial. In particular, relative abundancy of polar foraminifer *Neogloboquadrina pachyderma* sinistrally coiled indicates the coldest conditions during DO stadials associated with the North Atlantic HE. Furthermore, it is shown that the picks of sand fraction correspond to condensed layers formed during the Greenland DO interstadials and the interglacials, as confirmed by absolute ^{14}C ages obtained from bulk foraminifera and shells, and by the $\delta^{18}O$ record[9]. The reason for the decrease in sedimentation rate is attributed to rapid sea-level rise that prevents sediments to reach the shelf edge. Therefore, the effect of winnowing is increased and results in increased sand percentage (mainly warmer foraminifers)[26]. The most pronounced seismic

reflections correspond in fact to the sandy layers associated to major interstadials that follow HE. In other words, there is a relationship between seismic reflection amplitude and the magnitude of the climatic transition between Heinrich cold stadials and warm DO interstadials. The seismic reflections are attributed to the period of highest sea-level (when sediment supply is minimum) and correspond to maximum flooding surfaces. At the position of the borehole and throughout the study area, transitions from H6 to GI-16/GI-14, H4 to GI-8, and H2 to GI-2 are at the origin of the highest seismic reflections.

On the outer continental shelf, S5 is not entirely preserved. The boundaries of internal units become erosional in a landward direction and the stratal geometry of each unit displays internal clinoforms with toplap erosional terminations (Fig. 3). This geometry is typical of "forced regressive" deposits where progradation occurs in response to sea-level fall[12]. Erosional surfaces between each unit are downward shift surfaces formed during small-scale sea-level falls within an overall marine regression. The two upper units that have been reached by cores on the outer shelf display a shallowing upward pattern with coarse-grained erosional termination, within an overall shallowing upward trend at the scale of S5. [14]C dates indicate that sedimentation occurred during cooling intervals. The units are topped by erosion surfaces (indicative of low sea-level) that formed, respectively, around Heinrich event 2 and LGM[27].

Finally, the most obvious seismic reflections correspond, on the outer shelf to erosion surfaces formed during sea-level falls whereas they are maximum flooding surfaces formed during high sea-levels on the upper slope. Besides sea-level changes, two other factors might influence the stratal geometry of the last glacial sequence. First, the lateral migration of deltaic lobes that were situated at the shelf edge during glacial periods may be at the origin of bounding surfaces that mimic sequence boundaries. In such a case, however, they could not be tracked within the canyon heads and throughout the study area. Changes in sediment flux represent another complication: when sediment supply decreases with constant sea-level, condensation and even erosion surfaces may form because of the increased relative effect of waves and currents. In that case, the erosion surfaces observed on the outer shelf would correspond to periods of low sediment supply. This hypothesis is ruled out by the calculation of sedimentation rate at the position of the deep borehole PRGL1-4[9]. It shows that sedimentation rate increases during cooling phases of Bond cycles[3] for reaching a maximum value around Heinrich events, whereas it is minimal during ensuing Greenland interstadials. This implies that the discontinuities are formed by episodic small-scale sea-level falls rather than by changes in sediment flux. More precisely, the stratal geometry of seismic units and

the available time constraint imply that relatively low sea-level directly preceded the major DO interstadials; around the time of HE. This led us to a scenario of formation of depositional sequences at the shelf edge controlled by rapid sea-level oscillations linked to short-term climatic fluctuations (Fig. 4). In this scenario, sea-level highstands are associated to DO interstadials. During sea-level falls associated to cooling phases, erosion occurs on the shelf whereas sedimentation increases on the upper slope resulting in an overall downward shift of prograding depositional units. This phase terminates at the time of HE that has no particular sedimentary signature on the slope and corresponds to an erosion surface on the outer shelf. It is a small-scale sequence boundary. The ensuing sea-level rise is marked by decreased sedimentation rate on the upper slope and slight aggradation on the outer shelf. It terminates during the following interstadial with a coarse-grained condensed level on the upper slope that represent a small-scale maximum flooding surface. Finally, such depositional sequences are the stratigraphic expression of the climatic Bond cycles[3].

During MIS 3, the association between the longest NGRIP stadials and the warmest Antartica interstadials define the most pronounced climatic events[2]. These events (interstadials 12, 8 and 4) are more likely to influence global sea-level changes, and this is why they have the clearest stratigraphic imprint. Because of erosion of interstadial deposits on the outer shelf during ensuing stadials, it is not possible to evaluate precisely the magnitude of sea-level changes during each cycle. However, by extrapolating the landward termination of preserved surfaces, we may consider that the associated sea-level fall was at least in the order of 5 to 10 m, a value in agreement with that proposed by other authors[5-7]. Finally, our study independently confirms the existence of millennial-scale sea-level changes associated to Bond cycles, and shows the stratigraphic expression of such cycles. They represent up to 15-20 m thick para-sequences formed in relation with 6th-order glacio-eustatic cycles.

3. References

1. Dansgaard, W. et al. Evidence for general instability of past climate from a 250-kyr ice-core record. Nature 364, 218-220 (1993).

2. EPICA Community Members. One-to-one coupling of glacial climate variability in Greenland and Antarctica. Nature 444, 195-198 (2006).

3. Bond, G. et al. Correlations between climate records from North Atlantic sediments and Greenland ice. Nature 365, 143-147 (1993).

4. Cacho, I. et al. Dansgaard-Oeschger and Heinrich event imprints in Alboran Sea paleotemperatures. Paleoceanography 14, 698-705 (1999).

5. Chappell, J. Sea-level changes forced ice breakout in the Last Glacial cycle: new results from coral terraces. Quaternary Science Reviews 21, 1229-1240 (2002).

6. Lambeck, K., Esat, T. M. & Potter, E.-K. Links between climate and sea-levels for the past three million years. Nature 419, 199-206 (2002).

7. Siddall, M. et al. Sea-level fluctuations during the last glacial cycle. Nature 423, 853-858 (2003).

8. Haq, B. U., Hardenbol, J. & R., V. P. Chronology of fluctuating sea-levels since the Triassic. Science 235 (1987).

9. Sierro, F. J. et al. Rapid rises of sea-level during the longest interstadials of the last glacial period in Greenland. Nature (submitted).

10. Lisiecki, L. E. & Raymo, M. E. A Pliocene-Pleistocene stack of 57 globally distributed benthic $\delta^{18}O$ records. Paleoceanography 20, PA1003 (2005).

11. Shackleton, N. J., Hall, M. A. & Vincent, E. Phase relationships between millennial-scale events 64,000 - 24,000 years ago. Paleoceanography 15, 565-569 (2000).

12. Posamentier, H. W., Allen, G. P., James, D. P. & Tesson, M. Forced regressions in a sequence stratigraphic framework: concepts, examples and exploration significance. American Association of Petroleum Geologists Bulletin 76, 1687-1709 (1992).

13. Berné, S. et al. Pleistocene forced regressions and tidal sand ridges in the East China Sea. Marine Geology 188, 293-315 (2002).

14. Rabineau, M. et al. Sedimentary sequences in the Gulf of Lion: a record of 100,000 years climatic cycles. Marine and Petroleum Geology 22, 775-804 (2005).

15. Trincardi, F. & Correggiari, A. in Sedimentary responses to forced regressions (eds. Hunt, D. & Gawthorpe, R.) (Geological Society Special Publication, London, 2000).

16. Winn, R. D. et al. Upper Quaternary strata of the upper continental slope, northeast Gulf of Mexico: sequence stratigraphic model for a terrigeneous shelf edge. Journal of Sedimentary Research 68, 579-595 (1998).

17. Rahmstorf, S. Ocean circulation and climate during the past 120,000 years. Nature 419, 207-214 (2002).

18. Heinrich, H. Origin and consequences of cyclic ice rafting in the Northeast Atlantic Ocean during the past 130,000 years. Quaternary Research 29, 142-152 (1988).

19. Stocker, T. F. The seesaw effect. Science 282, 61-62 (1998).

20. Blunier, T. & Brook, E. J. Timing of Millenial-Scale Climate Change in Antartica and Greenland During the Last Glacial Period. Science 291, 109-112 (2001).

21. Cacho, I., Grimalt, J. O., Sierro, F. J., Shackleton, N. & Canals, M. Evidence for enhanced Mediterranean thermohaline circulation during rapid climatic coolings. Earth and Planetary Science Letters 183, 417-429 (2000).

22. Moreno, A. et al. Links between marine and atmospheric processes oscillating on a millennial time-scale. A multi-proxy study of the last 50,000 yr from the Alboran Sea (Western Mediterranean Sea). Quaternary Science Reviews 24, 1623-1636 (2005).

23. Rohling, E. J. et al. Abrupt cold spells in the Northwest Mediterranean. Paleoceanography 13, 316-322 (1998).

24. Combourieu-Nebout, N. et al. Enhanced aridity and atmospheric high-pressure stability over the western Mediterranean during the North Atlantic cold events of the past 50 k.y. Geology 30, 863-866 (2002).

25. Canals, M. et al. Flushing submarine canyons. Nature 444, 354-357 (2007).

26. Sierro, F. J., Flores, J. A. & Baraza, J. Late glacial to recent paleoenvironmental changes in the Gulf of Cadiz and formation of sandy contourite layers. Marine Geology 155, 157-172 (1999).

27. Jouet, G. et al. Shoreface migrations at the shelf edge and sea-level changes around the Last Glacial Maximum (Gulf of Lions, NW Mediterranean). Marine Geology 234, 21–42 (2006).

28. Berné, S. et al. Notice de la carte morpho-bathymétrique du Golfe du Lion. 1, 48 (2002).

29. Hughen, K. A. et al. Marine04 Marine radiocarbon age calibration, 26 - 0 ka BP. Radiocarbon 46, 1059-1086 (2004).

30. Bard, E., Arnold, M., Hamelin, B., Tisnerat-Laborde, N. & Cabioch, G. Radiocarbon calibration by means of mass spectrometric 230Th/234U and 14C ages of corals. An

updated data base including samples from Barbados, Mururoa and Tahiti. Radiocarbon 40, 1085-1092 (1998).

4. End notes

Author Contributions: G.J. and S.B. processed and interpreted the seismic data. F.J.S. and the PROMESS Team provide plaleoclimatic proxies from PRGL1-4. All authors contributed equally to the integration of the seismic data and lithological observations.

Author Information Reprints and permissions information is available at www.nature.com/reprints. The authors declare no competing financial interests. Correspondence and requests for materials should be addressed to G.J. (gwenael.jouet@ifremer.fr).

PROMESS-1 Team A. Asioli[5], M.A. Bassetti[1], C. Beaudouin[6], S Berné[1], I Cacho[4], G. Cairanne[7], M. Canals[4], J.L. Casamor Bermudez[4], A. Cattaneo[1], S. Lafuerza[4], E. Colmenero-Hidalgo[3], A.M. Correggiari Anna[8], B. Dennielou[1], M. Diepenbroek[9], L. Droz[2], G. Floch[1], J.A. Flores[3], J. Frigola[4], R. Gelfort[10], B. Gonzalez-Mora[3], J. Gravalosa[3], J. Grimalt[11], E. Hutton[12], G. Jouet [1,2], H. Lee[13], J. Locat[14], F. Martinez Ruiz[15], P. Moal[1], A. Moreno[4], G. Mountain[16], G. Ollier[17], M. Perez-Folgado[3], M. Rabineau[2], D. Ridente[8], U. Röhl[18], C. Satra[1], R. Schneider[19], T. Schoolmeester[10], R. Schulz[10], F.J. Sierro[3], A. Skinner[20], M. Stoker Martyn[20], J-P. Suc[6], N. Sultan[1], N. Thouveny[21], F. Trincardi[8], N. Uchard[1], R. Urgeles[4], H-J. Wallrabe-Adams[18], T. Wonik[10], Y-H. de Roeck[1].

[1]Géosciences Marines, IFREMER, Plouzané, France, [2]UMR-CNRS 6538 Domaines Océaniques, IUEM, Université de Bretagne Occidentale, Plouzané, France, [3]Departamento de Geología, Universidad de Salamanca, Spain, [4]CRG Marine Geosciences, University of Barcelona, Spain, [5]Istituto di Geoscienze e Georisorse, Padova, Italy, [6]UMR 5125 PEPS-CNRS, Université Claude Bernard Lyon 1, France, [7]Université d'Aix Marseille III, France, [8]Istituto di Scienze Marine, Sezione di Bologna/Geologia Marina, Bologna, Italy, [9]WDC Marine Environmental Sciences, AWI/MARUM, Bremen/Bremerhaven, Germany, [10]Geowissenschaftliche Gemeinschaftsaufgaben, Nieders, Landesamt, Hannover, Germany, [11]Dept. of Environmental Chemistry, Inst. of Chemical and Environmental Research, Barcelona, Spain, [12]Institute of Arctic and Alpine Research, University of Colorado, USA, [13]United States Geological Survey, Western Region, Menlo Park, USA, [14]Département de Géologie et de Génie Géologique, Université Laval, Canada, [15]Instituto Andaluz de Ciencias de la Tierra, Univ. de Granada, Spain, [16]Lamont-Doherty Earth Observatory, Columbia University, USA, [17]Research Directorate-General, European Commission, Brussel, Belgium, [18]Department of Geosciences, Bremen University, Germany, [19]Institut für Geowissenschaften, Christian-Albrechts Universität, Kiel, Germany, [20]British Geological Survey, Edinburgh EH9 3LA, UK, [21]CEREGE, University of Aix-Marseille, Aix en Provence, France.

5. Figure legends

Figure 1 Bathymetric map of the Gulf of Lions[28]. The Gulf of Lions is a stable margin, characterized by high sediment supply and steady subsidence rate (about 250 m/Myr[14]). The main sediment source is from the alpine glaciers through the Rhone River. This allows an almost continuous record of sedimentary fluctuations associated with the global and environmental variations, at least around the shelf edge where accommodation space is sufficient. Grey pattern corresponds to sandy sediments marking shorefaces deposited during glacial and Younger Dryas stillstands. Position of seismic sections A and B, and of cores and borehole data is reported.

Figure 2 Seismic stratigraphy and correlation with Promess PRGL1-4 borehole data on the upper continental slope. A, Very-high resolution Chirp seismic profile and stratigraphic interpretation (position of section-A in Fig. 1). The sequence between D60m and D70m

corresponds to the last glacial cycle (ca 130,000 years). Within it, twelve stratigraphic units are defined on the basis of stratal terminations. **B,** PRGL1-4 borehole provides lithological and chrono-stratigraphic constraints. From right to left, proxy data[9] are reported: (a) ^{14}C dates, obtained on bulk foraminifera and shells. The ages reported herein are δ^{13}C-normelised AMS ^{14}C years, corrected for an assumed air-sea reservoir effect of -400 years, then converted into calibrated ages using the Cal. v5.1 version[29] and the Glacial polynomial[30] (b) percentage in cold water foraminifer *Neogloboquadrina pachyderma* sinistrally coiled, (c) percentage of fraction higher than 62 microns. These proxies allow the recognition of major climatic events (Marine Isotope Stages, Interstadials, Heinrich events), that can be correlated to our seismic data. Note the good correlation between highest seismic amplitudes and coarse layers that correspond to major warm periods and related high sea-levels.

Figure 3 Evidence of erosional surfaces formed by rapid sea-level falls on the Bourcart-Hérault interfluve. **A,** Very-high resolution Chirp seismic profile on the outer shelf (position of section-B in Fig. 1). **B,** Stratigraphic interpretation displaying erosional surfaces (in red) which mark the downward shift of succeeding clinoforms, and pass seaward to correlative conformities. The upper units have sampled by cores and reveal a shallowing upward pattern[27]. These discontinuities represent the time interval including the sea-level falls during the cooling phase of Bond cycles and the lowstand around the time of Heinrich events.

Figure 4 Conceptual model of sedimentation at the shelf edge during a time-equivalent Bond climatic cycle. This scenario requires an overall and progressive decreasing sea-level in response to the global cooling trend occurring during oxygen isotope stage 3. The initial stage corresponds to sea-level highstand associated to interstadial. Continental slope progradation and outer shelf erosion occur during sea-level fall until lowstand, close in time to the HE. The ensuing global sea-level rise and highstand favour the formation of a condensed layer on the continental slope, and deposition of sediments on the outer shelf (that can be removed by subsequent sea-level fall). As a result of the shift in position of depo-centers, shelfal seismic discontinuities formed during lowstands are in continuity with correlative conformities, on the continental slope, formed during highstand. They both correspond to coarse-grained beds that form one single continuous and high-amplitude seismic reflection (SR, in red). Only internal seismic terminations allow to distinguish these 2 types of surfaces.
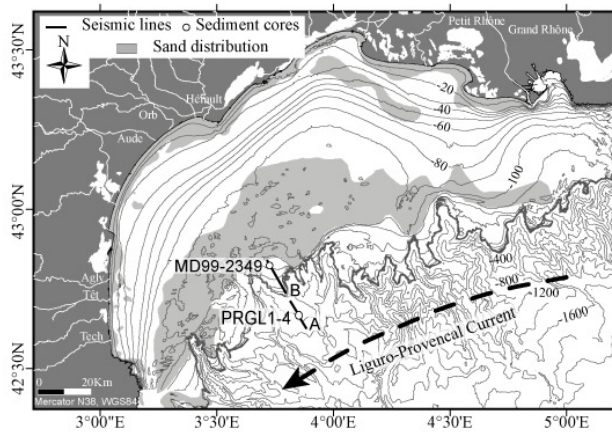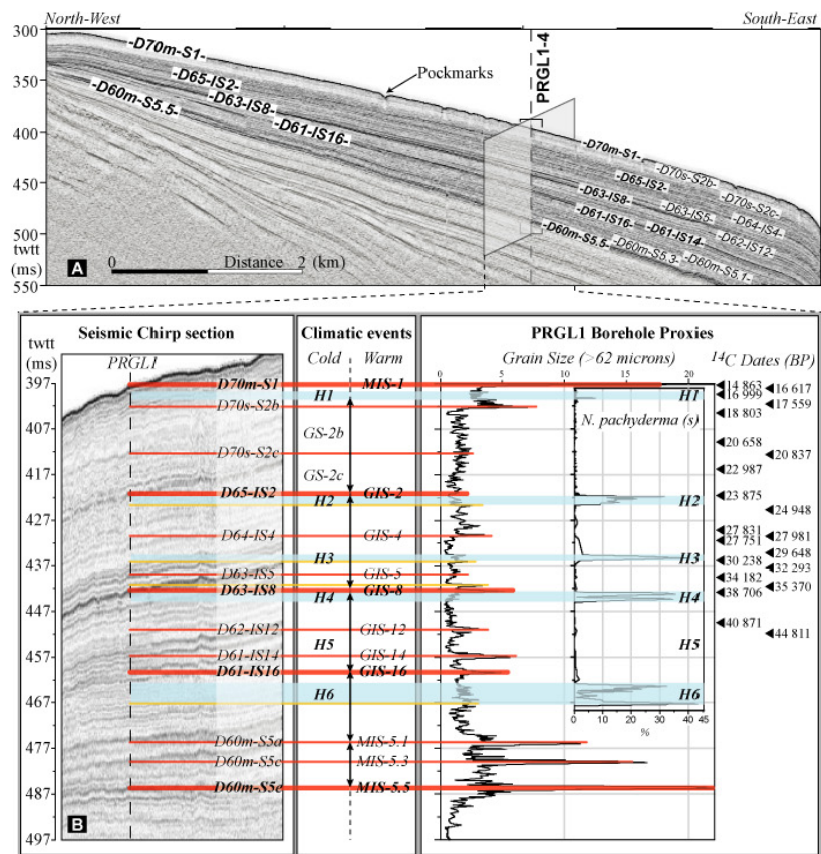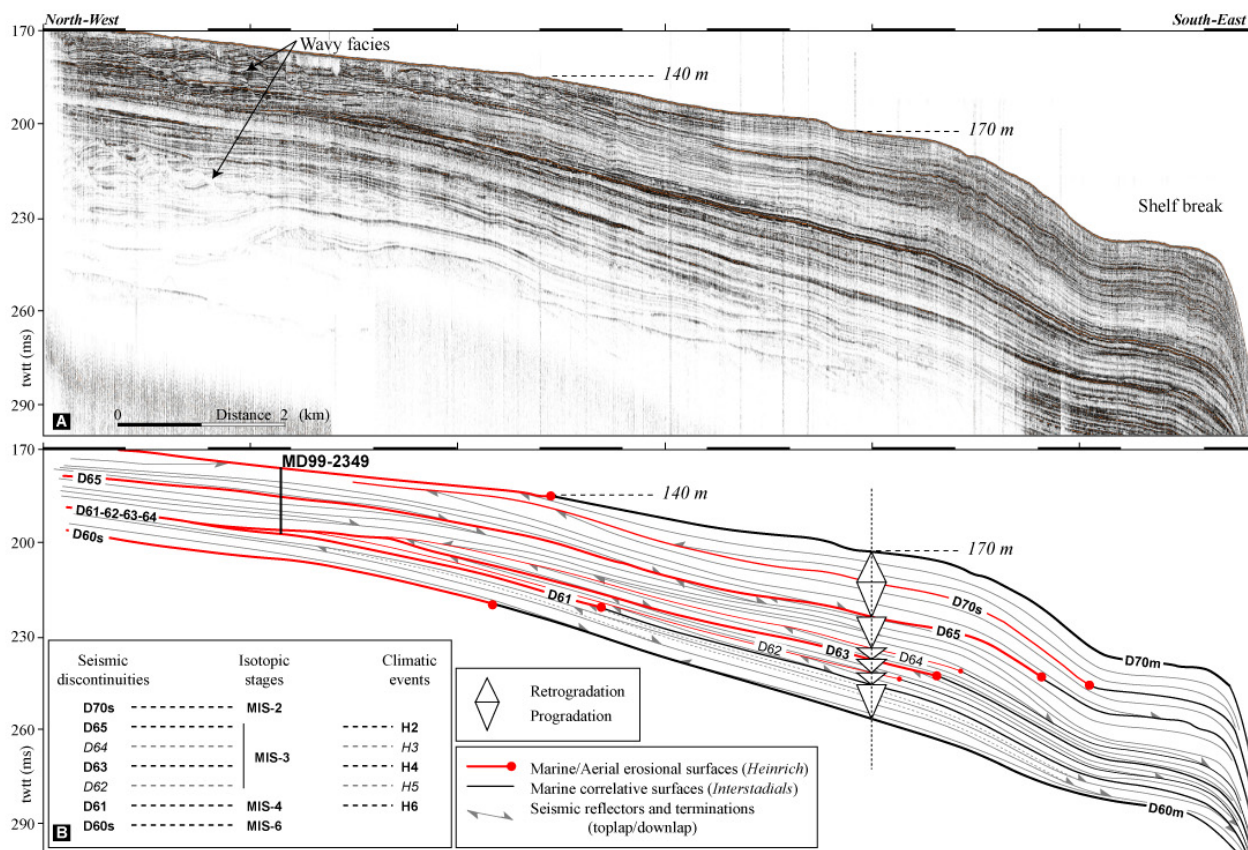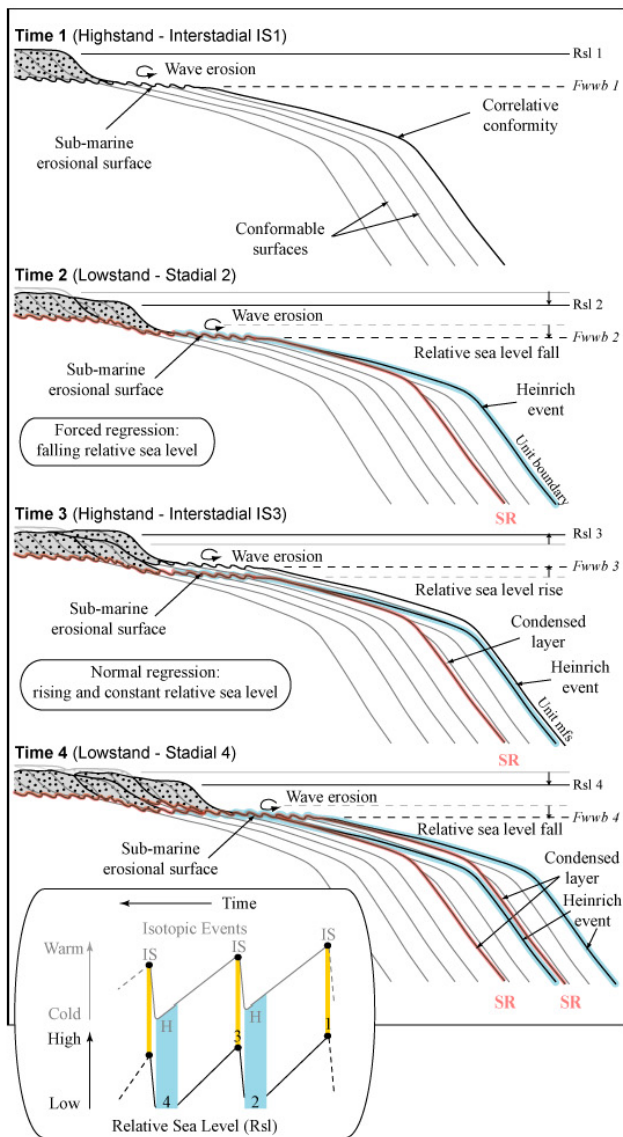
Fig.1 - Jouet et al.

Fig.2 - Jouet et al.

155

Fig.3 - Jouet et al.

Time 1 (Highstand - Interstadial IS1)
- Wave erosion
- Sub-marine erosional surface
- Conformable surfaces
- Correlative conformity
- Rsl 1
- Fwwb 1

Time 2 (Lowstand - Stadial 2)
- Wave erosion
- Sub-marine erosional surface
- Forced regression: falling relative sea level
- Relative sea level fall
- Heinrich event
- Unit boundary
- Rsl 2
- Fwwb 2
- SR

Time 3 (Highstand - Interstadial IS3)
- Wave erosion
- Sub-marine erosional surface
- Normal regression: rising and constant relative sea level
- Relative sea level rise
- Condensed layer
- Heinrich event
- Unit mfs
- Rsl 3
- Fwwb 3
- SR

Time 4 (Lowstand - Stadial 4)
- Wave erosion
- Sub-marine erosional surface
- Relative sea level fall
- Condensed layer
- Heinrich event
- Rsl 4
- Fwwb 4
- SR   SR

Isotopic Events
Time
Warm
Cold
IS   IS   IS
H   H
High
Low
4   3   2   1
Relative Sea Level (Rsl)

Fig.4 - Jouet et al.

ANNEXE - IV

PUBLICATIONS SUR LA PERIODE DEGLACIAIRE

ANNEXE-IV. P<small>UBLICATIONS SUR LA</small> P<small>ÉRIODE</small> D<small>ÉGLACIAIRE</small>

A-IV.1. Seismic stratigraphy of the Deglacial deposits of the Rhône prodelta and the adjacent shelf.

(Labaune, Jouet *et al.*, 2005)

A-IV.2. Sand bodies at the shelf edge in the Gulf of Lions (Western Mediterranean): deglacial history and modern processes.

(Bassetti, Jouet *et al.*, 2006)

A-IV.3. Late Glacial to Preboreal sea-level rise recorded by the Rhône deltaic system (NW Mediterranean

(Berné, Jouet *et al.*, *in press*)

MARINE GEOLOGY

INTERNATIONAL JOURNAL OF MARINE GEOLOGY, GEOCHEMISTRY AND GEOPHYSICS

ELSEVIER

Seismic stratigraphy of the Deglacial deposits of the Rhône prodelta and of the adjacent shelf

Caroline Labaune [a,*], Gwenael Jouet [b], Serge Berné [b], Bernard Gensous [a], Michel Tesson [a], Arnaud Delpeint [b]

[a]*Université de Perpignan, Laboratoire de Biophysique et Dynamique des Systèmes Intégrés, 52 avenue Paul Alduy, 66860 Perpignan, France*
[b]*Ifremer, DRO/GM Technopôle Brest-Iroise, P.O.Box 70, 29280, Plouzané, France*

Abstract

In order to achieve a synthesis of the stratigraphic organization of the Deglacial deposits of the inner/middle shelf in front of the Rhône delta plain, we merged high resolution (Mini-sparker and Sparker), and very high resolution (chirp and mud-penetrator) seismic data into a single seismic database. Thus, the merged seismic database improves the lateral correlation between eastern and western parts, separated by the Rhône Incised Valley deposits. As a result the interpretation of seismic units in relation to local and global environmental changes was refined.

The Deglacial deposits rest on a basal erosional discontinuity capping a complex of Pleistocene prograding wedges. The identified units make up Transgressive and Highstand Systems Tracts, and are bounded by flooding surfaces. The main flooding surfaces are (1) the transgressive surface (D200) which forms the lower boundary of the Deglacial deposits and (2) the maximum flooding surface which forms the boundary between the Transgressive and Highstand Systems Tracts. Regarding the data set the study area is divided into three parts depending on the stacking pattern and main control factors. In the western area the units present an aggradational stacking pattern and the rate of sediment supply and dynamic conditions seems coupled with glacio-eustacy role on sedimentary units building and evolution. In the central area the units present an overall backstepping pattern mainly controlled by glacio-eustacy. In the eastern area the units present an aggradational stacking pattern and both the glacio-eustacy and rate of sediment supply have an important role.

The lower parasequence of the Transgressive Systems Tract (U200) is due to the reworking of Würmian terraces. Above, the parasequence U300 is a transgressive body formed during a rapid sea-level rise. The two upper parasequences are interpreted as ancestral coastal systems with a backstepping pattern. The first coastal system (U400) is due to a decrease in the rate of sea-level rise that occurred during the Younger Dryas. The second coastal system (U500) may be due to a similar event or to an increased rate of sediment supply during a constant sea-level rise.

* Corresponding author. Tel.: +33 336 66 68 21 12.
  E-mail address: labaune@univ-perp.fr (C. Labaune).

Finally the Highstand Systems Tract is composed of three units: (i) unit U601, located to the West and interpreted as a subaqueous delta, (ii, iii) units U600 and U610, located to the East and interpreted as prograding deltaic lobes.
© 2005 Published by Elsevier B.V.

1. Introduction

During the last three decades, Deglacial deposits of shelf areas have been the field of numerous geological studies. On many inner continental shelves, shallow water depth and landward thickening prisms, several tenths of meter thick, provide expanded records of Deglacial deposits. The Rhône continental shelf, in particular, allows detailed analysis of various local and global factors controlling formation of depositional sequences formed during the last post-glacial hemi-cycle.

Several previous works deal with the Deglacial deposits of the northern part of the Gulf of Lions, including Aloisi et al. (1975); Marsset and Bellec (2002) and Gensous and Tesson (1997, 2003). Those papers defined a set of progradational, aggradational and/or backstepping units. Some differences

appear about the extension of the transgressive units and essentially about the interpretation and identification of the upper units of the prodelta system.

Through the "Eurodelta" European concerted action (Trincardi, 2003), the main prodeltas of the northern Mediterranean Sea and Black Sea are objects of synthesis of previous works and data. In this context, a synthetic study of the Deglacial Rhône prodelta and adjacent shelf deposits was done, using a large seismic database. The present study is based on the analysis of high and very high resolution (HR and VHR) seismic data acquired both by Ifremer and Perpignan University (GDARGO) on the inner and middle shelf of the northern part of the Gulf of Lions (Fig. 1).

The objectives were to achieve a synthesis of the stratigraphic organization of the Deglacial deposits, to improve the lateral correlation between eastern and
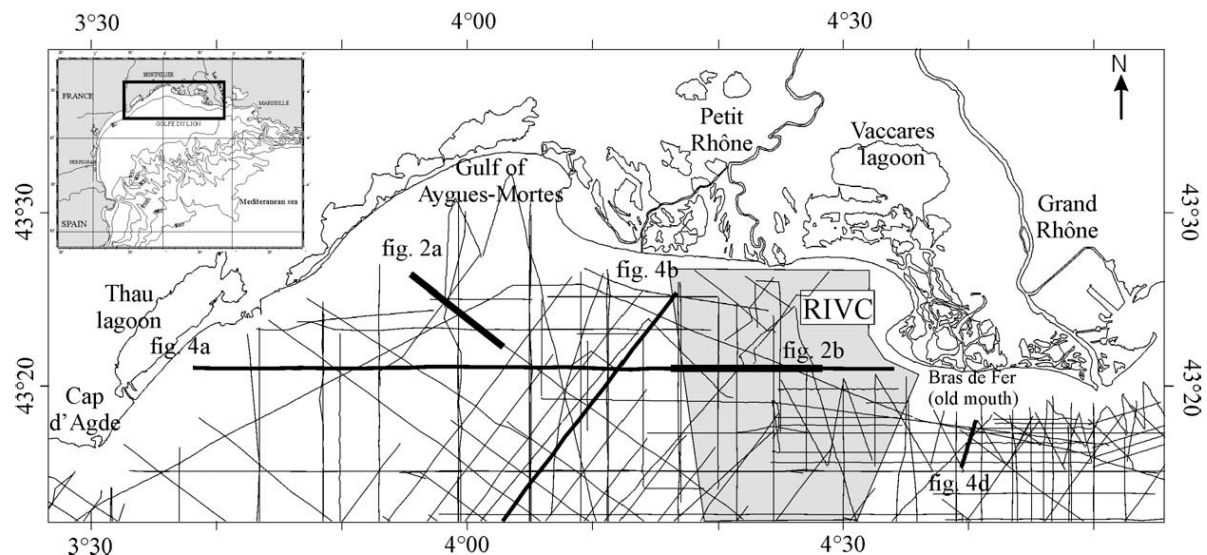

Fig. 1. Map of the northern part of the Gulf of Lion and location map of seismic sections acquired both by Ifremer and Perpignan University (GDARGO). The grey area indicates the location of the Rhône Incised Valley Complex (RIVC) which delimits the eastern from the western area.

162

western parts of the delta system, and to refine the interpretation of seismic units in terms of genetic factors.

2. Regional setting

The Gulf of Lions is a siliciclastic passive margin stretched between the Pyrenean and Alpine orogenic belts in the Northern part of the Western Mediterranean Basin (Fig. 1). The development of the margin was initiated by Oligocene rifting (Gueguen, 1995; Sioni, 1997) followed by oceanic opening during the Miocene (Speranza et al., 2002). The accumulation of the sedimentary wedge mainly occurred during the Plio-Quaternary period, principally controlled by glacio-eustacy (Bessis, 1986).

The Gulf of Lions is a wave-dominated area with, at the shoreline, extensive sand barriers isolating shallow lagoons ("étangs"). The Rhône sediment supply represents 80%, about 7.4×10^6 tons/yr, of the total sediment budget to the continental shelf (Pont et al., 2002) and forms a large delta system. At the coast, the southeasterly dominant wave-regime drives a southwestward longshore drift. The general oceanographic circulation is dominated by the geostrophic Liguro-Provencal current (Millot, 1994). The specific study area is bounded at the South by the 43°15 parallel.

From the mid-shelf to the shelf break, Pleistocene deposits are represented by a complex of superimposed prograding wedges thickening seaward. Those wedges are interpreted as prodeltaic deposits (Aloïsi, 1986; Tesson and Allen, 1995; Rabineau et al., 1998) that accumulated during falling-stage and lowstand sea-level episodes (Tesson et al., 2000; Posamentier et al., 1992). In the central part of the study area, the Pleistocene deposits are interrupted by an important incised valley system: the Rhône Incised Valley Complex—RIVC (Fig. 1). It extends from the deltaic plain down to the Petit Rhône canyon. The RIVC formed by successive Quaternary eustatic cycles (Tesson and Allen, 1995). The stacking pattern of Pleistocene units differs between the western and eastern parts of the RIVC. In the western area, some well-developed intercalated units appear between the prograding wedges at the mid/outer shelf. They represent nearshore sand bodies that accumulated either during the periods of maximum relative sea level lowstand and/

or during stillstands that occurred during overall sea-level rises (Berne et al., 1998; Rabineau et al., 1998; Tesson et al., 2000).

3. Data and methodology

The location map of all seismic sections used for this study is presented in Fig. 1. The database represents both the Ifremer and the University of Perpignan seismic data collected since 1990. The 5000 km seismic data comprise high resolution (HR) profiles, acquired with a mini-sparker (50 J) and a sparker (700 J). Very high resolution (VHR) seismic data were acquired with a chirp system (2–5 kHz) and a mud penetrator working at 3.5 kHz. Most of the data were digitally recorded using a Delph seismic system. Other data were recorded on analogic format, and were subsequently digitized. The navigation was based on GPS (100 m accuracy) and DGPS (about 10 m accuracy).

The following section summarizes key observations based on these data, especially on HR seismic data. The principles of seismic analysis are those described by Mitchum and Vail (1977) and Mitchum et al. (1977) who describe the key seismic facies and terminations (Fig. 2).

4. Seismic stratigraphy

The main characteristics of seismic surfaces and units are summarized in Tables 1 and 2.

4.1. Discontinuities

Nine surfaces, labeled D200 to D610 from base to top, are identified through the study area (Figs. 3 and 4). Each surface is defined as regional or local depending both on their correlation with previous works and on the correlation through the seismic database used in this study. Generally, the bounding surfaces present a flat morphology, except those located in the RIVC area. The basal discontinuity, D200, is amalgamated with D300 in the western area and is well-defined in the central and eastern areas where it overlays toplap terminations. D200 is an erosional discontinuity which is correlated down to
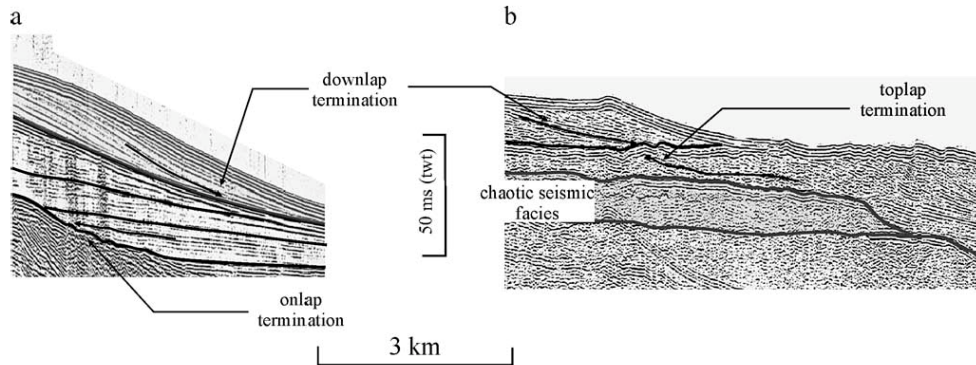
Fig. 2. Several types of seismic reflector terminations, after the terminology defined by Mitchum et al. (1977).

the shelf break by Gensous and Tesson (2003) and thus it is considered as a regional surface. D300 is defined by onlap terminations onto the RIVC to the east, and by coastal onlap onto Pleistocene deposits landward. The underlying reflectors show toplap terminations. It is an erosional and regional discontinuity amalgamated with D400 in the eastern area. D400 is a regional surface observed through the whole seismic database. It is an erosional discontinuity defined by toplap and essentially downlap terminations, and lateral sub-concordant reflectors. The surface D401 shows toplap terminations and is observed only in the north of the Gulf of Aigues-Mortes. D402 is a downlap surface restricted to the westernmost coast. D500 is an erosional and regional surface, observed through the whole seismic database. It is characterized by toplap terminations below and downlap terminations above except in the western end of the RIVC area where it is outcropping. The upper boundary surfaces, D600 and D610, are only identified in the eastern area as downlap surfaces. D601 is an erosional discontinuity characterized by toplap terminations. It

extends only in the western area. It is also a downlap surface.

4.2. Seismic units

Ten seismic units (from U200 to U610 from base to top) bounded by the above described unconformities have been identified.

Unit U200 is located in the central and eastern areas. Its maximum thickness is about 10 m (Fig. 5a). It erosionally overlies the deposits of the RIVC in the central area and the Pleistocene wedges in the eastern area. Its stratal pattern evolves from discontinuous reflectors or chaotic seismic facies in the axial part to continuous, slightly convex-upward reflectors which downlap eastward onto the underlying surface.

Unit U300 is observed in the western area from the middle shelf up to 30 m water depth. The isopach map (Fig. 5b) shows a crescent shape with a maximum thickness of about 20 m in the proximal part of the unit. Its internal structure is characterized by horizontal to sub-horizontal parallel continuous reflectors onlapping landward onto Pleistocene deposits and laterally onto U200 deposits and incised valley deposits. It is a regional seismic unit.

The prograding units U400 and U500 are superimposed or slightly backstepping. Both are regional units but they mainly developed in the western and central area where they outcrop on the inner shelf between 30 and 60 m of water depth. In the eastern area, in front of the present Rhône river mouth, U400 and U500 are relatively thin and arranged in an aggrading pattern; the presence of gas prevents seismic penetration and further observation.

Table 1
Main characteristics of seismic surfaces

Surfaces	Terminations	Type	Extent
D610	downlap	?	local
D601	toplap/downlap	erosional	local
D600	toplap/downlap	erosional	local
D500	toplap/downlap	erosional	regional
D402	downlap	?	local
D401	toplap	erosional	local
D400	toplap/downlap	erosional	regional
D300	toplap/onlap	erosional	regional
D200	toplap	erosional	regional

Table 2
Main characteristics of seismic units and named correspondence with previous works of Marsset and Bellec (2002) and Gensous and Tesson (2003)

Units	Seismic facies	Thickness	Extent	Area	Marsset and Bellec (2002)	Gensous and Tesson (2003)
U610	prograding clinoforms to sub-horizontal reflectors	up to 25 m	local	East	U8–U11	
U601	prograding sigmoids	up to 10 m	local	West		T4
U600	prograding clinoforms to sub-horizontal reflectors	up to 10 m	local	East	U8–U11	
U501	sigmoid to oblique-tangential reflectors	up to 20 m	local	West		
U500	prograding clinoforms to sub-horizontal reflectors	up to 30 m	regional	West	U7	T4
U402	oblique-tangential reflectors	up to 15 m	local			T3
U401	landward prograding clinoforms	up to 15 m	local	North-West	U6	T3
U400	prograding clinoforms to sub-horizontal reflectors	up to 30 m	regional		U5	T3
U300	sub-horizontal reflectors	up to 30 m	"regional"		U4b–U4c	
U200	chaotic to continuous reflectors	up to 10 m	local	RIVC/East	U4a	T2

Unit U400 is mainly developed in front of the Gulf of Aigues-Mortes (Fig. 5c). On cross section it appears as a lenticular to prismatic body, about 30 m thick, thinning seaward and eastward. Seismic facies pattern is oblique-tangential with high angle toplap terminations (1° to 1.5°). The distal toes of clinoforms gently downlap onto the lower boundary and merge with sub-parallel reflectors of U300. Shoreward, the inner part of U400 is erosionally overlaid by unit U401 (Fig. 5d) showing landward prograding clinoforms. In the eastern area U400 is thin (maximum 15 m) and is composed of horizontal to sub-horizontal reflectors. It rests on Pleistocene deposits or U200.

Unit U500 spreads on the inner shelf shoreward of U400. In the central area, it is a shore parallel lenticular to prismatic body (Fig. 6f), of up to 30 m thick, and presenting an offlap break. It shows seaward prograding clinoforms to sub-horizontal tangential reflectors. Towards the east, U500 prolongs under the modern delta plain; only the distal part of the unit, composed of horizontal to sub-horizontal reflectors, is observed on the inner shelf.

Unit U402 and unit U501 are located at the westernmost part of the study area, close to Cap d'Agde (Figs. 5e and 6g). Based on correlation of seismic profiles, they are considered as lateral equivalents of U400 and U500, respectively. Unit U402 is a lenticular body (Fig. 5e), 15 m thick, with prograding oblique-tangential reflectors onlapping onto the Pleistocene deposits. They present an accentuated dip in the proximal area.

Unit U501 (Fig. 6g) is a prismatic body up to 20 m thick. Its seismic facies presents sigmoid to oblique-tangential reflectors.

Units U600 and U610 are stacked units that develop in the eastern part of the study area, in front of the Rhône delta plain (Fig. 6h). Both units are wedge shaped thinning progressively offshore and thickening landward. They show prograding oblique-tangential reflectors. Maximum observed thick-
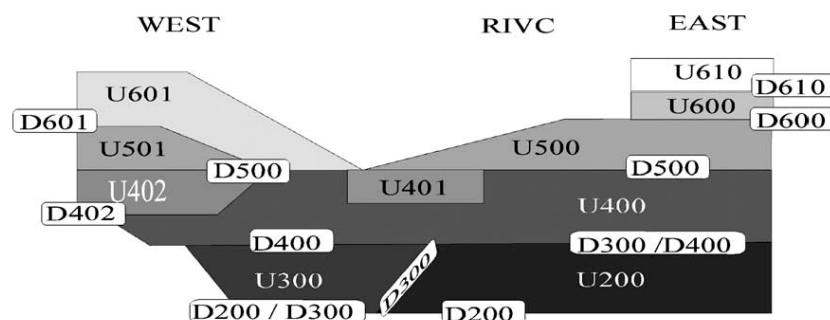

Fig. 3. Schematic stratigraphic organization of the Deglacial deposits and discontinuities in the western, RIVC and eastern parts of the study area (not scaled).
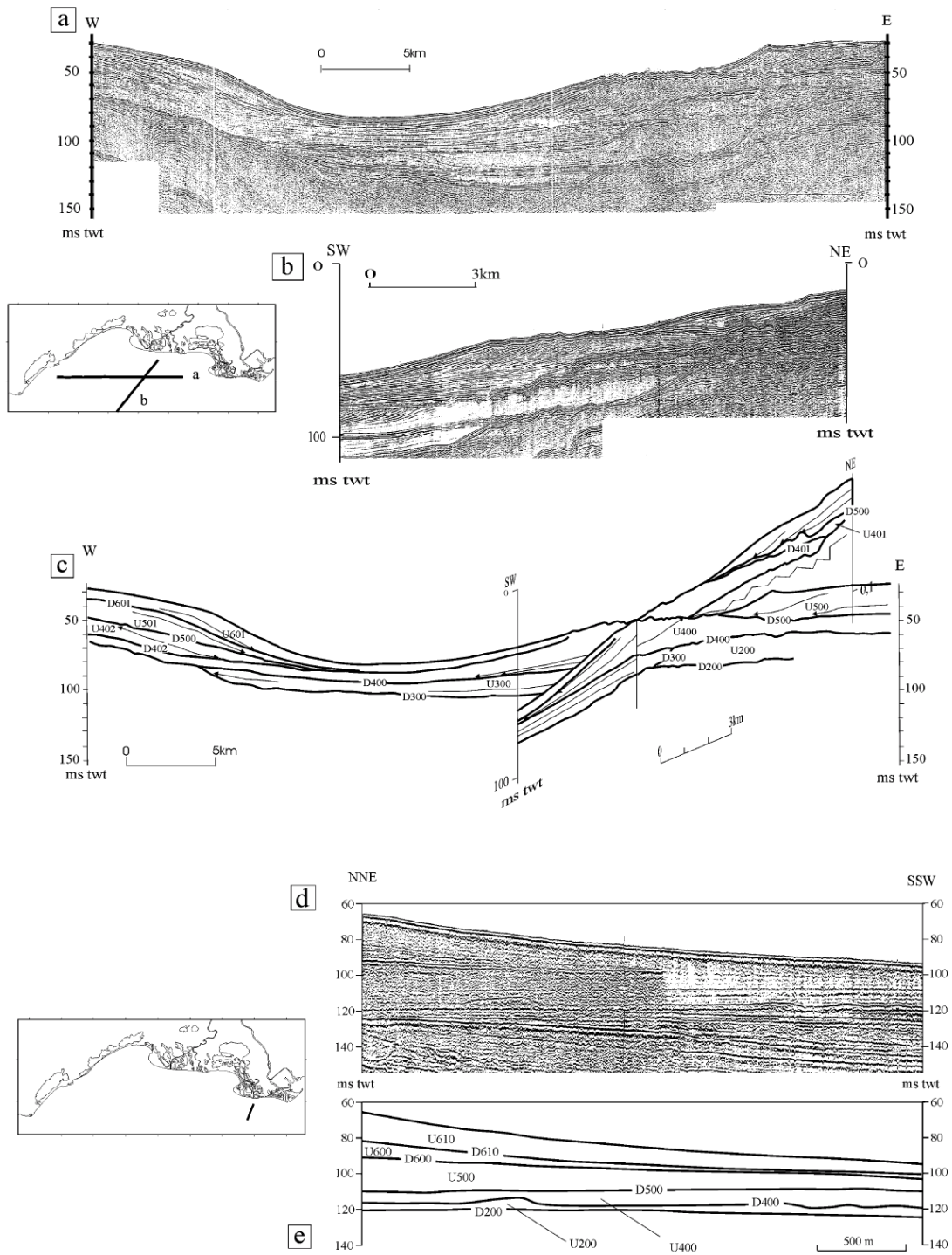
Fig. 4. Uninterpreted (a, b, d) and interpreted (c, e) seismic sections illustrating the main units and discontinuities, respectively, in the western area (a, b, c) and eastern area (d, e).
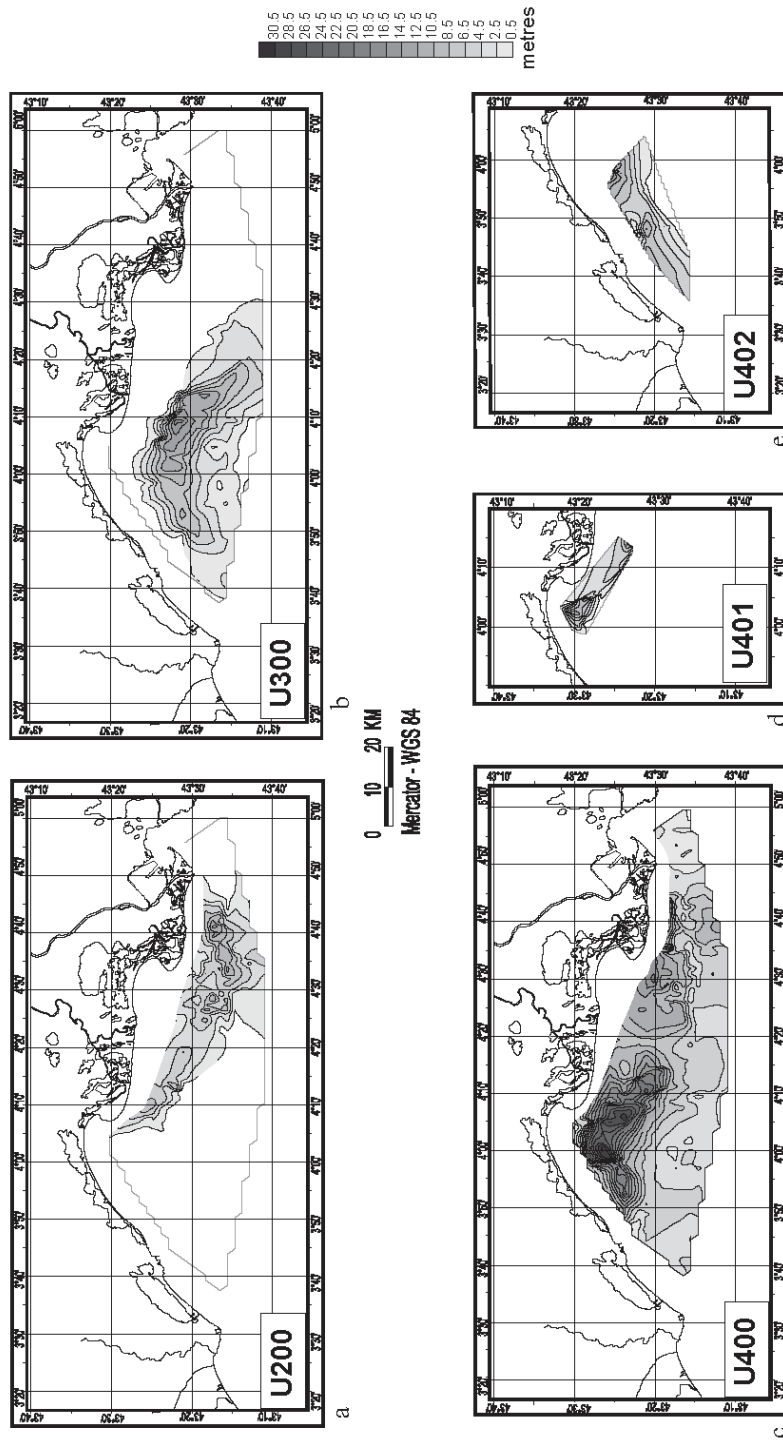
Fig. 5. Isopach maps of some of the units identified in the Rhône prodelta and adjacent shelf. The isopach maps from the basal to the fifth unit identified (from a to e) are here shown. Thickness in meters, based on an acoustic waves velocity of 1600 m/s in sediment.
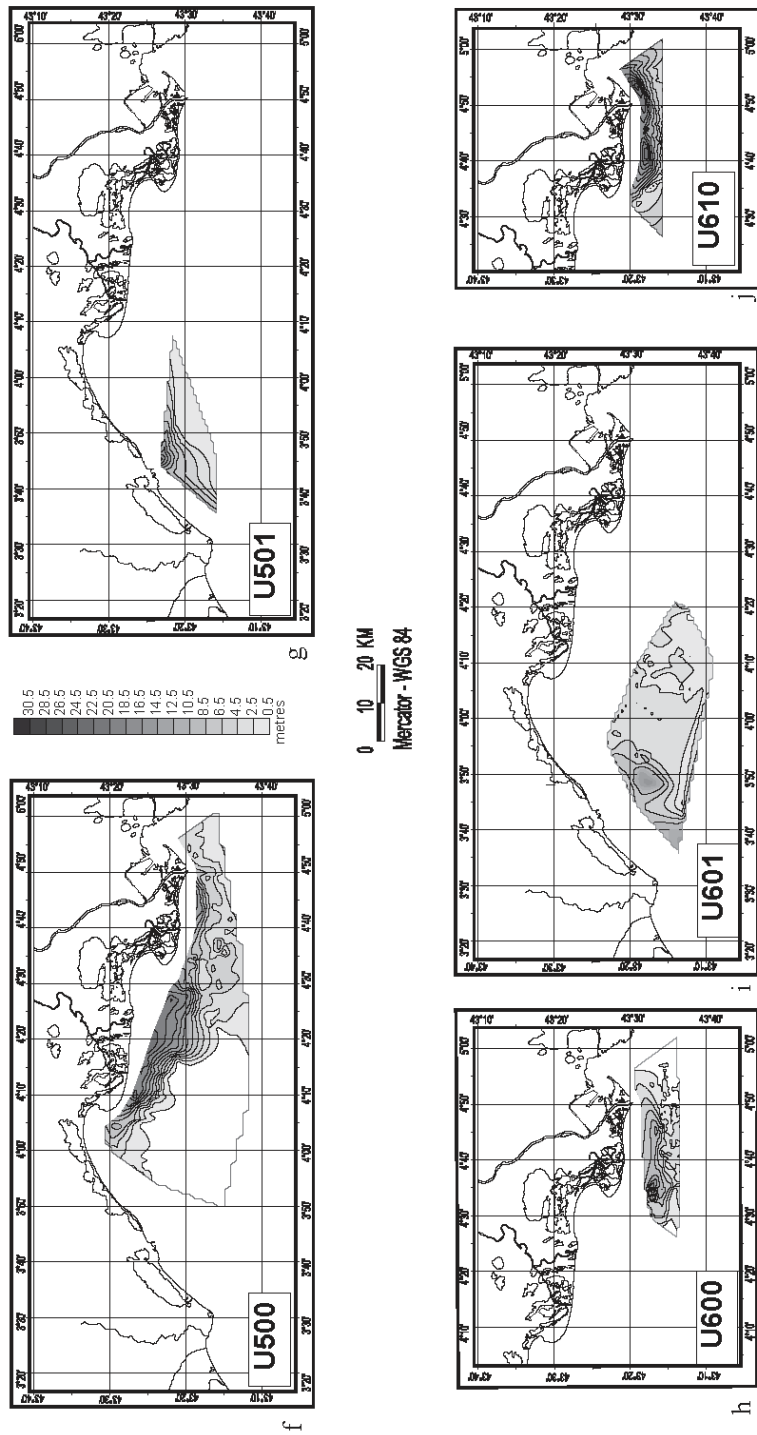
Fig. 6. Isopach maps of some of the units identified in the Rhône prodelta and adjacent shelf. The isopach maps from the sixth unit to the upper unit identified (from f to j) are here shown. Thickness in meters, based on an acoustic waves velocity of 1600 m/s in sediment.

ness is 10 m for U600 and 25 m for U610 in front of the "Grand Rhône" and "Bras de Fer" mouths.

Unit 601 is the uppermost unit in the western area (Fig. 6i). It appears as a lenticular body with a maximum thickness of 10 m. U601 shows clearly prograding sigmoids.

5. Interpretation

5.1. Stratigraphic interpretation

Two mains unconformities (Fig. 7) have been identified in terms of sequence stratigraphy (Mitchum et al., 1977).

(i) D200, which is merged with D300 in the western area, is located at the base of the Deglacial deposits. It is interpreted at once as the lowstand

erosional discontinuity (Marsset and Bellec, 2002) and as the Transgressive Surface (TS).

(ii) The unconformity D600 which separates backstepping units from aggrading/prograding units is a maximum flooding surface (mfs). In the central area, this surface is outcropping. In the western area the lateral equivalent of D600 (mfs) is represented by D601.

The other unconformities (D400, D500, D610) represent flooding surfaces.

On either side of the deltaic plain, the units rest on a Pliocene and Mesozoic substrate which has a relatively high gradient (1% to 3%). Three types of stacking pattern are observed (Fig. 7): (a) aggrading pattern in the eastern area, (b) backstepping pattern with mfs outcropping in the central area and (c) aggrading pattern with mfs outcropping in the westernmost area.
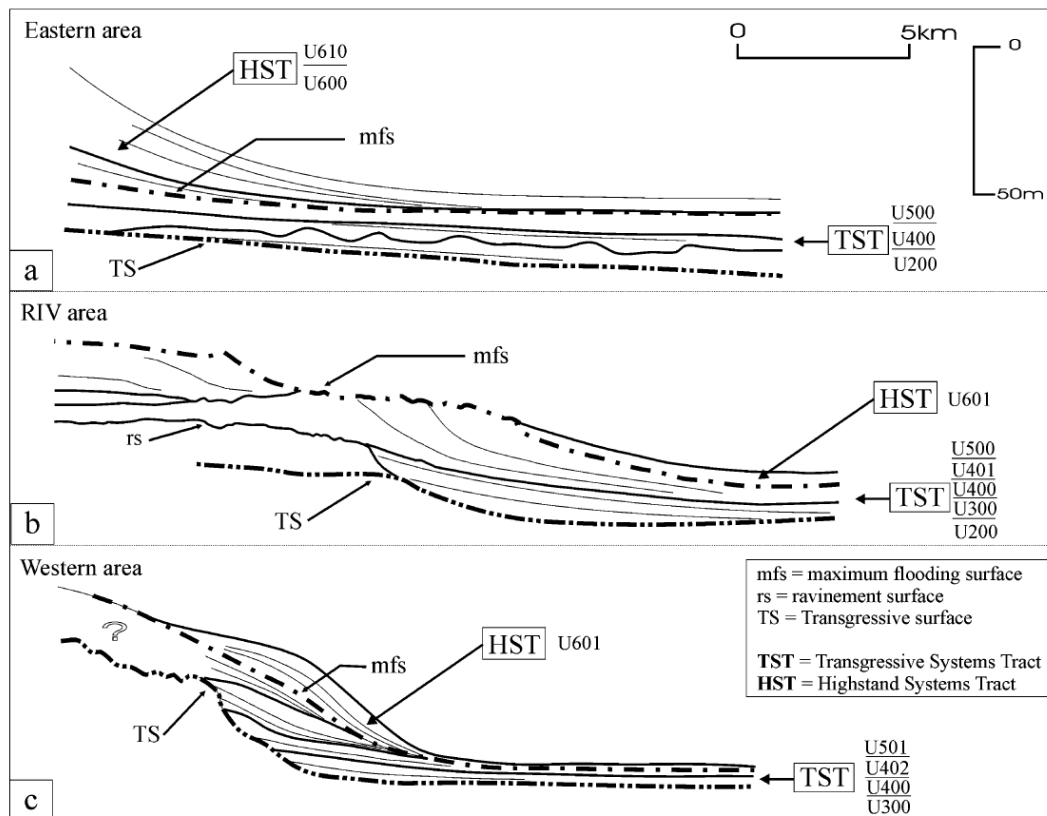

Fig. 7. Schematic patterns of the Deglacial deposits in each identified areas (a: eastern area, b: RIV area, c: western area). Location of key stratigraphic surfaces and systems tracts.

5.2. Depositional processes (environments)

The basal seismic unit, U200, built along the retreat path of the Rhône mouth across the shelf. In the central part, seismic facies indicate coarse-grained deposits probably resulting from the reworking of alluvial deposits of the RIVC (Würmian terraces). To the east, the continuous reflectors are interpreted as medium to fine grained overflow deposits.

The transgressive pattern within unit U300 suggests that this unit developed during a period of rapid landward migration of the shoreline.

The two prograding units, U400 and U500, have similar attributes to modern coastal depositional systems. The seaward prograding clinoforms are typical of a sandy coastal barrier, with lagoonal deposits possibly preserved (Fig. 5b) landward. Locally, the sudden acoustic wipe out of seismic reflections observed seaward of the coastal barrier (Fig. 5d) is attributed to the effects of shallow gas. It is commonly found in rapidly deposited sediments with a high organic content such as prodelta environments. U400 and U500 are interpreted as coastal systems resulting from the progradation of deltaic lobes which have been subsequently reworked and re-shaped into coastal barriers as it can be observed in the modern Rhône delta (Oomkens, 1967). Unit U401 may represent either backbarrier deposits synchronous of the U400 coastal system, or washover deposits associated with reworking of the top of U400 during the subsequent flooding event.

Units U400 and U500 prograded during periods of decreasing rate of sea level rise and/or increased sediment supply. These units are parasequences of the Transgressive Systems Tract (TST) bounded by flooding surfaces in the sense of Van wagoner et al. (1988); locally, the boundary of U400/U500 is a wave ravinement surface (D500). They are arranged in a backstepping pattern which reflects the transgressive character of the late Deglacial period. Because of their present bathymetric location (30 to 60 m), below storm wave base, they are not presently subject to reworking.

Units U402 and U501 are considered as the lateral equivalents to U400 and U500, respectively. Regarding their shapes and internal reflectors, they are compared to ancestral "subaqueous deltas" in the sense of Cattaneo et al. (2003). They would have form under the effect of westward littoral drift and regional cir-

culation, considered similar to the present-day oceanographic regime.

Units U600 and U610 constitute prodeltaic lobes. They correlate onshore with deposits of the upper part of the delta plain. They prograded onto the late transgressive deposits (U400 and U500) and they are interpreted as sedimentary bodies of the Highstand Systems Tract. Their lower boundary (D600) is the maximum flooding surface (mfs). Recent studies on the Rhône delta plain (Vella, 2002) show that at least two major Highstand delta complexes prograded during the last 4000 yr. The first one (Saint Ferreol complex) prograded between 4000 and 2000 yr BP in the western part of the Rhône delta plain, in front of units U400 and U500. The most recent system (Vieux Rhône complex) prograded since 2000 yr BP in the eastern part of the delta plain and correlates seaward with units U600 and U610. The upper prodeltaic lobe, U610, shows two depocentres. The first depocentre is correlated with the "Bras de Fer" deltaic lobe and the second depocentre with the presently active lobe (Roustang lobe).

Unit U601 is also interpreted as a modern "subaqueous delta" in the sense of Cattaneo et al. (2003) because there is no direct sediment supply source in the vicinity. The Rhône would therefore be the main sediment source of U601, sediment being transported by a southwestward current generated by the Liguro-Provencal current.

6. Discussion

6.1. Glacio-eustacy

Given the short time-span represented by the Deglacial deposits, and the moderate effect of tectonic subsidence in the area (Bessis, 1986) we consider that the main controlling factor on stratal architecture is related to glacio-eustatic sea-level changes. Nevertheless other controlling factors, especially sediment supply, ocean dynamics and the pre-existing morphology may have had an effect on the stacking pattern of the prodeltaic units.

It is now well-known that the last Deglacial sea level rise was not continuous and regular but was punctuated by steps (Fairbanks, 1989; Bard et al., 1993; Bard et al., 1996). In Lambeck and Bard

(2000), two sea-level variation models are presented. The first model represents a predicted relative sea-level curve which shows a regular relative sea-level rise along the French Mediterranean coast. The second model presents a corrected relative sea-level curve based on field observations and shows increased and decreased rate of relative sea-level rise.

On the Rhône shelf, the good correlation between the bathymetry of the upper boundaries of the transgressive units and the Deglacial sea-level curve suggests that glacio-eustatic changes are the main controlling factor.

6.2. Deglacial development

Unit U200, located along the axis of the paleo-Rhône, is observed all over the shelf (Gensous and Tesson, 2003), representing the retreating path of the Rhône delta.

Unit U300 built up during a period of rapid migration of the shoreline from outer to inner shelf (from −90 m to −70 m). We correlate it with the meltwater pulse 1A (MWP-1A) that started at around 14,200 yr Cal. BP and occurred during 500 yr (Fig. 8). Moreover, the low gradient of the middle shelf, inherited from the previous lowstand period, favored the rapid landward shift of the shoreline, when the rate of eustatic sea-level rise increased dramatically.

Units U400 and U500 prograded during periods of slowing down of eustatic rise. Age dating from cores cutting across U400 gives 9860 yr ^{14}C BP/11,300 yr Cal. BP (Aloisi et al., 1975) and 10,475 ± 40 yr ^{14}C BP/12,600 yr Cal. BP (Berne et al., 2003). From these data, it is assumed that U400 built up during the Younger Dryas after MWP 1A. Similarly, it would be proposed that U500 prograded during the period of decreased rate of sea-level rise that occurred after MWP 1B. However, the importance of this second meltwater pulse (MWP-1B) is controversial (Bard et al., 1996), and it is not absolutely certain that the backstepping pattern between U400/U500 is related to a changing rate of sea-level rise. Another possibility is that the progradation of U500 would be related to climatically induced increase in river supply.

Units U600 and U610 have prograded onto the late transgressive deposits since the period of reduced rate of sea-level rise at the end of the Holocene. A previous study of sea-level changes during the Highstand
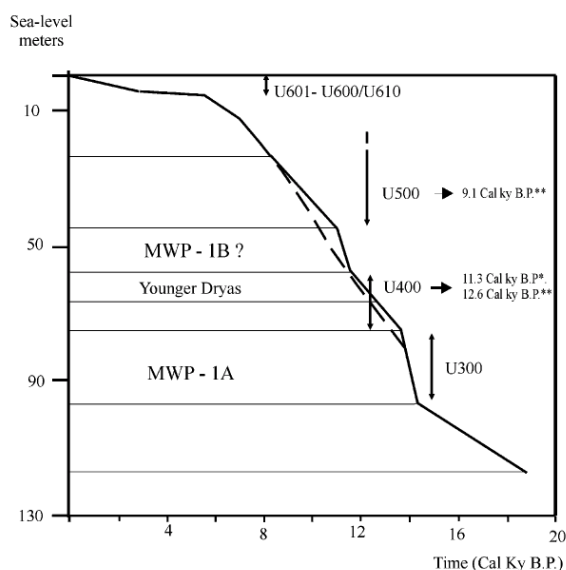

Fig. 8. Relation between glacio-eustacy and Deglacial units. Eustatic curves from Bard et al. (1996), showing the alternating period of increase and decrease rates of sea-level rise. MWP-1A and MWP-1B: brief periods of accelerated melting (i.e., meltwater pulse) of the continental ice and increase of sea-level rise. The continuous line presents the two MWP events whereas the dashed line presents a single MWP. YD: periods corresponding to the Younger Dryas cold period. *Age dating from Berne et al. (2003) corresponding to the unit U400, **age dating from Aloisi et al. (1975) corresponding, respectively to the units U500 and U400.

period that occurred in the delta plain (Vella and Provansal, 2000) indicates two periods of rapid sea-level rise. The first occurred between 6295 and 4585 yr ^{14}C BP (about 2 mm/yr) and the second, between 2120 and 1200 yr ^{14}C BP (1.9 mm yr). These periods were separated by a period of stability between 4085 and 2260 yr ^{14}C BP during which the Saint Ferréol lobe prograded in the western part of the delta plain. From studies carried out on the delta (Vella, 2002), the two depocentres of Unit 610 are correlated with the "Bras de Fer" delta lobe that prograded during the 17th and 18th Century (that is the Little Ice Age period) during a period of enhanced sediment supply and the presently active "lobe de Roustang", that was artificially channelled at the end of the19th century.

6.3. Other controlling factors

In the western area, units U402, U501 and U601 represent subaqueous deltas. In this work, they are

considered as time correlative (synchronous) of units U400, U500 and U600/U610, respectively.

The development of a large prograding body rather than a subaqueous delta is correlated to the hydrodynamic conditions and to the variation in sediment supply. In front of the Rhône mouth the sediment discharge was sufficient to build up an important prograding deltaic depositional system with continuity between the deposits of the delta plain, delta front and prodelta. Westward to the Rhône mouth the sediment supply decreased. Nevertheless the general oceanographic circulation could lead to a westward transport of suspended sediment of the Rhône which enabled to build up a prograding body, the relict subaqueous delta which is disconnected from the modern coastal barrier.

In the central part, off the deltaic plain, the shelf has a low gradient (0.1% to 0.5%) inherited from the deltaic plain environment of the previous lowstand period (and similar to the gradient of the Rhône river of the modern delta plain). This inherited topography favored the rapid landward migration of the shoreline during a phase of accelerated sea-level rise and the drowning of parasequences that are arranged in a retrogradational pattern (Fig. 7b).

7. Conclusions

From the synthesis of existing seismic data, a succession of 10 units separated by flooding surfaces have been observed on the Rhône delta shelf. The first seven are associated to the Transgressive Systems Tract and the last three are associated to the Highstand Systems Tract (HST).

From base to top the TST is composed of (i) reworking deposits of Würmian terraces due to the first step of the Deglacial transgression, (ii) transgressive deposits due to the rapid sea-level rise and landward migration of the shoreline and (iii) two backstepping coastal systems. The first coastal system is due to a decrease in the rate of sea-level rise associated to the Younger Dryas event. The second coastal system is due to a decrease in the rate of the sea-level rise or to an important increase in the rate of sediment supply associated to a constant rate of sea-level rise.

The HST is composed of prograding delta lobes in the eastern area and subaqueous delta in the western area. The prograding delta lobes are due to minor sea-

level variations during a stillstand sea-level, or, more probably, to lobe switching that could be linked to rapid climatic changes. The subaqueous delta is mainly fed by sediment supply reworked through the hydrodynamic circulation.

Glacio-eustacy seems to be the main factor controlling the overall stratigraphic organization of units. Good correlation exists between the shape of the global sea-level curve and the position of the units. Moreover, lateral variability observed within the Rhone sedimentary units would result from the ratio between the rate of sea-level rise and fluvial sediment supply, the location of the sediment input and differing slope gradients.

Without a detailed chronostratigraphic framework, it is difficult to disentangle effects from global (eustatic) changes and those due to local (climatic) changes. However, this study provides the first comprehensive view of the stratigraphic architecture of the Rhone prodelta, and provides the framework for future detailed sedimentological and paleoenvironmental studies.

References

Aloïsi, J.C., 1986. Sur un modèle de sédimentologie deltaïque. Contribution à la connaissance des marges passives. Thèse d'état, Université de Perpignan. 161 pp.

Aloisi, J.C., Monaco, A., Thommeret, J., Thommeret, Y., 1975. Évolution paléogéographique du plateau continental languedocien dans le cadre du golfe du Lion. Analyse comparée des données sismiques, sédimentologiques et radiométriques concernant le Quaternaire récent. Rev. Géogr. Phys. Géol. Dyn. XXXII (1), 13–22.

Bard, E., Arnold, M., Fairbanks, R.G., Hamelin, B., 1993. ^{230}Th–^{234}U ^{14}C ages obtained from mass spectrometry on corals. Radiocarbon 35, 191–199.

Bard, E., Hamelin, B., Arnold, M., Montaggioni, L., Cabioch, G., Faure, G., Rougerie, F., 1996. Deglacial sea-level record from Tahiti corals and the timing of global meltwater discharge. Nature 382, 241–244.

Berne, S., Lericolais, G., Marsset, T., Bourillet, J.F., De Batist, M., 1998. Erosional offshore sand ridges and lowstand shorefaces: examples from tide and wave dominated environments of France. J. Sediment. Res. 69 (4), 540–555.

Berne, S., Baton, J.M., Delpeint, A., Dennielou, B., Duval, F., Field, M., Lericolais, G., Le Roux, E., Satra, C., Taviani, C., 2003. Deglacial history of the Rhone prodelta form detailed morphology and preliminary stratigraphic data. ComDelta: Open conference on Comparing Mediterranean and Black Sea Prodeltas. Aix-en-Provence, France, 26–28 October 2003.

Bessis, F., 1986. Some remarks on the study of subsidence of sedimentary basins. Application to the Gulf of Lions margin. Mar. Pet. Geol. 3, 37–63.

Cattaneo, A., Correggiari, A., Langone, L., Trincardi, F., 2003. The late-Holocene Gargano subaqueous delta, Adriatic shelf: sediment pathways and supply fluctuations. Mar. Geol. 193 (1–2), 61–91.

Gensous, B., Tesson, M., 1997. Les dépôts postglaciaires de la plate-forme rhodanienne: organisation stratigraphique et conditions de mise en place. C. R. Acad. Sci., Paris II (317), 803–810.

Gensous, B., Tesson, M., 2003. L'analyses des dépôts postglaciaires et son application à l'étude des séquences de dépôt du Quaternaire terminal sur la plate-forme au large du Rhône (Golfe du Lion). Bull. Soc. Géol. Fr. 174, 401–419.

Gueguen, E., 1995. La Méditerranée Occidentale: un véritable océan. Exemple de segmentation des marges et de hiatus cinématiques. Implications sur les processus d'amincissement crustal. Thèse de doctorat, Université de Bretagne Occidentale.

Fairbanks, R.G., 1989. A 17000-year glacio-eustatic sea level record: influence of glacial melting rates on the Younger Dryas event and deep-ocean circulation. Nature 342 (6250), 637–642.

Lambeck, K., Bard, E., 2000. Sea-level change along the French Mediterranean coast for the past 30000 years. Earth Planet. Sci. Lett. 175 (3–4), 203–222.

Marsset, T., Bellec, V., 2002. Late-Pleistocene–Holocene deposits of the Rhône inner continental shelf (France): detailed mapping and correlation with previous continental and marine studies. Sedimentology 49, 255–276.

Millot, C., 1994. Models and data: a synergetic approach in the Western Mediterranean sea. In: Malanotte-Rizzoli, P. (Ed.), Ocean Processes in Climate Dynamics: Global and Mediterranean Examples. Kluwer Academic Publishers, pp. 407–425.

Mitchum, J.R., Vail, P.R., 1977. Seismic stratigraphy and global changes of sea level: Part 7. Seismic stratigraphy interpretation procedure. In: Payton, C.E. (Ed.), Seismic Stratigraphy—Applications to Hydrocarbon Exploration, 26, Mem. AAPG, pp. 135–143.

Mitchum, J.R., Vail, P.R., Sangree, J.B., 1977. Seismic stratigraphy and global changes of sea level, part: stratigraphic interpretation of seismic reflection patterns in depositional sequences. In: Payton, C.E. (Ed.), Seismic Stratigraphy—Applications to Hydrocarbon Exploration (Ed. Payton, C.E.), 26, Mem. AAPG, pp. 117–133.

Oomkens, E., 1967. Depositional sequences and sand distribution in a deltaic complex. Geol. Mijnb. 46, 265–278.

Pont, D., Simonnet, J.-P., Walter, A.V., 2002. Medium-term changes in suspended sediment delivery to the ocean: consequences of catchment heterogeneity and river management (Rhone River, France). Estuar. Coast. Shelf Sci. 54 (1), 1–18.

Posamentier, H., Allen, G., James, D.P., Tesson, M., 1992. Forced regressions in a sequence stratigraphic framework: concepts, examples, and exploration significance. AAPG Bull. 76, 1687–1709.

Rabineau, M., Berne, S., Ledrezen, E., Lericolais, G., Marsset, T., Rotunno, M., 1998. 3D architecture of lowstand and transgressive Quaternary sand bodies on the outer shelf of the Gulf of Lion, France. Mar. Pet. Geol. 15 (5), 439–452.

Sioni, S., 1997. Mer Ionienne et Apulie depuis l'ouverture de l'Océan Alpin. Thèse de Doctorat, Univ. Bretagne Occidentale.

Speranza, F., Villa, I.M., Sagnotti, L., Florindo, F., Cosentino, D., Cipollari, P., Matei, M., 2002. Age of the Corsica-Sardinia rotation and Liguro-Provencal Basin spreading: new paleomagnetic and Ar/Ar evidence. Tectonophysics 347, 231–251.

Tesson, M., Allen, G., 1995. Contrôle tectonique et eustatique haute-fréquence de l'architecture et de la stratigraphie de dépôts de plate-forme péricatonique. Exemple du Golfe du Lion (Méditerranée, France) et des dépôts quaternaires. C. R. Acad. Sci., Paris IIa (320), 39–46.

Tesson, M., Posamentier, H., Gensous, B., 2000. Stratigraphic organization of the Late Pleistocene deposits of the western part of the Golfe du Lion shelf (Languedoc shelf), western Mediterranean Sea, using high resolution seismic and core data. AAPG Bull. 84 (1), 119–150.

Trincardi, F., 2003. The impact of short term supply fluctuations on margin shaping over the last 20,000 years. Ocean Margin Research Conference, Paris 15th–17th September 2003.

Van wagoner, J.C., Posamentier, H.W., Mitchum Jr., R.M.Vail, P.R., Sarg, J.F., Loutit, T.S., Hardenbol, J., 1988. An overview of the fundamentals of Sequence Stratigraphy and key definitions. In: Wilgus, C.K., Hastings, B.S., Kendall, C.G.St.C., Posamentier, H., Ross, C.A., Van Wagoner, J. (Eds.), Sea Level Changes—An integrated approach. SEPM Special Publication, vol. 42, pp. 39–46.

Vella, C., 2002. Edification pulsée d'un appareil prodeltaïque progradant: le lobe de St. Ferréol, delta du Rhône. Colloque général du GDR marges, Reuil Malmaison.

Vella, C., Provansal, M., 2000. Relative sea-level rise and neotectonic event during the last 6500 yr on the southern eastern Rhône delta. Mar. Geol. 170, 27–39.

Sand bodies at the shelf edge in the Gulf of Lions (Western Mediterranean): Deglacial history and modern processes

M.A. Bassetti [a,b,*], G. Jouet [a,b], F. Dufois [c,d], S. Berné [a], M. Rabineau [b], M. Taviani [e]

[a] GM-IFREMER BP70 29280 Plouzané, France
[b] UMR6538 Domaines océaniques, IUEM, 29280 Plouzané, France
[c] EC-TP-IFREMER/BP 70/29280 Plouzané, France
[d] IRSN, Base Ifremer, BP 330, 83507 La Seyne sur Mer Cedex, France
[e] ISMAR-CNR, Via P. Gobetti, 101 Bologna, Italy

Abstract

The outer continental shelf of the Gulf of Lions is covered by thick, mainly regressive, sand deposits. A combination of seismic, sedimentological and geochronological methods allows us to demonstrate that a veneer of transgressive sand bodies, few m to less than 1 m thick, reworks these deposits. They take the form of sand ridges and transverse dunes that formed at different periods. In fact, the low-gradient outer shelf of the Gulf of Lions displays a complete record of deglacial history, including not only transgressive deposits that formed during sea-level rise, but also bedforms that still evolve under episodic high-energy events that occur under more highstand conditions.

Core lithology, ^{14}C dates and regional sea-level curve suggest that the formation of the sand ridges was favoured during a period of deceleration of sea-level rise, such as during the Younger Dryas event. The dunes are part of a "mobile carpet" (here U160). The deposition of this marine sand veneer is possibly related to the interplay between different factors that trigger the turning on/off for bottom currents sand deposition/transport on the outer shelf. In fact, the sands appear to have been reworked intermittently due to high-energy conditions in shallow water depth (currents, wave regime and wind-driven circulation) as well as they form current ridges superimposed to the transgressive deposits in the westernmost part of the studied area (at the Bourcart Canyon's head).
© 2006 Elsevier B.V. All rights reserved.

Keywords: sand ridges; outer shelf; deglacial transgression; sand transport; Gulf of Lions

1. Introduction

1.1. Background: "offshore sands" of outer continental shelves

The concept of relict "offshore sands" was first introduced by Emery (1968), who observed that sand belts were covering many continental shelves around the world, at water depths generally comprised between 80 and 120 m water depth. He noticed that they were not in

---

* Corresponding author. GM-IFREMER BP70 29280 Plouzané, France.
E-mail address: mabasset@ifremer.fr (M.A. Bassetti).

equilibrium with modern shelf processes, and concluded that these deposits were deposited during and immediately after the Last Glacial period. Later, Swift et al. (1971) suggested that shelf sands, although too coarse to have been transported by present-day processes, are being reworked and resorted by waves and currents, and referred to them as "palimpsest".

In the Gulf of Lions, which is considered as a relatively low energy continental shelf, most of the authors still consider that the offshore sands are relict features, only the transgressive processes, at a time when sea-level was lower by about 100 m, being able to rework sediments (Monaco, 1971; Aloïsi, 1986; Berné et al., 1998). However, ultra-high-resolution seismic data, coring and ^{14}C dating, as well as numerical modelling of wind stress on oceanic circulation, allow us to demonstrate that a mobile carpet of sand is periodically active at the shelf edge, feeding slope and rise deposits and contributing to the episodic reworking of shelf morphology.

Among the studies dedicated to the stratigraphy of the late Pleistocene in the Gulf of Lions (Monaco, 1971; Aloïsi, 1986; Tesson et al., 1990; Rabineau et al., 1998; Tesson et al., 2000; Rabineau, 2001; Berné et al., 2004, among the others), the present work concerns the definition of the post-glacial deposit geometry, as well as the distribution of sediments in relation with the latest Quaternary episodes and, in some cases, recent oceanographic events. As a matter of fact, we think that the most recent sedimentary unit is still under the influence of events able to mobilize at least the upper part of the well definable transgressive deposits. These consideration arise from the recently acquired data in the Gulf of Lions about the significant influence of cold water downwelling during winter storms on recent sedimentations (Palanques et al., 2004). In fact, seasonal modifications in the thermohaline circulation in the Gulf of Lions related to the wind action (Cers, Mistral and Tramontane wind complex) have been observed and we propose that the combination of regional interannual variability in water circulation and local hydrodynamic conditions (wind and wave-driven circulation) might lead to strong sea-bed stirring up and sediment transport.

In order to support this hypothesis and, therefore, to estimate the degree of preservation of the most recent sedimentation layer, a numerical model of bottom shear-stress, is here proposed.

On the other hand, the post-glacial unit interfaces are closely analyzed, combining sedimentological data (sedimentary facies and fossil content), radiocarbon dates and seismic features, to trace them on the basis of their distribution on the basal *ravinement* surface.

2. Regional and stratigraphic setting

The Gulf of Lions is a passive, prograding margin, located in the northwestern sector of the Mediterranean Sea bounded, to the west and east, by Pyrenean and Alpine orogenic belts, respectively. It comprises a wide (at least 70 km) shelf and a continental slope that is incised by numerous canyons descending down to the abyssal area of the Algero–Balearic Basin (Fig. 1A). This basin formed as a result of Oligocene–Miocene rifting (Gorini et al., 1994) and it hosted the accumulation of huge amount of clastic sediments forming a thick wedge (900 m) on the inner shelf, more than 2 km on the outer shelf (Lofi, 2002) that makes up the outbuilding shelf.

The post-rift sedimentation was severely affected by the Messinian Salinity Crisis (Hsü et al., 1973), when the sea-level dramatically dropped (Ryan, 1976) and the continental margins were exposed to intense erosion (Cita and Ryan, 1978). The Messinian unconformity bases the cyclically stacked Plio-quaternary bodies that have been object of investigation over the last 30 years by several authors that proposed a number of stratigraphic models (Monaco, 1971; Aloïsi, 1986; Tesson et al., 1990; Tesson et al., 2000; Rabineau, 2001, Lofi et al., 2003, Lobo et al., 2004). The last ca 500 kyr, in particular, display superimposed prograding wedges extending over the entire shelf seawards-thickening and pinching out landward beneath the 80 m isobath (Aloïsi, 1986). They are interpreted as deposited during 'forced regressions', in response to successive sea-level falls (Posamamtier et al., 1992). They correspond to units U140, 147 and 150 in Fig. 2 (Berné et al., 1998; Rabineau et al., 1998, 2005).

The deglacial (post-Last Glacial Maximum) succession overlies the major erosional discontinuity related to emersion of the continental shelf during the Last Glacial Maximum (LGM). It consists of basal transgressive deposits, subsequently reworked, on the outer shelf, into dunes and sand ridges (U155; Berné et al., 1998; Rabineau, 2001; Perez-Belmonte, 2003) overlaining the regressive prograding body. It thickens toward the inner shelf, especially on the Rhône prodeltaic area, between 35 and 70 m water depth (Aloïsi, 1986; Gensous and Tesson, 2003; Berné et al., 2004). The shelf "relict" sands, whose distribution is shown in Fig. 1A, were deposited from 80 m to about 120 m water depth, where they pass rapidly to marine muds. These sands were first described by Bourcart (1945) who called them "sables du large", an equivalent to the "offshore sands" of Emery (1968). The transition between sands and muds is outlined by a distinct regional step in the sea-floor
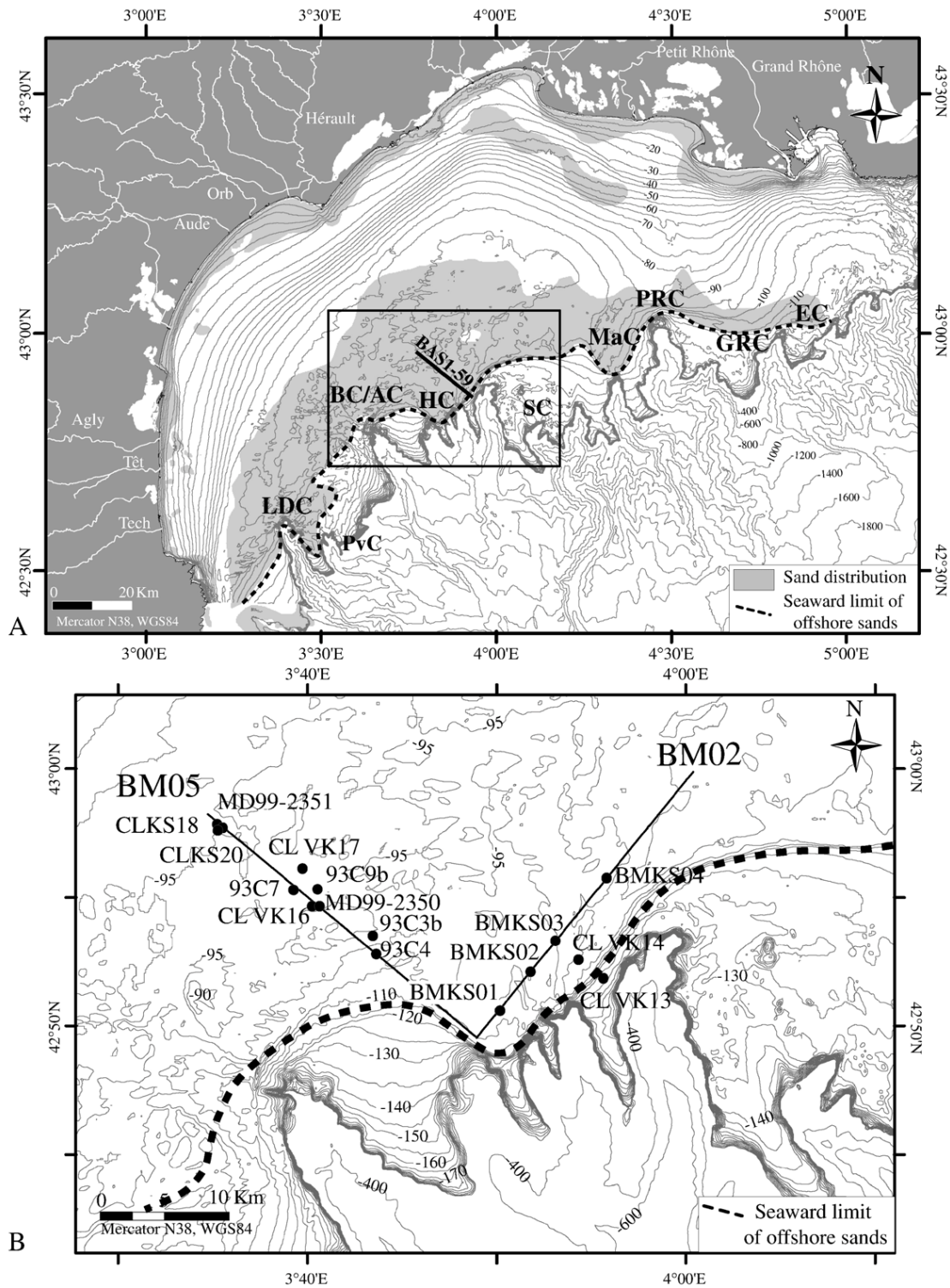
Fig. 1. (A) Bathymetric map of the Gulf of Lions and position of the study area on the outer shelf. LDC, Lacaze-Duthiers Canyon; PvC, Pruvot Canyon; BC/AC, Bourcart or Aude Canyon; HC, Herault Canyon; SC, Séte Canyon; MaC, Marti Canyon; PRC, Petit-Rhône Canyon; GRC, Grand-Rhône Canyon; EC, Estocade canyon; (B) location of seismic lines and cores, showed in this study, at the head of Herault Canyon.
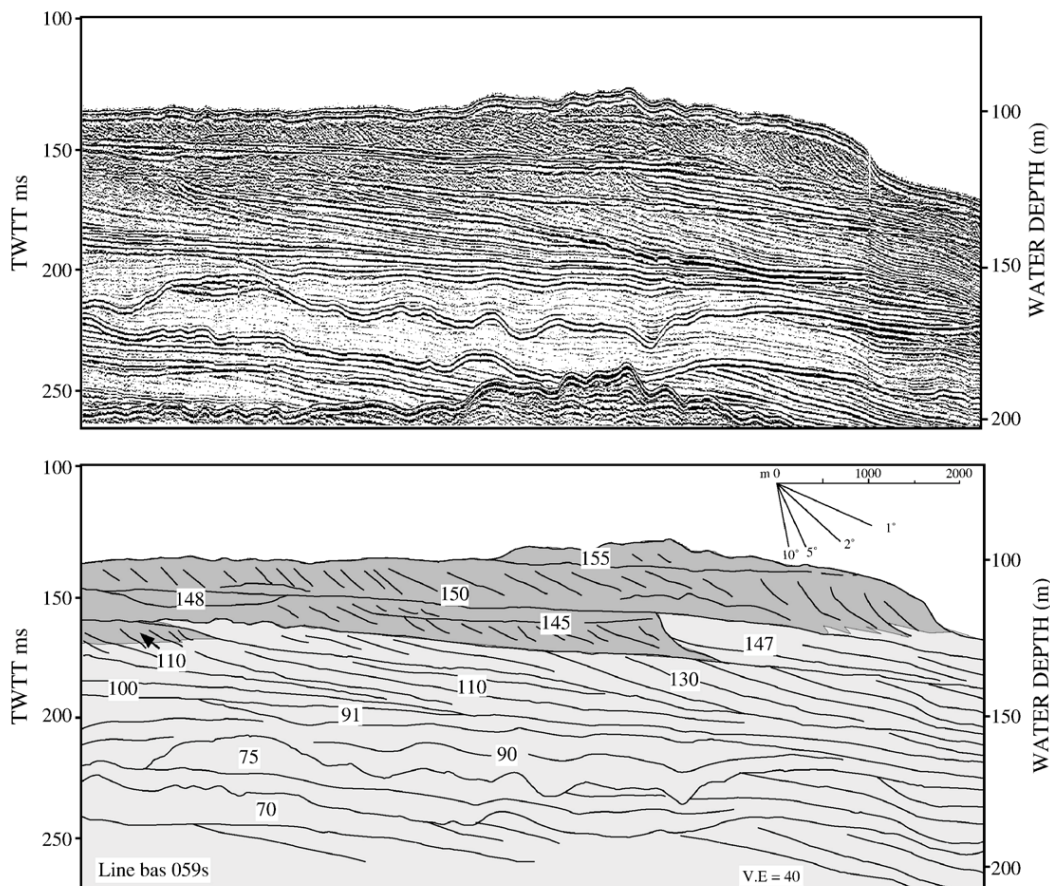
Fig. 2. Seismic section across the Pleistocene sand wedges (BAS 59 on Fig. 1) showing the vertical relationship of the seismic unit identified on the outer shelf of the Gulf of Lions (from Berné et al., 1998, modified).

morphology, that can reach up to 20–25 m of height and can be tracked all along the shelf edge (Berné et al., 2002). The sands are characterized by high carbonate content (25–50%), mainly due to a significant biogenic component (Got and Aloïsi, 1990).

3. Hydrodynamic setting

The continental shelf of the Gulf of Lions is a low-energy wave dominated area where tides have small amplitudes (a few cm) and associated currents are so weak that they cannot be measured (Lamy et al., 1981).

The general circulation and hydrodynamic conditions result from the interaction with the atmospheric phenomena, determining the formation of dense water, up and downwellings and oscillatory currents caused by winds (Tramontane, Mistral) and storms (Millot, 1990).

One of the main components of the general circulation in the western Mediterranean is the "Liguro–Provençal–Catalan Current" or "Northern Current"

which involves water of Atlantic origin, flowing south-westwards mainly along the continental slope and shelf break, following the continental margin. This current is characterized by speeds ranging from 50 cm s^{-1} near the surface and a few cm s^{-1} at a few hundreds of metres depth (Monaco et al., 1990). According to Millot (1990), the core of the Northern Current follows the continental slope most of the time, but the trajectory can be temporally altered during northwesterly wind, when the superficial waters tend to penetrate onto the continental shelf forming a current front that can reach 30 cm s^{-1} after the wind decay (Millot and Wald, 1980). The hydrodynamic conditions on the continental shelf have a strong seasonal variability and the maximum current velocity is reached in winter (Millot, 1990; Estournel et al., 2003; Dufau et al., 2004).

An important parameter in the Gulf of Lions circulation is the meteorological forcing. In fact, local hydrodynamic conditions are determined by the interactions of wave regimes and wind-driven circulation.

The latter is generally dominated by the northwest Tramontane, or by the occurrence of Mistral and Tramontane winds that generate classical oceanographic features (up and downwellings, Palanques et al., 2006-this volume) and transitional circulation features such as inertial oscillations (Millot, 1990; Petrenko, 2003).

However, the winds are not homogeneous throughout the Gulf and especially easterly winds seem to generate the most significant bottom stress, according the modelling, year 2001 (Fig. 3A), despite their occasional occurrence (Fig. 3B). In fact, the surface wind stress, which occurs as individual storm events lasting several
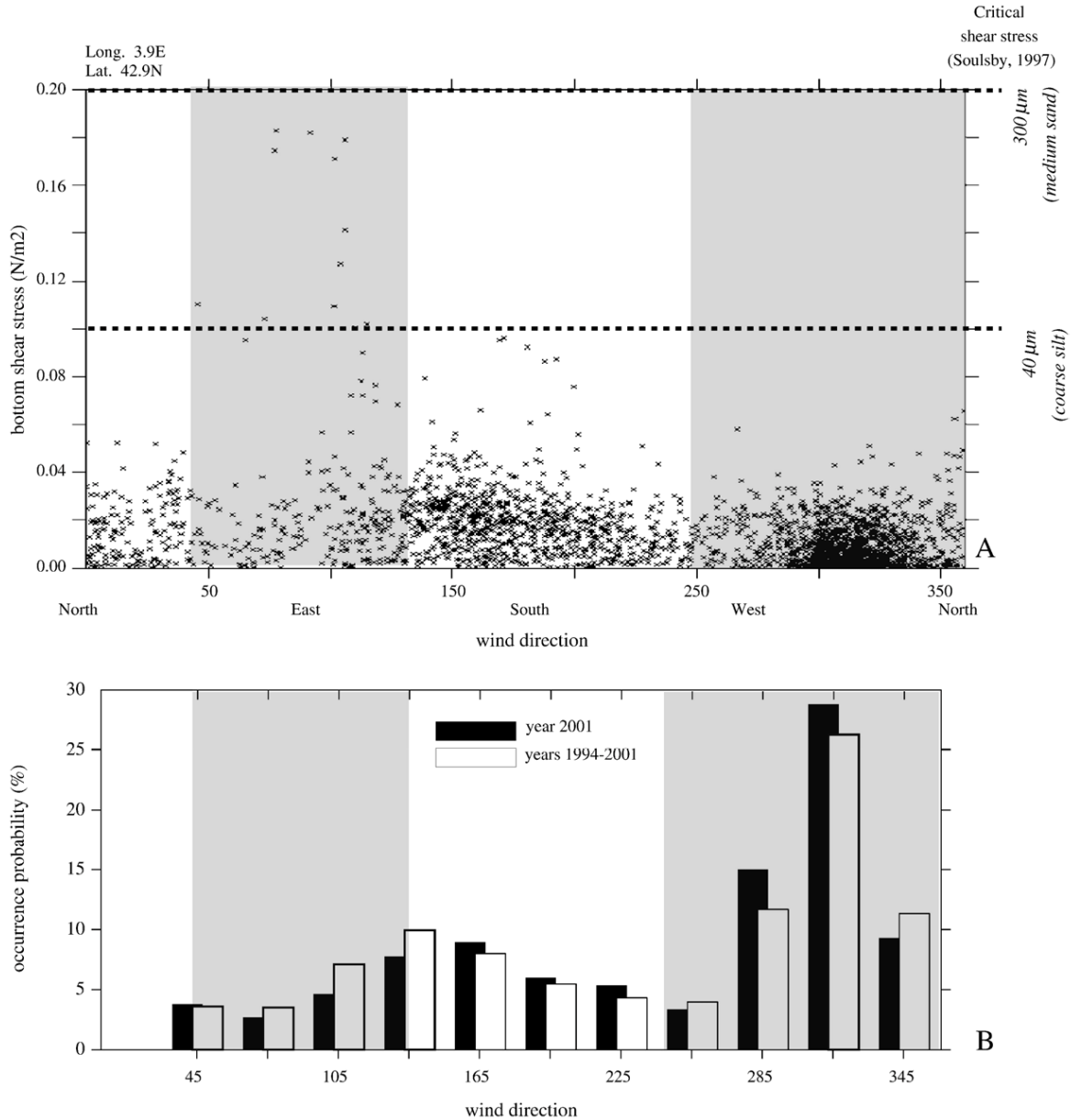

Fig. 3. (A) Comparison plot of wind distribution and the bottom shear stress that they generate measured at a fix point (Long 3.9E; Lat. 42.9 N). Remarkable difference is observed between the bottom stresses induced by easterly winds (up to 0.2 N/m^2) with respect to the ones linked to the Tramontane, Mistral, Cers wind complex, despite their lower occurrence in the gulf. Critical shear stress for sand (300 μm) and coarse silt (40 μm) transport is marked on the plot (after Soulsby, 1997). (B) Statistical record of wind annual (year 2001) and interannual occurrence (years 1994–2001) in the Gulf of Lions, based on the model Météo France ARPEGE. Note that the statistic probability of wind occurrence observed over several years is very similar to the one established during one single year.

days, can generate bottom currents able to transport sediment. This has been demonstrated by *in situ* measurements on other continental shelves (Drake, 1976; Drake and Cacchione, 1989; Nittrouer and Wright, 1994), as well as studies on the genesis of Holocene sand banks (East Texas, Rodriguez et al., 1999; Snedden and Darlymple, 1999).

Nonetheless, extensive measurements of real current speeds at the bottom and its influence on sediment transport are not yet available in the Gulf of Lions. Recent studies demonstrate the existence of strong links between the occurrence of catastrophic meteorological events (such as winter storms) and the formation of cold, dense water cascading that reinforces the transport of suspended sediments and may trigger the remobilization of recent deposits from the shelf towards the canyons (Palanques et al., 2006-this volume). On the other hand, the wave influence on the outer shelf can be neglected, since it results to be not particularly significant in bottom shear stress generation mechanisms (Ulses, 2005).

In this work, we will focus on an area of the outer shelf and shelf edge, in the vicinity of the Bourcart canyon (Fig. 1).

4. Methods

The data were acquired during several cruises with *R/V "Georges Petit", "L'Europe", "Le Suroît", "Beautemps-Beaupré"* and *"Marion Dufresne"*. During these cruises, we used several high-resolution seismic sources including (a) a 700 Joules SIG sparker, (b) a towed "EDO Western" 2.5 kHz sub-bottom profiler, and (c) a hull-mounted "Eramer" Chirp system. Swath bathymetry systems included a Simrad EM 1000 (on *"L'Europe"*), EM300 (on *"Le Suroît"*) and an EM 1002S on the *"Beautemps Beaupré"*. Cores were sampled with piston corers, vibro-corers, and the *"Calypso"* system onboard *"Marion Dufresne"*. Radiocarbon dates were performed on selected shells (Table 1) using both conventional radiocarbon method and accelerator mass spectrometer (AMS). The shells were collected from various parts in the listed cores. Well-preserved material has been chosen (as bivalves with the two valves).

All ^{14}C dates are given in calibrated ages, using the Cal v5.1 version (Hughen et al., 2004) or the polynomial in Bard et al., 1998, except for dates giving an age >40,000 years.

A correlation between the seismic units observed on very high-resolution (700 Joules sparker) and ultra-high (chirp) seismic data and the post-glacial climatic/sea-level changes was attempted. These data are "ground-truthed" by sedimentological interpretation of shallow

cores (piston cores and vibra-cores), analysis of mollusc assemblages and ^{14}C dates. Seismic lines and core samples that are shown in this work are located in Fig. 1B.

The hydrodynamics was modelled using MARS-3D (André et al., 2005), a three-dimensional model in sigma coordinates, which solves equations under the assumptions of Boussinesq and hydrostaticity. It was designed to simulate the three components of the currents, surface elevation, temperature and salinity in coastal areas. The set of equation solved is well known and is given for example in Blumberg and Mellor (1987).

The model is forced by several parameters: atmospheric conditions (wind, solar fluxes...), river discharges, lateral fluxes and elevation at the open boundaries. The latter allows forcing the model with large-scale circulation such as the Northern Current.

In order to estimate the erosion probability, the most interesting output of the model is the bottom shear stress (τ) that is calculated under the assumption that velocity profile is logarithmic in the turbulent bottom layer (Eq. (1))

$$\tau = \rho[\kappa u(z)/\ln(z/z0)]^2 \qquad (1)$$

where ρ is the water density, κ the von Karman constant (0.4), and $z0$ the roughness length of bed surface taken as 0.0035 m.

The observations of simulated bottom shear stress for all the 2001-year show that easterly winds have the strongest effect on bottom stress, generated in the western part of the shelf after a few hours. Therefore, a simulation with a constant wind of 20 m/s from the east for the entire area of Gulf of Lions, has been run to determine bottom stress during high easterly wind events (wind directions seem to be more significant than wind intensity to force bottom circulation in this area, Fig. 3A). Consequently, in this work, we do not consider the influence of N–NW winds since the bottom shear stress generated by these winds is estimated not strong enough for remobilizing sandy sediments.

5. Results

5.1. Morphology and seismic facies of post-glacial deposits

(a) *Sand ridges* in the studied area, the major morphological feature is represented by the sand ridges, localized between 95 and 110 m water depth (U155). They have limited areal distribution, variable heights (up to 9 m) a mainly WNW–ESE

Table 1
AMS and conventional ^{14}C datings of biogenic carbonate material

Core	Sample depth (cm)	Sample weight (mg)	Lat (N)	Long (E)	Water depth (m)	Core length (m)	Dated material	Dating technique	Conventional ^{14}C age (BP)	Calibrated age (y BP)	Calibration reference
93C3b	70	30	42°55.32	3°40.52'	96	1.96	Undet. bivalve	Conventional	6305±45	67.04–6.831	Hughen et al. (2004)
93C3b	161	93	42°55.32	3°40.52	96	1.96	Undet. bivalve	Conventional	9085±45	9.711–9.897	Hughen et al. (2004)
93C4	155	42	42°52.80	3°43.68	103	2.4	Undet. bivalve	Conventional	2140±40	1.682–1.797	Hughen et al. (2004)
93C9b-1	175	n.a.	42°55.32	3°40.52	96	1.96	Undet. bivalve	AMS	12.290±80	13.661–13.830	Hughen et al. (2004)
BMK01	250	120	42°50.52	3°50.13	103	2.73	Timoclea ovata	AMS	12.560	13.914–14.108	Hughen et al. (2004)
BMKS02	25–27	50	42°52.11	3°51.78	100	2,67	Caryophyllia smithii	AMS	250	6.014–6.578	Hughen et al. (2004)
BMKS02	85	14	42°52.11	3°51.78	100	2,67	Undet. bivalve (articulated shell)	AMS	12.980±60	14.638–14.976	Hughen et al. (2004)
BMKS02	160	35	42°52.11	3°51.78	100	2,67	Undet. bivalve (articulated shell)	AMS	12.590±50	13.980–14.111	Hughen et al. (2004)
BMKS02	260	0.45	42°52.11	3°51.78	100	2,67	Corbula gibba (articulated shell)	AMS	12.690±60	14.035–14.249	Hughen et al. (2004)
BMKS03	50	0.33	42°53.33	3°53.10	98	2,83	Veneridae sp.	AMS	8410±50	8.958–9.090	Hughen et al. (2004)
CLVK20	172–175	n.a.	42°57.55	3°35.56	95	2,35	Ostracods	Conventional	39.710±720	45.034	Bard et al. (1998)
CLVK20	68–74	n.a.	42°57.55	3°35.56	95	2,35	Undet. bivalve	Conventional	10.875±120	12.212–12.656	Hughen et al. (2004)
MD99-2350	14–17	190	42°54.64	3°40.63	98	2,57	Pitar rudis	AMS	9250	9.958–10.061	Hughen et al. (2004)
MD99-2350	43	n.a.	42°54.64	3°40.63	98	2,57	Undet. bivalve	Conventional	10.715±60	11.965–12.211	Hughen et al. (2004)
MD99-2350	240	1.01	42°54.64	3°40.63	98	2,57	Aequipecten opercularis	AMS	40.200±800	–	–
MD99-2350	53–54	443	42°54.64	3°40.63	98	2.57	Mytilus sp.	Conventional	24.170±140	27.947	Bard et al. (1998)
MD99-2350	99–101	13	42°54.64	3°40.63	98	2.57	Nucula sp.	AMS	42.500±900	–	–
MD99-2351	15–17	400	42°57.69	3°35.59	98	3.51	Corbula gibba	AMS	720	309–413	Hughen et al. (2004)
MD99-2351	22–25	450	42°57.69	3°35.59	98	3.51	Acanthocardia echinata	AMS	2190	1721–1849	Hughen et al. (2004)
MD99-2351	89–93	721	42°57.69	3°35.59	98	3.51	Mytilus sp.	Conventional	13.970±40	15947–16320	Hughen et al. (2004)
MD99-2351	325–327	23	42°57.69	3°35.59	98	3.51	Mixed benthic forams	AMS	45.100±1200	–	–

orientation, as recognized on the bathymetric maps (Fig. 4A). They have an irregular topography and mainly show a linear, elongated shape. On the chirp profiles their surface is smooth, they form bodies of

maximum length of 5 km and they rest on a major erosional surface (*ravinement* surface) that is possibly exposed beyond the ridge field (Fig. 5A). The ridges have an asymmetric transverse profile
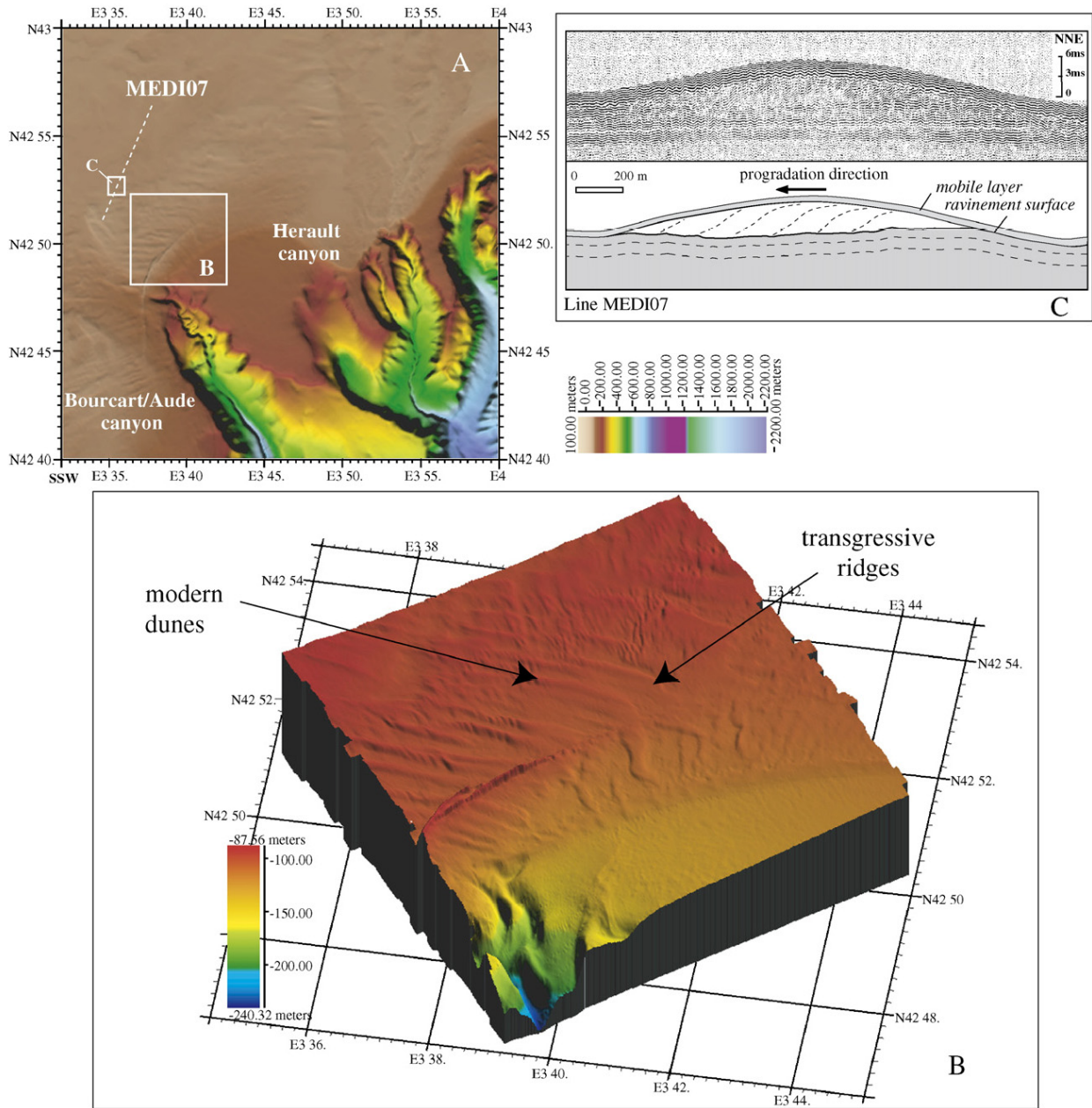

Fig. 4. Detailed morpho-bathymetric map of the study area: (A) morphological alignments are evident on the general map corresponding to the transgressive deposits (dunes); (B) closer view of the map of Fig. 4A. Note the superimposition of dunes on fossil ridges, possibly linked to modern hydrodynamics. Data and processing by Service Hydrographique de la Marine (SHOM); (C) internal structure of a sand ridge (2.5 kHz sub-bottom profile). Apparent WSW direction of migration is indicated by the dipping of clinoforms. The upper layers are not distinct at the resolution of the system, and create a thick packet of parallel reflections.
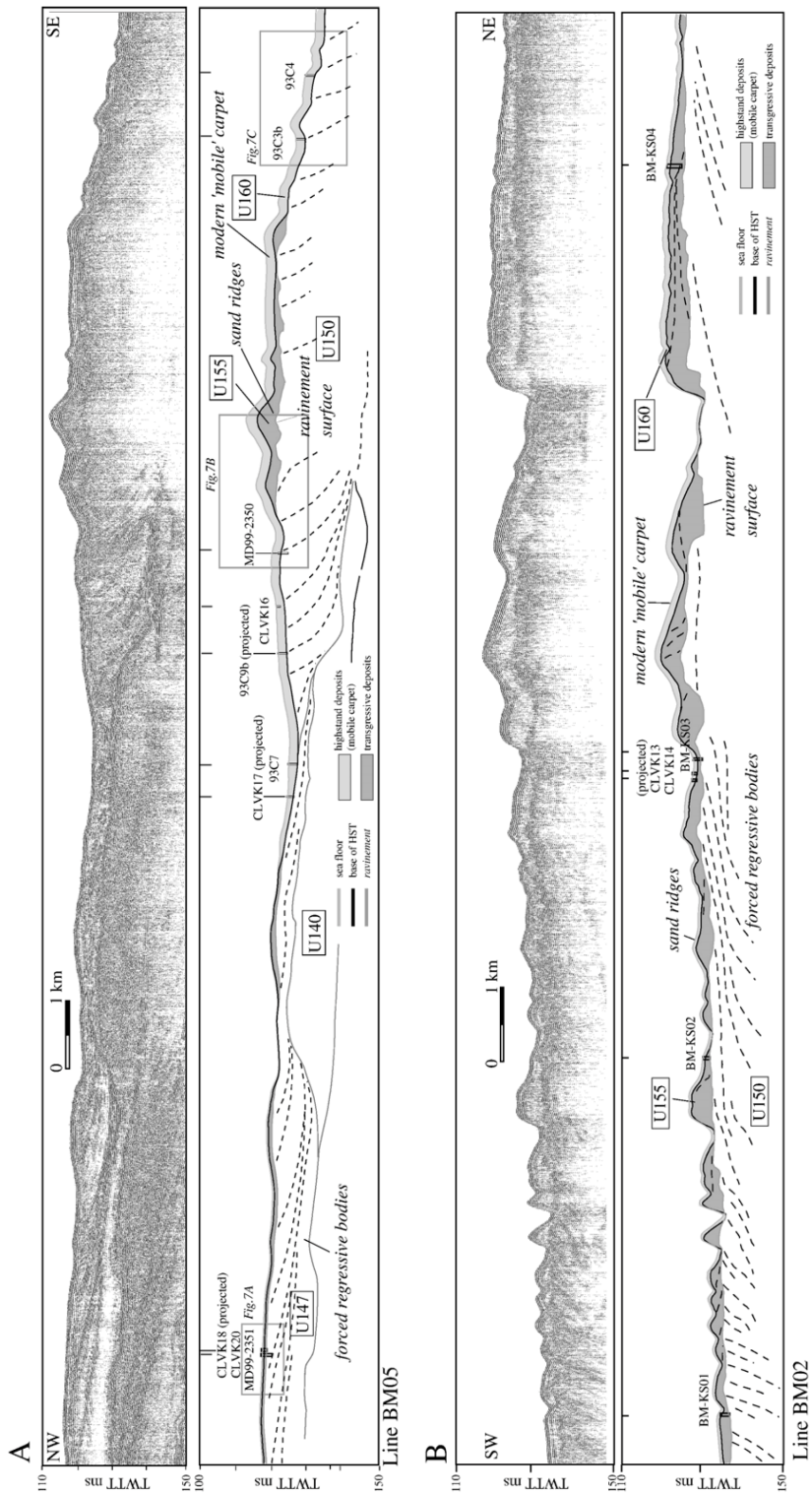
Fig. 5. Uninterpreted and interpreted seismic profile sections located on the outer shelf (A) and at the shelf break (B), which clearly show the stratigraphic relations between the forced regressive bodies (U140, 147, 150), transgressive deposits (U155) and deglacial unit (U160). The two profiles are approximately perpendicular (see Fig. 1B). The boxes point to the closer view showed in Fig. 7A–B–C.

183

(with the steepest slope facing the SW). At times, they show a nearly symmetric profile, but it concerns only the smaller bodies. They show distinct clinoforms, dipping in the SW direction (Figs. 2 and 4C) and some chaotic internal reflections (Fig. 5B), probably in relation with coarse-grained material diffracting seismic waves. However, some major erosional surfaces (discontinuities) can be recognized within the ridge, that may be related to storm events affecting the ridge growth, although they cannot be correlated from one ridge to another. These sand ridges correspond to seismic unit U155.

(b) *The dunes* were only detected when we used high-resolution swath bathymetric systems, such as the EM 1000 and EM1002S (Fig. 4B). They have an average spacing of 130 m and maximum height of 2 m. Their great axis has a NNW–SSE orientation in the NE part of the surveyed area, turning progressively to NW–SE in the SW corner (Fig. 4B). Their internal structure was not detectable considering their small size. They are classified as transverse dunes in the sense of Ashley (1990) and they clearly rework the shape of the sand ridges.

On top of the sand ridges, chirp and sub-bottom seismic profiles display a thick pattern of parallel reflections, that was first considered as the result of some ringing effect representing the pulse length of the seismic sources, instead of a real sedimentary layer (Figs. 5 and 7). However, extensive coring (see next section) and bathymetric data (Fig. 4B) demonstrated that a distinct layer actually exists at the sea-floor interface. All together, the dunes and the uppermost layers will be included into a new seismic unit named U160.

5.2. Sedimentary facies

Units U155 and U160 have been extensively sampled by vibrocoring and piston coring. The various sedimentary facies can be classified into three main types: (1) muddy sand facies, (2) sand facies and (3) gravel facies (Fig. 6).

The muddy sands (from medium to coarse grained) generally consists of a maximum of 2 m thick veneer of sediments (U160) covering U155. They are homogeneous and possibly bioturbated. They do not show bedding and contain abundant biogenic sand often concentrated into irregular layers.

The *sand facies* does not show any structure and consists of sand (rarely muddy sand) with or without shells or shell beds. The sand facies comprises the sand ridges (U155), the sediments are medium to coarse-grained and moderately to well sorted. The sand is dominantly siliciclastic with a minor amount of biogenic components (mollusc shell fragments). The shells that are found there are indicative of nearshore, shallow-water environment of a 10–100 m water range. Presence of reworked material is highly possible in this facies.

The *gravel facies* marks a sharp lithological passage with the underlying deposits, it consists of mixed clasts and biogenic fragments, often in a muddy matrix. The macrofaunal assemblage of this facies is prevalently a mixture of mollusc shells sourced from littoral-estuarine (*Mytilus* sp.) to infralittoral nearshore environments associated with bioturbation-driven younger shells from deeper environments. These shell assemblages contain typical cold guests (*Arctica islandica*, *Mya truncata*, *Buccinum* sp), likely indicating the latest glacial age (Fig. 6). In fact, the gravel facies is usually found at the transition between units U150 and U155, therefore it corresponds to the erosional surface that bases the post-glacial deposits (*ravinement*). The lithological passage between unit U155 and the underlying forced regressive bodies is always abrupt and easily detectable both on seismic profiles and on core sections (Figs. 5A–B, 6 and 7).

5.3. Chrono-stratigraphic constraints

Based on the numerous ^{14}C dates, it is possible to distinguish 2 groups of dates belonging to deposits that are separated by the *ravinement* surface situated between U155 and U150, despite the fact that some shells are likely reworked from older deposits. Under this surface, the forced regressive deposits of U150 are all dated more than 20 ka cal BP. Above it, the dates within U155 range from 15 ka to 12 ka cal BP. The uppermost U160 layer displays a very broad range of ages, from early Holocene (about 10 kyr cal BP) to recent (250 yr cal BP). The presence of a "modern" shell (1682 yr cal BP, core 93C4 in Fig. 6) at 145 cm below the sea-floor demonstrates the high amount of mobility of unit U160. In order to understand the processes at the origin of the mobility of U160, we utilized the output of the Mars 3D circulation model of the Gulf of Lions (Fig. 8).

5.4. Wind-induced bottom circulation

Based on the statistical analysis of Fig. 3, the easterly winds are likely the source of high shear stress in our
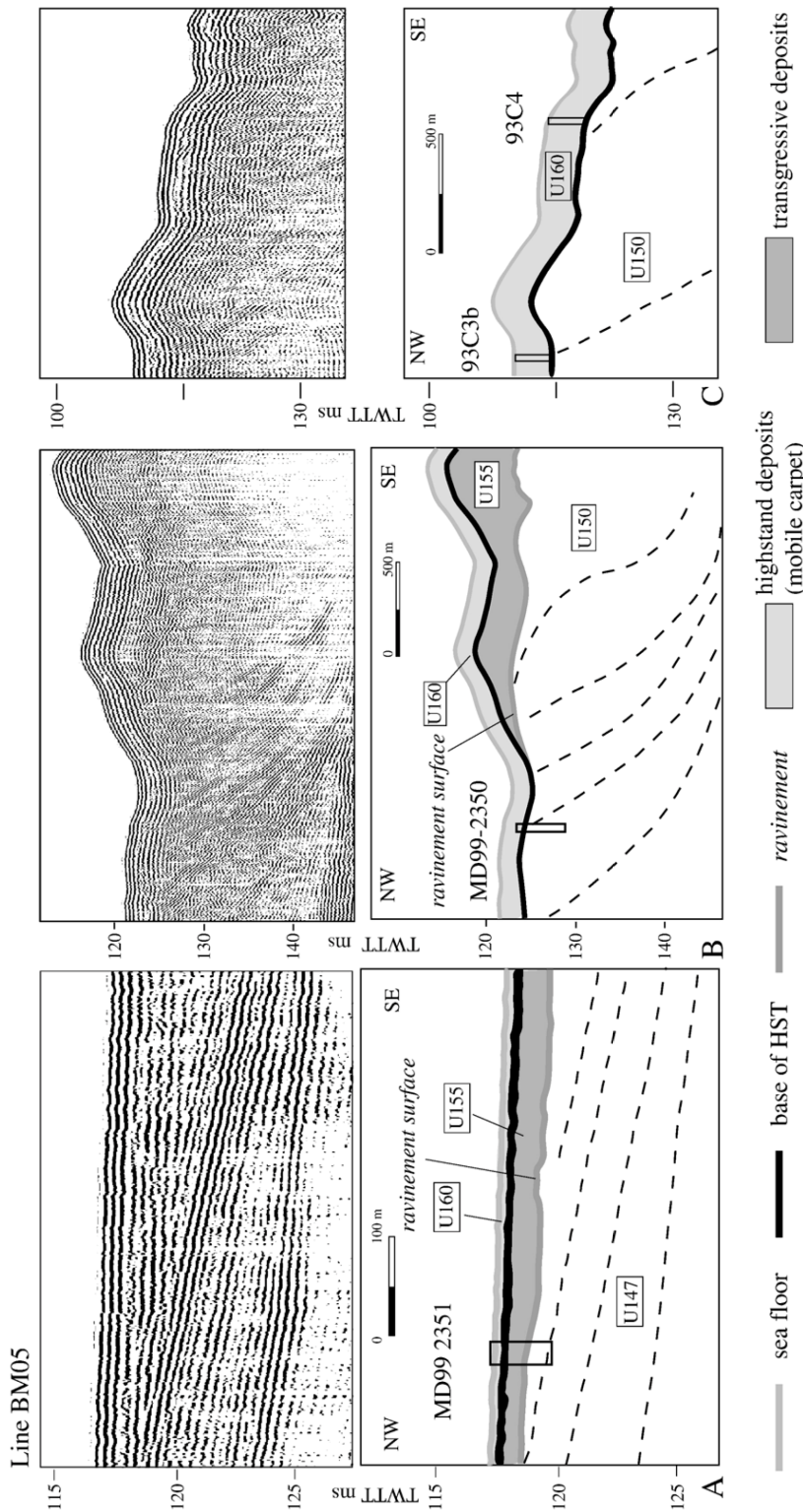
Fig. 6. Time correlation along the BM05 (A) and BM02 (B), see Fig. 1 for location. The time equivalency is based on ^{14}C dates, seismic features and facies analysis.

Fig. 7. (A) Unintepreted and interpreted portion of the high-resolution seismic profile BM05 showing the strongly lenticular geometry of unit 155 (transgressive sand ridges), draped by the modern mobile layer, as discussed in the text. Note the change in amplitude in the upper reflections, that supports the interpretation of a real upper mobile layer rather than a ringing effect of the seismic signal. The core MD 2350 is located at the lateral pinch out of the unit 155 (see Fig. 6 for log and lateral correlation) and, possibly, the uppermost part of the core was lost during coring operations; (B) landward thinning of units 155 and 160. However, there are no clear indications of the presence of the unit 160 on this area: tracing the U160 in this part of the shelf is mostly speculative and, possibly, the U155 is exposed at the sea bottom. In the figure C, the U160 is more than 2 m thick, as also confirmed by the ^{14}C dates (see Fig. 6).

study area. Therefore, we used a realistic constant wind velocity of 20 m/s, blowing during a period of 7 days, in order to evaluate the effect on the sea floor. It turns out that, after one day, intense bottom currents can be pro-

duced in the coastal zone, as expected, but also in the westernmost area of the shelf and at the shelf break (Fig. 8A). The maximum effect, occurring at the beginning of the events and showing tensions up to 0.24 N
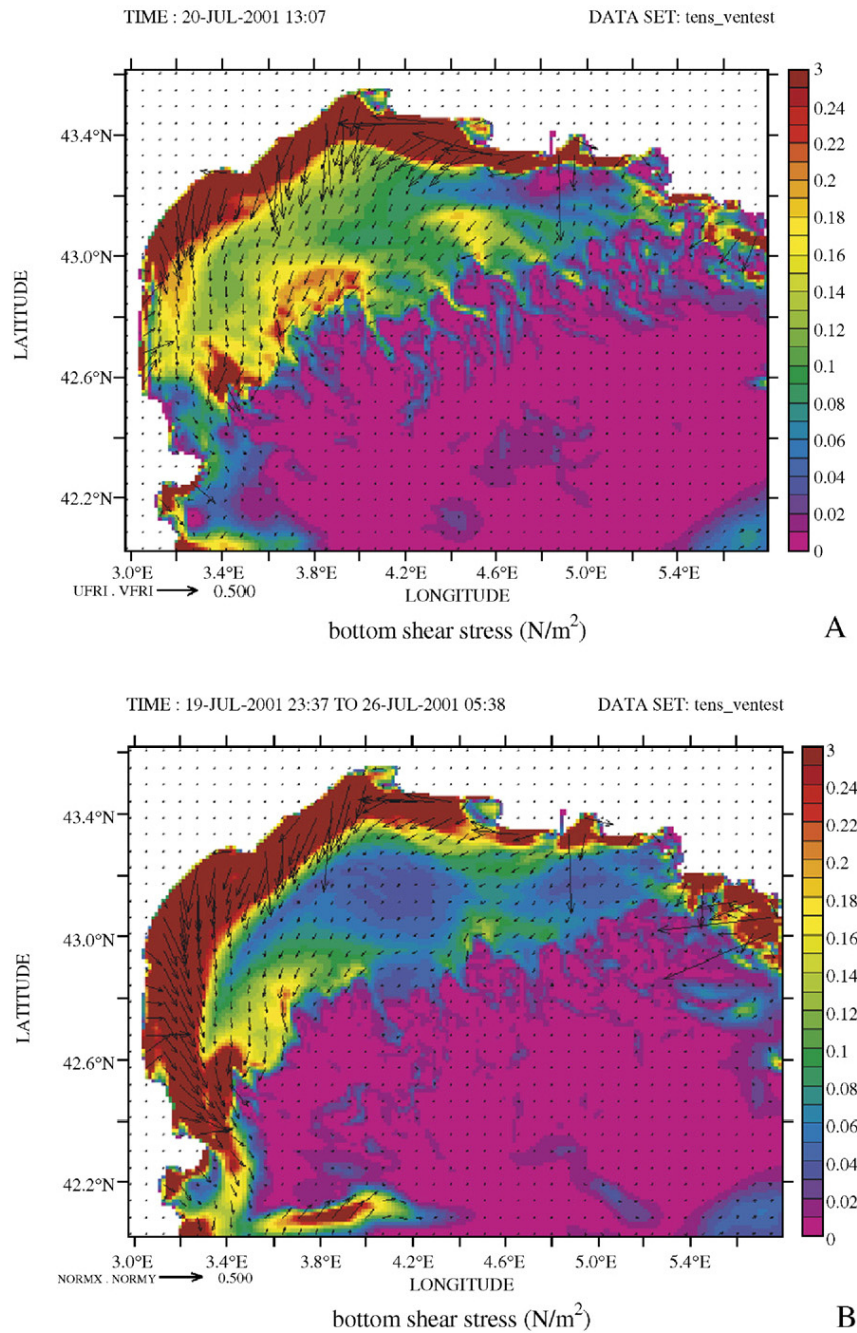

Fig. 8. The intense winds from east can induce a significant bottom shear stress (according to the model MARS 3D) in the western part of the outer shelf that is stronger at the beginning of the wind event due to the contribution of inertial-gravity oscillation signal (A). On a longer time frame (1 week, in this model), the stress on the bottom gradually decreases in intensity (B).
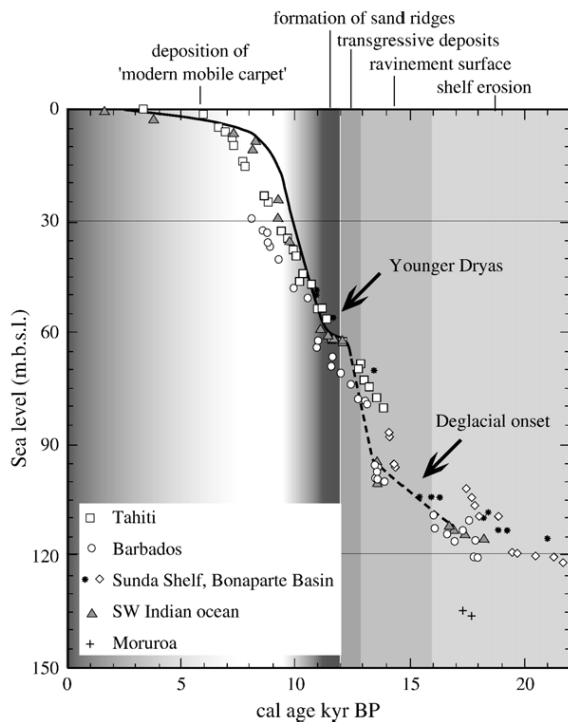
Fig. 9. Correlation of depositional events in the outer shelf of the Gulf of Lions during the last 20 ka to the global sea-level curve (from Camoin et al., 2004, modified).

m ^{2} at the sea-bottom, can be expected at about 100 m depth. The observation of the bottom currents evolution during several days demonstrates that the tensions progressively weakens during a 7-day period, and that the area where the bottom shear stress is the most intense progressively moves southwestwardly (Fig. 8B). The reason of this southwestward shifting is not clear: it could be related to a local acceleration of the flow due to a convergence of the shelf water transport towards the SW ends of the gulf. In summary, one single day of constant wind blowing at 20 m/s is sufficient for erosion and transport in the SW direction of fine sand in our study area. This direction is consistent with that predicted from the asymmetry of transverse dunes. More precisely, it might be noted that the progressive change in direction of transverse dunes observed on the swath bathymetric map of Fig. 4 coincide with the progressive shift of predicted directions of sand transport from WSW to SW in Fig. 8. Compared to this very conservative 20 m/s scenario, there is no doubt that much more severe meteorological conditions that likely occurred during the last hundred years, allowed episodic transport of all classes of sand and rejuvenation of transverse dunes, which therefore can be considered as "active".

6. Discussion

6.1. Bounding surfaces associated with transgressive deposits

Our investigation demonstrates that, on the outer shelf, the transgressive deposits only consist of a thin veneer (0 to 9 m thick) of sandy sediment resting on a marine *ravinement* surface. These transgressive deposits rework the sandy facies that formed between Marine Isotope Stage (MIS) 3 and the Last Glacial Maximum. The shoreface sands form a thick (up to 30 m) regressive wedge that was misinterpreted by some authors as a transgressive parasequence (Gensous and Tesson, 1997). In fact, the top of regressive deposits were reworked into transgressive dunes and ridges during the deglacial sea-level rise (Fig. 9), making difficult the seismic and lithological distinction of the two units. However, the base of the transgressive deposits is clearly detectable on ultra-high-resolution seismic profiles (Fig. 5). In addition, ^{14}C dates, despite some age inversions due to reworking, allow to distinguish transgressive (<16 ka cal BP) and regressive deposits (45 to 20 ka cal BP). In between, time-transgressive erosional (or *ravinement*) surface made of coarse sand with abundant shells and shell fragments are observed. Similar erosional surfaces are reported in many continental shelves such as the Adriatic sea (Trincardi et al., 1994) or the Gulf of Mexico (Anderson et al., 2004). However, because of a relatively high-energy situation compared to the above-mentioned areas, the surface is more distinct in the Gulf of Lions.

6.2. Sand ridges formation and implications for sea-level reconstruction

Active, "moribund" and relict sand ridges are described over most continental shelves around the world. If we have clear evidences for proposing that transverse dunes are still episodically actives, it is difficult to determine what is the status of sand ridges. However, according to some authors (see review by Berné, 2002) their spacing is an indirect way to estimate paleo-water depths at which they were created. Different equations have been proposed that link bedform spacing and water depth:

(1) $H = 0.167h$ (Yalin, 1964)
(2) $H = 0.086h^{1.19}$ (Allen, 1984)

Where H is the dune height and h is the water depth. With both equations, we obtain a maximum water depth

of about 50 m for ridge formation. Considering that present water depth of these features is between 95 and 110 m, and using a sea-level curve as that of Fig. 9, it gives an age of 11 to 12 ka Cal BP, at least, for ridge formation that may correspond to the Younger Dryas event. During this period, sea-level rise deceleration or a short-lived stillstand possibly favoured the formation of these sedimentary bodies. This age is consistent with most of the ^{14}C dates found within unit U155.

Additional support to the estimated shallow water nature of the sand ridges may be derived from the macrofaunal assemblage indicating a 3–50 m depth range. In particular, within this unit (155) the basal erosional surface (*ravinement*) contains shells unquestionably sourced from littoral-estuarine (i.e *Mytilus* cf *galloprovincialis*) to infralittoral-nearshore environments, while those hosted in the ridges muddy sand suggest a deeper sub-littoral environment in the order of 30–50 m approximately.

On the other hand, macrofaunal assemblages of unit 160 are enriched in benthic bivalves (*Bathyarca grenophia, Nuculana commutata, Pseudoamussium clavatum, Corbula gibba, Timoclea ovata...*), gastropods (*Aporrhais* cf. *pespelecani, Turritella communis, Alvania testae* etc.), scaphopods (*Dentalium* sp.) and occasional holoplanktic thecosomatous pteropods (*Creseis acicula, Diacria trispinosa*), characterizing macrofaunal communities inhabiting offshore middle to outer shelf setting, from 50 m down, thus supporting the interpretation of a "modern" bed.

The best estimate for the age of the ravinement surface in our study area comes from core MD992351, where a shell of *Mytilus* sp. yield an age of 15,947 a cal B.P. The corresponding water depth is 98+1=99 m (Figs. 6 and 9).

6.3. Sediment transport during late Holocene and modern oceanographic conditions

Sediment deposition on the shelf is related to the sediment input from land, topography of the sea floor and wave and current energy. For those sediments, subsequent transport can result from processes linked to occasional events.

In the Gulf of Lions, numerical modelling shows that oceanographic and meteorological processes can combine to generate ample bed shear stresses to move fine sands. Wind-induced tensions during extreme meteorological conditions are capable of reaching the sea floor at the outer shelf depth (100 m approximately), producing currents that have an erosive potential and possibly producing bottom stresses triggering sediment transport on and offshore, in particular down the submarine canyons.

A distinctive feature associated with the Gulf of Lions setting resulting from the modelling is that of shear bed stresses are mainly generated in the area where dunes are found (western outer shelf), whereas the flat mid shelf is weakly affected by the wind-induced bottom tensions.

This fact suggests that during extreme meteorological events linked to easterly winds (as showed in the model, Fig. 8), the flow jetting is bypassing the mid shelf where the bottom shear stress is <0.1 N m ^{1}, whereas, according to the model, bathymetric influence induces a rapid increase of bottom shear stress up to 0.24 N m ^{1} toward the SW outer shelf area. The proposed mechanism would imply a large remobilization of at least the uppermost sediment layer that blankets the outer shelf and this is actually the area where the draping unit 160 is detected on the high-resolution seismic profiles (Figs. 5 and 7).

7. Conclusions

The correlation between the seismic units defined on the outer shelf, the numerous sediment cores, and the sea-level curve allows us to establish a scenario for the evolution of shelf edge sand bodies (Fig. 9):

1. During the LGM sea-level lowstand, the platform underwent intensive erosion and, at the onset of deglaciation, the landward migration of shoreline activated the deposition of a transgressive unit, based by a *ravinement* surface that can be followed throughout the whole outer shelf. Such a discontinuity is unambiguously recognized on the basis of characteristic seismic and lithological features and ^{14}C dates. This surface is dated at 15,900 y cal BP at 99 m water depth;

2. The transgressive deposits take the form of sand ridges that cover a portion of the outer shelf (U155). They usually show asymmetric transverse profiles (with a lee side toward SW). ^{14}C dates, core lithology and inferences from the depth of formation of modern sand ridges, suggest that they formed during a slow down of sea-level rise, around the Younger Dryas;

3. These transgresssive deposits are toped by a thin (<2 m) layer of sands or muddy sands (here called U160) that blankets the outer shelf, sometimes shaped into transverse dunes. Numerical modelling demonstrates that easterly winds can be at the origin of sea-floor shear stress sufficient for sand transport,

in our study area as well as in the Western Gulf of Lions (where larger dunes are also observed). Therefore, these bedforms can be considered as "active" features.

4. The occurrence of strong energy events able to remobilize and transport sand from former shoreface deposits situated at the shelf edge is a mechanism for supplying sand to canyon heads, as observed by Gaudin et al. (2006-this volume). This mechanism, and others such as dense water cascading (Palanques et al., 2006-this volume; Ulses, 2005), can be the source of sand to the deep-sea during modern (highstand) conditions.

Acknowledgments

References

Allen, J.R.L., 1984. Principles of Physical Sedimentology. Allen and Unwin, London. 272 pp.

Aloïsi, J.-C., 1986. Sur un modèle de sédimentation deltaïque: Contribution à la connaissance des marges passives. PhD thesis, University of Perpignan, 162 pp.

Anderson, J.B., Rodriguez, A., Abdulah, K.C., Fillon, R.H., Banfield, L.A., McKeown, H.A., Wellner, J.S., 2004. Late Quaternary stratigraphic evolution of the northern Gulf of Mexico margin: a synthesis. In: Anderson, J.B., Fillon, R.H. (Eds.), Late Quaternary Stratigraphic Evolution of the Northern Gulf of Mexico Margin. SEPM (Society for Sedimentary Geology), Tulsa, pp. 1–23.

André, G., Garreau, P., Garnier, V., Fraunie, P., 2005. Modelled variability of the sea surface circulation in the North-western Mediterranean Sea and in the Gulf of Lions. Ocean Dyn. 55, 294–308.

Ashley, G.M., 1990. Classification of large-scale subaqueous bedforms: a new look at an old problem. J. Sediment. Petrol. 60 (1), 160–172.

Bard, E., Arnold, M., Hamelin, B., Tisnerat-Laborde, N., Cabioch, G., 1998. Radiocarbon calibration by means of mass spectrometric $^{230}Th/^{234}U$ and ^{14}C ages of corals. An updated data base including samples from Barbados, Mururoa and Tahiti. Radiocarbon 40 (3), 1085–1092.

Berné, S., 2002. Offshore sands. In: Middleton, G.V. (Ed.), Encyclopedia of Sediments and Sedimentary Rocks. Kluwer Academic Publishers, pp. 492–499.

Berné, S., Lericolais, G., Marsset, T., Bourillet, J.F., de Batist, M., 1998. Erosional shelf sand ridges and lowstand shorefaces. Examples from tide and wave dominated environments of France. J. Sediment. Res. 68 (4), 540–555.

Berné, S., Satra, C., Aloïsi, J.C., Baztan, J., Dennielou, B., Droz, L., Dos Reis, A.T., Lofi, J., Méar, Y., Rabineau, M., 2002. Carte morpho-bathymétrique du Golfe du Lion, notice explicative. Ifremer, Brest.

Berné, S., Rabineau, M., Flores, J.A., Sierro, F.J., 2004. The impact of Quaternary global changes on strata formation. Oceanography 17 (4), 92–103.

Blumberg, A.F., Mellor, G.L., 1987. A description of a three dimensional coastal circulation model. In: Heap, N.S. (Ed.), Three Dimensional Coastal Ocean Models. Coastal and Estuarine Sciences, vol. 4. American Geophysical Union, Washington, D.C., pp. 1–16.

Bourcart, J., 1945. Etude des sediments pliocènes et quaternaries du Roussillon: service Carte Géologique de France. Bullettin 45, 395–476.

Camoin, G.F., Montaggioni, L.F., Braithwhite, C.J.R., 2004. Late to post glacial sea levels in the Western Indian Ocean. Mar. Geol. 206, 119–146.

Cita, M.B., Ryan, W.B.F. (Eds.), 1978. Messinian erosional surfaces in the Mediterranean. Mar. Geol., vol. 27, pp. 193–365.

Drake, D.E., 1976. Suspended sediment transport and mud deposition on continental shelves. Marine Sediment Transport and Environmental Management. John Wiley and Sons, New York, pp. 127–158.

Drake, D.E., Cacchione, D.A., 1989. Field observations of bed shear stress and sediment resuspension on continental shelves, Alaska and California. Cont. Shelf Res. 6, 415–429.

Dufau, C., Marsaleix, P., Petrenko, A., Dekeyser, Y., 2004. 3D modeling of the Gulf of Lion's hydrodynamics during January 1999 (MOOGLI 3 experiment) and Late winter 1999: WIW formation and cascading over the shelf break. J. Geophys. Res. 109 (C11), C11002. doi:10.1029/2003JC002019.

Emery, K.O., 1968. Relict sediments on continental shelves of the world. Bull. Am. Assoc. Pet. Geol. 52, 445–464.

Estournel, C., Durrieu de Madron, X., Marsaleix, P., Auclair, A., Julliand-Dufau, C., Vehil, R., 2003. Observation and modelisation of the winter coastal oceanic circulation in the Gulf of Lions under wind conditions influenced by the continental orography (FETCH experiment). J. Geophys. Res. 108 (C3), 8059. doi:10.1029/2001JC000825.

Gaudin, M., Berné, S., Jouanneau, J.-M., Palanques, A., Puig, P., Mulder, T., Cirac, P., Rabineau, M., Imbert, P. 2006-this volume. Massive sand

beds deposited by dense water cascading in the Bourcart canyon head, Gulf of Lions (northwestern Mediterranean Sea). Mar. Geol. 234, 111–128.

Gensous, B., Tesson, M., 1997. Postglacial deposits of the Rhone shelf: stratigraphic organisation and growth patterns. C.r. Acad. Sci., Ser. 2, Sci. -Earth Planet. Sci. 325 (9), 695–701.

Gensous, B., Tesson, M., 2003. L'analyse des dépôts postglaciaires et son application à l'étude des séquences de dépôt du Quaternaire terminal sur la plate-forme au large du Rhône (golfe du Lion). Bull. Soc. Geol. Fr. 174 (3), 401–419.

Gorini, C., Mauffret, P., Guennoc, P., Le Marrec, A., 1994. The structure of the Gulf of Lions (Northwestern Mediterranean Sea): a review. In: Mascle, A. (Ed.), Hydrocarbon and Petroleum Geology of France. Springer–Verlag, New York, pp. 223–243.

Got, H., Aloïsi, J.-C., 1990. The Holocene sedimentation on the Gulf of Lions margin: a quantitative approach. Cont. Shelf Res. 10 (9–11), 841–855.

Hughen, K.A., Baillie, M.G.L., Bard, E., Bayliss, A., Beck, J.W., Bertrand, C.J.H., Blackwell, P.G., Buck, C.E., Burr, G.S., Cutler, K.B., Damon, P.E., Edwards, R.L., Fairbanks, R.G., Friedrich, M., Guilderson, T.P., Kromer, B., McCormac, F.G., Manning, S.W., Bronk Ramsey, C., Reimer, P.J., Reimer, R.W., Remmele, S., Southon, J.R., Stuiver, M., Talamo, S., Taylor, F.W., van der Plicht, J., Weyhenmeyer, C.E., 2004. Marine04 Marine radiocarbon age calibration, 26–0 ka BP. Radiocarbon 46, 1059–1086.

Hsü, K.J., Ryan, W.B.F., Cita, M.B., 1973. Late Miocene desiccation of the Mediterranean. Nature 242, 240–244.

Lamy, A., Millot, C., Molines, J.M., 1981. Bottom pressure and sea-level measurements in the Gulf of Lions. J. Phys. Oceanogr. 11, 394–410.

Lobo, F.J., Tesson, M., Gensous, B., 2004. Stratal architectures of late Quaternary regressive–transgressive cycles in the Roussillon Shelf (SW Gulf of Lions, France). Mar. Pet. Geol. 21 (9), 1181–1203.

Lofi, J., 2002. La crise de salinité messinienne: conséquences directes et différées sur l'évolution sédimentaire de la marge du Golfe du Lion, Lille 1, Lille. 260 pp.

Lofi, J., Rabineau, M., Gorini, C., Berne, S., Clauzon, G., De Clarens, P., Tadeu Dos Reis, A., Mountain, G.S., Ryan, W.B.F., Steckler, M.S., Fouchet, C., 2003. Plio-Quaternary prograding clinoform wedges of the western Gulf of Lion continental margin (NW Mediterranean) after the Messinian Salinity Crisis. Mar. Geol. 198 (3–4), 289–317.

Millot, C., 1990. The Gulf of Lions' hydrodynamics. Cont. Shelf Res. 10 (9–11), 885–894.

Millot, C., Wald, L., 1980. The effect of Mistral wind on the Ligurian Current near Provence. Oceanol. Acta 3, 399–402.

Monaco, A., 1971. Contribution à l'étude gééologique et sédimento-logique du plateau continental du Roussillon. PhD thesis, Unveristy of Perpignan, pp. 295.

Monaco, A., Courp, T., Heussner, S., Carbonne, J., Fowler, S.W., Deniaux, B., 1990. Seasonality and composition of particulate fluxes during ECOMARGE-I, western Gulf of Lions. Cont. Shelf. Res. 9–11, 959–987.

Nittrouer, C.A., Wright, L.D., 1994. Transport of particles across the continental shelves. Rev. Geophys. 32, 85–113.

Perez-Belmonte, L., 2003. Enregistrement de la dernére transgression dans le Gulf du Lion. Memoire DEA. University of Lille, p. 52.

Palanques, A., Puig, P., Durrieu de Madron, X., Guillén, J., Calafat, A., Fabrés, A., Bourrin, F., Heussner, S., Canals, M., 2004. Suspended sediment fluxes in the Gulf of Lion submarine canyons during the November–May 2003 high resolution experiment. Eurodelta–Eurostrataform meeting, Venice 2004. Abstr. Book, p. 29.

Palanques, A., Durrieu de Madron, X., Puig, P., Fabres, J., Guillén, J., Calafat, A., Canals, M., Bonnin, J., 2006-this volume. Suspended sediment fluxes and transport processes in the Gulf of Lions submarine canyons. The role of storms and dense water cascading. Mar. Geol. 234, 43–61. doi:10.1016/j.margeo.2006.09.002.

Petrenko, A.A., 2003. Circulation features in the Gulf of Lions, NW Mediterranean Sea; importance of inertial currents. Oceanol. Acta 26, 323–328.

Posamamtier, H.W., Allen, G.P., James, D.P., Tesson, 1992. Forced regression in a sequence stratigraphic framework: concepts, examples, and exploration significance. AAPG Bull. 76, 1687–1709.

Rabineau, M., 2001. Un modéle géométrique des sequences des dépôts quaternaires sur la marge du Gulf du Lion: enregistrement des cycles climatiques de 100.000 ans. PhD thesis, University of Rennes, pp. 394.

Rabineau, M., Berné, S., Ledrezen, E., Lericolais, G., Marsset, T., Rotunno, M., 1998. 3D architecture of lowstand and transgressive Quaternary sand bodies on the outer shelf of the Gulf of Lion, France. Mar. Pet. Geol. 15, 439–452.

Rabineau, M., Berné, S., Aslanian, D., Olivet, J-L., Joseph, P., Guillocheau, F., Bourillet, J.-F., Ledrezen, E., Granjeon, D., 2005. Sedimentary sequences in the Gulf of Lion: a record of 100,000 years climatic cycles. Mar. Pet. Geol. 22 (6–7), 775–804.

Ryan, W.B.F., 1976. Quantitative evaluation of the depth of the Western Mediterranean before, during, and after the Late Miocene salinity crisis. Sedimentology 23, 791–813.

Rodriguez, A.B., Anderson, J.B., Siringan, F.P., Taviani, M., 1999. Sedimentary facies and genesis of Holocene sand banks on the East Texas inner continental shelf. In: Bergman, K.M., Snedden, J.V. (Eds.), Isolated Shallow Marine Sand Bodies: Sequence Strati-graphic Analysis and Sedimentologic Interpretation. Spec. Publ., vol. 64. SEPM, pp. 165–178.

Snedden, J.W., Darlymple, R.W., 1999. Modern shelf sand ridges: from hystorical perspective to a unified hydrodynamic and evolutionary model. In: Bergman, K.M., Snedden, J.V. (Eds.), Isolated Shallow Marine Sand Bodies: Sequence Stratigraphic Analysis and Sedimentologic Interpretation. Spec. Publ., vol. 64. SEPM, pp. 13–28.

Soulsby, R.L., 1997. Dynamics of marine sands. A Manual for Practical Applications. Thomas Telford Publications. 249 pp.

Swift, D.J.P., Stanley, D.J., Curray, J.R., 1971. Relict sediments on continental shelves; a reconsideration. J. Geol. 79 (3), 322–346.

Tesson, M., Gensous, B., Allen, G., Ravenne, C., 1990. Late Quaternary lowstand wedges on the Rhône continental shelf, France. Mar. Geol. 91, 325–332.

Tesson, M., Posamentier, H.W., Gensous, B., 2000. Stratigraphic organisation of Late Pleistocene deposits of the western part of the Rhone shelf (Languedoc shelf) from high resolution seismic and core data. AAPG Bull. 84 (1), 119–150.

Trincardi, F., Correggiari, A., Roveri, M., 1994. Late Quaternary transgressive erosion and deposition in a modern epicontinental shelf: the Adriatic semi-enclosed basin. Geo Mar. Lett. 14, 41–51.

Ulses, C., 2005. Dynamique océanique et transport de la matière dans le Golfe du Lion: crue, tempêtes et période hivernale. PhD Thesis, University Paul Sabatier, 247 pp.

Yalin, M.S., 1964. Geometrical properties of sand waves. Proc. Am. Soc. Civ. Eng., J. Hydraul. Div. 90, 105–119.

Late Glacial to Preboreal sea-level rise recorded by the Rhône deltaic system

(NW Mediterranean)

S. Berné[a*], G. Jouet[a,b], M.A. Bassetti[a], B. Dennielou[a], M. Taviani[c]

[a] *Ifremer, Géosciences Marines, BP 70, 29280 Plouzané, France*

[b] *UMR-CNRS 6538, Domaines Océaniques, IUEM, Plouzané, France*

[c] *ISMAR-CNR, Via Gobetti 101, 40129,Bologna, Italy*

*Corresponding author. tel: +33(0)298224249, fax: +33(0)298224570, email: sberne@ifremer.fr

Abstract

A unique late Glacial–Preboreal record of changes in sea-level and sediment fluxes originating from the Alps is recorded in the Rhône subaqueous delta in the Western Mediterranean Sea. The compilation of detailed bathymetric charts, together with high-resolution seismic profiles and long cores, reveals the detailed architecture of several sediment lobes, related to periods of decreased sea-level rise and/or increased sediment flux. They are situated along the retreat path of the Rhône distributaries, from the shelf edge and canyon heads up to the modern coastline. They form transgressive backstepping parasequences across the shelf, the late Holocene (highstand) deltas being confined to the inner shelf. The most prominent feature is an elongated paleo-shoreface/deltaic system, with an uppermost sandy fraction remolded into subaqueous dunes. A long piston core into the bottomsets of this prograding unit allows precise dating of this ancient deltaic system. In seismic data, it displays aggradation, starting at ~ 15 cal kyr BP, followed by progradation

initiated during the first phase of the Younger Dryas, a period of reduced sea-level rise or stillstand. The delta kept pace with resumed sea-level rise during the Preboreal (which is estimated at about 1 cm/yr), as a result of increased sediment supply from the Alps (melting of glaciers and more humid climate "flushing" the sediment down to the sea). Abandonment of the delta occurred around 10,500 cal yr BP, that is to say about 1,000 yr after the end of the Younger Dryas, probably because decreased sediment flux.

1. Introduction and background

The direct record of sea-level rise for the last deglacial period has been mainly determined from the position of reef-crest *Acropora* corals living at less than 5 m of water depth (Fairbanks, 1989; Bard et al., 1996). Another way to explore this record is to study the retreat path of fluvial systems. Estuaries and deltas are depocenters that may leave on the shelf large quantities of sediments from their landward migration. The amount of preserved deposits is thought to be mainly a function of the energy of coastal and marine processes, of the amount of sediment supplied, and of the rate of relative sea-level rise. For instance, some authors have estimated the last deglacial sea-level rise by dating continental fragments of coastal sedimentary environments deposited along the retreat path of large rivers on the Sunda Shelf (Hannebuth et al., 2000). In areas where sediment supply is high, prograding transgressive deposits (parasequences in the sense of Van Wagoner et al. (1990)) formed during periods of deceleration of sea-level rise. First described in the stratigraphic record, they have also been identified in Quaternary sedimentary environments (Anderson and Thomas, 1991). However, autogenic processes (such as the change of sediment flux due to increased rainfall, or the

avulsion of deltaic systems) may mimic parasequences induced by sea-level forcing, as discussed by Harris (1999).

In the Gulf of Lions (Fig. 1), Aloïsi et al. (1975) were the first who recognized the architecture of sediment bodies linked to the Rhône retreat during the last sea-level rise. Using seismic and core data, they demonstrated that an elongated sediment body, roughly parallel to the bathymetric contour lines, was situated at a water depth of about 50 m. They suggested that this sediment body was Younger Dryas in age, and formed during a sea-level stillstand followed by a slight fall in sea-level. Further investigations more precisely defined the morphology of the subaqueous delta (Tesson et al., 1998) and the shape of some of its constituting sediment bodies (Gensous et al., 1993; Marsset and Bellec, 2002). The compilation of a large set of seismic data allowed Labaune et al. (2005) to propose a synthesis of the architecture of various seismic units composing the transgressive subaqueous Rhône delta, but details of the morphology and chronostratigraphic framework were not available until now.

2. Terminology

2.1. Subaqueous deltas

The term of subaqueous delta employed in this study corresponds to the sediment bulge which formed by accumulation of sediments during the retreat of the Rhône river during the last deglacial sea-level rise and subsequent highstand. It includes remains of various submarine and subaerial depositional environments left by the retreat: delta plain, beach barriers, delta front, prodelta. It does not include the modern wedge-shaped sediment body that extends westward of the Rhône, a subaqueous delta in the sense of Cattaneo et al. (2003), that results from westward alongshore sediment transport.

195

2.2. Shoreface

The shoreface of many authors is the portion of shallow-marine depositional system that lies between low tide level and the fair-weather wave base, generally situated at 5-15 m below sea-level (Walker and Plint, 1992). The *fair-weather wave base* corresponds to the limit of the zone where sand transport occurs on a day-to-day basis. In our view, this definition is not precise and does not correspond to an easily identified sedimentological boundary. As proposed by Van Wagoner et al. (1990), we will consider the *storm-wave base* as the lower boundary of the shoreface because the shape and structure of shoreface deposits described in this paper likely represent the long-term product of episodic storms.

2.3. Parasequence

Parasequence is used in the sense of van Wagoner et al. (1990) as "relatively comformable successions of genetically related beds or bedsets bounded by marine flooding surfaces or their correlative surfaces". They are separated by a marine-flooding surface, across which there is evidence of an abrupt increase in water depth. In transgressive deltaic environments of the stratigraphic record, parasequences form backstepping units that are often attributed to short period (<100 kyr) cycles of relative sea-level changes. From a sedimentary environment point of view, a parasequence includes the shoreface, as previously described, and the foreshore (beach) deposits. In a deltaic setting, it would include the delta plain, beach ridges, delta front and prodelta.

3. General setting

3.1. Structural framework

The Gulf of Lions is a passive margin which formed in response to late Eocene-Oligocene rifting and subsequent drifting of Corsica and Sardinia (see reviews by Guennoc et al. (2000)

and Berné and Gorini (2005)). The margin prograded during the Miocene, accommodation space being mainly provided by thermal subsidence due to the cooling of the oceanic crust. On the shelf, Miocene deposits are topped by a major erosional surface formed during the Messinian salinity crisis (Ryan and Cita, 1978). The existence of the Rhône during the Messinian is attested by a deeply incised valley that formed in response to a sea-level fall of about 1,500 m (Clauzon, 1974). Seaward, the incision is easily mapped up to the pre-Messinian shelf edge (Guennoc et al., 2000; Lofi et al., 2005).

3.2. The Quaternary

The thickness of Quaternary deposits (sediments deposited since 1.87 Ma) at the position of the modern Rhône outlet is about 400 m (Debrand-Passard et al., 1984). In fact, some of the sediments that constitute the present Rhône deltaic plain originate from the Durance, a stream that became a tributary of the Rhône only during the last glacial period. Studies of the modern deltaic plain show that it is made of sandy beach ridges, flood plain and lagoonal deposits, dissected by numerous paleo-channels (L'Homer et al., 1981; Arnaud-Fassetta, 1998; Vella, 1999). The position of the early highstand shoreline is about 15 km landward, the Holocene deposits (marine and terrestrial) thickness reaching about 50 m below the delta plain (Vella et al., 2005).

The architecture of the Rhône subaqueous delta is mainly known from seismic surveys that revealed the organization of late Pleistocene/Holocene deposits (Fig. 2). These investigations demonstrate that the transgressive/highstand deposits form a lobate wedge with a maximum thickness at sea of about 50 m (Aloïsi et al., 1975; Aloïsi, 1986). Because of the littoral drift and the general anti-clockwise water circulation in the Gulf of Lions, there is a strong asymmetry in the thickness of these deposits between the eastern and the western sides of the

Rhône subaqueous delta, the transgressive/highstand deposits forming an elongated sediment body stretching to the west (Fig. 3). Further west, the littoral prism is also fed by Languedocian and Pyrenean streams such as Herault, Aude, Agly, Tet, but they presently account for less than 10% of the total sediment budget in the Gulf of Lions (Arnaud-Fassetta, 1998).

3.3. Hydrodynamic setting

The water circulation in the Gulf of Lions is mainly driven by the cyclonic Liguro-Provencal or Northern Current (Millot, 1987, 1999). A shallow branch of this current occasionally penetrates over the shelf, whereas the main outer branch permanently flows southwestward along the slope. This latter branch has a width of about 30-50 km and a thickness of about 300-500 m. The current speed decreases from 30 to 50 cm/s at the surface to a few cm/s at 500 m depth (Durrieu de Madron et al., 1999). On the western Gulf of Lions continental shelf, measurements have been carried out during extreme events (Guillen et al., 2006). They show that during easterly storms, significant wave heights are in excess of 7 m, with period of about 12 s. Corresponding orbital velocities near the bed reach up to 1.2 m/s at 28 m water depth.

The shelf, about 60 km wide in the central part of the Gulf of Lions, narrows to both the east and west. The shelfbreak is located at water depths ranging from 100 to 150 m, depending on the occurrence or not of recent slope failures within the submarine canyons (Berné et al., 2002a).

4. Data and methods

4.1. Bathymetry

The source data mainly consists of 76 sounding charts at the 1/10000 scale (i.e., soundings along a square grid with a 100 m x 100 m spacing) for water depths ranging from 0 to 50 m,

and 54 sounding charts at the 1/20000 scale for water depths ranging from 50 to 150 m. The data set covers the entire Gulf of Lions (Fig. 1). These data, acquired in the 70's and 80's by the Hydrographic Service of the French Navy (Service Hydrographique et Océanographique de la Marine, SHOM), were positioned with the Syledis radio-electrical system, giving a horizontal accuracy better than about 10 m. The vertical accuracy of sounding data, after correction from tidal and meteorological effects, is better than 1 m.

Manual interpretation of this large data set (with 1 m-spaced contour lines) was digitized. Geostatistical interpolation and gridding with 50 m spacing allowed creating Digital Terrain Models (DTM) with spacing of 50 and 100 m (Berné et al., 2002a). In addition, some areas were surveyed by Ifremer with SIMRAD EM950 and SIMRAD EM1000 swath bathymetric systems during cruises in 1995, 2002 and 2003. Additional mapping with "Beautemps Beaupré" was carried out by SHOM in 2004, using a Simrad EM1002S swath bathymetric system.

4.2. Geophysical data

During the same cruises, we employed an SIG sparker (200-600 Hz, 700 Joules) for high-resolution sub-bottom studies, with a shoot interval of 1 or 2 s, at a ship speed of ~ 6 knots. Digital data were acquired and processed on board using a Delph 2 system (swell filtering, gain adjustements, etc.). They were post-processed using Ifremer proprietary software. A hull-mounted Chirp sub-bottom profiler, working at a frequency of 2,500 to 5,200 Hz, was also utilized for ultra-high resolution. For all of these cruises, vessel location data were obtained with a Differential Global Positioning System, providing accuracy in the range of few meters.

4.3. Sedimentology data

In total, 28 cores from the Rhone subaqueous delta were collected and examined, but only 5 are presented in this paper. Piston corers, including the giant piston corer "Calypso" of R/V "Marion Dufresne", were utilized. Cores in muddy areas are of good quality and undisturbed. Because of the shallow water depth of the sites, "stretching" of the cores (Skinner and McCave, 2003) did not occur. Using distinct seismic horizons for evaluating actual core penetration, we found a loss of about 0.5 m at the top of the long (16 m) Calypso core MD992352. The position of a major discontinuity (D350) on seismic profiles correlates well with the actual position of a coarse lag at the bottom of this core, using measured sonic velocities, thus confirming the absence of core deformation. In sandy areas, a vibracorer designed by Rice University was utilized. Well-preserved mollusc and bivalves shells plus calcareous tests from microfauna associations were collected from 5 cores (position in Fig. 3). Radiometric dates of these samples were obtained with accelerator mass spectrometer (AMS) ^{14}C at the Lawrence Livermore National Laboratory (LLNL) and at the Poznan Radiocarbon Laboratory (PRL). The ages reported herein are delta13C-normalised conventional 14C years. All ages being comprised between 0 and 21,880 yr ^{14}C BP, calendar (i.-e. calibrated) ages were calculated using the Calib 5.0 sofware (Stuiver and Reimer, 1993). For marine material, the Marine04 calibration curve (Hughen et al. 2004) was used with no deviation from the average reservoir age (-408 years). For continental material (namely the organic debris of the St Ferreol prodelta) the Intcal04 calibration curve (Reimer et al., 2004) was used.

Data were incorporated into a Geographic Information System (GIS), allowing easier comparison of various data sets.

5. Results

5.1. Overall architecture of the subaqueous deltaic complex

A general topographic/seismic profile across the continental shelf in the Gulf of Lions illustrates the various morphologies and stacking patterns related to the late Quaternary history of the Rhône system (Fig. 2). From south to north (in the direction of shore retreat during the deglacial sea-level rise), they consist of:

-Prograding sequences (S0 to S5) with internal clinoforms corresponding to Pleistocene forced regressions that formed during 100 kyr glacial cycles (Aloïsi, 1986; Rabineau et al., 2005). Outcropping of the last lowstand shoreface sands ("offshore sands") between 90 and 120 m water depth form a distinct morphology, bounded to the south by a major step that corresponds to the limit between upper shoreface sands and lower shoreface muds. The sea-floor on the outer shelf is characterized by erosional morphology. Remnants of beaches cemented during glacial periods (beach rocks) form several meter high pinnacles (Berné et al., 1998).

-Backstepping units (U300 to U500 in Fig. 2) form the deglacial and highstand Rhône subaqueous delta. The seafloor lithology is dominated by silts and clays, except for an elongated sand body situated at about 45-50 m water depth, that will be described hereafter.

The bathymetric map reveals the main geomorphic features that constitute the Rhône subaqueous delta (Fig. 3). Using the same data set, a slope map was created in order to better visualize slope gradients (Fig. 4).

Several geomorphic features are identified, from south to north:

- In the vicinity of the "Petit Rhône" canyon head, very distinct steps at 110-115 m (1 in Figs. 3 and 4) and 98 m (2 and 3 in Figs. 3 and 4) are features observed elsewhere in the Gulf of Lions (Berné et al., 2002a; Jouet et al., 2006). They

correspond to periods of decreased sea-level rise during the early deglacial. Further to the west, they have been dated at 18,000-17,000 cal. yr BP (feature 1) and >15,500 cal. yr BP (features 2-3) (Jouet et al., 2006).

- The main retreat path of the Rhône (4 in Figs. 3 and 4) appears to be clearly visible from its canyon head (the "Petit Rhône" canyon head) to the south up to the −60 m contour line to the north. Between the −75 m and −65 m contour lines, preserved channel/levee facies can be observed, suggesting that the sea-level rise was fast enough to limit erosion by wave action. This facies disappears landward at about −65 m, where it is buried by muds from more proximal prograding units. Other, similar but less distinct features (4w1, 4w2 and 4e) are attributed to other distributaries of a Lowstand Rhône deltaic system. It is worth noting that 4w1 connects to the Marti canyon head, indicating that the "Petit Rhône" canyon was not the only sink for sediments from the Rhône during the last glacial cycle.

- On the inner shelf, 6 major elongated or semi-circular sediment bodies can be identified, based on increased gradient in seafloor slope (5 to 10 in Figs. 3 and 4). These features are inferred to correspond to the remains of past deltaic lobes. The most distinguishable feature is located in the western part of the subaqueous delta, between the −55 and −35 m contour lines (Lobe 5 in Figs. 3 and 4). It roughly corresponds to the position of the sand body that was initially described by Aloïsi et al. (1975). Other, more recent features (Lobes 6 to 10 in Figs. 3 and 4) are also preserved. The upper 5.60 m of Lobe 6 were sampled by core BMKS21 (position in Fig. 3). It consists of clayey silt which yield ages, from bottom to top, between 2,500 and 2,050 yr cal. BP (Table 1). These dates are compatible with the age of the St Ferreol deltaic lobe mapped onshore (2,000-4,000 yr cal BP (Vella et al., 2005)) and Lobe 6 is likely the marine (prodeltaic) equivalent to the St Ferreol

delta. Similarly, the NW-SE bathymetric step running from Pointe de l'Espiguette to the -25 m contour line (Lobe 7 in Figs. 3 and 4) may correspond to a former Peccais deltaic lobe, and/or could be the submarine prolongation of a sand spit formed by modern processes (Sabatier et al., 2006). The Lobe 8 in Fig. 3 is the marine component of the "Bras de Fer" system recognized onshore (Arnaud-Fassetta, 1998), that formed during the Little Ice Age, whereas the Lobe (9) certainly corresponds to the remains of the "Peygoulier" lobe, that formed after the avulsion of the Bras de Fer during the major floods of 1709-1712, and was active until it was diverted toward the modern "Roustan" delta lobe (feature (10) in Figs. 3 and 4) during the 20 th century (Arnaud-Fassetta, 1998). Comparison of bathymetric data sets acquired since 1842 show that these two lobes are presently experiencing erosion (Sabatier et al., 2006).

5.2. The Early Rhône Deltaic Complex (ERDC)

Besides the "offshore sands" that blanket the entire outer continental shelf, beyond about 90 m water depth, the largest sand body in the Gulf of Lions is the one labeled as "Lobe 5" in Figures 3 and 4. In fact, this sand body represents the topset region of a prograding system corresponding to unit U400 of Figure 2. We will successively examine its morphology, lithology, and internal structure.

5.2.1- Detailed morphology and surficial lithology of the Early Rhône Deltaic Complex

Part of the ERDC was mapped with swath bathymetric systems that reveal two types of bedforms at the top of the sand body (Fig. 5):

Longitudinal bedforms, oriented NW-SE. They are less than 3 m high, with a spacing of about 600 m. In fact, the orientation of these features changes from the west to the east, the

overall shape being curvilinear. To the north, they are buried under unit U500 (that corresponds to the more recent St Ferreol deltaic lobe), and therefore considered to be fossil. They are very similar in shape and orientation to the beach ridges described in the recent St Ferreol deltaic lobe (L'Homer et al., 1981) and are therefore interpreted as preserved beach ridges.

Transverse dunes, up to 4 m high, with a spacing of about 500 m. The dunes have a main axis oriented in a N-S direction; however, they often display a polygonal character that could be due to varying directions of sediment transport under different wind-driven circulation regimes.

When compared to the sediment distribution in the area (Fig. 1), it appears that the occurrence of both longitudinal and transverse bedforms corresponds to the availability of sandy sediment. It can be noted that the water depth of dune distribution does not strictly follows the bathymetric contour lines: the lower limit of dunes is around -60 m to the east, whereas it is only 45 m to the west.

5.2.2- Seismic facies and architecture

In cross section, the ERDC displays clinoforms (seismic unit U400 of Fig. 2) topped by a zone remolded by dunes. U400 is better seen on profiles with less vertical exaggeration (Line Bas1-38, Fig. 6). It forms a seismic sequence, up to 30 m thick, that pinches out seaward at about 90 m water depth. Landward, this seismic unit is overlain by late transgressive or highstand deposits of the Rhône subaqueous delta (U500 and other seismic units, see Labaune et al. (2005) for detailed geometrical description). Its internal seismic geometry corresponds to large-scale (10-20 m) tangential clinoforms, truncated at their top by a wavy surface, downlapping on unit U350. The maximum angle of dip of the clinoforms is between 0.5 and

1°, that is to say about the same as the muddy clinoforms of the Adriatic shelf (Cattaneo et al., 2004), but less than the very sandy clinoforms of the Gulf of Lions outer continental shelf where angles are as high as 5° (Berné et al., 1998). In detail, chirp seismic profiles show that the upper erosion surface that overlies U400 is a distal equivalent to D500 (that separates U400 from U500 in the landward direction), and sometimes separates the clinoforms of U400 from an upper thin unit, not distinguished on sparker profiles. Within the upper part of the clinoforms, there is also a distinct change in seismic facies (Fig. 7), with:

An upper, chaotic facies (Fig. 7-1), with numerous cut and fill structures, typical of deltaic environments (Berné et al., 2002b; Abdulah et al., 2004; Roberts et al., 2004; Correggiari et al., 2005).

A lower clinoform facies (Fig. 7-2) with continous and parallel to sub-parallel reflections, typical of prodeltaic environments (Cattaneo et al., 2004; Trincardi et al., 2004).

Medium-scale (1-3 m) clinoforms with an apparent angle of dip in the Northern direction are stacked in the upper part of unit U400 (close-up view 1 in Fig.2). This implies that some sediment transport in a landward or shore-parallel direction occurred at the end of the deposition of U400 (washover or alongshore transport in a lagoon isolated by a barrier island).

The lower boundary of U400 (D400) is not a pronounced reflector, and was therefore omitted in earlier interpretation (Labaune et al., 2005). It corresponds, however, to a distinct downlap surface, sometimes underlined by the presence of shallow gases underneath (Fig. 11). It can be mapped regionally on strike seismic profiles (Fig. 12).

5.2.3. Sedimentary facies and environments, chronostratigraphy

Piston and vibracores where collected from the topset, foreset and bottomset regions of the ERDC in order to characterize lithologies, determine sedimentary environments from primary structures and mollusc assemblages, and obtain chronostratigraphic constraints through radiocarbon dating.

Lithology of the topset area (sand dune/sand ridge area)

All the 16 sediment cores available from the topset region are fairly short, due to difficulty of core penetration and recovery in sandy material. Therefore, the cores did not reach the underlying deltaic facies that are observed on chirp seismic profiles. Most of the cores, such as core BMVK06 shown in Fig. 8, or core BMKS16 positioned in Fig. 5 exhibit a distinct coarsening-upward pattern, with, from bottom to top, fine to medium sand beds alternating with silty intervals, progressively or abruptly passing to massive fine to medium sands (up to 1.50 m thick). They are topped by coarse bed(s) 5-30 cm thick, with shells, shell debris and some pebbles and cobbles. Most of individual sand beds observed in the zone of alternating sand and silt exhibit a fining-upward pattern. The erosion surface observed at the top of U400 on seismic profiles is consistent with several cores containing a very coarse lag including shell and shell fragments originating from shoreface and very shallow water environments. At the top of most of the cores, especially in vibracores where the upper beds are better preserved, unconsolidated silty clay, up to 80 cm thick, is observed, suggesting that the underlying dunes are not in equilibrium with the hydrodynamic regime, at least during periods of fair weather. The coarsest samples were found at the eastern end of the ERDC, with a zone blanketed by cobbles and pebbles (core STKS 25, Fig. 9), indicative of the vicinity of a fluvial system. It is worth noting that along the modern Rhône, pebbles are not found south of Arles, about 50 km upstream of the present river outlet (Vella, Pers. Comm.). This implies

that the capacity of bedload transport of the Rhône was much higher at the time of deposition of the ERDC.

Lithology of the foreset/bottomset area (core MD992352)

The longest core from the foreset/bottomset region was obtained with the "Calypso" piston corer of "Marion Dufresne". Core MD992352 is 15.40 m long and provides the most expanded record of seismic units U400 and U350 (Fig. 8 and Table 1).

At its base (1538-1529 cm), this core displays a very coarse and shell-bearing horizon with flat cobbles (up to 2 cm in diameter) interpreted as a ravinement surface. This strata likely corresponds to seismic surface D350. The skeletal assemblage above that surface is a muddy-shell hash that contains mollusc shells of diverse ages sourced from various littoral and sublittoral environments. In particular worn bioclasts belonging to the bivalve *Mytilus* sp. (cf *galloprovincialis*) dated at ~ 15,000 cal yr BP, together with *Chamelea gallina* and the gastropod *Nassarius reticulatus*, represent the shallowest (therefore oldest) components included in such assemblage and interpreted as a very shallow-water environment (0-2 m water depth) cannibalized during the transgression. Other components in this same hash include the boreo-celtic guest *Mya truncata*, and holoplanktic molluscs such as thecosomatous pteropods (*Limacina* sp.).

Above the ravinement surface, the core displays a long interval of clayey silts, interrupted by mm-thick laminae to cm-thick beds of sandy silt or fine sand, indicative of a lower shoreface/prodeltaic environment. Molluscs representative of muddy, prodeltaic settings, such as *Turritella communis* and *Corbula gibba*, confirm this interpretation.

Between 102 and 140 cm, a shell bed and shell hash in a matrix of fine sand is observed, and this likely corresponds to seismic surface D500 (if we consider that about 0.5 m of upper fine sediments were lost during the coring operation). The skeletal assemblage is very diverse and

includes molluscs, bryozoans and serpulids from different shelf environments. This bed is interpreted as documenting a phase on intense sea-floor winnowing (condensed interval).

The upper 102 cm is a bioturbated, beige, silty clay with some shells and shell debris. The occurrence of *Parvicardium minimum*, *Acanthocardia echinata*, *Nassarius pygmaeus* and especially *Corbula gibba*, documents a modern prevalently muddy shelf environment with episodic reworking of sediment (e.g., Cabioch, 1968; Di Geronimo and Robba, 1989; Taviani et al., 1998). Pteropods such as *Cavolinia inflexa* indicate a pelagic contribution.

The ages of dated material are reported in Table 1. Except for one sample composed of mixed material (benthic foraminifera, bivalves, gastropods and ostracods), the results do not show any age inversion within the 1-sigma error interval. From these results, an age model was established for the interval situated between the two erosion surfaces (D350, the ravinement surface situated at the bottom of the core, D500, the upper erosion surface) (Fig. 10).

6. Discussion

6.1. What is the ERDC and when did it form ?

The elongated geometry and internal seismic architecture of the ERDC present similarities with that of the *infralittoral prograding wedges* described along the Spanish Mediterranean coast (Hernandez-Molina et al., 2000). These sand bodies have been interpreted by these authors as the product of downwelling storm currents and are therefore modern sand bodies in equilibrium with present oceanographic processes. In contrast, the age of the bottomsets of the ERDC demonstrates that it is a relict feature, even though modern processes might episodically reactivate its surface during extreme events. We have seen that the sandy upper part of the ERDC likely corresponds to the remains of a shoreline that deposited during a slow down of the deglacial sea-level rise. It is difficult to date precisely beach deposits, that incorporate material of very different origin and age. Therefore, we used the dates from the

coeval deposits of the lower shoreface/prodelta domain. Using the ultra-high resolution seismic profiles, we used clinoforms as time-lines, in order to propagate the radiocarbon age model from the bottomset region (core MD992352) to the foreset/topeset area.

Each clinoform on the seismic profile (labeled 1 to 11 in Figure 11) is a time-line which can be dated at the intercept with the position of core MD992352 (Table 2). If we plot these time lines from the position of the core in a landward direction, we may infer the age of the corresponding sandy foresets, as well as the age of the transition zone between the deltaic/prodeltaic seismic facies, that approximates sea-level position. This technique indicates that deposition of the ERDC began, in our study area, around 15,000 yr cal BP, above the coarse lag of the ravinement surface (D350), and stopped around 10,500 yr cal BP. We cannot exclude that marine sedimentation began earlier, and in that case older ravinement surfaces would be preserved below D350, but the age and nature of Unit 300 seen in Fig. 6 are unknown as we have not been able to collect any core from this interval. This 15,000-10,500 yr cal BP time-frame encompasses the end of the Bølling-Allerød, the Younger Dryas and the Preboreal. Maximum sedimentation at the position of our core occurred between 11,500 and 10,500 cal yr BP, during the Preboreal. Seismic surface D400, identified as a downlap surface, has an interpolated age of about 12,049±62 cal yr BP (Fig. 10). This age corresponds to the beginning of the Younger Dryas, a time of reduced sea-level rise (Fairbanks, 1989) or even still-stand when the ERDC shifted from aggradation to progradation. The end of deposition of the EDRC does not coincide with the termination of the Younger Dryas, but lasted until ~ 10,500 cal yr BP, about 1,000 years after the end of this cold event.

The erosional surface observed at the top of the ERDC (D500) is younger than 10,500 cal yr BP. Therefore, it can not be attributed to a sea-level fall during the Younger Dryas, as hypothesized by Aloïsi (1986). On the contrary, it might correspond to a phase of starvation

during a phase of increased sea-level rise. It is an equivalent to the transgressive condensed interval described on the outer shelf (Bassetti et al., 2006).

6.2. Relative sea-level changes and shoreline progradation

A way to evaluate sea-level position from our seismic data is to measure the depth of the transition between the distinct deltaic and prodeltaic seismic facies shown in Fig. 7. This transition point, which roughly represents the *shoreline trajectory* (as described by Helland-Hansen and Martinsen (1996) and discussed by Hampson and Storms (2003)), has been plotted on chirp seismic profiles (marked by X symbols in Fig. 11). This boundary between seismic facies is not extremely precise, but certainly has a depth error bar similar to that of *Acropora* used in coral reef studies (i.e., about 5 m). Furthermore, the migration of this transition zone, as it can be tracked across clinoforms, is a good indicator of the *rate* of sea-level change. Our results are not corrected for any glacio- or hydro-isostatic effect, and therefore should be considered as *relative* sea-levels. Estimates of hydro-isostatic effect at the shelf edge is in the order of 20 m for the last 20kyr (Jouet et al., in press). However, numerical modeling of mantle rheology suggests that, in our study area and for the considered period, the glacio-isostatic contribution roughly balanced the hydro-isostatic effect (Lambeck and Bard, 2000). In all of our results, we do not take into account the depth of the brinkpoint (-47 m) observed on bathymetric and seismic data because we do not know whether it corresponds to the top of a paleo-delta front or to a preserved coastal dune.

The depth of the transition zone between deltaic and prodeltaic seismic facies can be measured on Clinoforms 6 to 11, with corresponding ages comprised between ~ 11,100 and ~ 10,600 cal yr BP (Table 2), that is to say the end of the Preboreal chronozone. The validity of our method is confirmed by the age of the bottom of core BMVK06 from the topset region (10,665-10,899 cal yr BP, Table 1), compared to the age of the nearest clinoform (clinoform

11, dated at 10,595±161 cal yr BP, Table 2). According to our data, relative sea-level rose from about -55 m to about -50m during this interval, at an average rate of 1.02 cm/yr. More precisely, the rate of sea-level rise was on the order of 0.3-0.6 cm/yr between ~ 11,100 and 10,900 cal yr BP, then about 1.2 cm/yr from ~ 10,900 to 10,600 cal yr BP.

Shoreline advance in our study area can also be estimated from the intercept between the top of the clinoforms and the sea-floor in a shore-normal direction. This measurement is only possible between about 11,000 cal yr BP (Clinoform 8) and the brink point. It decreases from about 15 m/yr around 11,000 cal yr BP to 2.4 m/yr around 10,600 cal yr BP. Without any avulsion or change in sediment flux, this decrease could simply be explained by an increased rate of sea-level rise creating more accommodation.

6.3. Sequence stratigraphic interpretation of the ERDC

In a sequence stratigraphic framework, the ERDC corresponds to a *transgressive parasequence* bounded by *flooding surfaces* (Fig. 13) in the sense of Van Wagoner et al. (1990). Our precise chronology allows us to link key surfaces to phases of (relative) sea-level change:

- The basal bounding surface corresponds to sea ingression during the Bølling-Allerød, and is therefore a true flooding surface.

- The downlap surface (D400) that mimics a maximum flooding surface represents the end of this rapid sea-level rise. It formed during the first phase (around 12,000 cal yr BP) of the Younger Dryas stillstand or decelerating sea-level rise. It is a *surface of maximum transgression* in the sense of Helland-Hansen and Martinsen (1996).

- The upper boundary (surface D500) is also a flooding surface, but it formed with a delay of about 1,000 yr with respect to the resumed sea-level rise. This implies that

it can no more be considered as an erosion surface formed by stillstand or sea-level fall at the end of the Younger Dryas (Aloïsi et al., 1975; Gensous and Tesson, 2003; Labaune et al., 2005).

- The sand that constitutes the upper part of the ERDC originates from an ancient shoreline/delta front, with the possible position of a Rhône outlet at the position of core KSTR 25 where cobbles and pebbles are found. Longitudinal bedforms parallel to this paleo-shoreline are relict feature, their northern termination being buried by the Holocene muds. It is not clear whether transverse dunes from the same area are fossil or still subject to episodic migration during high-energy events, such as the outer shelf dunes described by Bassetti et al. (2006).

The bathymetric position of the ERDC and the chronology of its deposition is similar to other transgressive parasequences described elsewhere. For instance, the extensively studied Northern Gulf of Mexico margin displays several transgressive backstepping deltas that formed during the same time period (Anderson et al., 2004). In particular, the Colorado river formed, between 14,000 and 11,000 yr BP, a backstepped delta at -45 m (Abdulah et al., 2004) that corresponds, in time and position, to the ERDC. In the Adriatic, several backstepped units are also preserved in similar stratigraphic and bathymetric positions (Trincardi et al., 1996; Cattaneo and Trincardi, 1999; Asioli et al., 2001; Cattaneo et al., 2003).

6.4. Processes controlling the late progradation and abandonment of the ERDC

Changes in the rate of relative sea-level rise (that control accommodation) and/or changes in the amount of sediment supply may explain the evolution of the ERDC, and its abandonment at ~ 10,500 cal yr B.P, that represents a delay of ~1,000 yr following the Younger Dryas cold interval.

6.4.1. Sea-level

Positions of sea-level inferred from our data correspond very well with that from global studies (Fig. 14), even though they are uncorrected sea-levels. We note in Table 2 an increase in the slope of the shoreline trajectory that suggests an increase in the rate of sea-level rise at the end of the progradation phase of the ERDC. However, this observation is based on only 2 measurements, and, for this 11,100-10,600 cal yr BP time-period, there is a large consensus about a constant sea-level rise. For instance, Lambeck et al. (2002) propose a constant global sea-level rise of 1.52 cm/yr for the Post Younger Dryas- 8,500 cal yr BP time window. Similarly, Camoin et al. (2004) propose for the Indian Ocean a minimum value of 1.16 cm/yr for the 11,600–9,640 cal yr BP time window, that can be compared to the 1.2 cm/yr measured in the Gulf of Lions. Some authors have argued that, besides MWP1A and MWP1B, other Melt Water Pulses occurred during the last deglacial sea-level rise (Liu et al., 2004). However, even if real, the chronology of these events, especially their so-called MWP 1c, does not correspond to our period of possible increased sea-level rise.

6.4.2. Sediment flux

Sequence stratigraphers have shown that shoreline progradation (regression) may occur in a context of sea-level rise, provided that sediment flux is sufficient to fill the available space (Posamentier et al., 1992). The ~ 1,000 yr delay between the end of the Younger Dryas and the period of delta abandonment may be explained by a phase of increased sediment flux during the beginning of the Preboreal. This hypothesis is supported by studies in the catchment area of the Rhône, for instance in Lake Lautrey of Jura where Younger Dryas is characterized by very low sedimentation rate (about 0.2 mm/yr), whereas the warmer Preboreal has a sedimentation rate about 6 times higher (Magny et al., 2006). It is very likely that melting of Alpine glaciers due to Preboreal warming, and increased rainfall during the

same period, favored the supply of a huge amount of sediment to the sea, following the dry and cold Younger Dryas. As to the abandonment of the ERDC at 10,500 cal yr BP, it could be due to a purely autocyclic process, the delta being switched further west, as suggested by the WNW-ESE trend of the ERDC and the progressive shallowing of the sand/silt transition in the WNW direction. A climatic control is however likely, as a phase of aridification is observed all around the Western Meditteranean Sea at the same time (Magny et al., 2002).

In summary, we consider that the initiation and growth of the ERDC was mainly controlled by a decreased rate of sea-level rise. In contrast, the ERDC was able to keep pace with renewed increase of sea-level rise after the Younger Dryas mainly because increasing sediment flux.

In the future, it will be interesting to explore the relative effect of changes in temperature and rainfall on the amount of sediment supplied to the ERDC, and more generally to the Rhône deltaic system. 3D stratigraphic modeling constrained by seismic geometries and ^{14}C dates will permit to test these hypothesis, and to quantify the relative impact of sediment flux and sea-level changes on sequence architecture.

Conclusions

The morphology and internal architecture of the Rhône subaqueous delta exhibit the imprint of deglacial sea-level rise strongly influenced by changes in sediment supply. Early phases in the rise are evidenced by 2 morphological steps at 110-115 and 98 m water depth. The rapid sea-level rise during Meltwater Pulse 1A resulted in the retreat of the Rhône along a N-S path that is well preserved in the present seafloor morphology, in the form of a channel-levee system. The ERDC was deposited between about 15,000 and 10,500 cal yr BP, forming a major transgressive parasequence on the middle/inner shelf. This complex consists in a lower

retrograding/aggrading unit, that formed during a period of rapid sea-level rise (15,000 to 12,000 cal yr BP), and an upper prograding unit initiated during the slow sea-level rise of the Younger Dryas. However, due to increased sediment flux during the Preboreal, progradation was maintained until about 10,500 cal yr BP, about 1,000 yr following the end of the Younger Dryas, at a time when the rate of sea-level rise was in the order of 1 cm/yr. The abandonment of the deltaic complex at 10,500 cal yr BP is attributed to a decrease in sediment supply, rather than to an increased rate of sea-level rise. The origin of this sediment starvation can be linked to a phase of aridity and/or to a shift of the Rhône to the West.

Despite the general idea that the last deglacial sea-level rise was too fast for allowing deposition of large sediment bodies on the shelf, our study demonstrates that most of the sediment accumulated on the inner and mid shelf off the Rhône corresponds to transgressive deposits, late Holocene sediments being accumulated along the coastal zone.

References

Abdulah, K.C., Anderson, J.B., Snow, J.N., Holford-Jack, L., 2004. The Late Quaternary Brazos and Colorado deltas, offshore Texas, USA- Their evolution and the factors that controleld their deposition. In: J.B. Anderson and R.H. Fillon (Editors), Late Quaternary Stratigraphic evolution of the northern Gulf of Mexico margin. SEPM (Society for Sedimentary Geology) Special Publication 79, Tulsa, pp. 237-269.

Aloïsi, J.C., Monaco, A., Thommeret, J., Thommeret, Y., 1975. Evolution paléogéographique du plateau continental languedocien dans le cadre du Golfe du Lion. Analyse comparée des données sismiques, sédimentologiques et radiométriques concernant le Quaternaire récent. Revue de Géologie Dynamique et de Géographie Physique, 17, 13-22.

Aloïsi, J.C., 1986. Sur un modèle de sédimentation deltaïque: contribution à la connaissance des marges passives. Unpublished Doctoral Thesis, University of Perpignan, 162 p.

Anderson, J.B., Thomas, M.A., 1991. Marine ice-sheet decoupling as a mechanism for rapid, episodic sea-level change: the record of such events and their influence on sedimentation. Sedimentary Geology, 70, 87-104.

Anderson, J.B., Rodriguez, A., Abdulah, K.C., Fillon, R.H., Banfield, L.A., McKeown, H.A.Wellner, J.S., 2004. Late Quaternary Stratigraphic evolution of the northern Gulf of Mexico margin: a synthesis. In: J.B. Anderson and R.H. Fillon (Editors), Late Quaternary Stratigraphic evolution of the northern Gulf of Mexico margin. SEPM (Society for Sedimentary Geology), Tulsa, pp. 1-23.

Arnaud-Fassetta, G., 1998. Dynamiques fluviales holocènes dans le delta du Rhône. PhD Thesis, Université de Provence, Aix en Provence, 329 pp.

Asioli, A., Trincardi, F., Lowe, J.J., Ariztegui, D., Langone, L., Oldfield, F., 2001. Sub-millennial scale climatic oscillations in the central Adriatic during the Lateglacial: palaeoceanographic implications. Quaternary Science Reviews, 20, 1201-1221.

Bard, E., Hamelin, B., Arnold, M., Montaggioni, L., Cabioch, G., Faure, G., Rougerie, F., 1996. Deglacial sea-level record from Tahiti corals and the timing of global meltwater discharge. Nature, 382, 241-244.

Bassetti, M.A., Jouet, G., Dufois, F., Berné, S., Rabineau, M., Taviani, M., 2006. De-glacial sedimentary processes and deposits in the outer continental shelf of the Gulf of Lions (western Mediterranean). Marine Geology, 234, 93-109.

Berné, S., Lericolais, G., Marsset, T., Bourillet, J.F., de Batist, M., 1998. Erosional shelf sand ridges and lowstand shorefaces: examples from tide and wave dominated environments of France. Journal of Sedimentary Research, 68, 540-555.

Berné, S., Carré, D., Loubrieu, B., Mazé, J.P., Normand, A., 2001. Carte morpho-bathymétrique du Golfe du Lion. Ifremer, Brest.

Berné, S., Satra, C., Aloïsi, J.C., Baztan, J., Dennielou, B., Droz, L., Dos Reis, A.T., Lofi, J., Méar, Y., Rabineau, M., 2002a. Carte morpho-bathymétrique du Golfe du Lion, notice explicative, Ifremer, Brest.

Berné, S., Vagner, P., Guichard, F., Lericolais, G., Liu, Z., Trentesaux, A., Yin, P., Yi, H.I., 2002b. Pleistocene forced regressions and tidal sand ridges in the East China Sea. Marine Geology, 188, 293-315.

Berné, S., Rabineau, M., Flores, J.A., Sierro, F.J., 2004. The impact of Quaternary Global Changes on Strata Formation. Exploration of the shelf edge in the Northwest Mediterranean Sea. Oceanography, 17, 92-103.

Berné, S., Gorini, C., 2005. The Gulf of Lions: An overview of recent studies within the French 'Margins' programme. Marine and Petroleum Geology, 22, 691-693.

Camoin, G.F., Montaggioni, L.F., Braithwaite, C.J.R., 2004. Late glacial to post glacial sea levels in the Western Indian Ocean. Marine Geology, 206, 119-146.

Cabioch, L., 1968. Contribution à la connaissance des peuplements benthiques de la Manche occidentale. Cahiers de Biologie Marine 9, 493-720.

Cattaneo, A., Trincardi, F., 1999. The Late-Quaternary transgressive record in the Adriatic Epicontinental Sea: Basin widening and facies partitioning. In: K.M. Bergman and J.W. Snedden (Editors), Isolated Shallow Marine Sand Bodies: Sequence Stratigraphic Analysis and Sedimentological Interpretation. SEPM Special Publication, Tulsa.

Cattaneo, A., Correggiari, A., Langone, L., Trincardi, F., 2003. The late-Holocene Gargano subaqueous delta, Adriatic shelf: Sediment pathways and supply fluctuations. Marine Geology, 193, 61-91.

Cattaneo, A., Trincardi, F., Langone, L., Asioli, A., Puig, P., 2004. Clinoform generation on Mediterranean margins. Oceanography, 17, 105-117.

Clauzon, G., 1974. L'hypothèse eustatique et le creusement prépliocène de la vallée du Rhône. Annales de Géographie, 456, 129-140.

Correggiari, A., Cattaneo, A., Trincardi, F., 2005. The modern Po Delta system: Lobe switching and asymmetric prodelta growth. Marine Geology, 222-223, 49-74.

Debrand-Passard, S., Courbouleix, S., Lienhardt, M.J., 1984. Synthèse géologique du Sud-Est de la France, 125. Bureau de Recherches Géologiques et Minières, Orléans, 615 pp.

Di Geronimo, I., Robba, E., 1989. The structure of benthic communities in relation to basin stability. In: A. Boriani, M. Bonafede, G.B. Piccardo and G.B. Vai (Editors), The Lithosphere in Italy, Atti del Convegno Lincei 80, Accademia Nazionale dei Lincei, pp. 341-352.

Durrieu de Madron, X., Radakovitch, O., Heussner, S., Loye-Pilot, M.D., Monaco, A., 1999. Role of the climatological and current variability on shelf-slope exchanges of particulate matter: Evidence from the Rhone continental margin (NW Mediterranean). Deep Sea Research Part I: Oceanographic Research Papers, 46, 1513-1538.

Fairbanks, R.G., 1989. A 17,00-year glacio-eustatic sea-level record: influence of glacial melting rates on the Younger Dryas event and deep-ocean circulation. Nature, 342, 637-642.

Gensous, B., Williamson, D., Tesson, M., 1993. Late-Quaternary transgressive and highstand deposits of a deltaic shelf (Rhône delta, France). In: H.W. Posamentier, C.P. Summerhayes, B.A. Haq and G.P. Allen (Editors), Sequence stratigraphy and facies associations. International Association of Sedimentologists Spec. Pub. 18, Blackwell, Oxford, pp. 197-212.

Gensous, B., Tesson, M., 2003. L'analyse des dépôts postglaciaires et son application à l'étud des séquences de dépôt du Quaternaire terminal sur la plate-forme au large du Rhône (golfe du Lion). Bulletin de la Société Géologique de France, 174, 401-419.

Guennoc, P., Gorini, C., Mauffret, A., 2000. Histoire géologique du Golfe du Lion et cartographie du rift oligo-aquitanien et de la surface messinienne. Géologie de la France, 3, 67-97.

Guillen, J., Bourrin, F., Palanques, A., Durrieu de Madron, X., Puig, P., Buscail, R., 2006. Sediment dynamics during wet and dry storm events on the Tet inner shelf (SW Gulf of Lions). Marine Geology, 234, 129-142.

Hampson, G.J., Storms, J.E.A., 2003. Geomorphological and sequence stratigraphic variability in wave-dominated, shoreface-shelf parasequences. Sedimentology, 50, 667-701.

Hannebuth, T.J.J., Statteger, K., Grootes, P.M., 2000. Rapid flooding of the Sunda Shelf- A late-glacial sea-level record. Science, 288, 1033-1035.

Harris, P.T., 1999. Sequence architecture during the Holocene transgression: an example from the Great Barrier Reef shelf, Australia-comment. Sedimentary Geology, 125, 235-239.

Helland-Hansen, W., Martinsen, O.J., 1996. Shoreline trajectories and sequences: description of variable depositional-dip scenarios. Journal of Sedimentary Research, 66, 670-688.

Hughen, K.A. et al., 2004. Marine04 Marine radiocarbon age calibration, 26 - 0 ka BP. Radiocarbon, 46, 1059-1086.

Jouet, G., Berné, S., Rabineau, M., Bassetti, M.A., Bernier, P., Dennielou, B., 2006. Shoreface migrations at the shelf edge and sea-level changes around the Last Glacial Maximum (Gulf of Lions, NW Mediterranean Sea). Marine Geology, 234, 21-42.

Jouet, G., Hutton, E.W.H., Syvitski, J.P.M., Berné, S., in press. Response to loading and subsidence of the Rhône deltaic margin during the Last Climatic Cycle. Computers & Geosciences.

L'Homer, A., Bazile, F., Thommeret, J., Thommeret, Y., 1981. Principales étapes de l'édification du delta du Rhône de 7000 B.P. à nos jours ; variations du niveau marin. Oceanis, 7, 389-408.

Labaune, C., Jouet, G., Berné, S., Gensous, B., Tesson, M., Delpeint, A., 2005. Seismic stratigraphy of the Deglacial deposits of the Rhone prodelta and of the adjacent shelf. Marine Geology, 222-223, 299-311.

Lambeck, K., Bard, E., 2000. Sea-level change along the French Mediterranean coast for the past 30 000 years. Earth and Planetary Science Letters, 175, 203-222.

Lambeck, K., Yokoyama, Y.Purcell, T., 2002. Into and out of the Last Glacial Maximum: sea-level change during Oxygen Isotope Stages 3 and 2. Quaternary Science Reviews, 21, 343-360.

Lofi, J., Gorini, C., Berne, S., Clauzon, G., Tadeu Dos Reis, A., Ryan, W.B.F., Steckler, M.S., 2005. Erosional processes and paleo-environmental changes in the Western Gulf of Lions (SW France) during the Messinian Salinity Crisis. Marine Geology, 217, 1-30.

Magny, M., Miramont, C., Sivan, O., 2002. Assessment of the impact of climate and anthropogenic factors on Holocene Mediterranean vegetation in Europe on the basis of palaeohydrological records. Palaeogeography, Palaeoclimatology, Palaeoecology, 186, 47-59.

Magny, M., Aalbersberg, G., Begeot, C., Benoit-Ruffaldi, P., Bossuet, G., Disnar, J.-R., Heiri, O., Laggoun-Defarge, F., Mazier, F., Millet, L., 2006. Environmental and climatic changes in the Jura mountains (eastern France) during the Lateglacial-Holocene transition: A multi-proxy record from Lake Lautrey. Quaternary Science Reviews, 25, 414-445.

Marsset, T., Bellec, V., 2002. Late Pleistocene-Holocene deposits of the Rhône inner continental shelf (France): detailed mapping and correlation with previous continental and marine studies. Sedimentology, 49, 255-276.

Millot, C., 1987. Circulation in the Western Mediterranean Sea. Oceanologica Acta, 10, 143-149.

Millot, C., 1999. Circulation in the Western Mediterranean Sea. Journal of Marine Systems, 20, 423-442.

Posamentier, H.W., Allen, G.P., James, D.P., Tesson, M., 1992. Forced regressions in a sequence stratigraphic framework: concepts, examples and exploration significance. American Association of Petroleum Geologists Bulletin, 76, 1687-1709.

Provansal, M., Vella, C., Arnaud-Fassetta, G., Sabatier, F., Maillet, G., 2003. Role of fluvial sediment inputs in the mobility of the Rhône delta coast (France). Géomorphologie: relief, processus, environnement, 4, 271-282.

Rabineau, M., Berne, S., Aslanian, D., Olivet, J.-L., Joseph, P., Guillocheau, F., Bourillet, J.-F., Ledrezen, E., Granjeon, D., 2005. Sedimentary sequences in the Gulf of Lion: A record of 100,000 years climatic cycles. Marine and Petroleum Geology, 22, 775-804.

Reimer, P.J., Baillie, M.G.L., Bard, E., Bayliss, A., Beck, J.W., Bertrand, C.J.H., Blackwell, P.G., Buck, C.E., Burr, G.S., Cutler, K.B., Damon, P.E., Edwards, R.L., Fairbanks, R.G., Friedrich, M., Guilderson, T.P., Hogg, A.G., Hughen, K.A., Kromer, B., McCormac, F.G., Manning, S.W., Ramsey, C.B., Reimer, R.W., Remmele, S., Southon, J.R., Stuiver, M., Talamo, S., Taylor, F.W., van der Plicht, J., Weyhenmeyer, C.E., 2004. IntCal04 Terrestrial radiocarbon age calibration. Radiocarbon, 46, 1029-1058.

Roberts, H.H., Fillon, R.H., Kohl, B., Robalin, J.M., Sydow, J.C., 2004. Depositional architecture of the Lagniappe delta:sediment characteristics, timing of depositional events, and temporal relationship with adjacent shelf-edge deltas. In: J.B. Anderson and R.H. Fillon (Editors), Late Quaternary Stratigraphic evolution of the northern Gulf of Mexico margin. SEPM (Society for Sedimentary Geology), Tulsa, pp. 143-188.

Ryan, W.B.F., Cita, M.B., 1978. The nature and distribution of Messinian erosional surface-indication of a several kilometer-deep Mediterranean in the Miocene. Marine Geology, 27, 193-230.

Sabatier, F., Maillet, G., Provansal, M., Fleury, T.-J., Suanez, S., Vella, C., 2006. Sediment budget of the Rhone delta shoreface since the middle of the 19th century. Marine Geology, 234, 143-157.

Skinner, L.C., McCave, I.N., 2003. Analysis and modelling of gravity- and piston coring based on soil mechanics. Marine Geology, 199, 181-204.

Stuiver, M., Reimer, P.J., 1993. Extended 14C database and revised CALIB radiocarbon calibration program. Radiocarbon, 35, 215-230.

Taviani, M., Roveri, M., Impiccini, R., Vigliotti, L., 1998. Segnalazione di Quaternario marino nella Val Chero (Appennino Piacentino). Bollettino della Società Paleontologica Italiana 36, 331-338

Tesson, M., Gensous, B., Naudin, J.-J., Chaignon, V.Bresoli, J., 1998. Carte morpho-bathymétrique de la plate-forme du golfe du Lion: un outil pour la reconnaissance et l'analyse des modifications environnementales récentes. Comptes Rendus de l'Academie des Sciences - Series IIA - Earth and Planetary Science, 327, 541-547.

Trincardi, F., Cattaneo, A., Correggiari, A., Langone, L., 1996. Stratigraphy of the late-Quaternary deposits in the central Adriatic basin and the record of short-term climatic events In: P. Guilizzoni and F. Oldfield (Editors), Palaeoenvironmental analysis of Italian crater lake and Adriatic sediments. Mem. Ist. Ital. Idrobiol., pp. 39-70.

Trincardi, F., Cattaneo, A., Correggiari, A., 2004. Mediterranean prodelta systems: natural evolution and human impact investigated by Eurodelta. Oceanography, 17, 34-45.

van Wagoner, J.C., Mitchum, R.M., Campion, K.M., Rahmanian, V.D., 1990. Siliciclastic sequence stratigraphy in well logs, cores and outcrops. Methods in Exploration Series N° 7. American Association of Petroleum Geologists, 55 pp.

Vella, C., 1999. Perception et évaluation de la mobilité du littoral holocène sur la marge orientale du delta du Rhône. PhD Thesis, Aix-Marseille 1, Aix, 225 pp.

Vella, C., Fleury, T.-J., Raccasi, G., Provansal, M., Sabatier, F.Bourcier, M., 2005. Evolution of the Rhone delta plain in the Holocene. Marine Geology, 222-223, 235-265.

Walker, R.G.Plint, A.G., 1992. Wave- and storm- dominated shallow marine systems. In: R.G. Walker and N.P. James (Editors), Facies Models - Response to Sea Level Changes. Geological Association of Canada, St John, pp. 219-238.

Figure captions

Fig. 1: General bathymetric map of the Gulf of Lions (based on Berné et al. (2001)). The distribution of sand is modified from Aloïsi (1986). Isobath contour line interval is 5 m from 0 to 150 m water depth, 200 m beyond 150 m. The arrow represents the direction of the Northern contour current. LDC: Lacaze-Duthiers Canyon; PvC: Pruvot Canyon; AC: Aude Canyon (or Bourcart canyon); HC: Hérault Canyon; SC: Sète Canyon; MaC: Marti Canyon; PRC: Petit Rhône Canyon; GRC: Grand Rhône Canyon; EC: Estaque Canyon.

Fig. 2: Seismic (chirp) section STch 93 across the western Rhône subaqueous deltaic complex (modified from Berné et al. (2004)). The sandy upper shoreface (upper part of unit U400) forms a step well visible on the detailed bathymetric map (see Fig. 3). Note the very exaggerated vertical scale. CS: Cemented sands. Units including U300 through U500 represent the trangressive and highstand deposits that are studied in this paper. "1" and "2" are close-up views of unit U400. "m": multiple. D70, D60, D50 and D45 are surfaces of subaerial erosion that formed during Marine Isotope Stages 2, 6, 8 and 10, respectively. They bound regressive or "falling stage" systems tracts.

Fig. 3: Detailed morphology of the Rhône subaqueous delta and main morpho-sedimentary features offshore and onshore. This map is based on the compilation of sounding charts from the French Hydrographic Service of the Navy (SHOM). Contour lines are every 50 cm in order to highlight morphologic features. The thick arrow corresponds to the boundary between two Digital Terrain Models, that generate an artifact along the –50 m contour line (see text for explanation). The deglacial retreat path of the Rhône from the Petit Rhône canyon head (PRC) can be inferred with, from South to North: (1), (2) and (3): lowstand and early transgressive shorelines and/or delta fronts; (4): retreat path of the Rhône presumably during MWP1A; (4w1), (4w2), and (4e) correspond to the retreat path of other Rhône distributaries. (5): sandy delta front of the Early Rhône Deltaic Complex; 6: remnants of the Early St Ferreol delta; (7): remnants of a Peccais (?) delta front; (8): remnants of a Little Ice Age delta front (Bras de Fer); (9): remnants of the Peygoulier delta front; (10): modern Roustan delta front. The modern delta plain exhibits two distributaries, the "Petit Rhône" (little Rhône) to the west and the "Grand Rhône" (large Rhône) to the east. STKS25, MD992352 BMVK06, and BMKS16 are cores described or mentioned in the text. Paleo-shorelines, sand ridges and onshore deltaic lobes (in red) are from L'Homer et al. (1981),

Arnaud-Fassetta (1998), Vella (1999), Provansal (2003). Sand distribution is based on Aloïsi (1986), modified according to our samples.

Fig. 4: Slope map calculated from the Digital Terrain Model shown in Fig. 3. Note the steep slope of the modern Rhone prodelta compared to older lobes. Legend is the same as for Fig. 3.

Fig. 5: Swath bathymetric (EM1000 and EM 300) map of part of the Early Rhône Deltaic Complex (position in Fig. 3). Note elongated NW-SE ridges (interpreted as beach ridges), slightly oblique relative to present bathymetric contour lines, with superimposed subaqueous N-S sand dunes (possibly active during extreme events).

Fig. 6: Sparker profile BAS1-38 across the western Rhône subaqueous delta (position in Fig. 3). The location and actual penetration depth (with vertical scale in m) of cores MD992352 and BMKS16 is shown. The difference in core lengths is explained by different lithologies: clayey silt for the bottomsets, fine to medium sand for the topsets. Sequences and surfaces are the same as in Figure 2.

Fig. 7. Chirp seismic data from the upper chaotic facies (1) and the lower clinoform facies (2) (position in Fig. 3).

Fig. 8: Lithologic description and photographs of cores BMVK06 and MD992352 (positions in Figs. 3 and 6). For clarity, different vertical scales are used. Calibrated ages of dated samples (stars) are also reported.

Fig. 9: Photograph of the upper part of core KSTR25 (position in Fig. 3) with cobbles and pebbles (water depth at -55mbmsl).

Fig. 10: Age model curve for core MD992352, with 1 sigma error bars. Numbered lozenges represent the position along clinoforms of Figure 11 (the corresponding ages are reported in table 2). Only dates below the erosion surface D500 are taken into account, the time span represented by this surface being unknown.

Fig. 11: Part of Chirp seismic profile STch93. Core length is converted into milliseconds using an average sonic velocity of 1580 m/s (as measured in the core). The coarse lag observed between 1 m and 1.20 m on the core corresponds to the erosion surface named D500 on the seismic profile, implying that the upper 50 cm of sediment was lost during the coring operation. The lower coarse lag situated at the bottom of the core matches the depth of the ravinement surface (D350) seen on seismic profiles. X symbols correspond to the boundary between deltaic and prodeltaic seismic facies (see text and Fig. 7 for explanation), numbers are used for identification of clinoforms.

Fig. 12: Chirp seismic profile STch123 (strike section, position in Fig. 3). Note the chaotic seismic facies that underlies D350 (the ravinement surface). D400 is positioned by crossing with sparker profiles where downlap termination are seen more clearly than on chirp profiles.

Fig. 13: Schematic representation of the Early Rhone Deltaic Complex transgressive parasequence, with key components and corresponding chronology of deposition. This complex consists of an aggrading/retrograding unit (U350) topped by a prograding unit (U400). U350 formed during a period of rapid sea-level rise (the Bølling-Allerød, noted B/A,

including Melt Walter Pulse 1A, noted MWP1A). The transition between aggradation and progradation corresponds to the onset of the Younger Dryas (YD), a phase of decreased sea-level rise. Progradation of U400 occurred during YD, but was maintained during the Preboreal (PB) due to high sediment supply, until about 10,500 yr cal BP. It is a downlap surface named Maximum Transgression Surface (MTS) in the senses of Helland-Hansen and Martinsen (1996). This complex represents a transgressive parasequence bounded by flooding surfaces (FS1 and FS2). Note that none of the key surfaces or units is in phase with sea-level changes, except for MTS which corresponds to the onset of the Younger Dryas. The sea-level curve is from Bard et al. (1996).

Fig. 14: Relative sea-level curve in the Gulf of Lions for the last 20 kyr. The point at -99 m below present sea-level is from Bassetti et al. (2006), the one between -110 and -115 m is from Jouet et al. (2006). Our data are not corrected from isostatic effects and are therefore relative sea-levels.

Table 1: Summary of the dated samples used for this study. Absolute dates were obtained with accelerator mass spectrometer (AMS) ^{14}C dating of well-preserved shells and microfauna. They were made at Lawrence Livermore National Laboratory (LLNL), and at Poznan Radiocarbon Laboratory (PRL). The ages reported herein are delta ^{13}C-normalised conventional ^{14}C years. For ages between 0 and 21,880 yr 14C BP, calendar (i.-e. calibrated) ages were calculated using the Calib 5.0 sofware (Stuiver and Reimer, 1993). For marine material, the Marine04 calibration curve (Hughen et al., 2004) was used with no deviation from the average reservoir age (-408 years). For continental material (namely the organic debris of the St Ferreol prodelta) the Intcal04 calibration curve (Reimer et al., 2004) was used.

Table 2: Average age of clinoforms of Figure 11 (using the age model of Fig. 10) and depth of the deltaic/shoreface to prodeltaic transition (black crosses in Fig. 11), using a sonic velocity of 1580 m/s in sediment.
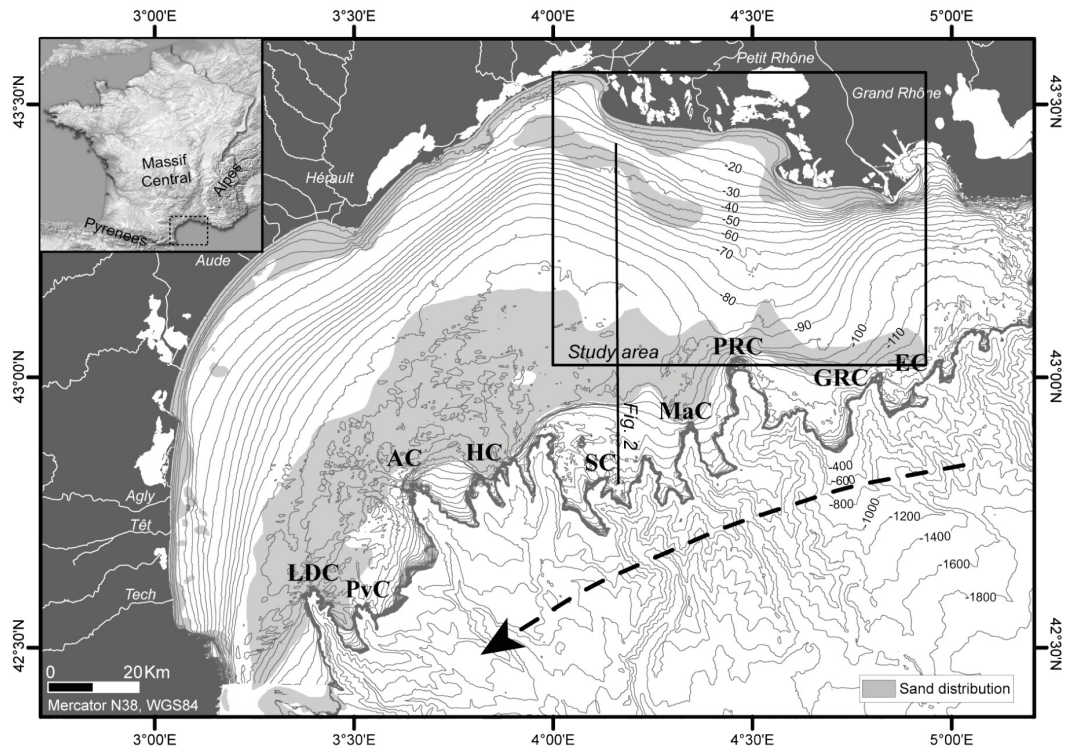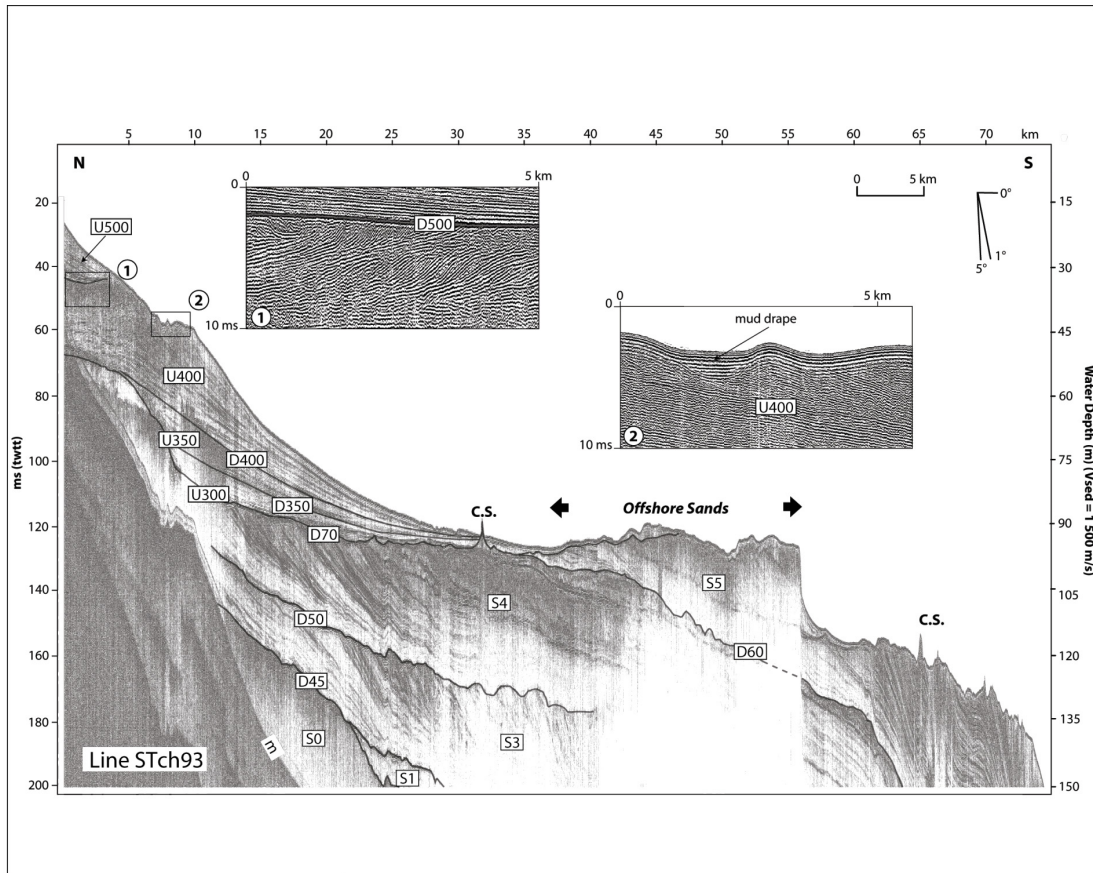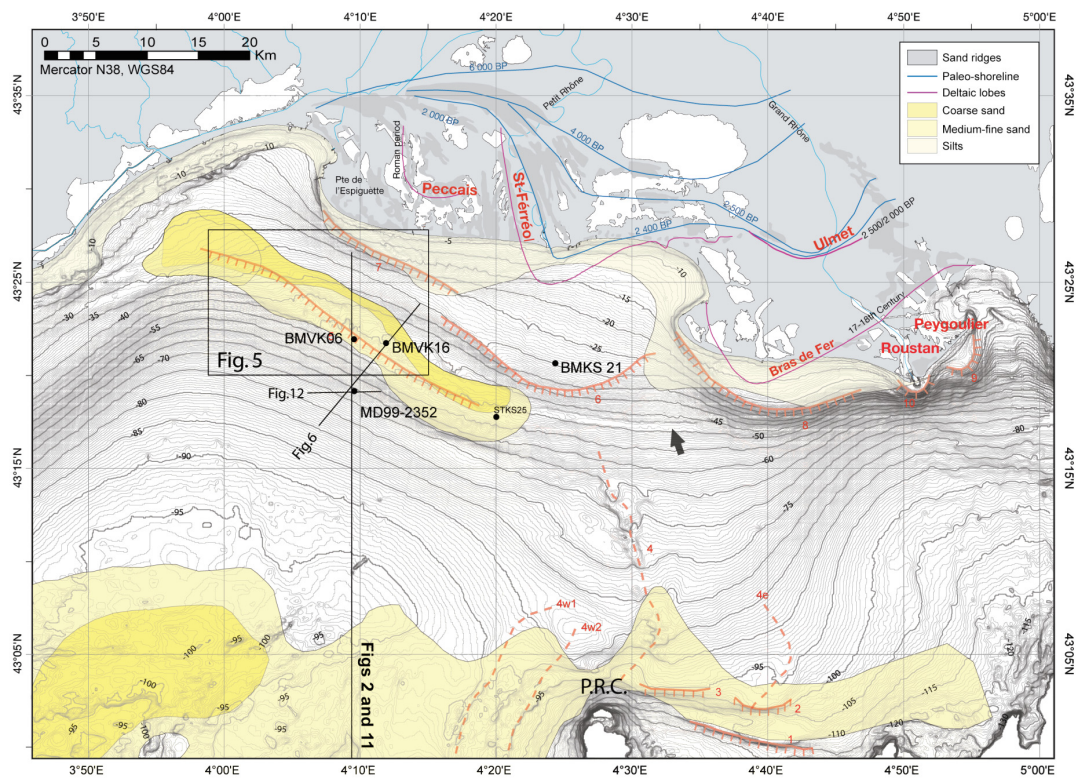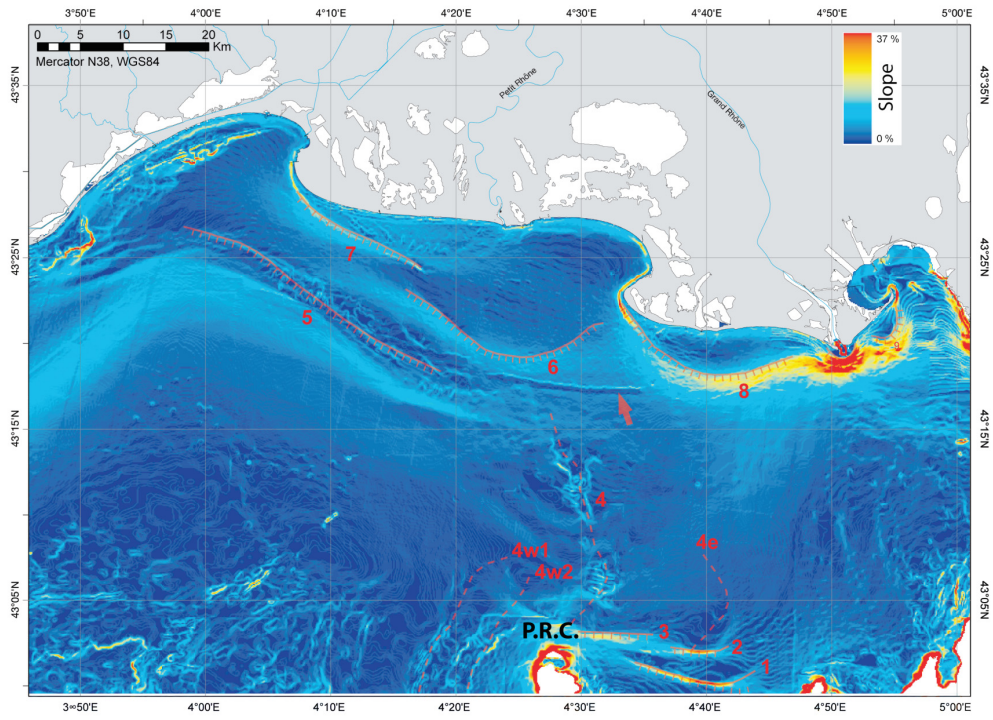
Fig. 1 Berné et al.

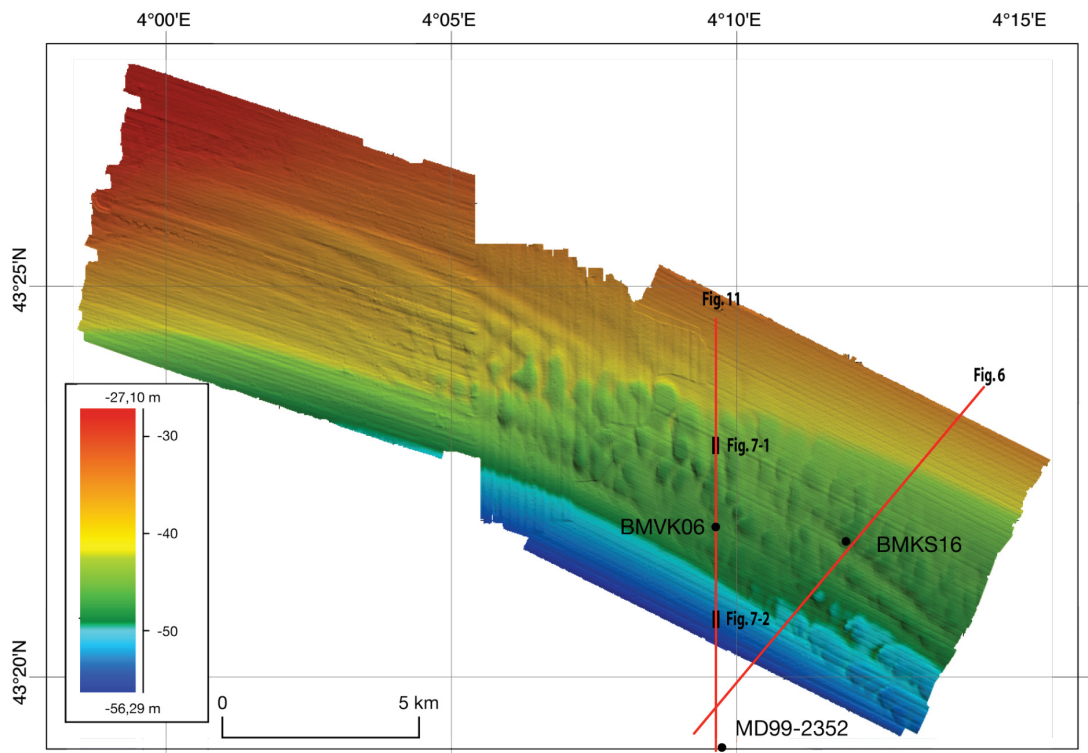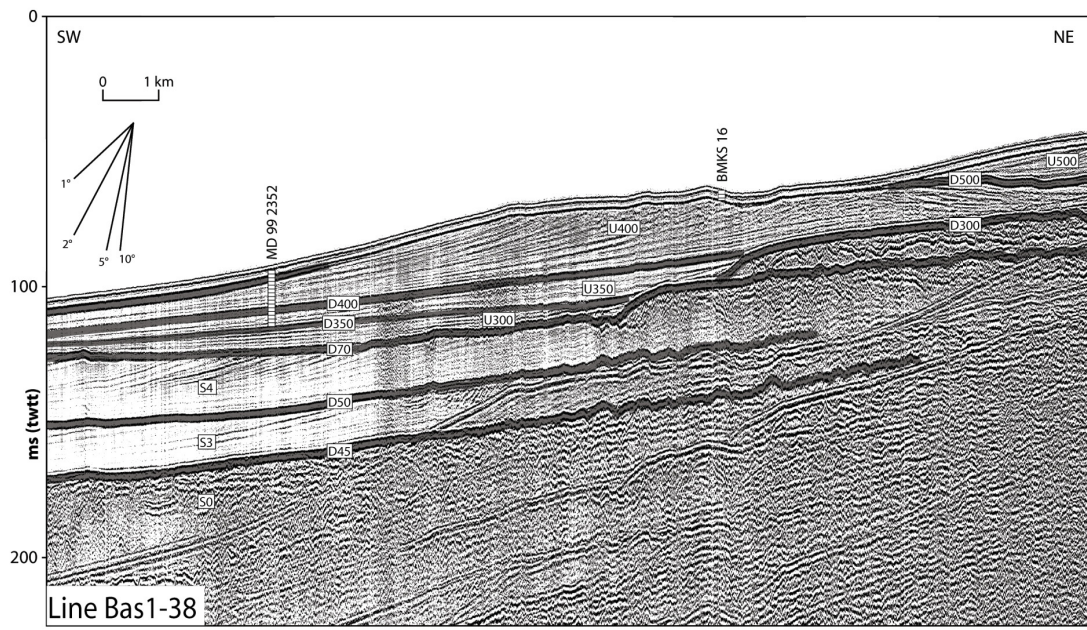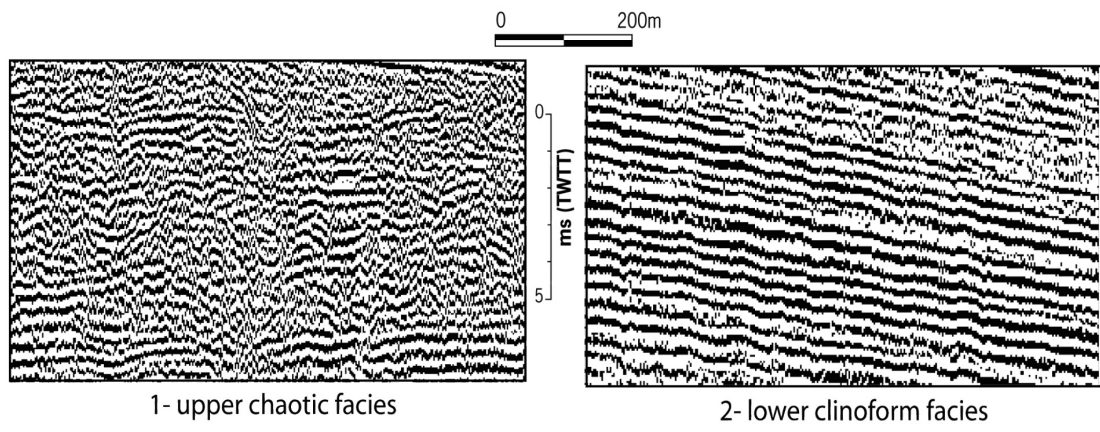Fig. 2 Berné et al.

Fig. 3: Berné et al.

228

Fig. 4 Berné et al.

Fig. 5   Berné et al.

230

Fig. 6 Berné et al

1- upper chaotic facies   2- lower clinoform facies

Fig.7 Berné et al.

BM-VK06

MD99-2532

BM-VK06

Description   Lithology
                        Sand
                    C S vff mc
cm 0

0-40: Highly heterogeneous
interval made of
mud and coarse- grained sand
mixed
with biogenic fragments

10

20   ★ 5.754-
              5.786 y BP

30

40

40-60: Homogeneous,
well-sorted sand.

50

60

70

60-91: Sand/clay alternations
The clay intervals (massive)
contain sand laminae
The fine-grained material shows
Organic Matter spots.

80

90

100

91-154: Clay/very fine
sand alternation

110

120

130

140

150   ★ 10.665-
              10.899 y BP

MD99-2532

Description   Lithology   Pebble
                        Sand
                    C S vff mc
                                    m 0

0-1.3 m: Brownish massive clay with
sand-silt pockets, containing shell
debris, fragments, spines,
forams.....with a coarse-grained
shell lag at the base

1

– – – – D500 – – – –   ★ 5.249-
                              5.362 y BP

2

3   ★ 10.661-
             10.925 y BP

1.3-14.5 m: Silt/very fine sand
alternations.
Abundant black spots
(hydrotroilite), wood debris,
sparse shell fragments and
occasional presence of
Turritella

4   ★ 10.909-
             11.110 y BP

5   ★ 11.019--
             11.117 y BP

6

U400   7   ★ 11.216-
                     11.333 y BP

8   ★ 12.845-
             12.908 y BP

9   ★ 11.738-
             11.954 y BP
           ★ 11.560-
             11.718 y BP

– – – D400 – – – 10

11   ★ 12.856-
             12.913 y BP

12

U350

13   ★ 13.225-
             13.317 y BP

14   ★ 13.244-
             13.326 y BP

Clay interval with some sandy
horizons interbedded

15   ★ 14.280-
             14.648 y BP
           ★ 15.031-
– – – – D350 – – – – 15.258 y BP
                      ★ 14.870-
Coarse grained bed consisting of   15.111 y BP
pebbles in a sandy matrix, mixed
with shell debris and fragments

16

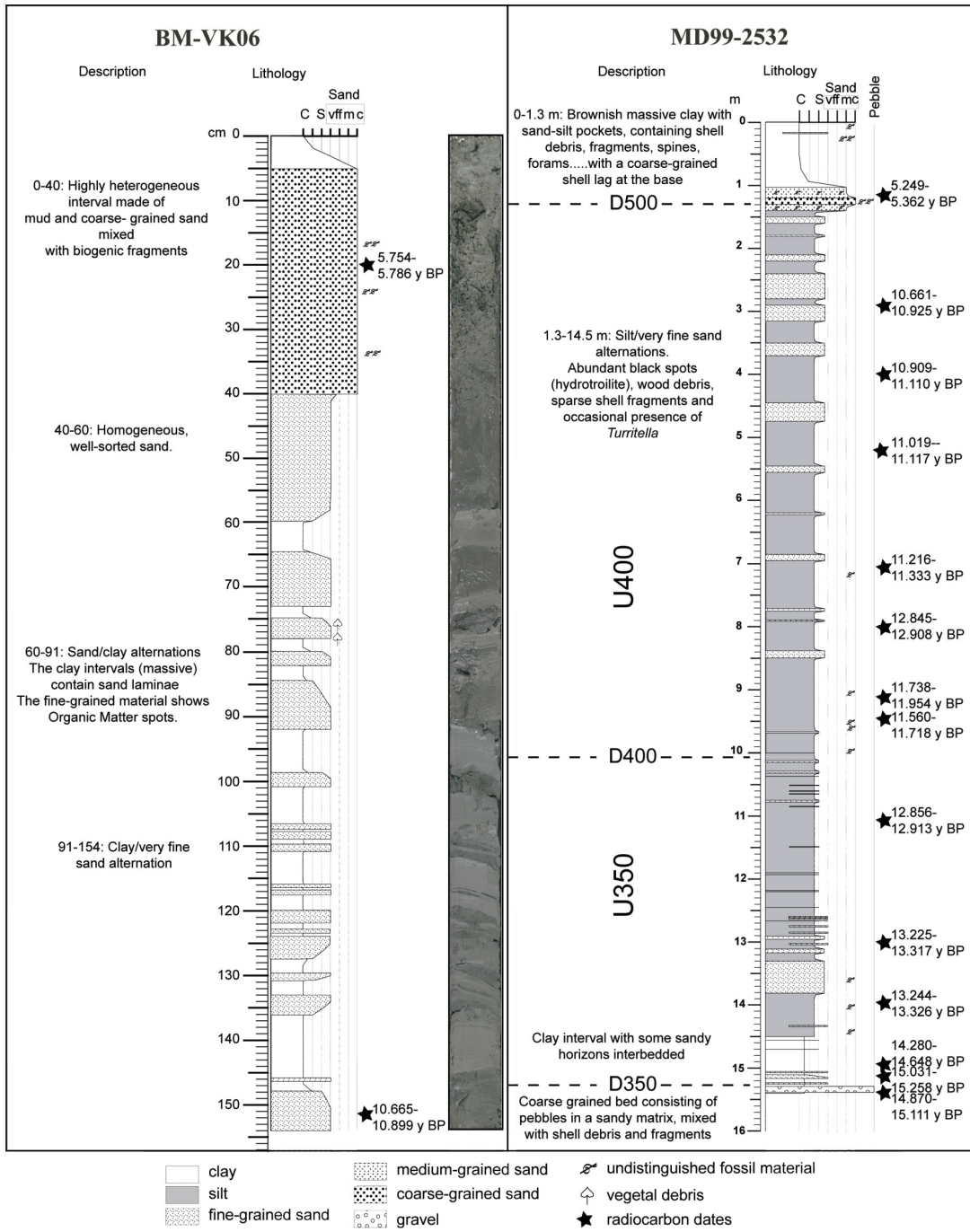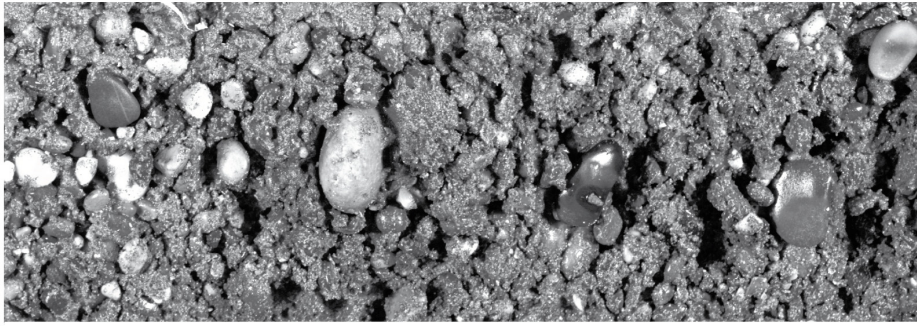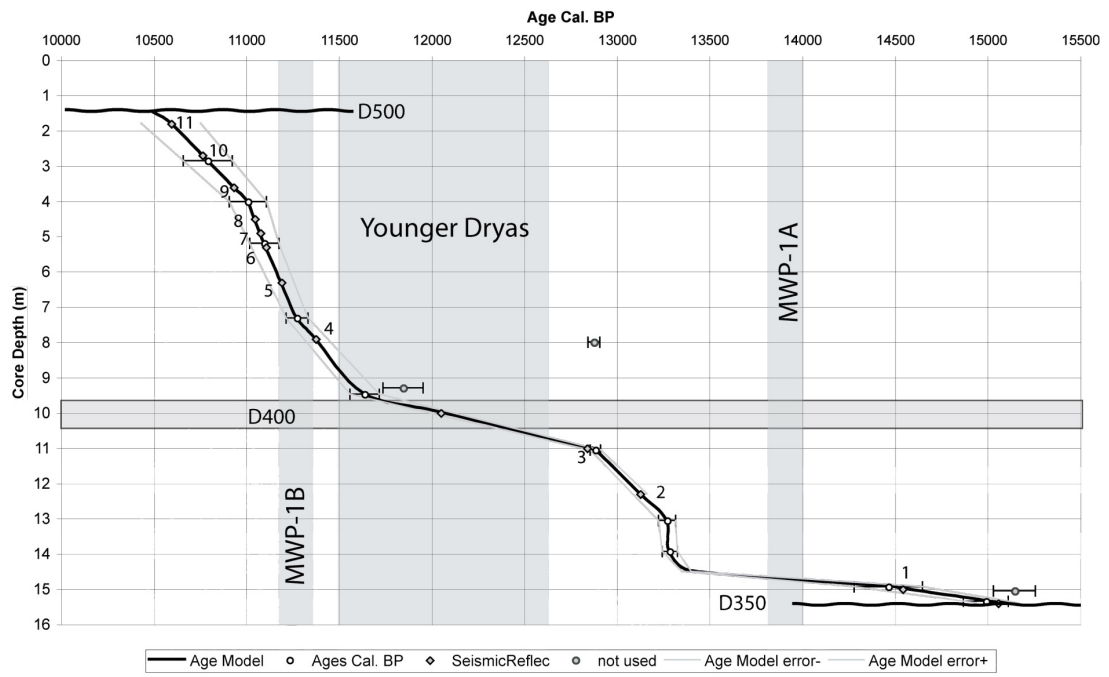| ▢ | clay | ▨ | medium-grained sand | ☞ | undistinguished fossil material |
| ▨ | silt | ▨ | coarse-grained sand | ♤ | vegetal debris |
| ▨ | fine-grained sand | ◦◦◦ | gravel | ★ | radiocarbon dates |

Fig. 8 Berné et al.
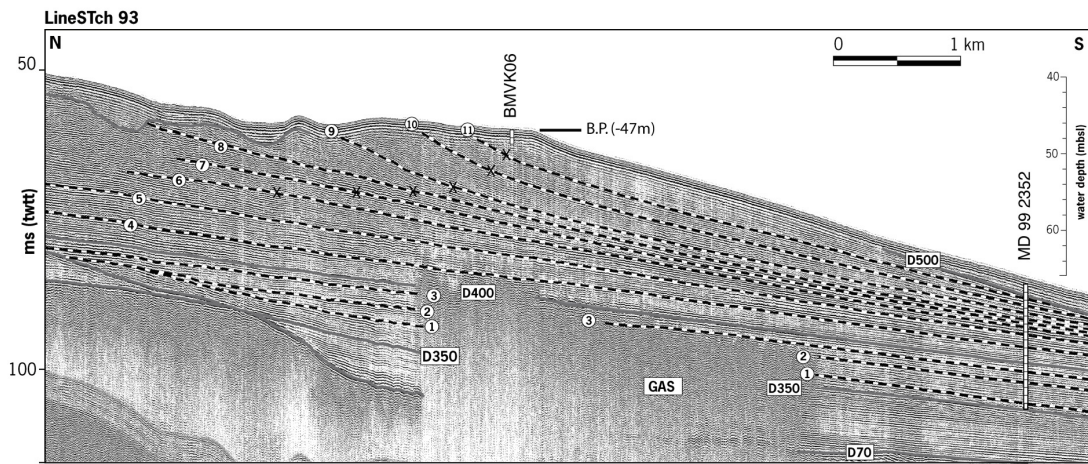
233

5cm

Fig. 9 Berné et al.

Figure 10 Berné et al.
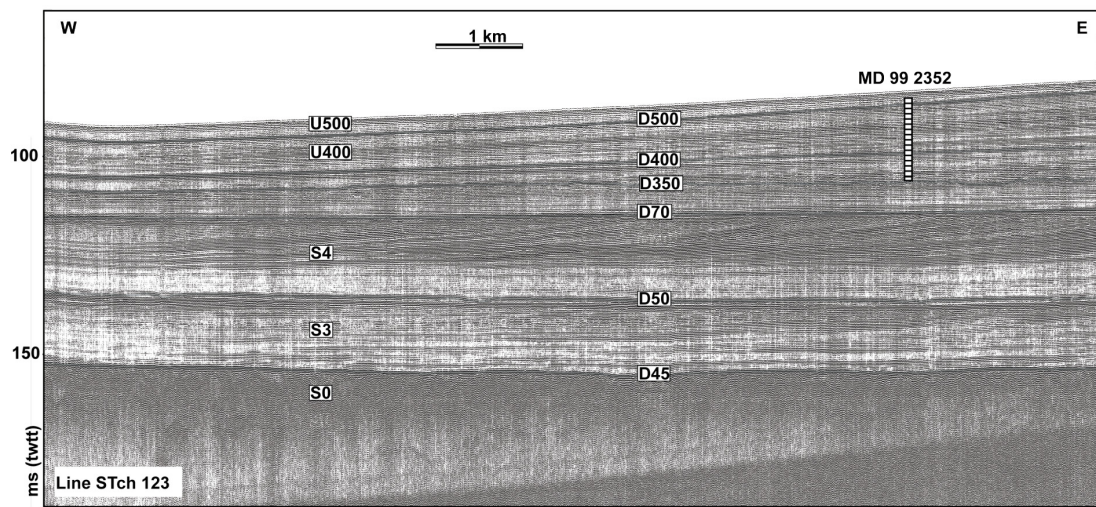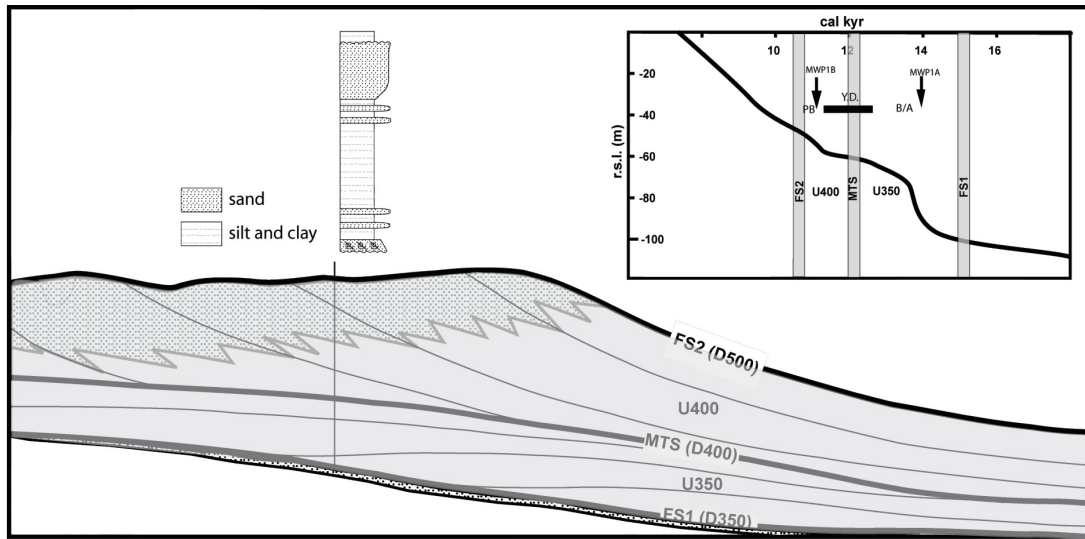
Fig. 11   Berné et al.

236

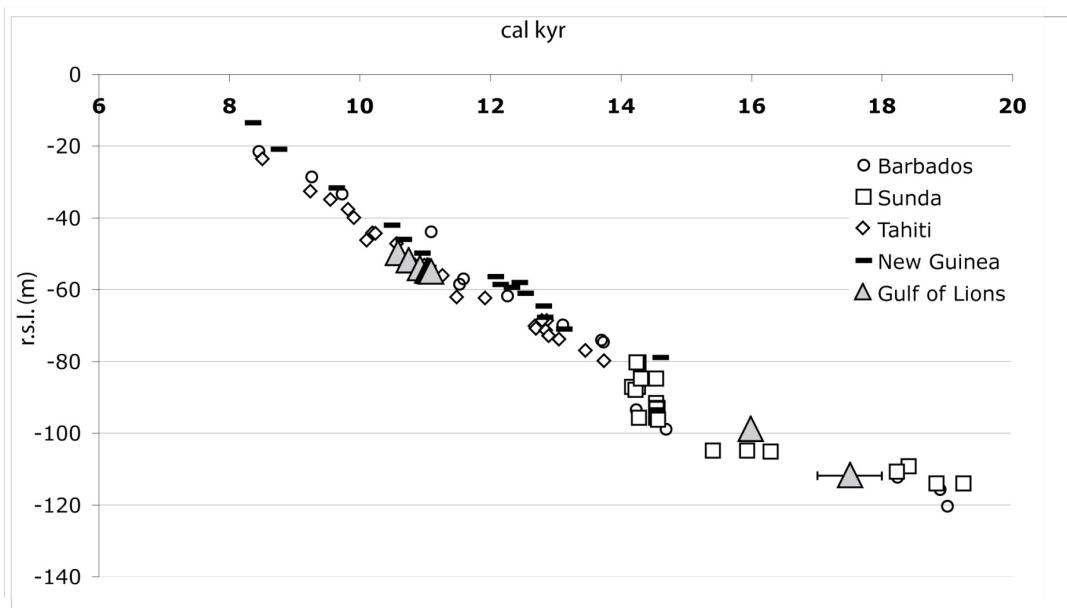Fig. 12 Berné et al.

237

Fig. 13 Berné et al.

238

Fig. 14 Berné et al.

Core	sample depth (cm)	sample weight (mg)	dated material	sample number	Conventional C14 age (BP)	1 sigma calibrated age (yr BP)	probability distribution (/1)
MD992352	123	340	*Acanthocardia echinata*	LLNL-95846	4 955 ± 45	5249-5362 ; 5367-5388	0.91 0.099
	286	109	*Nucula sp.(nucleus)*	poz-3842	9890 ± 60	10661-10925	1.000
	401-403	9,6	*Turitella communis*	poz-3843	10000 ± 50	10909-11110	1.000
	519-521	10,7	small benthic forams + few bivalves, gastropods and ostracods	poz-3844	10070 ± 60	10949-10953 ; 11019-11177	0.011 0.99
	731	59	*Turitella communis*	poz-3845	10310 ± 50	11216-11333	1.000
	799-801	15,3	mixed benthic forams + few bivalves, gastropods and ostracods	poz-3846	11320 ± 60	12845-12908	1.000
	928-932	19,2	*Corbula gibba*	poz-3848	10590 ± 50	11738-11954	1.000
	948	105	*Corbula gibba*	LLNL-95847	10 475 ± 40	11409-11523 ; 11560-11718	0.41 0.59
	1105-1107	19,6	mixed benthic forams + few bivalves, gastropods and ostracods	poz-3849	11340 ± 50	12856-12913	1.000
	1305-1307	42,6	*Ammonia beccarii or Elphidium crispum* + few bivalves	poz-3850	11820 ± 50	13225-13317	1.000
	1393	31	*Corbula gibba*	LLNL-95848	11 840 ± 40	13244-13326	1.000
	1494	64	*Turitella communis*	LLNL-95849	12 855 ± 40	14280-14648	1.000
	1505	290	*Mya truncata*	LLNL-95850	13 245 ± 40	15031-15258	1.000
	1534-1536	35.7	*Mytilus sp.*	LLNL-98908	13 090 ± 50	14870-15111	1.000
BMKS 21	20-23	151	*Turritella sp.*	Poz-11198	2050 ± 30	1573-1673 (1618)	1.000
	111-113	60	sediment >63 μm with vegetal debris	Poz-11459	2040 ± 35	1946-2046	1.000
	220-222	166	sediment >63 μm with vegetal debris	Poz-11461	2245 ± 35	2179-2241 2302-2334	0,64 0,33
	337-339C	25	sediment >63 μm with vegetal debris	Poz-11377	2060 ± 30	1988-2062 2086-2104	0.85 0.13
	337-339T	376	*Turritella sp.*	Poz-11199	2120 ± 30	1659-1767 (1705)	1.000
	445-446	4,3	*Turritella sp.*	Poz-11200	2135 ± 30	1683-1781 (1725)	1.000
	553-555	153	sediment >63 μm with vegetal debris	Poz-11462	2480 ± 40	2058-2206 (2137)	1.000
BMV K06	22	598	*Tellina serrata*	Poz-12147	5430 ± 35	5754-586 (5804)	1.000
	148-150	139	*Spisula subtruncata*	Poz-12148	9880 ± 50	10665-10899 (10788)	1.000

Table 1 Berné et al.

Seismic reflection	Depth (m) at MD992352	Inferred age (cal yr BP)	Relative sea-level (m)	Rate of r.s.l. rise (cm/yr)	Rate of shoreline progradation (m/yr)
D500	1.50	<10,500	-		
"Brink Point"	-	10,500			
11	1.80	10595±161	50,0	1.2	2.4
10	2.70	10763±136	52.1	1.2	5.4
9	3.60	10931±112	54.2	0.6	14,8
8	4.50	11046±92	54.9	0.3	
7	4.90	11076±84	55.0	0.7	
6	5.30	11106±78	55.2		
5	6.30	11190±68			
4	7.90	11374±64			
D400	10.0	12049±62			
3	11.00	12837±30			
2	12.30	13124±39			
1	15.00	14541±135			
D350	15.40	15055±113			

Table 2. Berné et al.